One Dimensional Computer Analysis of Simultaneous Consolidation and Creep of Clay

Vincent J. Perrone

Dissertation submitted to the Faculty of the
Virginia Polytechnic Institute and State University
in partial fulfillment of the requirements for the degree of

Doctor of Philosophy
in
Civil Engineering

J. Michael Duncan, Chair
T. Kuppusamy
James K. Mitchell
George M. Filz
Ron D. Kriz

August 7, 1998
Blacksburg, Virginia

Keywords: Consolidation, Creep, Clay, Computer Program, Elasto-visco-plastic

One Dimensional Computer Analysis of Simultaneous Consolidation and Creep of Clay

Vincent J. Perrone

(ABSTRACT)

This dissertation describes the development and verification of a general purpose computer program, CONSOL97, for analysis of one dimensional consolidation of multi-layered soil profiles. The program uses an elasto-visco-plastic model that can simulate both consolidation and creep in a single consistent analysis. The finite element program uses standard oedometer test data to model stress-strain-time relationships, and the effect of strain rate on preconsolidation stress observed in the laboratory and in the field. Validation of the computer program by simulating standard oedometer tests is described and the applicability of the program in predicting field behavior is examined.

The oedometer test simulations indicate good agreement with stress-strain and strain-log time test results during loading. Unloading behavior produces excessive rebound. Well-instrumented field tests at Väsby, Sweden, Skå-Edeby, Sweden and Berthierville, Canada indicate that elasto-visco-plastic CONSOL97 analyses produce better predictions of field behavior than conventional elasto-plastic models. CONSOL97 results were in good agreement for the Väsby and Berthierville test fills but underestimated displacements and pore pressures near the center of the normally consolidated clay layer beneath the Skå-Edeby test fill.

Acknowledgments

I have discovered that researching and writing a dissertation is a creative endeavor and an opportunity for personal growth. It has been a journey of self discovery and a fascination with my own creative process, rather than the mere acquisition of technical knowledge. Surprisingly, I found that my previous mountaineering adventures in remote areas produced many of the same emotions and struggles as the creative process. Both required persistence and courage, in the face of despair, to achieve lofty goals.

This journey would not have been possible without support from a diverse group of friends and teachers:

- Professor J. Michael Duncan for demonstrating "clear" thinking and the mechanics of dissecting a difficult problem. It was an honor to spend so much time with the best teacher I have ever known;

- Professors George Filz, Ron Kriz, T. Kuppusamy, and James K. Mitchell for taking the time to serve on my research committee;

- My good friend Dave Goodenough who taught me the "dance of life" and who would not let me take the easy way;

- Joe Keaveny for sharing his humor and his enthusiasm for music, art and literature and Dean Ryden who lived his life with courage and integrity;

- Roger Eddy and Jack Gorsuch for listening with soul;

- Jean Pierre Rajot for responding promptly and cheerfully to my questions about his theory, and for his encouragement and occasional philosophical musings. I look forward to meeting you and continuing our conversations at a Parisian cafe;

- Y.C. Eugene Chang, John Hawley and Rolf Larsson for their willingness to share their knowledge;

- Riley Chan and R.J. Harvey for their patient generosity and advice on computer maintenance and troubleshooting. Your suggestions spared me many long hours of frustration;

- Atsushi Iizuka for unexpectedly showing up and who tried to teach me how to have fun with research;

- Fellow students Diane Baxter, Chris Baxter, David Bentler, Harry Cook, Jaco Esterhuizen, Carmine Polito, and Alan Rauch, for their friendship and stimulating discussions;

- Mary Ruth McDonald, Vicki Graham, Judy Clark and Anne Crate for their friendly assistance on the many administrative matters that needed attention;

- My parents Rose and Paul Perrone. They gave me everything I needed to succeed on my own.

Finally, heartfelt thanks to my wife Chere, and my children, Andrew and Claire for enthusiastically embracing our three year (now five year) "family adventure" in Blacksburg, Virginia. Chere steadfastly endured my frustrations and long hours while working equally long hours as a Mom, a community volunteer, and a nursing instructor at Radford University. Andrew and Claire sacrificed many hours of playtime so Dad could "do his homework;" I hope that they might be encouraged to seek knowledge and truth throughout their lifetime.

"We shall not cease from exploration
And the end of all our exploring
Will be to arrive where we started
And know the place for the first time."

T.S. Elliot

Table of Contents

Appendix B: CONSOL97 USER'S MANUAL (continued)

List of Figures

Chapter 4

Chapter 5

Appendix A

Appendix B

Appendix B (continued)

List of Tables

List of Symbols

English

av : Coefficient of compressibility
C : Inverse of the tangent modulus, D, relating stress and strain (C=1/D)
C_α : Coefficient of secondary compression ($d\varepsilon/d(\log t)$)
$C_{\alpha e}$: Secondary compression index ($de/d(\log t)$)
C_c : Compression index
$C_{\varepsilon c}$: Compression ratio
C_r : Recompression index
$C_{\varepsilon r}$: Recompression ratio
CRS : Constant rate of strain test
c_v : Coefficient of consolidation
D : Tangent modulus relating stress and strain
e : Void ratio
$\dot{e}$: Void ratio rate
e_o : Initial void ratio
EOP : End of primary
EVP : Elasto-visco-plastic
Δe : Change in void ratio
Δe_p : Change in void ratio during primary consolidation
Δe_s : Change in void ratio during secondary compression
F : Plastic potential function
F_i^k : Boundary traction for element, i. Force traction when k=1 and flow traction for k=2

$$F_i^1 = \int_{\Omega^e} \left\{ \Delta\tilde{\sigma}' \frac{\partial \psi_i}{\partial z} + \Delta f_z \psi_i \right\} d\Omega^e + \left[\Delta T_z \Psi_i \right]_{z_a}^{z_b}$$

$$F_i^2 = \int_{\Omega_e} -k \frac{\partial \psi_i}{\partial z} d\Omega^e + \left[\psi_i q \right]_{z_A}^{z_B}$$

f_z : Unit body force
k : permeability
k_c^p : Tangent stiffness of the spring used in the creep portion of rheologic models
k_i^e : Tangent stiffness of the spring used in the instant compression portion of rheologic models
k_z : Vertical permeability
K_{ij}^{kl} : Stiffness matrix coefficients for element, i, and node, j.

$$K_{ij}^{11} = \int_{\Omega^e} C \frac{\partial \psi_i}{\partial z} \frac{\partial \psi_j}{\partial z} d\Omega^e$$

$$K_{ij}^{12} = \int_{\Omega^e} \frac{\partial \psi_i}{\partial z} \Psi_j d\Omega^e$$

$$K_{ij}^{22} = \int_{\Omega_e} \frac{\partial \psi_i}{\partial z} \frac{k}{\gamma_w} \frac{\partial \psi_j}{\partial z} d\Omega^e$$

LIR : Load increment ratio equal to $\frac{\Delta\sigma}{\sigma}$

M_{ij}^{kl} : Flow matrix coefficients for element, i, and node, j.

$$M_{ij}^{21} = \int_{\Omega_e} \psi_i \frac{\partial \psi_j}{\partial z} d\Omega^e$$

$$M_{ij}^{22} = \int_{\Omega_e} \psi_i \frac{n}{Q} \psi_j d\Omega^e$$

m_v : Coefficeint of volume change, $m_v = \frac{\partial \varepsilon_z}{\partial \sigma_z'}$

n : Porosity

NPE : Number of nodal points on the element

OCR : Overconsolidation ratio

P_p : Preconsolidation stress ($\sigma_{p-ref}^{\prime(o)}$)

Q : Bulk modulus of the pore fluid

q : Rate of flow per unit area

t : time duration

t* : Equivalent time used in Magnan's model

t_e : Equivalent time used in Christi and Tonks and other Type II models

t_{eop} : Time at end of primary consolidation

t_p : Time at end of primary consolidation

t_{ref} : Reference time

Tol : Allowable tolerance between the yield stress and the current effective stress

u : Pore pressure

u_e : Excess pore pressure

u_o : Hydrostatic pore pressure

u_j : Pore pressure solution at element node, j

Δu : Interpolated pore pressure increment in the finite element domain

$$\Delta u = \sum_{j=1}^{NPE} \Delta u_j \psi_j$$

u(z,t) : Interpolated pore pressure in the finite element domain at time, t

$$u(z,t) = \sum_{j=1}^{NPE} u_j(t) \psi_j(z)$$

$\dot{u}(z,t)$: Interpolated pore pressure rate in the finite element domain at time, t

$$\dot{u}(z,t) = \sum_{j=1}^{NPE} \dot{u}_j(t) \psi_j(z)$$

u_t : Pore pressure at each node at time, t

w_t : Displacement at each node at time, t

Greek

α : Creep parameter used in Embankco computer program, $\alpha = C_\alpha - (\beta_{\alpha s} \cdot \Delta\varepsilon)$

β : Scalar factor for time-dependent behavior

$\beta_{\alpha s}$: Change in secondary compression coefficient during soil compression used in Embankco computer program, $\beta_{\alpha s} = \Delta C_\alpha / \Delta\varepsilon$.

ε : Strain

$d\varepsilon$: Change in strain

$\dot{\varepsilon}$: Total strain rate

ε_{eop} : Strain at the end of primary consolidation

$\tilde{\varepsilon}^{(n)}$: Time-dependent strain at time step increment, n and when the effective stress is equal to or greater than the critical stress, σ'_c

$\Delta\tilde{\varepsilon}^{(n)}$: Change in time-dependent strain at time step increment, n

$\tilde{}_{e\ n}$: Time-dependent strain component at time step increment, n and when the current effective stress is less than the critical stress, σ'_c.

ε_c^p : Plastic creep strain

$d\varepsilon_c^p$: Change in plastic creep strain

$\dot{\varepsilon}_c^p$

$\dot{\varepsilon}_{c-ref}^p$: Reference plastic creep strain rate

$d\varepsilon_c^p$: Change in plastic creep strain

$\ddot{\varepsilon}_c^p$: Rate of change of the plastic creep strain rate.

ε_i^e : Instant elastic strain

$d\varepsilon_i^e$: Change in instant elastic strain

ε_i^p : Instant plastic strain

$d\varepsilon_i^p$: Change in instant plastic strain

ε_{ij}^{vp} : Visco-plastic strain tensor

ε_v : Volumetric strain

$\dot{\varepsilon}_v$: Volumetric strain rate

ε_v^p : Vertical or volumetric visco-plastic strain

$d\varepsilon_v^p$: Change in vertical visco-plastic strain

$\dot{\varepsilon}_v^p$: : Vertical visco-plastic strain rate

$\dot{\varepsilon}_{v-ref}^p$: Reference vertical visco-plastic strain rate

$\dot{\varepsilon}_{ij}^{vp}$: Visco-plastic strain rate tensor

ε_z : Vertical strain

γ_w : Unit weight of water

η : Viscosity of the dashpot in rheologic physical models (units are stress-time)

η_o : Viscosity constant (units are stress-time)

η^{tl} : Viscosity of the dashpot when convergence to the C_α-relationship begins

θ : Coefficient that varies from 0 to 1 and used to approximate time derivatives.

σ' : Effective stress

$\tilde{\sigma}'^{(n)}$: Time-dependent effective stress at time step increment, n

σ'_c : Critical effective stress ($\sigma'_c = \sigma'_p$)

σ'_v : Effective vertical stress

σ'_o : Initial effective stress

$\sigma'^{(o)}$: Initial effective stress

σ'_f : Final effective vertical stress

σ'_{ij} : Effective stress tensor

$\sigma'^{(o)}_{p-ref}$: Reference preconsolidation stress for the reference strain rate

σ'_p : Strain rate dependent effective preconsolidation stress or critical stress ($\sigma'_p = \sigma'_c$)

σ'_{ref} : Critical effective stress on the reference time line (Niemunis and Krieg model)

s'_t : Effective stress at each element at time, t

σ'_{vf} : Final effective vertical stress

σ_z : Total vertical stress

σ'_z : Effective vertical stress

ν_j : Displacement solution at element node, j

$\Delta\nu$: Displacement increment in the finite element domain

$$\Delta\nu = \sum_{j=1}^{NPE} \Delta\nu_j \psi_j$$

$\nu(z,t)$: Interpolated displacement solution in the finite element domain

$$\nu(z,t) = \sum_{j=1}^{NPE} \nu_j(t)\psi_j(z)$$

$\dot{\nu}(z,t)$: Interpolated displacement rate in the finite element domain at time, t

$$\dot{\nu}(z,t) = \sum_{j=1}^{NPE} \dot{\nu}_j(t)\psi_j(z)$$

ψ_j : Interpolation (shape) functions

Λ : Time-dependent multiplier

Ω : Finite element domain

Γ_j : Boundary "j" in the finite element domain

Chapter 1

INTRODUCTION

The development of time dependent models of one dimensional consolidation began about a decade after Terzaghi published his consolidation theory (Terzaghi, 1925) which described pore water pressure dissipation. Laboratory tests and field observations reported by Buisman (1936) and Taylor (1942) clearly indicated the effect of time on the compressibility of clays. Buisman found that settlements increased linearly with log of time under constant effective stress for clay and peat loaded in the field and in the lab. Taylor developed one of the first time dependent consolidation models (Taylor and Merchant, 1940; and Taylor 1942) to describe the behavior. These early efforts attempted to model creep during primary consolidation (increasing effective stress) and during secondary compression (constant effective stress). The effects of creep compression on preconsolidation pressure were generally not considered before Bjerrum's development of the time lines theory (Bjerrum 1967) and subsequent development of constant rate of strain (CRS) testing devices. Leroueil et al (1985) demonstrated the effect of rate of loading (strain rate) on the preconsolidation pressure.

Despite recent advances in our understanding of creep effects on one dimensional consolidation behavior, most geotechnical engineers use conventional methods of analysis that do not include the effects of strain rate, duration of loading, or creep on consolidation behavior. These methods, when they involve numerical computer analyses, may account for changes in permeability and non-uniform strain profiles that previously limited the applicability of Terzaghi's consolidation theory. Computer programs such as CONSOL (Duncan et al 1988) are used to predict the magnitude and rate of settlement during primary consolidation. At the end of primary

consolidation, secondary compression is added to the calculated settlement. Thus consolidation and secondary compression are separated for ease of computation, ignoring the fact that secondary compression (creep) and consolidation occur simultaneously.

This thesis describes the development and verification of a general purpose computer program, CONSOL97, for analysis of one dimensional consolidation of multi-layered soil profiles. It is based upon the Rajot theory (Rajot 1992) of time-dependent clay compressibility that can simulate both consolidation and creep in a single consistent analysis. Using standard oedometer test data, the theory can model stress-strain-time relationships, and the effect of strain rate on preconsolidation pressure observed in the laboratory and in the field.

Chapter 2 reviews the development of computer programs for one dimensional analysis of consolidation and creep. The list of programs includes ones that are currently available and ones that describe computer programs that are no longer available but made a significant contribution in the historical development of current day computer programs. Each model and its implementation in a computer program is described. The chapter concludes with a comparison of each program's simulation of loading of a thin lab sample and a thick field layer.

Chapter 3 describes Rajot's model, it's implementation in the CS1 finite element program, and the results of numerical simulations of standard oedometer tests to validate the computer program. Modification of CS1 to improve numerical stability, and predictive capabilities is also described in this chapter. The new program is named CONSOL97.

Operation of CONSOL97 is described in Chapter 4. The input parameters are described and the results of analyses that indicate the program's capabilities in predicting Bjerrum's time lines, aged OCR, and non-uniqueness of end of primary strain. The chapter concludes with a summary of the effects of time dependent behavior on magnitude of settlement, preconsolidation pressure, rate of settlement, and pore pressure dissipation.

The applicability of Rajot's model in predicting field behavior is decribed in Chapter 5. Data from three well- instrumented and carefully documented field cases are compared to CONSOL97 simulations. Three of the field cases are test embankments constructed on natural clay deposits in Väsby, Sweden; Skå-Edeby, Sweden and; Berthierville, Canada.

Conclusions derived from this research are summarized in Chapter 6. Recommendations for future research are presented in Chapter 7. A user's manual for CONSOL97 can be found in Appendix B.

1.1 TIME-DEPENDENT PHENOMENA

When clay is subjected to an increase in load, either in the laboratory or the field, compression continues at a diminishing rate after effective stress has reached a constant value, as shown in Figure 1.1(a). This time dependent compression at constant effective stress, or "secondary compression," is an important aspect of clay compressibility. In incremental laboratory consolidation tests, where loads are applied at 24 hour intervals, secondary compression strains that occur between the end of primary consolidation and 24 hours influence the position of the measured stress-strain curve (Figure 1.1(b)). If the duration of each load increment was longer, the measured strains would be larger, because more secondary compression would occur in the longer loading period. If the duration of each load was shorter, the measured strains would be smaller, because less secondary compression would occur.

The effects of time on clay compressibility are evident not only in the position of the stress-strain curve but also in the magnitude of the preconsolidation pressure measured in laboratory tests. Taylor (1942, 1948), Crawford (1964, 1988), and Bjerrum (1967) have shown that, as a result of secondary compression, there is not a single stress-strain curve for one-dimensional compression

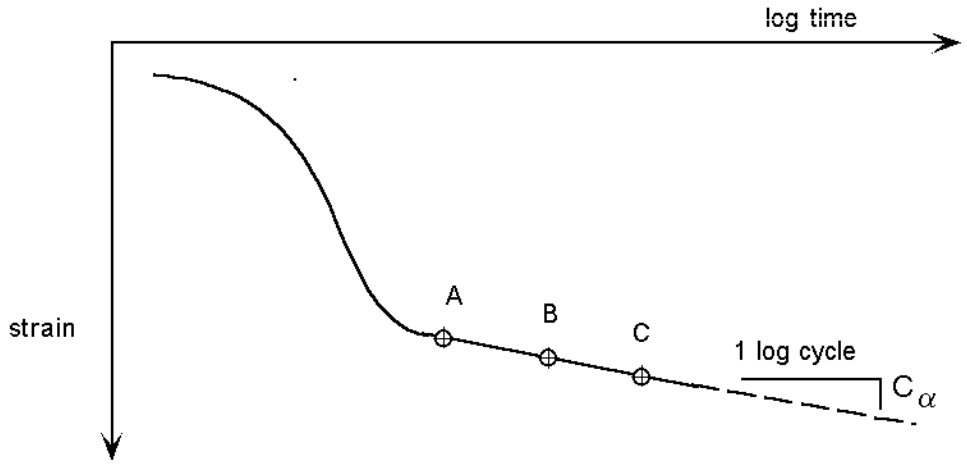

(a) Strain versus time curve for load increment from σ'_o to σ'_f

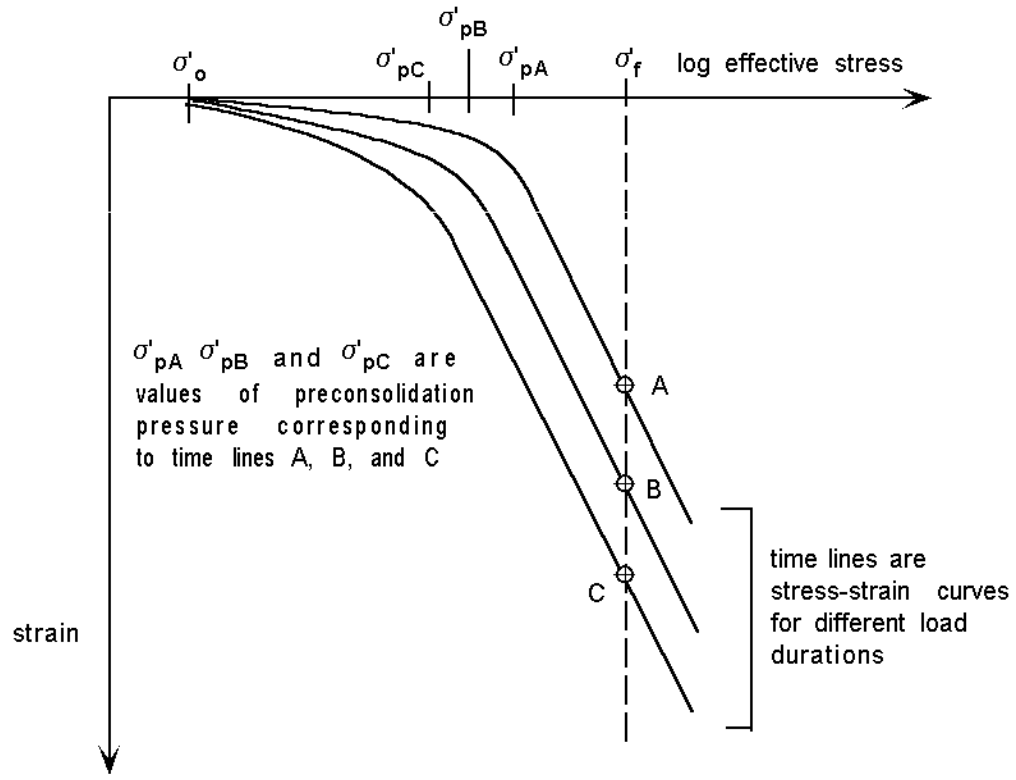

(b) Stress-strain curves

Figure 1.1: Strain versus time and stress-strain curves for consolidation tests on clay

of clay, but a family of curves, called "time lines," each corresponding to a different duration of the applied load, and each having a different preconsolidation pressure (P_p') as shown in Figure 1.1. Longer loading durations produce lower preconsolidation pressures. Since a clay has only one value of maximum past pressure, we must consider the lab determined "preconsolidation pressure" to be a time-dependent or strain rate-dependent parameter, $P_p = P_p(\dot{\varepsilon})$, designating the yield stress to be used in the constitutive model.

The terms "primary consolidation" and "secondary compression", illustrated in Figure 1.2a, are commonly understood by geotechnical engineers as consecutive phases of the one dimensional compression process. These are "descriptive" terms for the characteristic behavior observed during consolidation. The behavior they characterize includes the effects of pore water pressure dissipation with time after loading (which is governed by the phenomena of flow through porous media) and the response of the soil skeleton to the resulting increase in effective stress (which is governed by the constitutive behavior of the consolidating material). In particular, primary consolidation refers to the total change in void ratio caused by pore pressure dissipation [$(d\sigma'_v/dt) > 0$] and can be expressed by the compressibility index, C_c:

$$C_c = \frac{de}{d(\log \sigma'_v)} \tag{1.1}$$

or the coefficient of compressibility, a_v:

$$a_v = \frac{de}{d\sigma'_v} = \frac{C_c}{0.434 \times \sigma'_v} \tag{1.2}$$

Secondary compression refers to the creep rate or rate of change in void ratio at constant effective stress after pore pressure dissipation [$(d\sigma'_v/dt) = 0$]. The coefficient of secondary compression is typically used to express this behavior:

$$C_{\alpha e} = \frac{de}{d(\log t)} \tag{1.3}$$

where: t is the time after completion of primary consolidation.

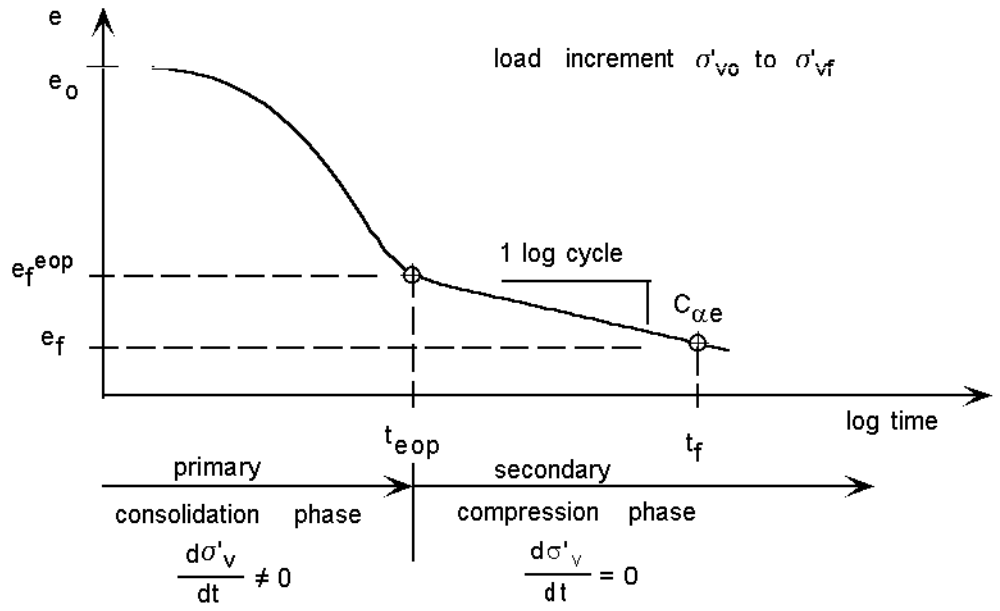

(a) Void ratio versus log time

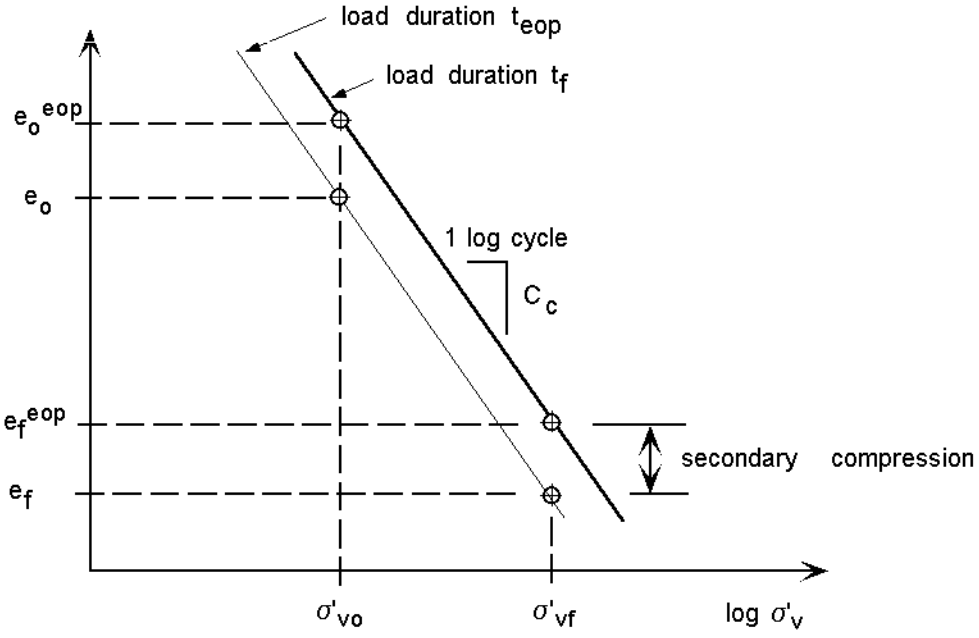

(b) Void ratio versus log effective stress

Figure 1.2: Consolidation phases

The effects of pore water pressure dissipation on the stress-strain behavior of clays are schematically illustrated in Figure 1.3 for a lab oedometer sample loaded in incremental steps. The loads are applied instantaneously but the increase in effective stress, which is shown by the dashed line in Figure 1.3a, is delayed due to hydrodynamic lag in pore pressure dissipation. The solid lines represent a hypothetical condition of instantaneous increase in effective stress. The hydrodynamic time lag slows the increase in of effective stresses and the corresponding changes in void ratio as compared to the case with no hydrodynamic lag. The characteristic consolidation behavior is illustrated by the *e vs. log t* plot in Figure 1.3b and the *e vs. log* s'_v plot in Figure 1.3c.

The basic constitutive behavior illustrated by the *e vs. log* s'_v plot (Figure 1.3c) consists of instant compression and creep compression. Instant compression, which is partly recoverable, represents the soil skeleton response to an immediate effective stress increase which would occur without the inherent time dependent creep effects. Creep compression is the time dependent behavior of the soil skeleton. An instantaneous increase in effective stress that would occur near the drainage boundary produces instant compression followed by creep compression at constant effective stress. Further from a drainage boundary, the effective stress increases more slowly and the proportion of creep strain at each effective stress level increases with respect to the amount of instant compression. Although the strain may vary with distance from the drainage boundary, only the average void ratio of the sample is measured and reported in conventional oedometer tests. The average behavior of a conventional oedometer test sample is represented by line A-C-E in Figure 1.3c, with a compressibility coefficient, C_c.

The basic constitutive behavior for the rate of void ratio change due to an increase in effective stress and time dependent creep behavior is:

$$\frac{de}{dt} = \left(\frac{\partial e}{\partial \sigma'_v}\right)_t \frac{d\sigma'_v}{dt} + \left(\frac{\partial e}{\partial t}\right)_{\sigma'_v} \qquad (1.4)$$

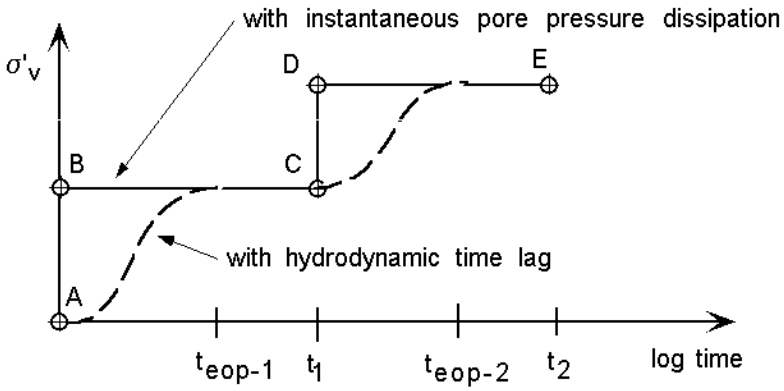

(a) Effective stress versus log time

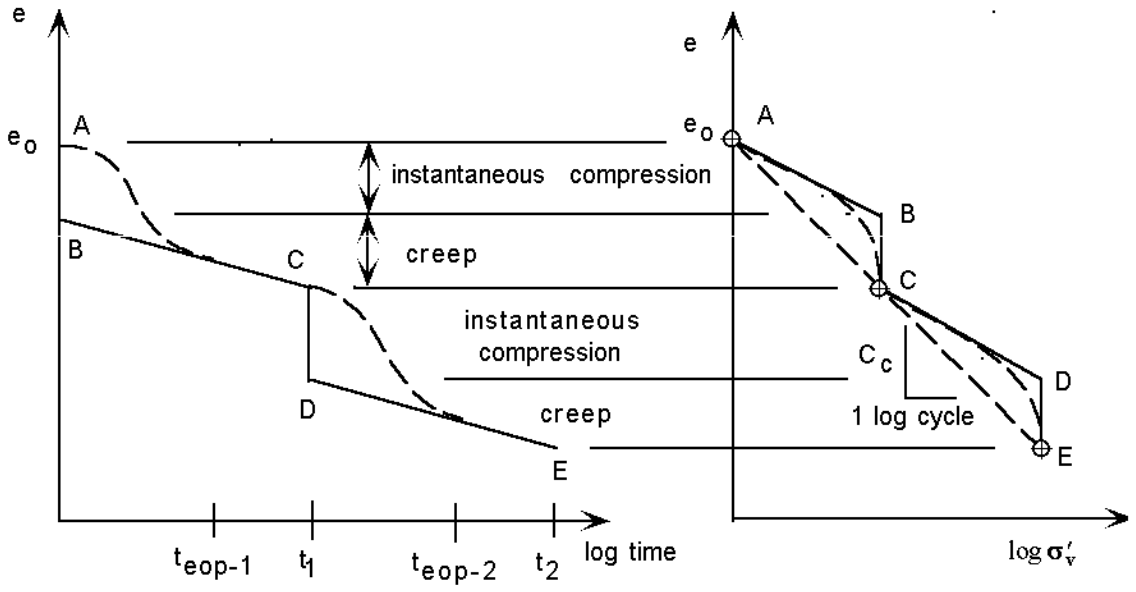

(b) Void ratio versus log time

(c) Void ratio versus log effective stress

— — — — — with hydrodynamic lag

——————— with instantaneous pore pressure dissipation

Figure 1.3: Effects of hydrodynamic lag

where: e = void ratio; σ'_v = effective vertical stress; $\left(\frac{\partial e}{\partial \sigma'_v}\right)_t \frac{d\sigma'_v}{dt}$ = rate of instant elastic compression due to a change in effective stress only; $\frac{\partial e}{\partial t}$ = creep rate.

Both instant compression and creep compression occur simultaneously during primary consolidation. When pore pressure dissipation is complete and effective stresses become constant, only creep compression occurs.

In principle, the total change in void ratio can be obtained by integrating equation 1.4:

$$\Delta e = \int_0^t \left[\left(\frac{\partial e}{\partial \sigma'_v} \right)_t \frac{d\sigma'_v}{dt} + \left(\frac{\partial e}{\partial t} \right)_{\sigma'_v} \right] dt \qquad (1.5)$$

Separating this expression into a primary consolidation phase and a secondary compression phase we have:

$$\Delta e = \Delta e_p + \Delta e_s \qquad (1.6a)$$

$$\Delta e = \int_0^{tp} \left[\left(\frac{\partial e}{\partial \sigma'_v} \right)_t \frac{d\sigma'_v}{dt} + \left(\frac{\partial e}{\partial t} \right)_{\sigma'_v} \right] dt + \int_{t_p}^{t} \left(\frac{\partial e}{dt} \right)_{\sigma'_v} dt \qquad (1.6b)$$

where: Δe_p = change in void ratio during primary consolidation; Δe_s = change in void ratio during secondary compression; t_p = time at end of primary consolidation; **t** = time since load application.

The relative contributions of $\left(\partial e/\partial \sigma'_v\right) d\sigma'_v/dt$ and $\partial e/\partial t$ cannot be measured during primary consolidation. However, equation 1.4, which includes the effect of time, indicates that the constitutive model for clay is of the form:

$$e = f(\sigma', t) \qquad (1.7)$$

In field situations, the time required to reach the end of primary consolidation can be many years whereas the time to end of primary for a thin lab sample may be about one hour. The corresponding strain rates in the field are orders of magnitude slower than in the lab. The effect of the strain rate on the soil compressibility may be much greater in the field than in the lab.

1.2 IMPORTANCE OF USING TIME DEPENDENT MODELS

Thick deposits of clay in the field have long consolidation periods and strain rates that are many orders of magnitude slower than for lab samples. The corresponding smaller strain rates result in lower preconsolidation pressures. Conventional consolidation analyses that ignore creep effects will underestimate the magnitude and the rate of settlement and over-estimate the rate of pore pressure dissipation in the field.

Figure 1.4a illustrates a subsurface profile of San Francisco Bay Mud that was analyzed using conventional and time-dependent theories. The time-dependent analysis was performed using a computer program based on Rajot's (1992) theory. The conventional analyses were performed using the computer program, CONSOL (Duncan et al, 1988) which can simulate non-uniform strain through the thickness of the layer and, non-linear stress-strain models without secondary compression effects.

The effective stress-strain behaviors for a soil element located in the center of the 10 meter thick layer are shown in Figure 1.4b for the time-dependent and conventional analyses. The conventional stress-strain path also corresponds to a stress-strain path for a lab sample. The time-dependent path is below the conventional stress-strain path because of the slower rate of consolidation at the center of the thick layer. It can be seen that the time-dependent theory predicts an apparent preconsolidation pressure that is lower than the preconsolidation pressure from conventional theories.

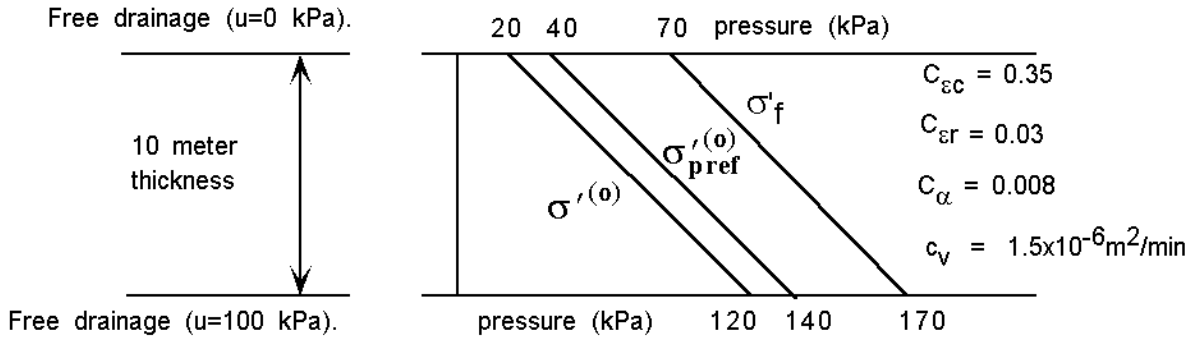

(a) Soil profile and loading conditions

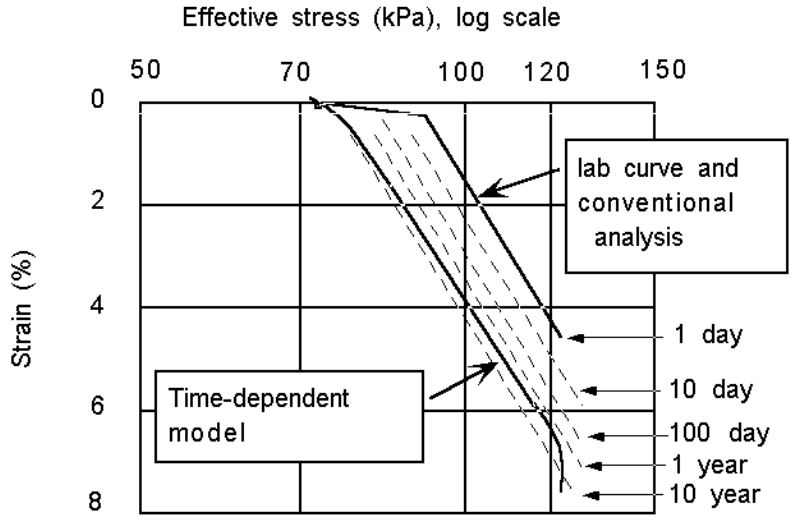

(b) Strain-effective stress at the center of the soil layer according to conventional and time-dependent models

Figure 1.4: Soil profile and stress-strain curves for conventional and time-dependent models

Figure 1.5 indicates that the average rate of settlement is faster and the magnitude of settlement is larger for the time-dependent analysis than for the conventional method that does not include

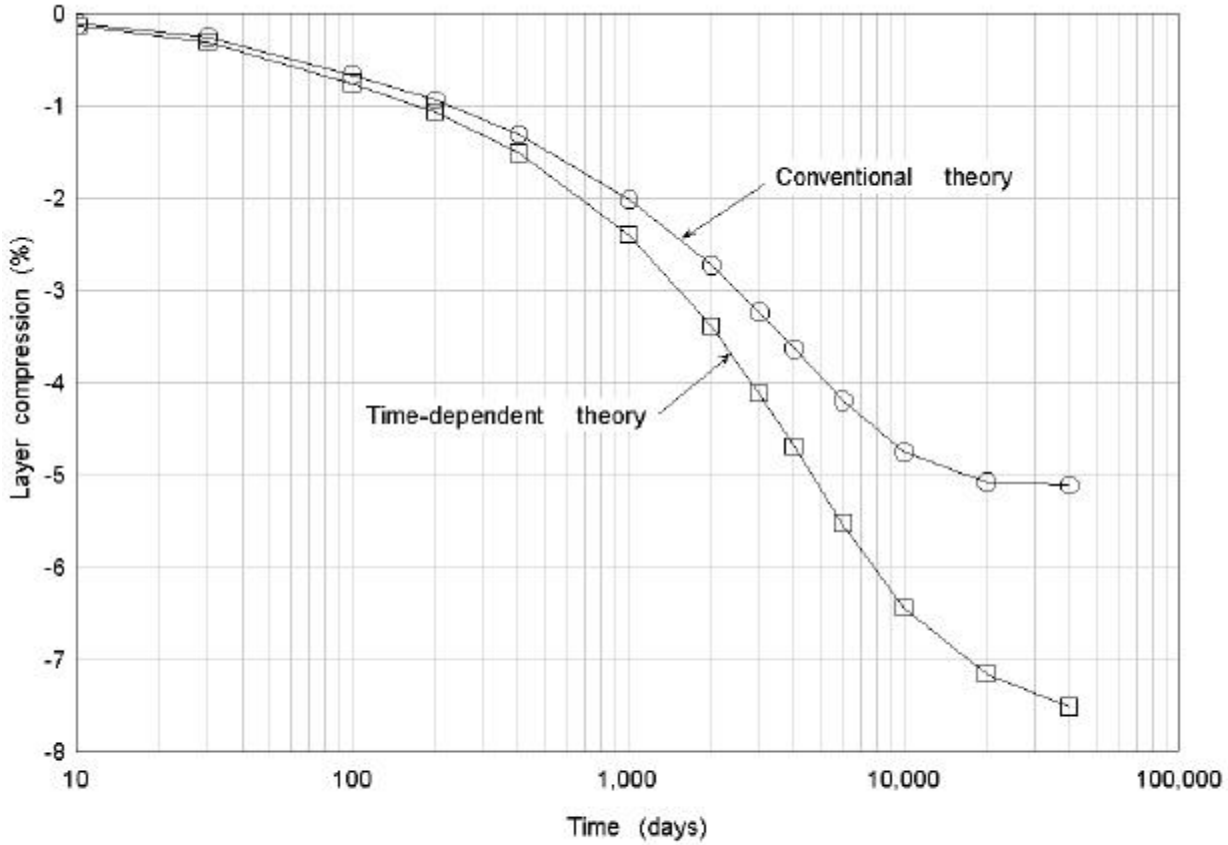

Figure 1.5: Calculated consolidation curves using conventional and time-dependent theories

creep compression effects. The differences in magnitude and rate of settlement would be expected to be even larger for more plastic clays and more organic soils.

Pore pressure magnitudes and dissipation rates calculated by the time-dependent method are larger than those predicted by conventional methods. Figure 1.6 illustrates pore pressure profiles after 1000 days of consolidation. Depending on the subsurface profile and the type of loading, some field measurements indicate that excess pore pressures may continue to increase after

loading ceases, or that significant settlement may continue after excess pore pressures have diminished to insignificant amounts (Crooks et al, 1984, Kabbaj et al, 1988). These effects can be important in many practical applications.

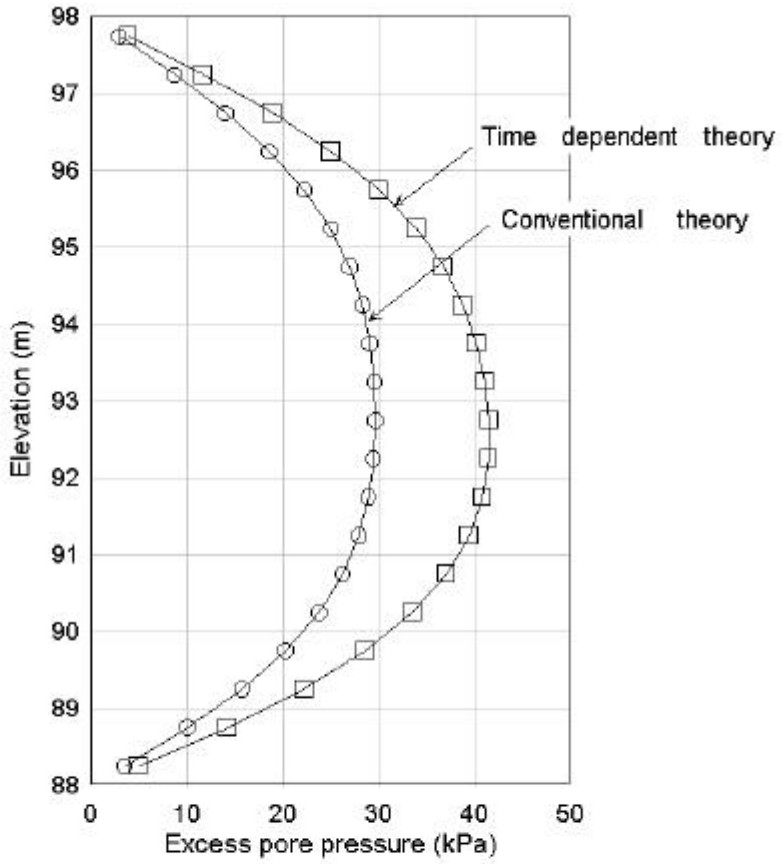

The soil profile and loading conditions are shown in Figure 1.4

Figure 1.6: Calculated excess pore pressures after 1000 days using conventional and time-dependent theories

Chapter 2

ONE-DIMENSIONAL MODELS OF CLAY COMPRESSIBILITY FOR NUMERICAL ANALYSIS OF CONSOLIDATION

2.1 METHODS OF MODELING TIME-DEPENDENT BEHAVIOR OF CLAY

Due to a lack of a general purpose computer program for analysis of simultaneous consolidation and creep compression, and the lack of long term field data to substantiate time-dependent behavior, geotechnical engineers often neglect time-dependent effects. They typically use the 24 hour stress-strain curve, preconsolidation pressure, and coefficient of consolidation to estimate settlement rates and magnitude. Jamiolkowski et al. (1985) noted that the use of these parameters has been justified by the hypothesis that the amount of strain at the end of primary consolidation (EOP) is the same for any layer thickness or time to end of primary (t_{eop}). However, this procedure is seen by some leading geotechnical engineers as an approximation of the complex behavior of clays--a procedure chosen for simplicity rather than fundamental accuracy. Jamiolkowski et al. (1985) suggested two extreme possibilities that they called Hypothesis A and Hypothesis B, which are illustrated in Figure 2.1:

> "Hypothesis A predicts that sample thickness ..... has no effect on the location of the end of primary (EOP) compression curve and hence of the value of [preconsolidation pressure]. Furthermore, the strain versus log t relationship for a given load increment is simply displaced in proportion to [the square of the length of the drainage path] as commonly assumed in practice.

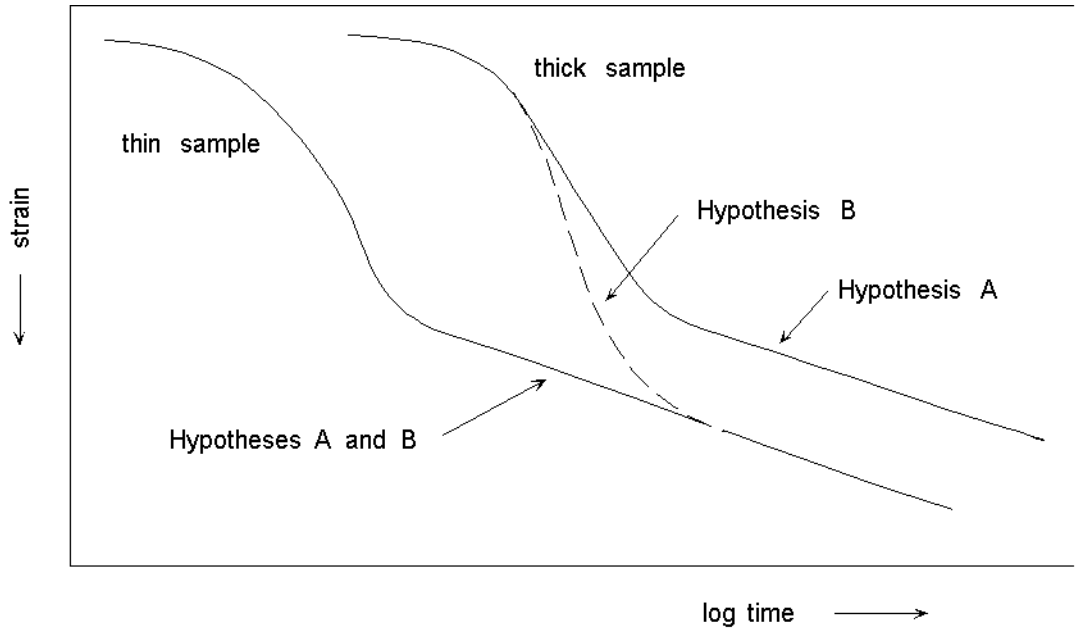

Figure 2.1: Hypothesis A and B as described by Jamiolkowski et al. (1985)

> Hypothesis B ..... predicts a significant shift in the location of the field versus laboratory EOP compression curves, with a corresponding decrease in [preconsolidation pressure] and increased consolidation settlements."

Since the state of the practice review by Jamiolkowski et al. (1985), researchers have made considerable progress toward developing time-dependent models for one-dimensional consolidation and simultaneous creep compression. Some have developed computer programs that include these effects in analyses. When programs are available for analysis of field loading situations, grossly simplifying assumptions regarding time-dependent behavior are not required.

A suitable time-dependent constitutive model for analysis of simultaneous consolidation and secondary compression should ideally have the capability of simulating the following aspects of clay behavior:

- Secondary compression;
- Coefficients of secondary compression that are constant in the normally consolidated range and that decrease with increasing over-consolidation ratio;
- Increases in preconsolidation pressure due to creep during sustained loading (aging);
- Preconsolidation pressures that depend on strain rate, effective stress, and total strain;
- Creep hardening during reloading;
- A rate of secondary compression that is independent of load magnitude in the normally consolidated range of effective stress.

To be useful in engineering practice, the model should be implemented in a computer program that is capable of simulating field subsurface conditions with multiple soil layers and internal as well as external drainage boundaries. The soil model parameters should preferably be familiar properties determined from conventional oedometer tests.

Most computer programs for analysis of time-dependent behavior use constitutive models that are based upon "macro-mechanical" approaches (Feda, 1992). In a macro-mechanical approach the phenomenon of one-dimensional creep behavior observed in the field or laboratory is modeled by mathematical expressions relating strain to the magnitude and duration of loading. The governing mathematical equations are founded on experimental evidence and are therefore physically interpretable. This method of representing constitutive behavior of clay is also known as the "phenomenological" approach.

In contrast to macro-mechanical approaches, micro-mechanical approaches model soil behavior at the particulate or molecular level. Rate process theory (Mitchell et al., 1968) is an example of a micro-mechanical approach which was used in a computer program by Kuhn and Mitchell (1992) to model creep. Although the model simulates the qualitative time-dependent behavior of soil, further research is required to develop a general purpose analytical tool.

Meso-mechanical approaches, which combine micro- and macro-mechanical approaches, have been used to develop computer programs with time-dependent models. Fox, Edil and Malkus (1994) have had some success using a discrete model computer program to simulate time-dependent one-dimensional compression of peat.

Discussion of computer programs that implement theories based on micro and meso-mechanical approaches is not included here because the computer programs do not include coupled consolidation, they generally require computer run times of several hours, and the theories have not yet matured to a practical level.

Although the models discussed here are macro-mechanical or phenomenological, it can be argued that they are also conceptual with regard to predicting field behavior. For example, in either field or lab data, we cannot separate the amount of instant strain due to a change in effective stress from creep strain that occurs simultaneously. Although a constitutive model may correctly simulate experimentally observed behavior such as time lines and secondary compression, it must be considered conceptual with regard to its ability to predict time effects in field situations with thicker clay layers and more complex loading sequences. Therefore, until the behavior of a model can be verified by comparison with field measurements, it must be considered conceptual.

In the phenomenological approach the required mathematical expressions for time-dependent constitutive models can be obtained in three ways: (1) Curve fitting data from lab tests with specific boundary conditions and loading sequence, and assuming the curve-fit model applies to field situations; (2) Modeling the constitutive stress-strain-time behavior with physical elements (springs, dashpots, and sliders); (3) Applying elasto-visco-plastic theory to experimental data on the behavior of clay.

2.1.1 Curve Fitting

The first computer program for analysis of simultaneous consolidation and secondary compression was developed by Garlanger (1973) using Bjerrum's concept of time lines (Figure 2.2) which was based on oedometer test data and field observations. Bjerrum's lab data on Drammen clay illustrated the effects of sustained laboratory loading on preconsolidation pressure (aging) and location of stress-strain-time lines. Garlanger expressed these constitutive relationships mathematically and incorporated them in the consolidation theory formulation. Similarly, Kabbaj et al. (1986) used the results of laboratory constant rate of strain (CRS) tests to formulate time-dependent constitutive relationships.

2.1.2 Rheologic Mechanical Models

Rheologic mechanical models consist of arrangements of springs, dashpots and sliders to represent soil behavior. Each element represents behavior that is elastic, viscous, or plastic. The structural or fabric changes that occur at the particle level are represented by non-linear behavior of the elements. Rheologic models were developed by Taylor (1940), Taylor and Merchant (1942), Gibson and Lo (1961) and, Barden (1965) as research tools to examine a particular aspect of time-dependent soil behavior: secondary compression after pore pressure dissipation or pore pressure dissipation and settlement rates during the early stages of the consolidation process. The effects of time on the preconsolidation pressure were not captured by these models.

The various combinations of linear and non-linear springs, dashpots and sliders for simulating soil behavior required unfamiliar parameters whose values could not be determined directly from standard laboratory tests. For this reason rheologic mechanical models were not widely used. A notable exception is Rajot's (1992) model which overcame previous difficulties associated with rheologic approaches. Rajot developed a model that could be characterized by familiar soil parameters ($C_{\varepsilon c}$, $C_{\varepsilon r}$, P'_p, and c_v) obtained from standard incremental oedometer tests. Rajot's model is described in Chapter 3.

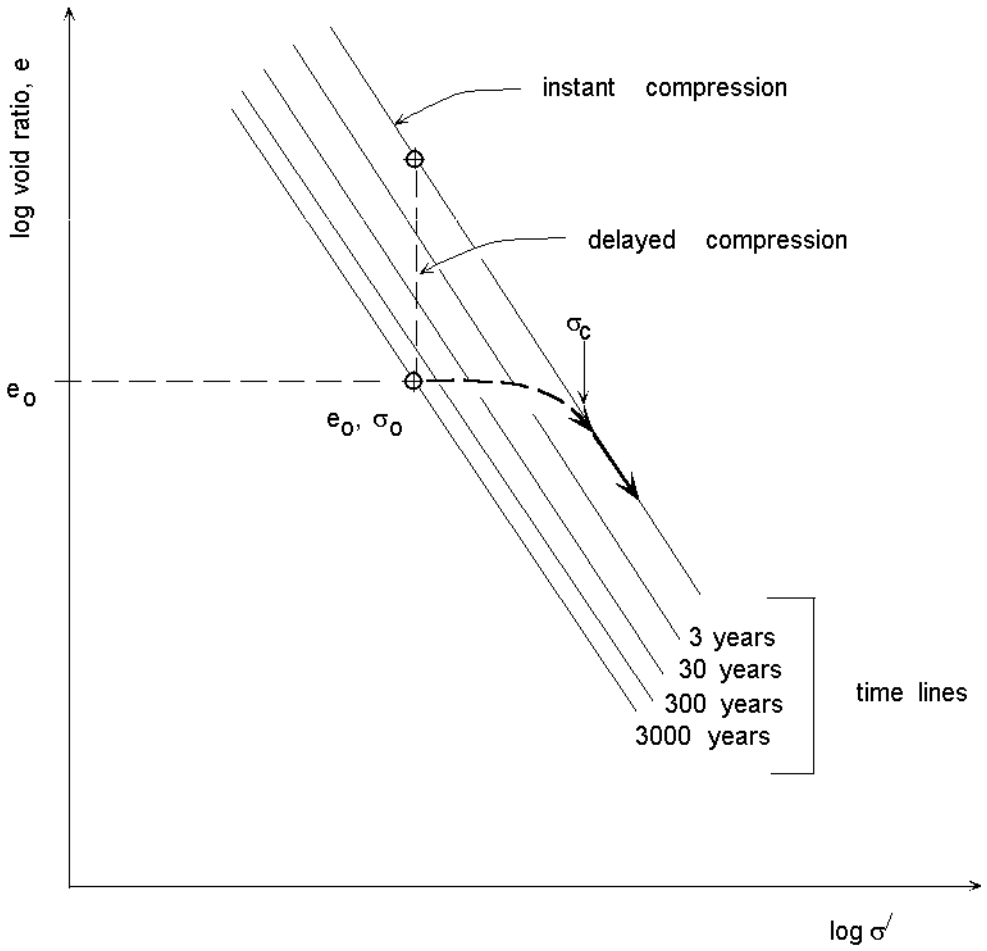

Figure 2.2: Bjerrum's time lines

2.1.3 Elasto-visco-plastic Theory

The elasto-visco-plastic approach to modeling clay behavior is based on Perzyna's visco-plastic over-stress theory (1963) and Olszak-Perzyna's (1966) theory of non-stationary flow surfaces. Much like elasto-plastic theory, these models are founded upon a physical interpretation of soil response. They incorporate the principal features of experimentally observed soil behavior such as dilatancy and soil hardening. For example, the hardening or softening function used in visco-

plastic formulations, describes the variation of the state parameters such as void ratio, strain rate, and effective stress that determine the mechanical response of the soil.

One-dimensional visco-plastic models are adaptations of Perzyna's elasto-visco-plastic theory (Perzyna, 1963) for multi-dimensional stress space. Perzyna's original model assumed that visco-plastic strains can occur only when the stress state reaches the yield surface, and that visco-plastic strains were not significant in the elastic zone below the yield surface (Figure 2.3a). The direction of the visco-plastic strain, $d\varepsilon_v^p$, which consists of instant plastic strain and creep strain, is specified by an associated flow rule. The visco-plastic strain rate depends on the amount that the effective stress exceeds the current static yield stress (the over-stress). In this model the yield surface does not change with time when the visco-plastic strains are held constant (i.e. there are no aging effects). In addition the visco-plastic strain rate is zero when the over-stress is zero.

Olszak-Perzyna (1966) subsequently modified Perzyna's visco-plastic theory to include the concept of a yield surface that changes in time due to creep behavior. The yield surface does not separate viscous from non-viscous behavior, but yielding (plastic strain) is always occurring and the yield surface represents a specific visco-plastic strain rate (Figure 2.3b). This theory was based on a time-dependent yield surface (visco-plastic potential function, F) of the form:

$$F = F\left(\sigma'_{ij}, \varepsilon_{ij}^{vp}, \beta\right) \qquad (2.1)$$

where: σ'_{ij} is the effective stress component *i* in the *j* direction; ε_{ij}^{vp} is visco-plastic strain and; β is a scalar parameter for time-dependent material behavior. Selection of the parameter β and specifying its physical nature distinguishes the various visco-plastic models. For 1-D consolidation, β has been defined either as a function of total or delayed strain rate or as a function of duration of loading.

Applying the associated flow rule:

$$\dot{\varepsilon}_{ij}^{vp} = \Lambda \frac{\partial F}{\partial \sigma'_{ij}} \qquad (2.2)$$

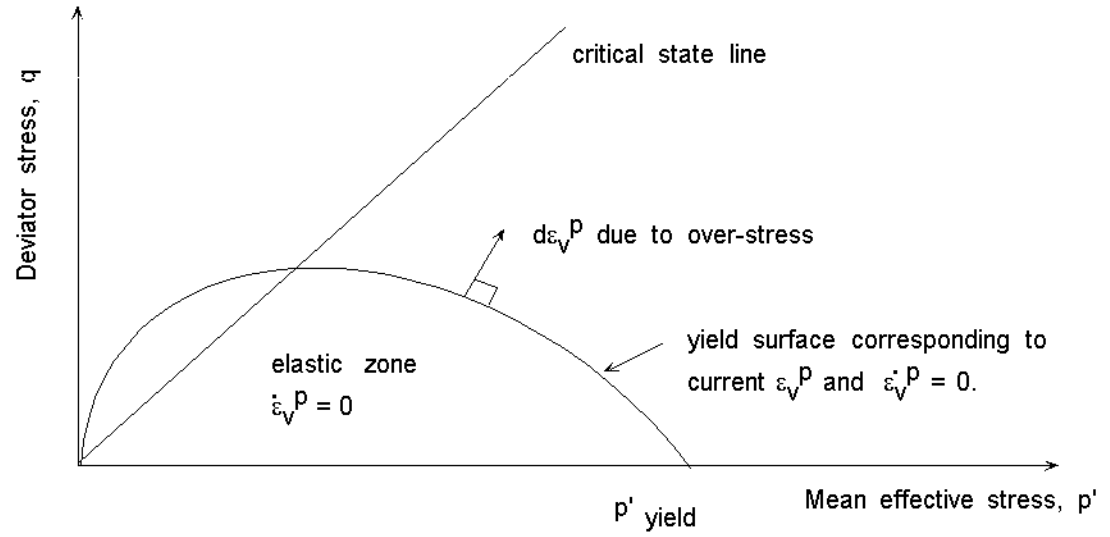

(a) Perzyna's visco-plastic theory

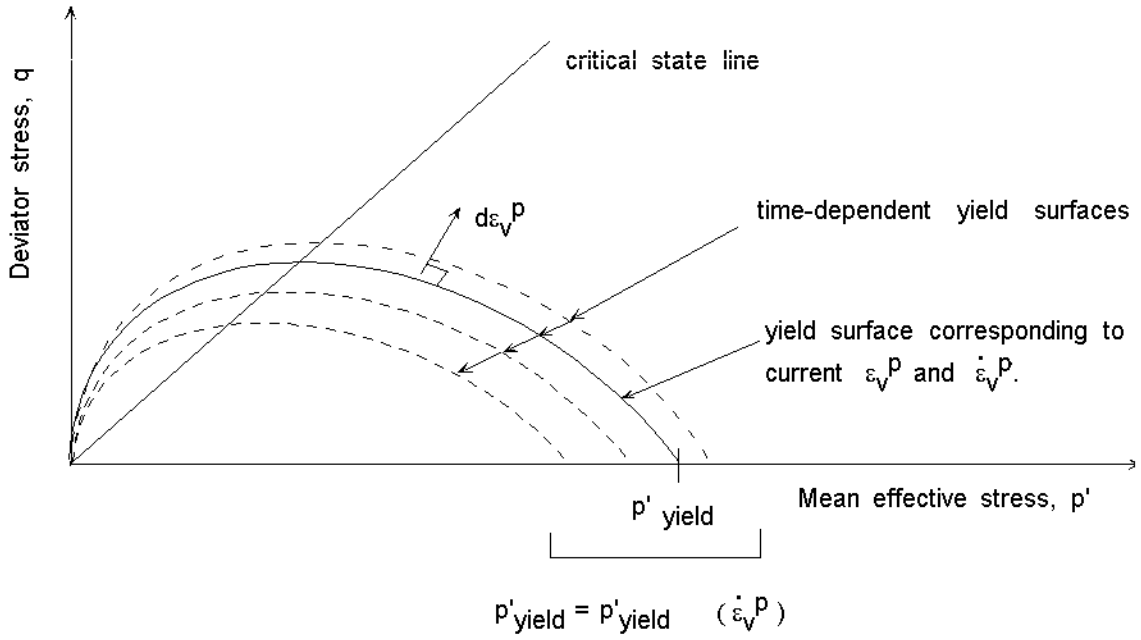

(b) Olszak-Perzyna visco-plastic theory

Figure 2.3: State boundaries for visco-plastic theories

where: Λ = time-dependent multiplier. Elastic compression occurs when F<0. When F=0, visco-plastic flow occurs. Therefore, visco-plastic flow occurs when:

$$\dot{F} = \frac{\partial F}{\partial \sigma'_{ij}} \dot{\sigma}'_{ij} + \frac{\partial F}{\partial \varepsilon^{vp}_{ij}} \dot{\varepsilon}^{vp}_{ij} + \frac{\partial F}{\partial \beta_{ij}} \dot{\beta}_{ij} = 0 \qquad (2.3)$$

By substituting Equation 2.2 in Equation 2.3, we can solve for Λ and develop solutions for multi-dimensional visco-plastic strain.

In one-dimensional space with only vertical effective stress and vertical strain, the incremental visco-plastic strain rate, $\dot{\varepsilon}^{vp}_{ij}$ is the volumetric and vertical visco-plastic strain rate, $\dot{\varepsilon}^{p}_{v}$. The volumetric strain rate is the "state variable" that controls hardening or change in the yield surface of the material. Therefore, we could use Bjerrum's time lines to express the volumetric strain increment, $d\varepsilon^{p}_{v}$, and by integration obtain the hardening function, ε^{p}_{v}, which is also the visco-plastic potential function, F.

Visco-plastic flow theory has been the basis of subsequent work by Oka (1981), Matsue and Abe (1982) and, Sekiguchi (1984), for multi-dimensional formulations of time-dependent soil behavior. Niemunis and Krieg (1996) developed a one-dimensional computer program by extending the Olszak-Perzyna theory such that viscous plastic strain (creep) can occur both inside and outside the reference yield surface. In essence, Niemunis and Krieg's model assumes that plastic strains occur at all stress levels, and that a continued elastic state does not exist.

2.2 MODEL SIMILARITIES AND DIFFERENCES

Regardless of the approach used to develop time-dependent constitutive models, all of the models are fundamentally elasto-visco-plastic (EVP) models and they therefore differ from conventional elasto-plastic models. An elasto-plastic model requires definition of elastic properties, a yield surface in stress space, a hardening rule, and a plastic potential. The yield surface separates elastic behavior from plastic behavior and, in a one-dimensional consolidation test, the yield stress

is defined by the preconsolidation pressure, σ'_p. The consistency condition requires that yielding or non-recoverable plastic compression occurs when the current effective stress is on the yield surface. The hardening rule describes how plastic deformations change the yield surface or preconsolidation pressure. The plastic potential describes the relative magnitude of volumetric strains and shear strains.

Unlike elasto-plastic models, visco-plastic models assume that the soil skeleton is always yielding or hardening because plastic creep strains are always occurring. In order to avoid confusion with the definition of yielding in elasto-plasticity theory, we shall use the term critical surface and critical stress in these time-dependent, visco-plastic models. The time-dependent models reviewed in this thesis differ in the way the hardening rule is specified. All of the models use a hardening rule that is fundamentally based on Bjerrum's time lines concept and they all include an instant elastic compression component that is generally defined by $C_{\varepsilon r}$ at over-consolidation ratios greater than about 2. However, the models differ in the method of decomposing the plastic strains and the method of expressing the corresponding constitutive relationships.

Two different methods of strain decomposition are used in the models. Both include an instant component of compression in series with a time-dependent creep component of compression:

$$d\varepsilon = f(\sigma') + g(t) \qquad (2.4)$$

where: f is the instant compression function and g is the creep compression function. In the first method of strain decomposition the instant compression function, f, is elastic and the strain components can be expressed in the following form:

$$d\varepsilon = d\varepsilon_i^e + d\varepsilon_v^p \qquad (2.5)$$

where: $d\varepsilon_i^e$ is the instant elastic strain increment and; $d\varepsilon_v^p$ is the visco-plastic strain. The second method of strain decomposition uses elastic and plastic components for the function, f, such that:

$$d\varepsilon = d\varepsilon_i^e + d\varepsilon_i^p + d\varepsilon_c^p \qquad (2.6)$$

where: $d\varepsilon_i^e$ is the instant elastic strain increment; $d\varepsilon_i^p$ is the instant plastic strain increment, which occurs when the effective stress is greater than or equal to the critical stress; and $d\varepsilon_c^p$ is the plastic

creep strain increment. By combining the plastic strain components in Equation 2.6, we arrive at the strain decomposition in Equation 2.5.

Figure 2.4 illustrates an oedometer test load increment from an initial effective overburden stress, σ'_o, located on the time line t_{aged} corresponding to the age of the deposit, to a final effective stress, σ'_f. In the first method of strain decomposition (equation 2.5) the strain increment from o to b′ defines the amount of instant elastic compression and the location of the time line at $t = 0^+$. The amount of visco-plastic strain depends on the duration of loading: path b′-b corresponds to end of primary t_{eop}, and path b′-c corresponds to t = 1 day. The second method of strain decomposition (equation 2.6) includes the same amount of instant elastic strain (path o-b′) and visco-plastic strain (path b′-b or path b′-c) but the visco-plastic strain includes both instant plastic and creep components. As we shall see, determining the magnitude of the creep component is required for models that define the time lines in terms of creep rate.

Time-dependent models used in computer programs for one-dimensional analysis of simultaneous creep and consolidation may be categorized according to the method of strain decomposition and the method of determining the creep rate. Three types of models have been identified. For convenience they are classified as Type I (instant time lines model), Type II (total strain rate model) and Type III (creep rate model).

2.3 COMPUTER PROGRAMS FOR ANALYSIS OF CLAY COMPRESSIBILITY

This section describes the evolution of computer programs for simultaneous analysis of one-dimensional consolidation and creep. The programs are grouped in subsections according to the time-dependent models they use (Type I, II, or III). Thirteen one-dimensional computer programs cited in published literature were reviewed. Letters requesting additional program

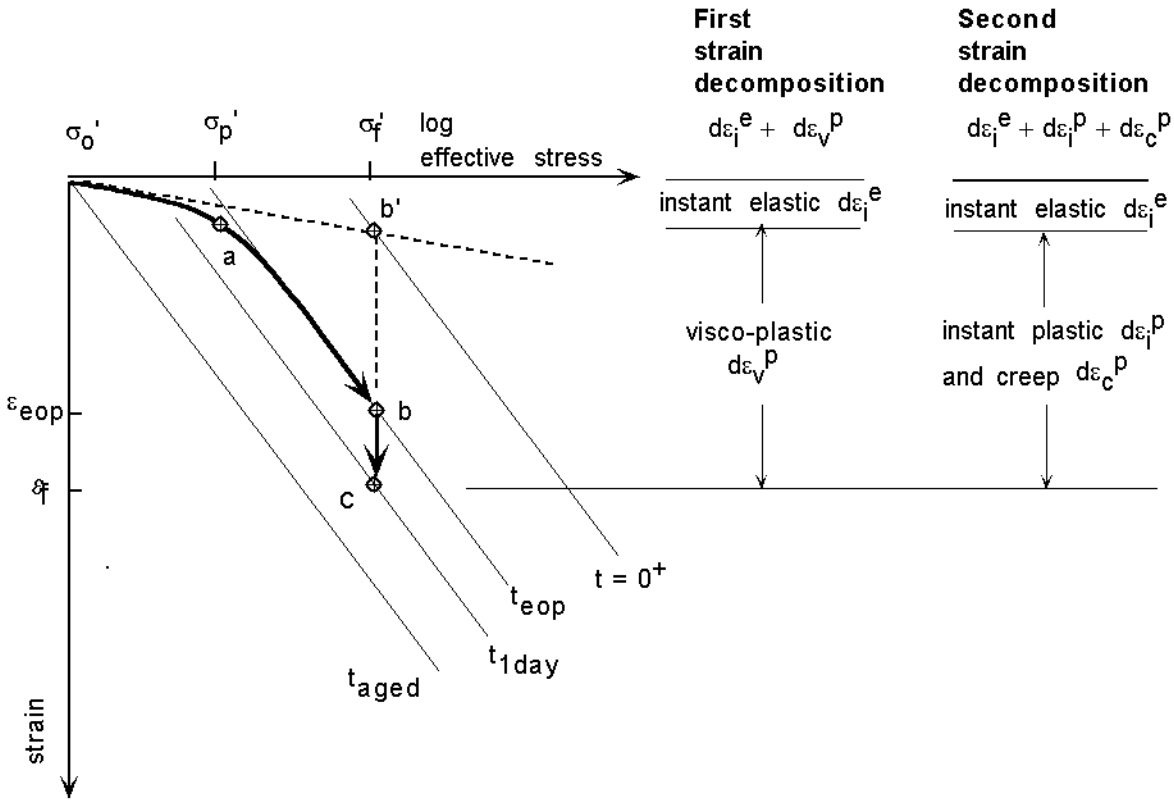

DEFINITIONS:

$t = 0+$	:	time line for instantaneous loading to σ_f'
t_{eop}	:	time to reach end of primary consolidation in oedometer test
t_{1day}	:	one day time line
t_{aged}	:	time line corresponding to the age of the soil deposit
σ_p'	:	preconsolidation pressure

STRESS-STRAIN PATHS:

o-a-b	:	oedometer test at the end of primary consolidation.
o-a-b-c	:	load increment from σ_o' to σ_f' after one day.

Figure 2.4: Strain decompositions

information were sent to each of the authors and five of the 13 authors responded. Table 2.1 is a descriptive summary of the constitutive model used in the computer programs. Table 2.2 summarizes the computational features of each computer program and its availability.

Table 2.1
Constitutive Models Used in 1-D Computer Programs

Reference	Model Type	Strain components	σ'_p depends on:	Stress-strain relationship	Creep rate depends on:
Garlanger (1972)	I	instant elastic, instant plastic, creep	effective stress, void ratio, load duration	linear ln e vs. ln p'	Distance to laboratory instant compression line.
Hawley and Borin (1973)	II	instant elastic, visco-plastic	effective stress, void ratio, total strain rate	linear e vs. ln p'	Included in total plastic strain rate determined by the distance to the ultimate and limit walls in e-log p' space. Assumes finite amount of creep strain.
Mesri and Rokhsar (1974)	I	instant elastic, instant plastic, creep	effective stress, void ratio, load duration	linear e vs. ln p'	Distance to lab end of primary compression line and the degree of consolidation, β and $\mathbf{C_{\alpha e}/C_x = constant}$ where: $C_x = C_c$ when $\sigma' \geq \sigma'_p$ and $C_x = C_r$ when $\sigma' < \sigma'_p$
Magnan et al (1979)	I	instant elastic, instant plastic, creep	effective stress, void ratio, load duration	linear e vs. ln p'	Distance to the one day reference time line and $\mathbf{C_{\alpha e}/C_x = constant}$ where: $C_x = C_c$ when $\sigma' \geq \sigma'_p$ and $C_x = C_r$ when $\sigma' < \sigma'_p$
Mesri and Choi (1985)	I	instant elastic, instant plastic, creep	effective stress, void ratio	linear e vs. ln p'	Distance to instant compression line and $\mathbf{C_{\alpha e}/C_x = constant}$ where: $C_x = C_r$ when $\sigma' \geq \sigma'_p$ and $C_x = C_c$ when $\sigma' < \sigma'_p$

Reference	Model Type	Strain components	σ'_p depends on:	Stress-strain relationship	Creep rate depends on:
Christie and Tonks (1985)	II	instant elastic, visco-plastic	effective stress, void ratio, total strain rate	linear ln e vs. ln p'	Included in total plastic strain rate determined by distance to the limit line which is determined for each effective stress increment in each time step increment.
Larsson (1986)	I	instant elastic instant plastic creep	effective stress, void ratio, load duration	ε vs. ln p'	Distance to the lab one day compression line and empirical relationships for C_α loading and unloading where: C_α depends on the maximum C_α, value near σ_p , and changes in C_α with strain.
Kabbaj et al (1986)	II	instant elastic, visco-plastic	effective stress, strain, strain rate	linear ε vs. ln p'	Included in total plastic strain rate lines determined from CRS lab tests.
Rajot (1992)	III	instant elastic, instant plastic, creep	effective stress, strain, creep rate	linear ε vs. ln p'	Distance from the reference compression line with known creep strain rate.
Niemunis and Krieg (1996)	II	instant elastic, visco-plastic	effective stress, strain, strain rate	linear ε vs. ln p'	Included in total plastic strain rate determined by the distance from reference CRS test compression line with known total visco-plastic strain rate.
Yin and Graham (1996)	II	instant elastic, visco-plastic	effective stress, strain, strain rate	linear ε vs. ln p'	Included in total plastic strain rate determined by the distance from reference compression line with known total strain rate.
den Haan (1996)	II	instant elastic, visco-plastic	effective stress, strain, strain rate	linear ln ε vs. ln p'	Included in total plastic strain rate determined by the distance from reference compression line with known total strain rate.

Table 2.2
Description of 1-D Computer Programs with Secondary Compression

Author	Reply Rec'd?	Program Name	Is it Available?	Program Capabilities					Data Input		
				Multiple Layers	Multiple drainage boundaries	Multiple load incre-ments	Initial pore pressure profile	Auto time step	Inter-active	Familiar soil para-meters*	Varying permea-bility
Garlanger (1972)	No	?	No	No	No	No	No	?	No	No	No
Hawley and Borin (1973)	Yes	?	No	?	?	Yes	Yes	Yes	?	No	Yes
Mesri and Rokhsar (1974)	No	?	No	No	Yes	No	No	?	No	Yes	Yes
Magnan et al (1979)	No	Conmult	?	Yes	Yes	Yes	Yes	Yes	No	Yes	Yes
Mesri and Choi (1985)	Yes	Illicon	No	Yes	Yes	Yes	Yes	?	No	Yes	Yes
Christie and Tonks (1985)	No	?	?	?	?	?	?	?	?	Yes	?
Larsson et al (1986)	Yes	Embankco	Yes	Yes	Yes	Yes	Yes	Yes	Yes	No	Yes
Kabbaj et al (1986)	No	?	?	?	?	Yes	?	?	?	No	Yes
Rajot (1992)	Yes	CS1	No	No	No	Yes	Yes	Yes	No	Yes	Yes
Fox et al (1994)	Yes	Fiber	No	No	?	?	?	?	No	No	?
den Haan (1996)	No	Consef	?	No	?	Yes	No	Yes	No	No	Yes
Niemunis and Krieg (1996)	Yes	?	?	No	?	Yes	?	?	?	No	Yes
Yin and Graham (1996)	Yes	?	No	No	No	No	Yes	Yes	Yes	No	No

* Compression coefficient, C_c; recompression coefficient, C_r; secondary compression coefficient, $C\alpha$; coefficient of consolidation, c_v; preconsolidation pressure, P_p

2.3.1 Type I: Instant Time Line Model

Type I programs use a model that assumes the strain decomposition defined by Equation 2.6, a linear relationship between strain and log effective stress, and time lines that are equally spaced with respect to the log of time. Bjerrum's time line concept (Figure 2.2) uses two different stress-strain relationships. Both are of the general form:

$$\varepsilon = f(\sigma'_v, t) \tag{2.7}$$

When the effective stress is equal to or greater than the preconsolidation stress, the strain increment includes instant elastic, instant plastic and creep strains:

$$d\varepsilon_i^e + d\varepsilon_i^p + d\varepsilon_c^p = \frac{C_{\varepsilon c}}{2.3}\left(\frac{d\sigma'}{\sigma'}\right) + \frac{C_\alpha}{2.3}\left(\frac{dt}{t}\right) \tag{2.8}$$

Otherwise the instant component of strain is elastic and the strain increment includes instant elastic and creep strains:

$$d\varepsilon_i^e + d\varepsilon_c^p = \frac{C_{\varepsilon r}}{2.3}\left(\frac{d\sigma'}{\sigma'}\right) + \frac{C_\alpha}{2.3}\left(\frac{dt}{t}\right) \tag{2.9}$$

Integrating equations 2.8 and 2.9:

$$\varepsilon = \frac{C_{\varepsilon c}}{2.3}\ln\left(\frac{\sigma'}{\sigma'_p}\right) + \frac{C_\alpha}{2.3}\ln\left(\frac{t}{t_{ref}}\right) \tag{2.10}$$

$$\varepsilon = \frac{C_{\varepsilon r}}{2.3}\ln\left(\frac{\sigma'}{\sigma'_o}\right) + \frac{C_\alpha}{2.3}\ln\left(\frac{t}{t_{ref}}\right) \tag{2.11}$$

where: σ'_o is the initial effective stress, σ'_p is the preconsolidation stress on the instant time line, t_{ref} is the reference time determined from end of primary consolidation in an oedometer test. On the instant time line, $t = t_{ref}$ and equation 2.10 reduces to an expression for the instant elastic plus instant plastic strain:

$$\varepsilon = \frac{C_{\varepsilon c}}{2.3}\ln\left(\frac{\sigma'}{\sigma'_p}\right) \tag{2.12}$$

After Bjerrum published his concept of time lines to illustrate the effect of geologic aging on building settlements, Garlanger (1972) used it to develop the first computer program that included creep effects (Figure 2.2). Bjerrum introduced the terms “instant compression” and “delayed compression” to describe the constitutive behavior of the soil. The instant time line was defined from laboratory stress-strain data at the end of primary consolidation. Although Bjerrum (1967) used the term “time lines”, he also indicated that each time line represented a delayed strain rate. Therefore, the “instant” time line was in fact associated with a reference delayed strain rate at the end of the laboratory oedometer test.

Garlanger (1972) expressed the creep strain rate at the current void ratio and effective stress as a function of distance to the instant compression line. The distance between time lines was based on a delayed compression relationship defined as: d(log e) / d(log t). He assumed that if the computed creep rate exceeded the pore pressure dissipation rate, the pore pressures would be held constant. In this model, instant plastic strains could only occur when the current effective stress and void ratio was located on the instant time line; otherwise, the instant strain was elastic.

Garlanger’s numerical computations proceeded as follows for each time step increment:

1. Use conventional consolidation theory to compute the change in pore pressure due to dissipation of excess pore pressure;
2. Compute the instant strain components resulting from the effective stress increase;
3. Compute the change in pore pressure due to the creep strain based on the creep rate at the current time;
4. Add the creep pore pressures to the changes in pore pressures computed in step one;
5. Return to step one and compute the change in the new excess pore pressure profile.

Garlanger's computer program was somewhat limited because the constitutive model was based upon duration of loading and the instant time line. The physical meaning of the instant time line was not clearly understood, although Garlanger provided some guidelines for selecting a time value for the "instant" time line based on the estimated age, effective stress, and void ratio of the deposit. In addition, the program could only analyze one load increment because the time duration of loading with respect to the instant time line had no meaning if a second load was applied during the consolidation process.

Subsequent researchers (Mesri and Rokhsar, 1974; Magnan et al, 1979; Mesri and Choi, 1985; Larsson, 1986) maintained the basic structure of Garlanger's model in their computer programs, but they used different assumptions regarding the creep component of the constitutive relationship during pore water pressure dissipation and the computation of the instant strain component.

Mesri and Rokhsar (1974) assumed that C_α/C_c is constant, and Larsson (1986) included provisions for specifying C_α as a function of strain. These researchers assumed that the conditions for instant plastic compression were not limited to the instant time line as assumed by Garlanger. They allowed instant plastic strain when the current effective stress exceeded the laboratory preconsolidation stress. They also accounted for changes in permeability and non-uniform strain profiles that previously limited the applicability of the Terzaghi consolidation theory and Garlanger's computer program.

Magnan et al. (1979) developed the concept of equivalent time that made it possible to simulate any loading sequence and made the program generally applicable to field situations with multiple layers and drainage boundaries. This was accomplished by formulating creep compression in

terms of an equivalent time, t*, illustrated in Figure 2.5. The equivalent time, t*, corresponds to a

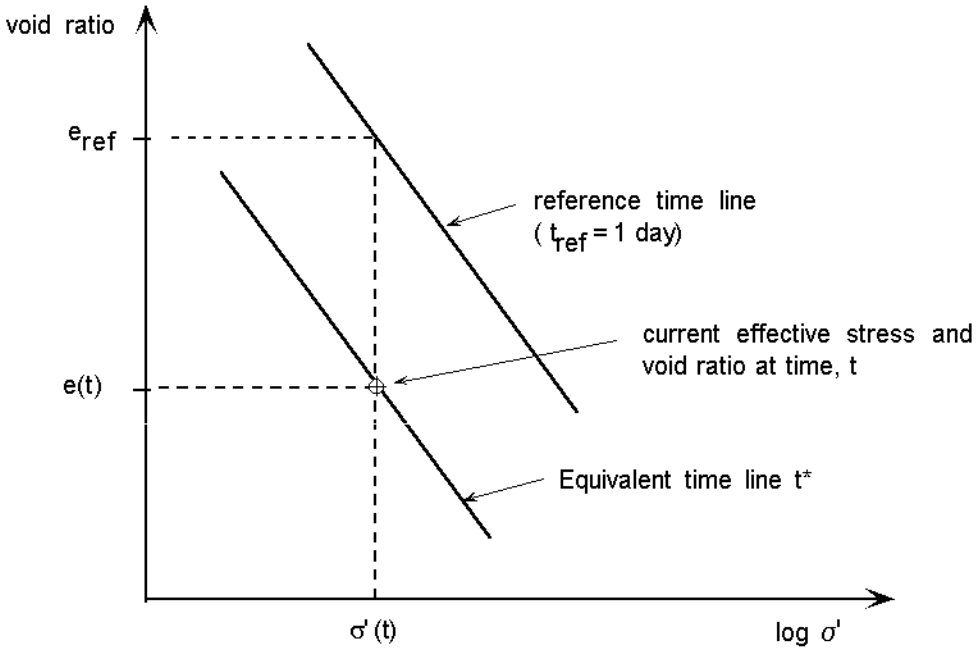

$$e_{ref} - e(t) = C_\alpha \log (t^* / t_{ref})$$

where: e_{ref} = void ratio on the reference time line for the current effective stress;
t = time since first load application;
t* = equivalent time. t*= t + constant

$$de / dt = (de / dt^*) \times (dt^* / dt) = C_\alpha / (2.3\, t^*)$$

$$t^* = C_\alpha / (2.3\, \dot{e})$$

Figure 2.5: Equivalent time used by Magnan et al. (1979)

time that would produce the void ratio, e(t), in the soil element if the creep strain rate, $\dot{\varepsilon}_c^p$ at the end of a standard one day oedometer test (t_{ref} = one day) was used as a reference value:

$$\dot{\varepsilon}_{c-ref}^{p} = \frac{C_\alpha}{2.3 \times t_{ref}} \qquad (2.13)$$

The creep rate at each time step increment was based on the equivalent time, t* which replaced time, t, in equations 2.8 and 2.9.

The computer program, Embankco, developed by Larsson et al (1986), is the only program based on this Type I (instant time line) model that was available for purchase. Embankco evolved from experiences at the Swedish Geotechnical Institute (SGI) with the computer program, Conmult. Conmult was originally developed at Laboratoire Central des Ponts et Chaussees (LCPC) in Paris, France under the direction Dr. Magnan and was subsequently modified at the University of Laval in Quebec, Canada and at SGI.

Mesri and Choi's (1985) computer program, Illicon, is based on the assumption that the strain at the end of primary consolidation is independent of the duration or rate of consolidation. This model predicts that a thick layer of clay would produce the same strain as a thin layer of clay, and that the preconsolidation pressure is independent of strain rate. Therefore, although their model includes the effects of creep behavior during consolidation, it is not a truly time-dependent model. The program can simulate subsurface profiles with multiple soil layers and a variety of loading conditions. It is not available for purchase or use by others.

2.3.2 Type II: Total Strain Rate Models

Researchers have developed computer programs based on Type II models using three approaches: (1) Olzsak-Perzyna's visco-plastic theory (Niemunis and Krieg, 1996); (2) Mathematical modeling the results of constant rate of strain oedometer tests (Kabbaj et al, 1985) and; (3) Extension of Garlanger's Type I model (Christie and Tonks, 1985; Yin and Graham, 1996; denHaan, 1996). Type II models use the strain decomposition given by Equation 2.5 and the assumption that each

parallel time line represents a locus of critical stresses for a particular total strain rate. The reference time line is determined by performing a constant rate of strain (CRS test) oedometer test at a particular rate of strain, $\dot{\varepsilon}_{ref}$. The locations of other time lines are determined based on the secondary compression coefficient, C_α.

To illustrate this model, consider a thin lab sample that is loaded in one increment from P'_o to P'_f in Figure 2.6. The load produces instant elastic strain defined by the slope of the recompression line from point o to b. The time line through point b is the "instantaneous" time line. The difference between the strains at c and b is the visco-plastic strain ε_v^p. In essence each effective stress increment stays on the critical surface ("yield surface" in Figure 2.3b) and the critical pressure, P'_c equals P'_f.

The visco-plastic strain increment between the reference time line and the instantaneous time line is used to calculate an equivalent time, t_e as follows:

$$d\varepsilon_v^p = \frac{C_\alpha}{2.3} \ln\left(\frac{t_e}{t_{ref}}\right) \tag{2.14}$$

then,

$$t_e = \frac{C_\alpha}{2.3 \cdot \dot{\varepsilon}_v^p} \tag{2.15}$$

No distinction is made between instant plastic or creep strains and the visco-plastic strain rate is assumed to be a scalar function of the total strain rate, $\dot{\varepsilon}$:

$$\dot{\varepsilon}_v^p = \dot{\varepsilon}\left(\frac{\lambda}{\lambda - \kappa}\right) \tag{2.16}$$

Substituting Equation 2.16 in 2.15,

$$t_e = \frac{C_\alpha}{2.3 \cdot \dot{\varepsilon}} \frac{\lambda}{(\lambda - \kappa)} \tag{2.17}$$

The strain increment is:

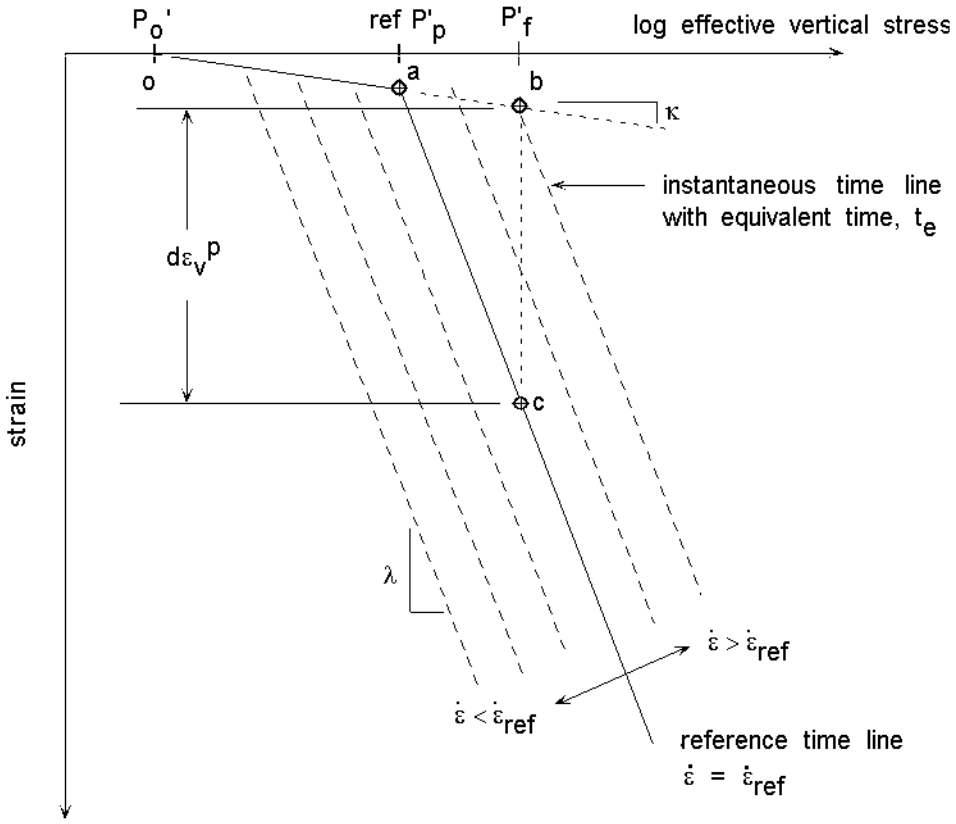

Figure 2.6: Type II total strain rate model

$$d\varepsilon_i^e + d\varepsilon_c^p = \frac{\kappa}{2.3}\left(\frac{d\sigma'}{\sigma'}\right) - \frac{C_\alpha}{2.3}\left(\frac{d\dot{\varepsilon}_v^p}{\dot{\varepsilon}_v^p}\right) \tag{2.18a}$$

or in terms of total strain rate by substituting Equation 2.16 in 2.18a:

$$d\varepsilon_i^e + d\varepsilon_c^p = \frac{\kappa}{2.3}\left(\frac{d\sigma'}{\sigma'}\right) - \frac{C_\alpha}{2.3}\left(\frac{d\dot{\varepsilon}}{\dot{\varepsilon}}\right) \tag{2.18b}$$

The negative sign before the last term on the right side of equation 2.18a and 2.18b results in a positive quantity because the strain rates, $\dot{\varepsilon}_v^p$ and $\dot{\varepsilon}$ are positive and the changes in strain rates, $d\dot{\varepsilon}_v^p$ and $d\dot{\varepsilon}$ are negative. Accordingly the form of the constitutive equation is:

$$\varepsilon = f(\sigma'_v, \dot{\varepsilon}) \qquad (2.19)$$

The strain decomposition in this type of model precludes the need for assuming a creep behavior during pore pressure dissipation because the time lines represent total strain rates. The amount of visco-plastic strain (hardening) is dependent upon the current effective stress, strain, and strain rate.

Computer programs for coupled pore water flow with Type II constitutive models reflect the fact that the consolidation process is governed by strain rate. Pore water dissipation due to an applied load imposes strain rates on each soil element and produces strain increments and corresponding effective stress increments for each time step. The new distribution of effective stresses produces new pore pressure distributions from which new strain rates arise. Conventional theories do not "impose strain rates" on each soil element but rather they impose strains that produce effective stress increments.

Hawley and Borin (1973) used this type of model when they proposed their "unified theory for the consolidation of clays." Their model required the definition of a "limit wall" and an ultimate line" in $e - \sigma' - \dot{e}$ space. The "limit wall" defines the e-σ' relationship when $\dot{e}$ equals infinity and the "ultimate line" defines the e-σ' relationship when $\dot{e}$ is zero. These relationships assume that there is a finite amount of creep strain and they are determined by fitting curves to laboratory oedometer test data. They used this model in a computer program that included changes in permeability during the consolidation process and could accommodate any loading schedule.

Christie and Tonks (1985) developed a model that clarified the meaning of Garlanger's instant time line. The time lines in their model were considered to include the total visco-plastic strain comprised of instant plastic and delayed compression. They proposed a "limit" line that was located above and parallel to Bjerrum's instant time line in log(e) vs. log(σ') space. This is the same as the "instantaneous" line used to describe model Type II (Figure 2.6) except that Christie and Tonks used a log(e) vs. log(σ') rather than an e vs. log(σ') relationship. The equivalent time

associated with this line provided a constitutive formulation based upon strain rate rather than time. The new limit line was calculated for each effective stress increment that occurred in each time step. This model was not limited to a single load.

DenHaan (1996) and Yin and Graham (1996) developed computer programs that were similar to the one developed by Christie and Tonks. Differences between the three programs include the relationship between void ratio and effective stress, large strain vs. small strain formulation, and the selection of the reference time line. Both DenHaan's and Yin and Graham's programs require unfamiliar input parameters whose values can be determined from standard oedometer tests.

In a different approach, Kabbaj et al developed a Type II model from constant rate of strain experimental data on normally consolidated sensitive clays. From their observations, they expressed the time-dependent behavior of the yield pressure, σ'_p, and strain, ε_v, as functions of total strain rate, $\dot{\varepsilon}_v$:

$$\sigma'_p = f(\dot{\varepsilon}_v) \qquad \text{and} \tag{2.20}$$

$$\varepsilon_v = g\left(\frac{\sigma'_v}{\sigma'_p(\dot{\varepsilon}_v)}\right) \tag{2.21}$$

Figure 2.7 illustrates these relationships for Batiscan clay (Kabbaj et al., 1986). The authors noted that the same constitutive model was derived by Oka (1981) who used a different approach based on Olszak-Perzyna's (1966) elasto-visco-plastic theory.

The authors cautioned against using this formulation for modeling field behavior until the rheologic model could be evaluated by long term observations of field behavior. The model was implemented in a finite difference program with an implicit time integration scheme. The computer program can analyze any time-dependent one-dimensional loading and unloading but it is limited to one material type throughout the profile.

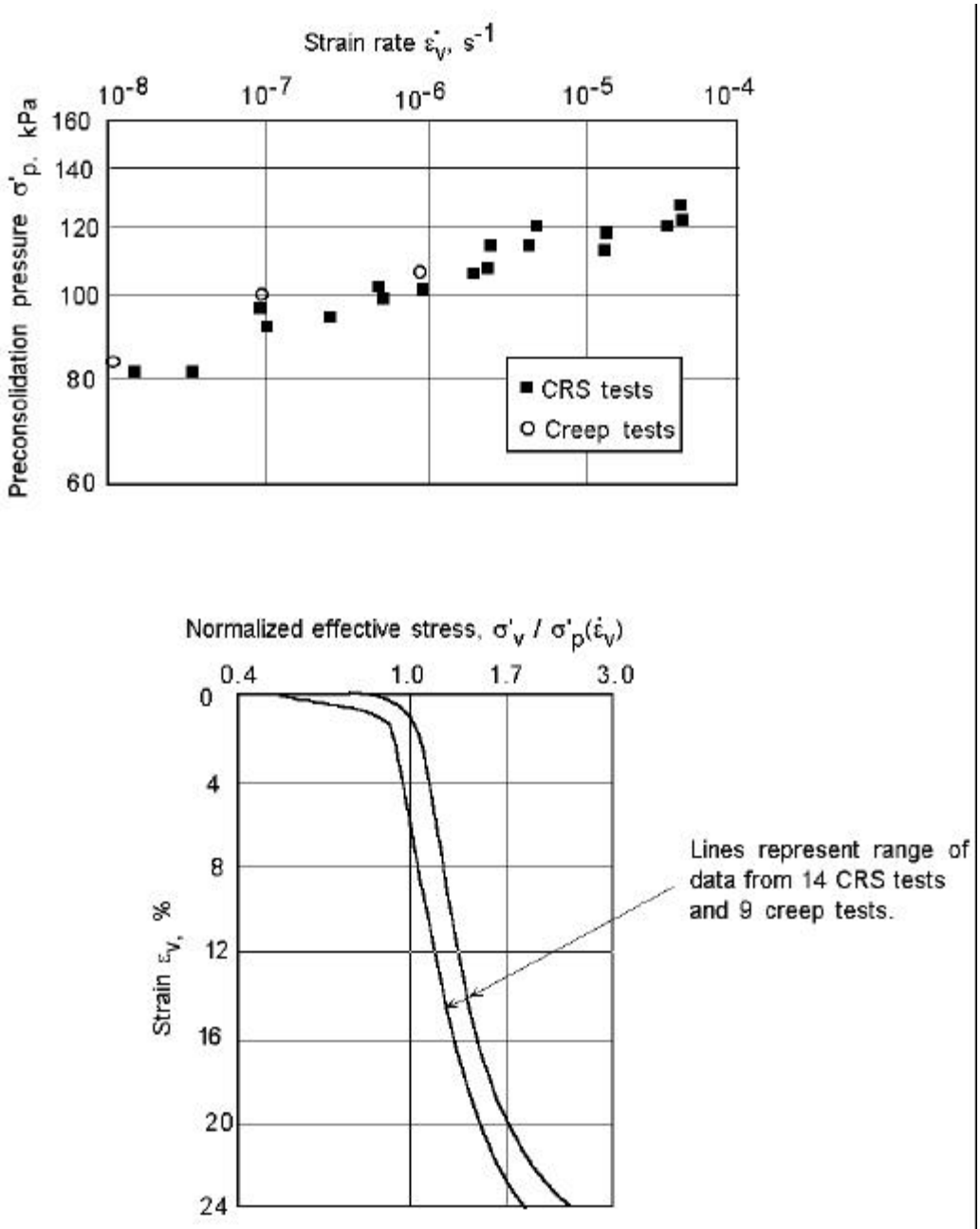

Figure 2.7: σ'_p - ε_v and σ_v / σ'_p - ε_v for Batiscan clay (from Leroueil et al. 1985)

Niemunis and Krieg (1996) extended Olszak-Perzyna's visco-plastic theory to develop their model which is illustrated in Figure 2.8. Although they use different terminology, the model is

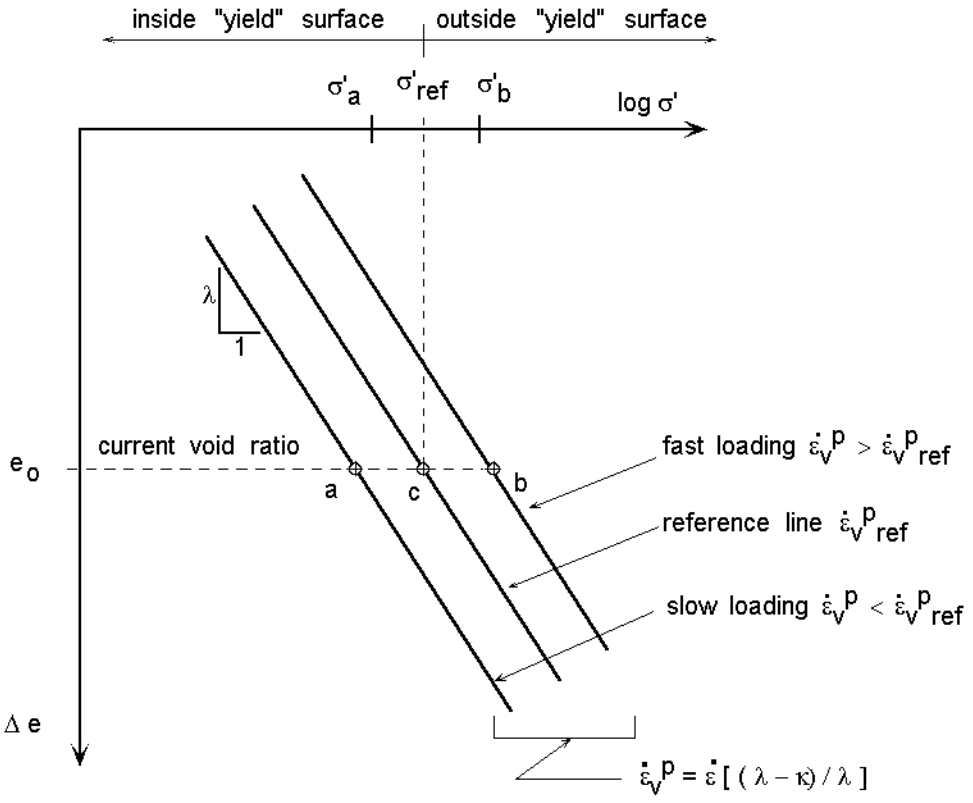

DEFINITIONS:

λ : slope of virgin compression line in constant rate of strain test.

κ : slope of recompression line.

$\dot{\varepsilon}_v^p{}_{ref}$: visco-plastic strain rate or the strain rate used for CRS test.

$\dot{\varepsilon}_v^p$: visco-plastic strain rate.

$\dot{\varepsilon}$: total strain rate.

Figure 2.8: Niemunis and Krieg visco-plastic model

essentially the same as model Type II illustrated in Figure 2.6. Niemunis and Krieg's model uses compression lines in e-log p' space that represent a particular visco-plastic strain rate. The critical stress σ'_{ref} that defines the "yield surface" in one-dimensional stress space is specified with respect to a reference line with a visco-plastic strain rate, $\dot{\varepsilon}^{p}_{v-ref}$. However, visco-plastic strains occur for each stress increment in e-log p' space and not only on the reference line. If at the current void ratio, e, the stress σ' equals σ'_{ref} (point c in Figure 2-8) then the visco-plastic strain is defined by $\dot{\varepsilon}^{p}_{v-ref}$. Otherwise if the current stress is inside the "yield surface" at point a, the viscous strain rate is slower than at the reference point c; outside the "yield surface" at point b, the viscous strain rate is faster than at point c. The authors define the over-consolidation ratio with respect to σ'_{ref} at the reference visco-plastic strain rate such that OCR = σ'_{ref}/σ'. This value can be smaller than unity.

At least one constant rate of strain (CRS) test is required to determine the values of the parameters involved in the model. The creep parameters may be evaluated from the results of two CRS tests or, alternatively, from the results of one CRS test and one incremental oedometer test in the normally consolidated range. The Niemunis and Krieg finite difference computer program can reproduce parallel time lines, and can simulate the effects of strain rate on yielding (preconsolidation pressure). The program can evaluate any loading history but it has not been developed for general application to multi-layer subsurface conditions, nor has it been coupled to pore water flow.

2.3.3 Type III: Creep Rate Models

These computer programs, like Type I computer programs, use models based on the strain decomposition given by equation 2.6. However, the "time lines" do not represent load durations; they represent loci of critical stresses at a particular creep rate.

When the current creep rate equals the creep rate of the time line passing through the current void ratio and effective stress, then the current effective stress equals the critical stress, P'_c. In this

condition the non-recoverable plastic strains consist of instant plastic strains and creep strains. The constitutive model for the elastic and plastic strains is given by:

$$d\varepsilon_i^e + d\varepsilon_i^p + d\varepsilon_c^p = \frac{C_{\varepsilon c}}{2.3}\left(\frac{d\sigma'}{\sigma'}\right) - \frac{C_\alpha}{2.3}\left(\frac{d\dot{\varepsilon}_c^p}{\dot{\varepsilon}_c^p}\right) \qquad (2.22)$$

When the current creep rate is less than the creep rate of the time line passing through the current void ratio and effective stress, the current effective stress does not equal the critical stress and plastic strains are due to creep only and the constitutive model for the elastic and plastic strains is given by:

$$d\varepsilon_i^e + d\varepsilon_c^p = \frac{C_{\varepsilon r}}{2.3}\left(\frac{d\sigma'}{\sigma'}\right) - \frac{C_\alpha}{2.3}\left(\frac{d\dot{\varepsilon}_c^p}{\dot{\varepsilon}_c^p}\right) \qquad (2.23)$$

The form of these constitutive equations is:

$$\varepsilon = f\left(\sigma'_v, \dot{\varepsilon}_c^p\right) \qquad (2.24)$$

The Type III model is illustrated in Figure 2.9 by the one dimensional effective stress-strain path for two soil elements in a clay layer. Each soil element in the field has a lab preconsolidation pressure, $P'_{p\text{-}lab}$ and an insitu effective overburden pressure of P'_o. Soil element "B" is located at a drainage boundary and it is assumed that the field creep rate, $\dot{\varepsilon}_c^p$, equals the lab creep rate at the end of primary consolidation. The critical pressure, P'_{cB}, corresponding to this strain rate equals $P'_{p\text{-}lab}$ and the effective stress-strain path in the field follows the laboratory stress-strain path o-b-c-d during time, t. Constitutive equation 2.23 defines path o-b and Equation 2.22 defines path b-c-d. Soil element "A" is located at the center of the clay layer and the field creep rate during loading is less than the lab creep rate at the end of primary consolidation. The critical pressure for this creep rate is P'_{cA} and the effective stress-strain path follows o-a-e for the same duration of loading as element "B". Constitutive equation 2.23 defines path o-a and equation 2.22 defines path a-e. The strain at the end of pore pressure dissipation is greater for element "A" (point e) than element "B" (point c).

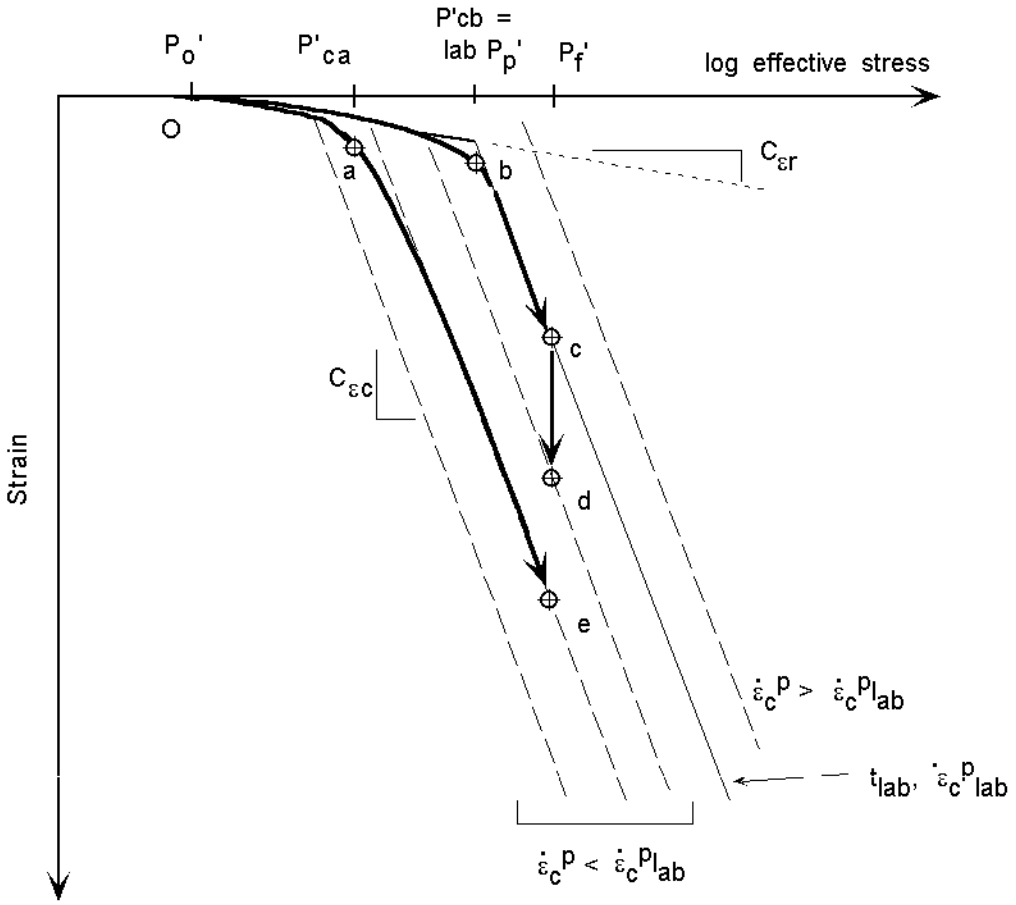

DEFINITIONS:

P'_o	: Initial effective overburden pressure
lab P'_p	: Lab determined preconsolidation pressure
P'_f	: Final effective stress
P'ca and P'cb	: Critical stresses for elements "A" and "B"

STRESS-STRAIN PATHS

Soil element "A" at the center of clay layer:

- o-a : Instant elastic and creep compression. P' < P'ca
- a-e : Instant elastic, instant plastic and creep compression. P' ≥ P'ca

Soil element "B" at the drainage boundary:

- o-b : Instant elastic and creep compression. P' < P'cb
- b-c : Instant elastic, instant plastic and creep compression. P' ≥ P'cb
- c-d : Creep compression (secondary compression).

Figure 2.9: Type III creep rate model

Rajot (1992) formulated a model of Type III using a physical model consisting of springs, dashpots and sliders (Figure 2.10). It differs from most Type II models in that hardening of the soil skeleton is dependent upon creep strain rate rather than total strain rate. The instant compression part of the model consists of an elastic spring and a plastic slider whose properties are dependent on the amount of plastic strain and the creep strain rate. The creep compression part of the model is an extended Kelvin element with a nonlinear spring in parallel with a non-linear dashpot. The fluidity of the dashpot depends on the total strain rate and a viscosity constant, η_o. The performance of the model is not very sensitive to the value of η_o, which has a set value.

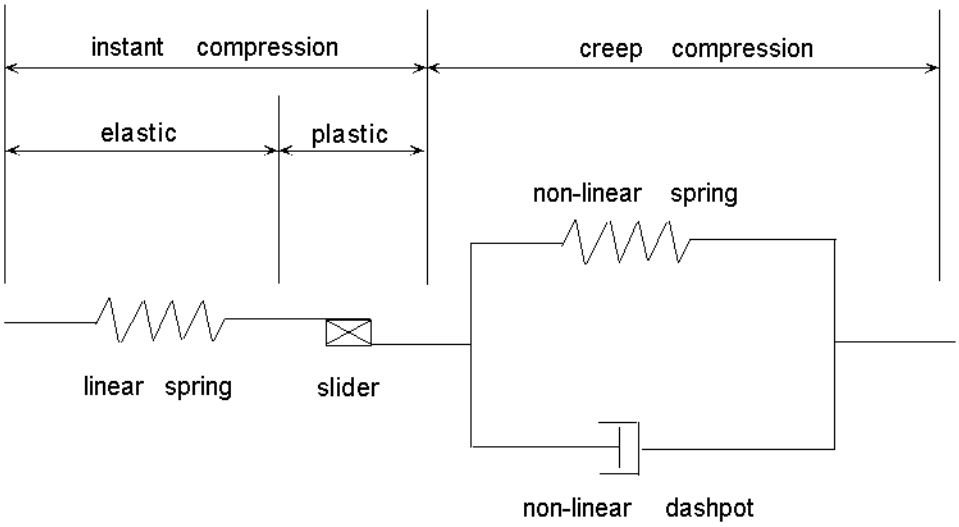

Figure 2.10: Rajot's rheologic mechanical model

Rajot assumed that each "time line" defined a set of values of effective stresses and plastic strains at which instant plastic compression would occur if the creep rate equaled the creep rate associated with the "time line". With this assumption, values of critical stress (the hardening

parameter) could be associated with the time lines, and conventional elasto-plasticity theory could be extended to include visco-plastic behavior. Also, in contrast to elasto-plastic theory, in which hardening only occurs on the yield surface, this model includes creep hardening when the effective stress is less than the critical stress, σ'_p. Therefore, Rajot's model incorporates a hardening rule at stresses less than σ'_p and a hardening rule when the effective stress is greater than σ'_p. A judging criteria is used to determine if the critical stress, σ'_p, corresponding to the current effective stress, strain, and creep strain rate is greater than or equal to the current effective stress, σ'.

Rajot implemented his model in his finite element program, CS1 (Rajot, 1992). It was capable of simulating Bjerrum's time lines. It predicted negligible secondary compression for over-consolidated clays and rates of secondary compression for normally consolidated clays that are consistent with laboratory test results (independent of load magnitude and duration). This is the only rheologic mechanical model that can predict changes in yield pressure due to changes in loading rates. The creep strain formulation based on creep rate rather than time permits analysis of loads applied at different times. The CS1 program has been further developed and renamed CONSOL97 as part of this research. The new program can analyze a subsurface profile with multiple soil layers and drainage boundaries. The user may specify any initial pore pressure distribution and any profile of change in vertical stress.

Rajot significantly improved the feasibility of using rheologic mechanical models for practical applications by developing the model using only standard oedometer test parameters: compression index, C_c; recompression index, C_r; coefficient of secondary compression, C_α; preconsolidation pressure, σ'_p; and consolidation coefficient, c_v. This program provides a consistent method for using all of the information obtained from laboratory consolidation tests to estimate rate and magnitude of field settlements.

2.4 COMPARISON OF COMPUTED RESULTS

Of the 13 computer programs in Table 2.2, only the program, Embankco, by Larsson et al. (1986), was available for use by others. The program by Magnan et al (1979) is a pre-cursor to the program Embankco by Larsson et al. (1986).

Embankco is a Type I program for analysis of road embankment settlements on soft fine-grained soil. The program incorporates the following assumptions: (1) The loads are of infinite length; (2) Vertical compression and flow of water during consolidation (one-dimensional consolidation); (3) The distribution of stress increase caused by the applied load can be calculated by the theory of elasticity and; (4) The compressibility characteristics of the soil can be evaluated from the results of oedometer tests. The program is easy to use because it has a Windows-based interface with on-line help for data input. The output consists of printed files or graphical files that can be displayed in the Windows environment or printed at the end of computation.

The model incorporates assumptions based on the behavior of Swedish soils. The creep model assumes that the coefficient of secondary compression is related to the void ratio of the soil. Soil compression produces a change in void ratio and C_α. The user must input the maximum coefficient of secondary compression, C_α, at the preconsolidation pressure, and $\beta_{\alpha s}$ where $\beta_{\alpha s} = \Delta C_\alpha / \Delta \varepsilon$. Embankco computes the creep parameter, α, at effective stresses larger than the preconsolidation pressure as: $\alpha = C_\alpha - (\beta_{\alpha s} \cdot \Delta \varepsilon)$. When the effective stress is less than 80% of the preconsolidation pressure (OCR ≥ 1.25), the model assumes that compression is only elastic. When the effective stress exceeds 80% of the preconsolidation pressure, the creep process begins and the creep parameter increases to a maximum value of C_α at the preconsolidation stress. The model also assumes that when compression rates exceed $C_\alpha \cdot 5 \cdot 10^{-6}$ per second, the laboratory oedometer test compression ratio, $C_{\varepsilon c}$, includes all the time effects.

The computer programs Embankco and CONSOL97 were used to simulate consolidation of a 9.6 meter thick layer of SanFrancisco Bay Mud. Figure 2.11 illustrates the subsurface profile, soil properties, initial and final effective stresses, and the variation of preconsolidation pressure with depth. The results of the analyses are summarized by plots of average strain vs log time (Figure 2.12) and by the variation of excess pore pressure with depth at various times during the consolidation process (Figure 2.13).

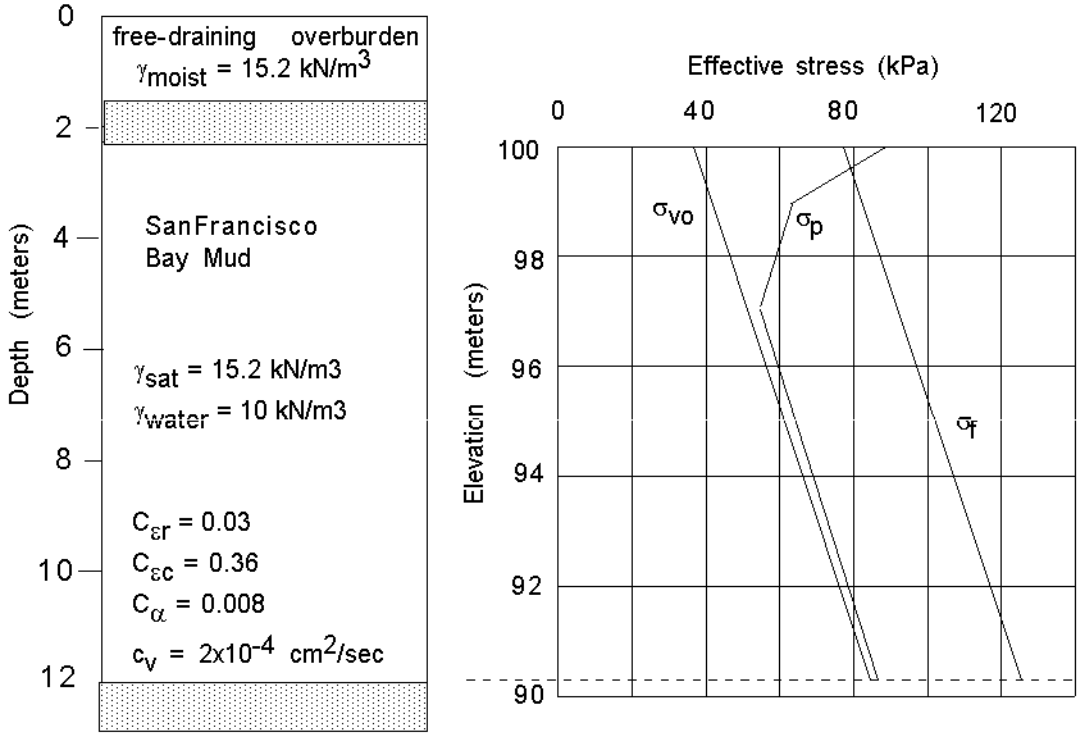

Depth (meters)	Elevation (meters)	σ_p' (kPa)	OCR
2.4	100	87.7	2.40
3.6	98.8	63	1.47
5.4	97.0	56	1.07
12.0	90.4	88	1.02

Figure 2.11: Field simulation for comparison of Embankco and Consol97

The results indicate that the Embankco program predicts larger settlement rates and about 45% more settlement over a period of 30,000 days (about 80 years) than CONSOL97 when creep effects are included in the analyses. In comparison to conventional methods of analysis, Embankco predicts about 60% more settlement whereas CONSOL97 predicts about 11% more settlement.

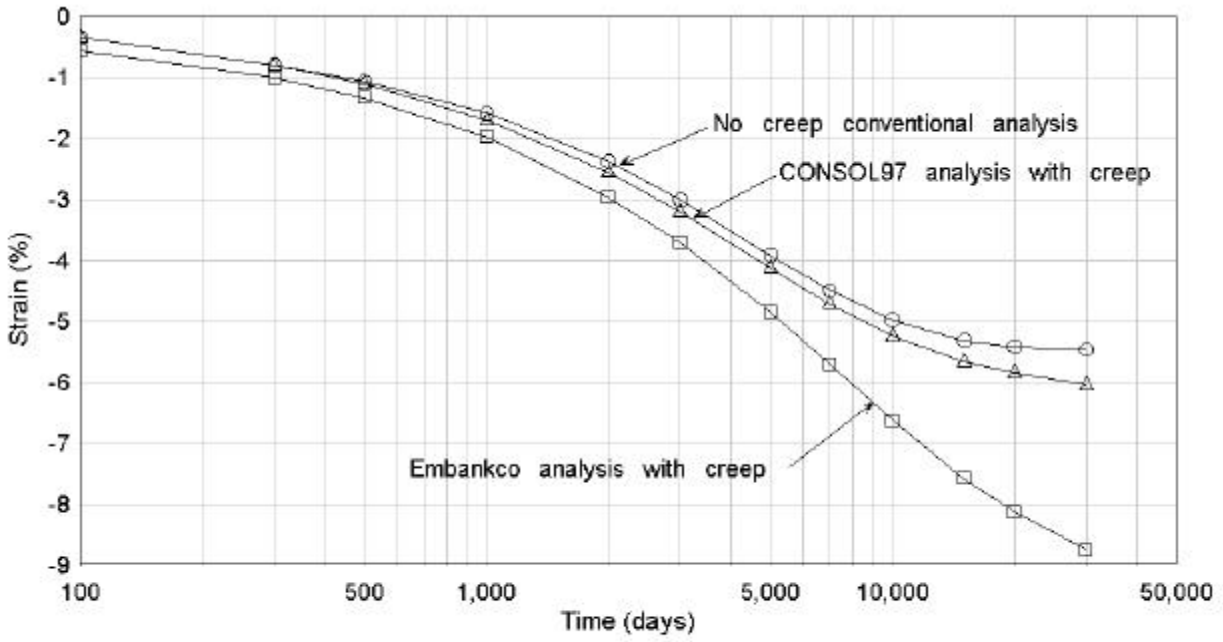

Figure 2.12: Comparison of strain-log time plots calculated using Embankco, Consol97 and conventional methods

The excess pore pressures in Figure 2.13 are substantially higher for Embankco than for CONSOL97. After 1000 days of consolidation, the effective stresses in the over-consolidated portion of the profile to about elevation 97.5 are less than about 80% of the preconsolidation pressure and the creep effects are not significant: Embankco and CONSOL97 predict nearly the same excess pore pressures in the top of the layer at this stage. However, below elevation 97, creep effects are significant because the effective stresses are close to the preconsolidation

pressure and the pore pressures predicted by Embankco are larger than those predicted by CONSOL97. The differences in excess pore pressures become more significant in all portions of the profile as the effective stresses exceed the laboratory preconsolidation stress.

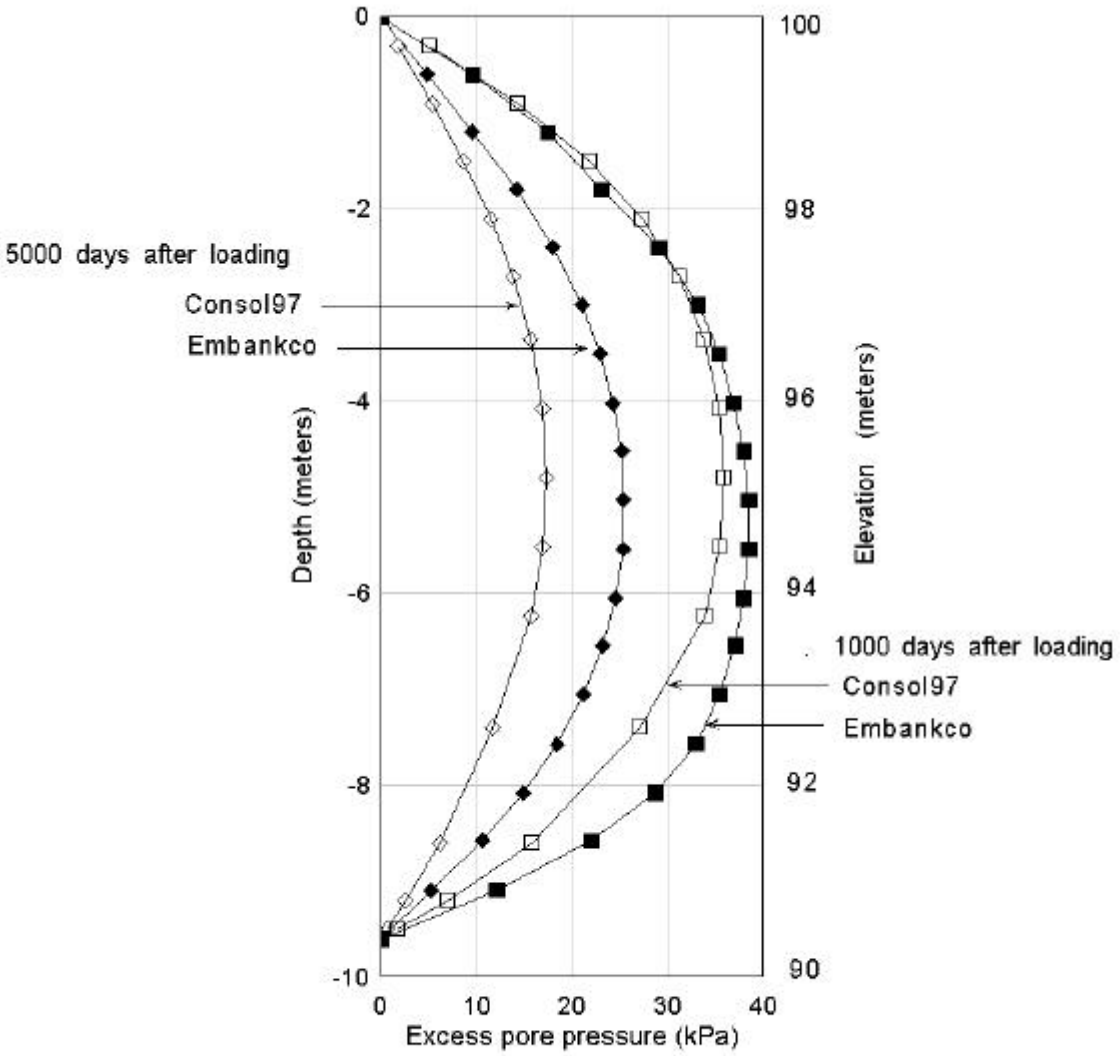

Figure 2.13: Comparison of excess pore pressures calculated using Embankco and Consol97

The slope dε/d(log t) of the ε vs. log time plot in Figure 2.12 is larger than the input value of C_α=0.008 as a result of the additional instant compression still on-going in the Embankco analysis. The slope of the ε vs. log time plot for the CONSOL97 analysis is close to the input value of C_α because instant compression is essentially complete.

The Embankco and CONSOL97 results are shown in Figure 2.14 with the strain-log time results of an "equivalent thin sample" for comparison to Hypotheses A and B (Jamiolkowski et al. 1985). The "equivalent thin sample" curve represents rapid consolidation of the 9.6 meter layer such that the time to end of primary consolidation is the same as a 2.5 cm doubly drained specimen. An extension of this curve represents the maximum strain for a thick layer conforming to Hypothesis B (refer to Figure 2.1). The results indicate that the Embankco curve converges to the "equivalent thin sample" curve as predicted by Hypothesis B, and that the CONSOL97 curve is between Hypothesis A and B.

The creep strain component computed by Embankco is much larger than CONSOL97 because the Embankco model assumes that the strain includes instant elastic, instant plastic and creep components when the effective stress is greater than 80% of the laboratory preconsolidation stress. This does not appear to be a reasonable assumption, however, because the instant plastic compression component, which is characterized by the slope ($C_{\varepsilon c}$) of the laboratory instant time line, already includes a creep component. The addition of pore pressures generated by creep at each time step is a key feature of the program, which appears to overestimate the amount of creep compression. After 10,000 days (about 27 years) Embankco predicts about 30% more settlement than CONSOL97. This difference is of practical significance. The amounts of creep calculated in the Embankco analysis appear to be excessive, and the resulting long-term settlements larger than are reasonable.

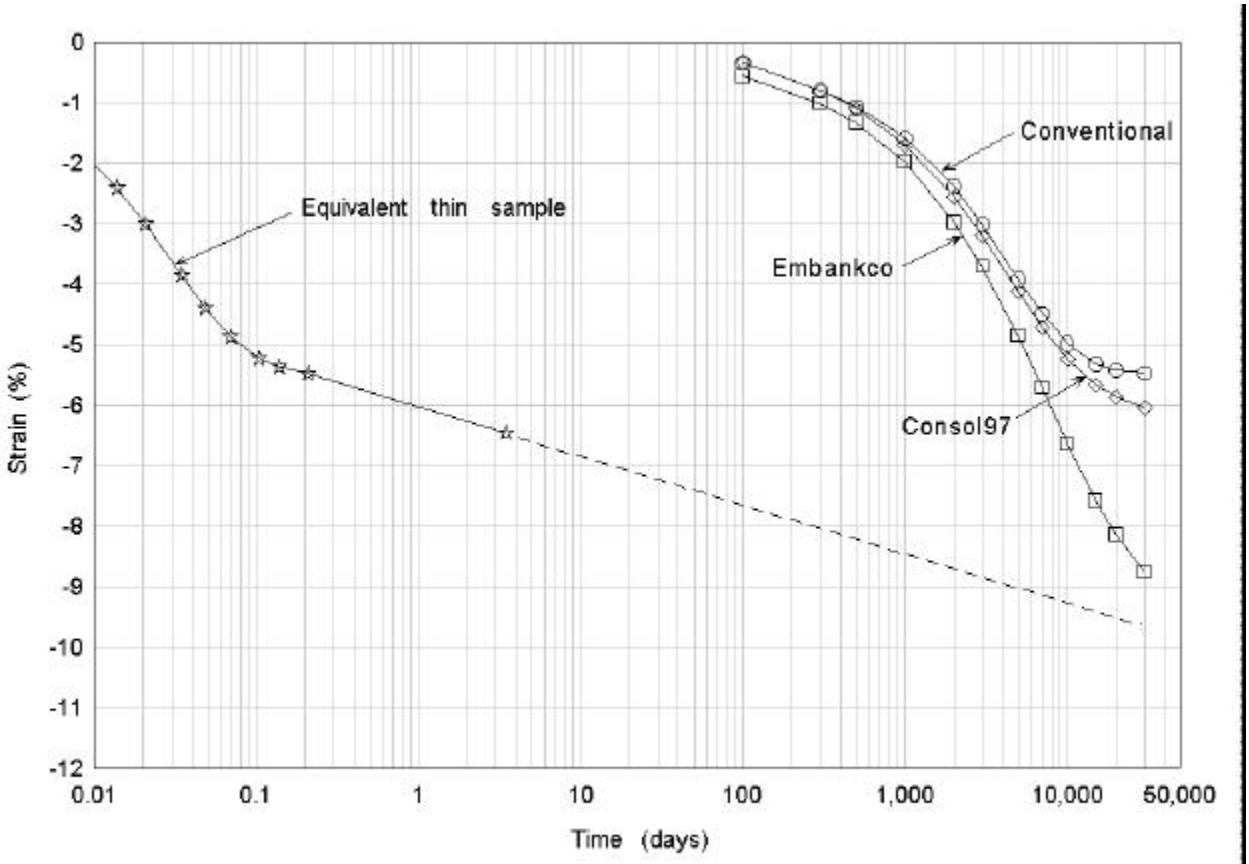

Figure 2.14: Embankco and Consol97 results compared to an equivalent thin sample

2.5 SUMMARY AND CONCLUSIONS

Significant work has been done in recent years to develop theories and computer programs for time-dependent analysis of one dimensional consolidation problems. Table 2.1 summarizes the models and the computer programs. Much of the research has focused on improvement of Garlanger's model that originated from Bjerrum's concept of time lines and in which hardening was related to the duration of loading. Models in which hardening is related to the plastic or total

strain rates have also been developed. Only one computer program (CS1) has been developed based on a rheologic mechanical model which relates hardening to creep rate.

A suitable constitutive model for time-dependent analysis of one-dimensional consolidation should simulate the following behavior:

- Secondary compression;
- Coefficients of secondary compression that are constant in the normally consolidated range and that decrease with over-consolidation ratio;
- Increases in preconsolidation pressure due to creep during sustained loading (aging);
- Critical stresses ("yield stresses") that depend on creep rate, effective stress, and total strain;
- Creep compression during reloading;
- Multiple loading.

In addition a computer program for soil consolidation should have the capability of simulating field subsurface conditions with multiple soil layers and internal and external drainage boundaries. Specification of the soil model parameters should preferably include familiar properties determined from standard oedometer test procedures. Table 2.2 summarizes the capabilities of computer programs for simultaneous analysis of one-dimensional consolidation and creep.

Many of the models formulated creep compression using time as the independent variable. These "Type I instant time line" models can simulate the effects of creep on the preconsolidation pressure, but they can only accommodate a single load increment (Garlanger, 1972; Mesri & Rokhsar, 1974). Other models use equivalent time formulations that are more flexible and accommodate any loading schedule (Magnan, Larsson). However, the time lines in Bjerrum's model represent instant plastic compression at specific creep rates. Therefore, these models are incomplete because they do not simulate instant plastic compression at void ratios and effective stresses below the reference time line. These programs produce excessive creep rates during pore pressure dissipation.

The "Type II total strain rate" models (Christie and Tonks, 1985; den Haan, 1996; Yin and Graham, 1996; Niemunis and Krieg, 1996) have been incorporated in computer programs that include instant plastic compression at stress states that are not on the instant time line. In essence the instant time line and therefore, the critical stresses ("yield stresses") are adjusted based on the current strain rate. These models can simulate the necessary time-dependent behavior but a general purpose computer program based on these theories is not available. Computer programs by Den Haan (1996) and Yin and Graham (1996) cannot evaluate multiple soil layers and the input data they use involve unfamiliar quantities determined by curve fitting to standard oedometer test data.

CONSOL97, based on Rajot's "Type III creep rate" model, is the only computer program that can simulate the required time-dependent behavior for any loading schedule and subsurface profile, and that uses familiar soil parameters. Because the model was specifically formulated with the reference time line and soil parameters based on standard laboratory testing methods, the data input for the program uses familiar soil properties (C_c , C_r , σ'_p , C_α , and c_v).

Only one other computer program, Embankco, was available for examination during this study. It uses a Type I instant time line model for analysis of embankment loading and includes a user friendly interface for data input, and for output. The model is empirically based on experiences with somewhat sensitive Swedish soils, and uses familiar input parameters derived from standard oedometer tests. A comparison of Embankco and CONSOL97 computer analysis of a 9.6 meter thick layer of SanFrancisco Bay mud indicates that Embankco predicts more clay compression than CONSOL97 at all times during the consolidation process. When excess pore pressures in the CONSOL97 analysis are less than 2% of the applied load, Embankco predicts about 50% more clay compression than CONSOL97 and residual excess pore pressures that are about 7% of the initial values.

Chapter 3

RAJOT'S ONE-DIMENSIONAL THEORY FOR TIME-DEPENDENT COMPRESSION OF CLAY

3.1 DESCRIPTION OF RAJOT'S MODEL

As explained in Chapter 2, Rajot's elasto-visco-plastic model of clay compressibility is a Type III creep rate model (see section 2.2.3) that can simulate observed phenomena of time lines, secondary compression and stress relaxation. Rajot used a mechanism consisting of two springs, a dashpot and a slider as shown in Figure 3.1 to formulate the time-dependent constitutive relationships. The instant component of compression is elasto-plastic, with an elastic spring and a rigid-plastic slider. Deformations of the spring correspond to recoverable volume changes ($d\varepsilon_i^e$). Deformations of the slider correspond to instant non-recoverable volume changes ($d\varepsilon_i^p$) that occur when the effective stress exceeds the critical effective stress. The non-recoverable creep component of compression ($d\varepsilon_c^p$) is represented by the extended Kelvin element shown on the right side of Figure 3.1. Deformation of this part of the model corresponds to time-dependent non-recoverable volume changes (creep). Since the extended Kelvin element is placed in series with the instant spring and slider, the model produces simultaneous plastic creep deformations and instant compression. As is the case with all elasto-visco-plastic models, the soil skeleton is always yielding due to any increase in loading.

Rajot extended Bjerrum's time lines theory to include: instant plastic compression of the soil skeleton when the current effective stress and void ratio is not on Bjerrum's "instant time line" and; creep compression during recompression loading. The new model developed by Rajot involved five assumptions: (1) a strain decomposition that includes instant elastic, instant plastic and creep

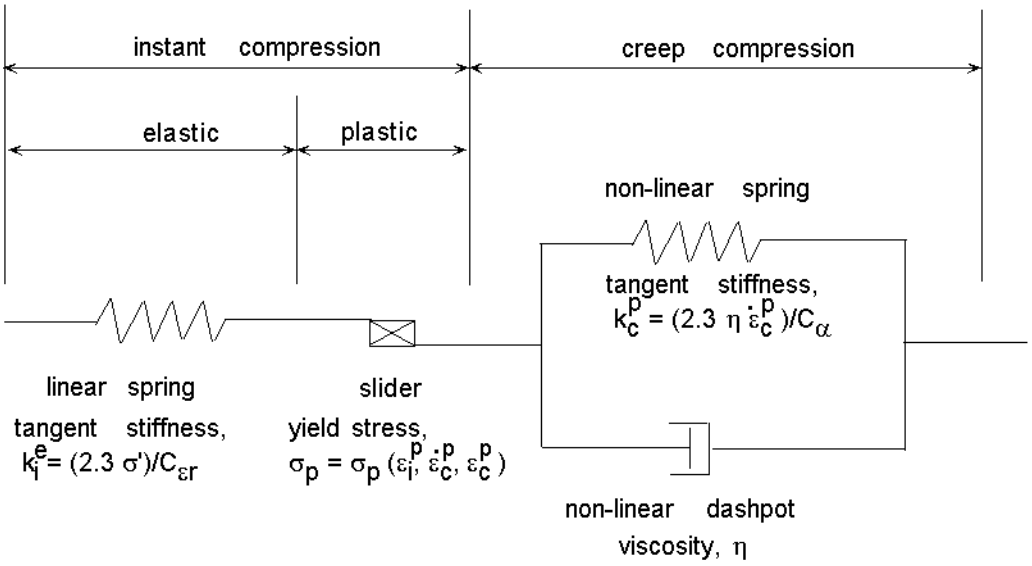

Figure 3.1: Rajot's Rheologic Mechanical Model

compression; (2) instant plastic compression occurs when the current effective stress equals the critical stress; (3) changes in the value of the critical stress are related to the amount of plastic strain (instant or creep) and the creep strain rate; (4) Bjerrum's time lines define a set of critical stress loci corresponding to different values of creep strain rate; (5) the time lines are equally spaced with respect to the log of time.

These assumptions produced a model in which the critical stress and creep are related. The physical model in Figure 3.1 illustrates this relationship. Although the slider is included in the instant compression component of the model, its properties are also dependent on the amount of creep and the creep rate from the creep compression component of the model. The preconsolidation stress that is determined from a laboratory oedometer test is a critical stress associated with the creep rate that occurs during the test. For other loading conditions and layer thicknesses, that produce creep rates that are not equal to lab creep rates, the critical stress is not equal to the lab preconsolidation stress.

3.1.1 Time-Dependent Yielding and Creep

Analyses with Rajot's model require continual computations of instant elastic deformation, instant plastic deformation, creep deformation and creep strain rate. The current creep strain rate is compared to the creep strain rate for the time line (the critical stress locus) at the current strain and effective stress to determine if the current effective stress equals the critical stress. Instant plastic compression occurs when the current effective stress equals the critical stress. The instant component of compression is elastic when the current effective stress is less than the critical stress.

Figure 3.2 illustrates the stress-strain path and critical stress determination for an over-consolidated soil sample loaded from an initial effective stress σ'_A to a final effective stress, σ'_c. The effective stress changes from point A to B produce creep rates that are faster than the creep rate on the time lines that are crossed by path AB. Therefore, for loading from point A to B, the critical stress, σ'_{px}, is always larger than the current effective stress, σ'_x . From point B to C, the current creep rate equals the creep rate of the time line on which BC lies. Because the stress-strain path follows the time line, the critical stress, σ'_p, is always equal to the current effective stress along path AB.

To derive the relationship between critical stress and creep, the system of time-lines was defined with respect to a reference line corresponding to a reference value of creep compression rate ($\dot{\varepsilon}^p_{c-ref}$). The creep strain rate observed after 24 hours in a conventional oedometer test is used as the reference creep strain rate, and the corresponding stress-strain curve (strain-log effective stress curve) is the reference time line. Other time-lines, corresponding to other load durations, and other values of creep compression rate ($\dot{\varepsilon}^p_c$) are located above and below the reference line. The distance from the reference time line to another ($\Delta\varepsilon$) is determined by the value of the creep strain rate on that time line ($\dot{\varepsilon}^p_c$):

$$\Delta\varepsilon = \varepsilon^p_c - \varepsilon^p_{c-ref} = C_\alpha \log\left(\frac{\dot{\varepsilon}^p_{c-ref}}{\dot{\varepsilon}^p_c}\right) \qquad (3.1)$$

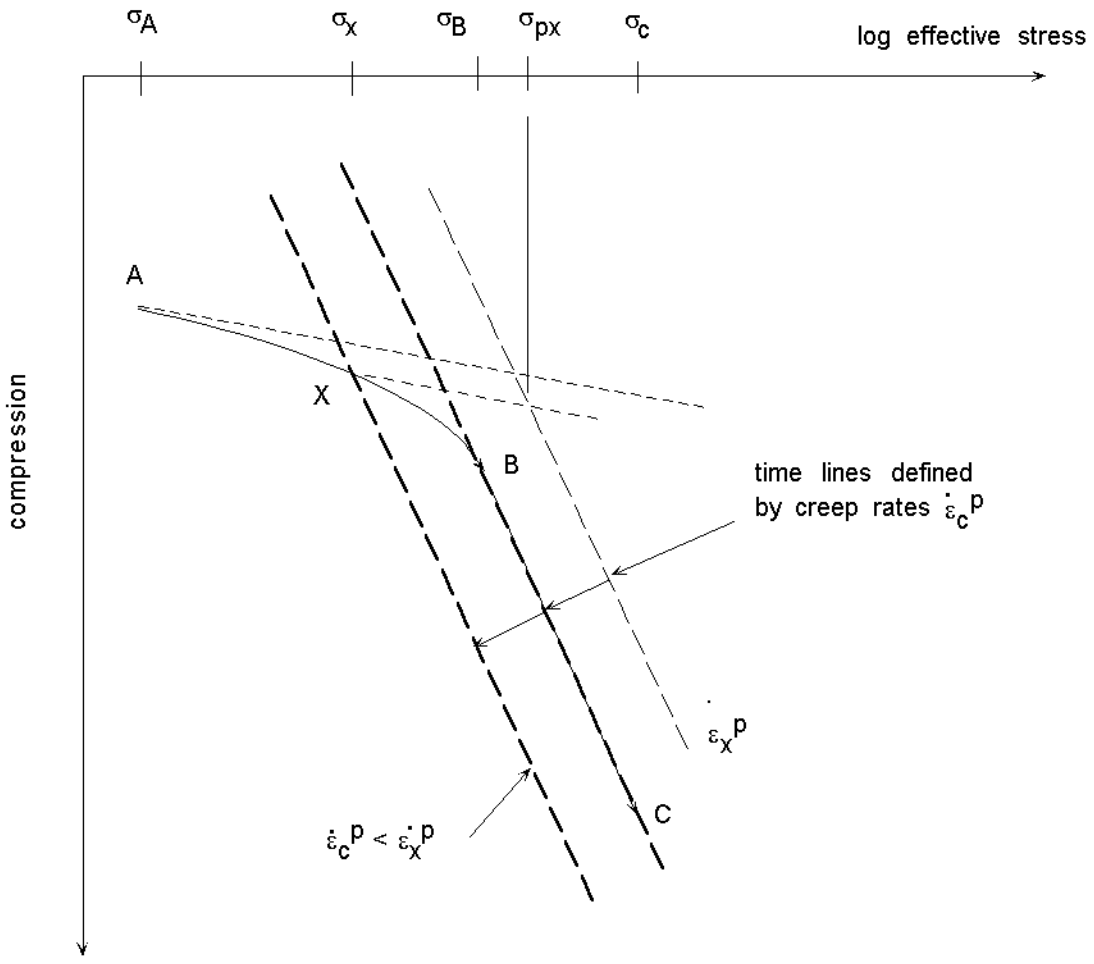

Figure 3.2: Critical stress determination for Rajot's model

This equation models a linear relationship between compression and log of time as implied by the concept of time lines that are equally spaced with respect to the log of time. The value of C_α used in this equation is the value in the normally consolidated range.

With these assumptions, the value of the critical effective stress at which instant plastic compression occurs (the preconsolidation pressure, σ'_p) may be expressed as follows for any amount of non-recoverable strain $\left(\varepsilon_i^p + \varepsilon_c^p\right)$ and any creep strain rate, $\dot{\varepsilon}_c^p$:

$$\sigma'_p = \sigma'^{(o)}_{pref} \times \exp\left\{\frac{2.3}{C\varepsilon c - C\varepsilon r}\left[\left(\varepsilon_i^p + \varepsilon_c^p\right) - \left(\varepsilon_i^{p(o)} + \varepsilon_c^{p(o)}\right)\right]\right\} \times \left(\frac{\dot{\varepsilon}_c^p}{\dot{\varepsilon}_{c-ref}^p}\right)^{\frac{C\alpha}{C\varepsilon c - C\varepsilon r}} \qquad (3.2)$$

where:

$\sigma_{pref}^{(o)}$ is the preconsolidation pressure for the reference time line and rate of creep compression. Superscript "(o)" refers to initial values. For a 24 hour reference line as used here, this is the conventional preconsolidation pressure.

ε_i^p is the instant plastic strain.

ε_c is the creep strain

$C_{\varepsilon r}$ is the slope of the recompression curve on a strain-log σ' plot. This is equal to the slope of σ' plot.

$C_{\varepsilon c}$ is the slope of the time lines on a strain-log σ' plot. This is equal to the slope of the conventional virgin compression curve plotted on a strain-log σ plot.

The relationship between yielding and creep compression during pore water pressure dissipation due to a load increment from σ'_o to σ_d is illustrated in Figure 3.3:

Point O to B: The rate of creep compression is higher than the creep strain rate for the time lines crossed, and thus is too high to allow instant plastic compression under the current effective stress. Compression is due to instant elastic strain and creep strain. Hardening occurs due to the creep strain and the one day reference preconsolidation pressure increases from σ'_{Po} σ'_{PB}. The effective stress-strain relationship for the model in this condition is:

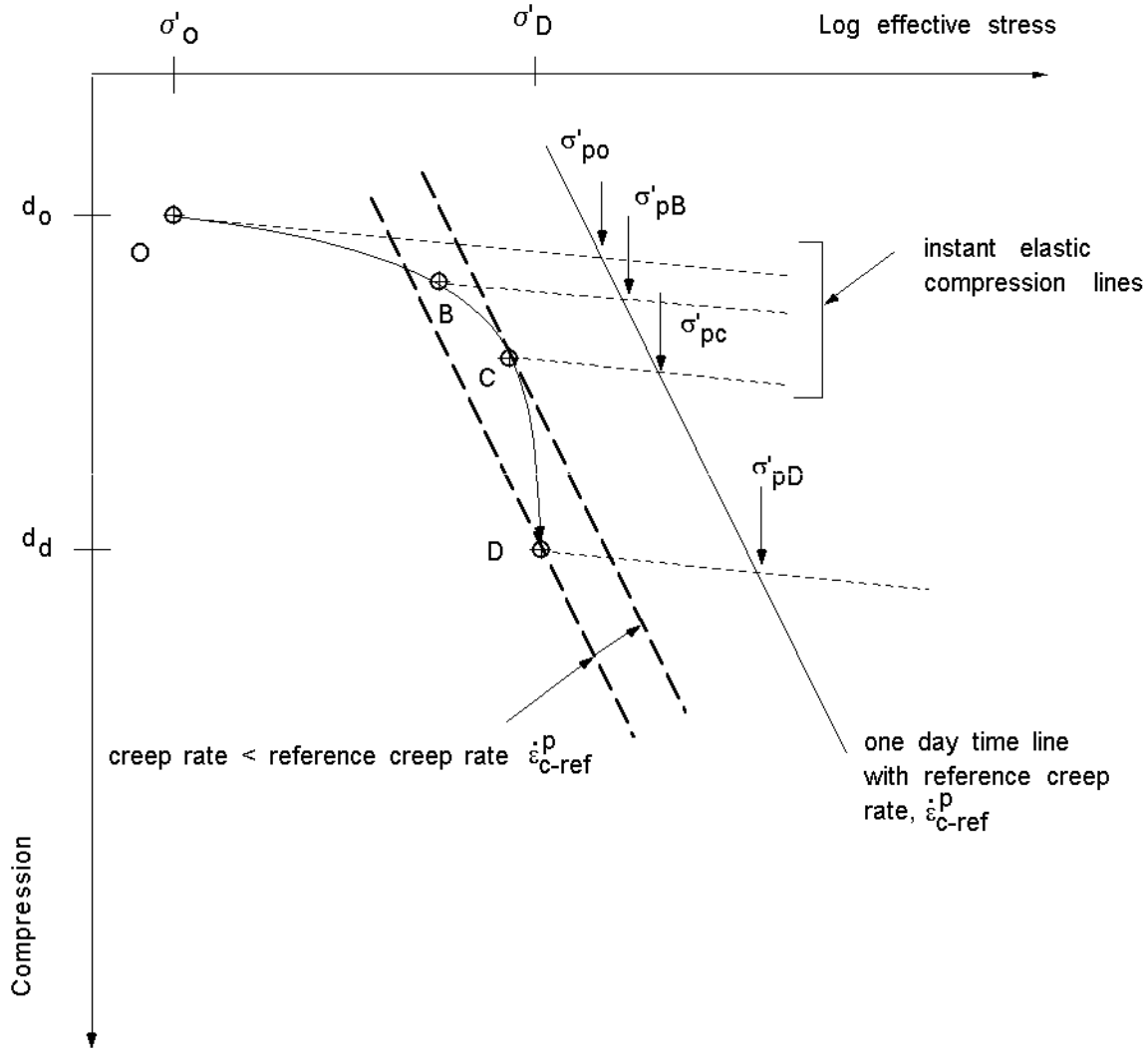

Figure 3.3: Yielding and creep during pore pressure dissipation

$$d\varepsilon = \frac{\varepsilon}{\sigma} d\sigma' - \frac{d\dot{\varepsilon}}{\dot{\varepsilon}} \qquad (3.3)$$

The negative sign before the last temr on the right side of equation 3.3 results in a positive quantity for path OB because the creep strain rate, $\dot{\varepsilon}_c$, is positive and the change in creep strain rate, $d\dot{\varepsilon}_c^p$, is negative.

Point B to D: Compression of the soil skeleton involves instant plastic and creep strain. The actual rate of creep compression corresponds to the creep strain rate of the time line at the current effective stress and strain for every point along the path BD. The current effective stress is thus equal to the critical stress at every instant. Hardening occurs due to instant plastic strain and creep strain, and the corresponding one day reference preconsolidation pressures increase to $\sigma'_{PB'}$ and σ'_{PD}. The effective stress-strain

$$d\varepsilon = \frac{C_{\varepsilon c}}{2.3\sigma'} d\sigma' - \frac{C_\alpha}{2.3} \frac{d\dot{\varepsilon}_c^p}{\dot{\varepsilon}_c^p} \tag{3.4}$$

The relationship among $d\sigma'$, $d\dot{\varepsilon}_c^p$ and $d\varepsilon$ represented by equation 3.4 and illustrated in Figure 3.4 may be characterized by three types of behavior: (1) When $d\dot{\varepsilon}_c^p$ is positive (the rate of creep compression is increasing), the compressibility ($d\varepsilon / d\sigma'$) is less than the compressibility along a time-line; (2) When $d\dot{\varepsilon}_c^p$ is zero (the rate of creep compression is constant), compression occurs along a time-line; and (3) When $d\dot{\varepsilon}_c^p$ is negative (the rate of creep compression is decreasing), the effective stress-strain curve is steeper than a time-line.

When the effective stress becomes constant, the model simulates the transition to secondary compression. A special case of equation 3.4 occurs for $d\sigma' = 0$, in which case all of the compression is time-delayed creep (secondary compression):

$$d\varepsilon = d\varepsilon_c^p = -\frac{C_\alpha}{2.3} \frac{d\dot{\varepsilon}_c^p}{\dot{\varepsilon}_c^p} \tag{3.5}$$

Integrating this differential equation leads to equation 3.1 which defines the distance between time-lines. When the effective stress becomes constant, the rate of creep compression is the rate

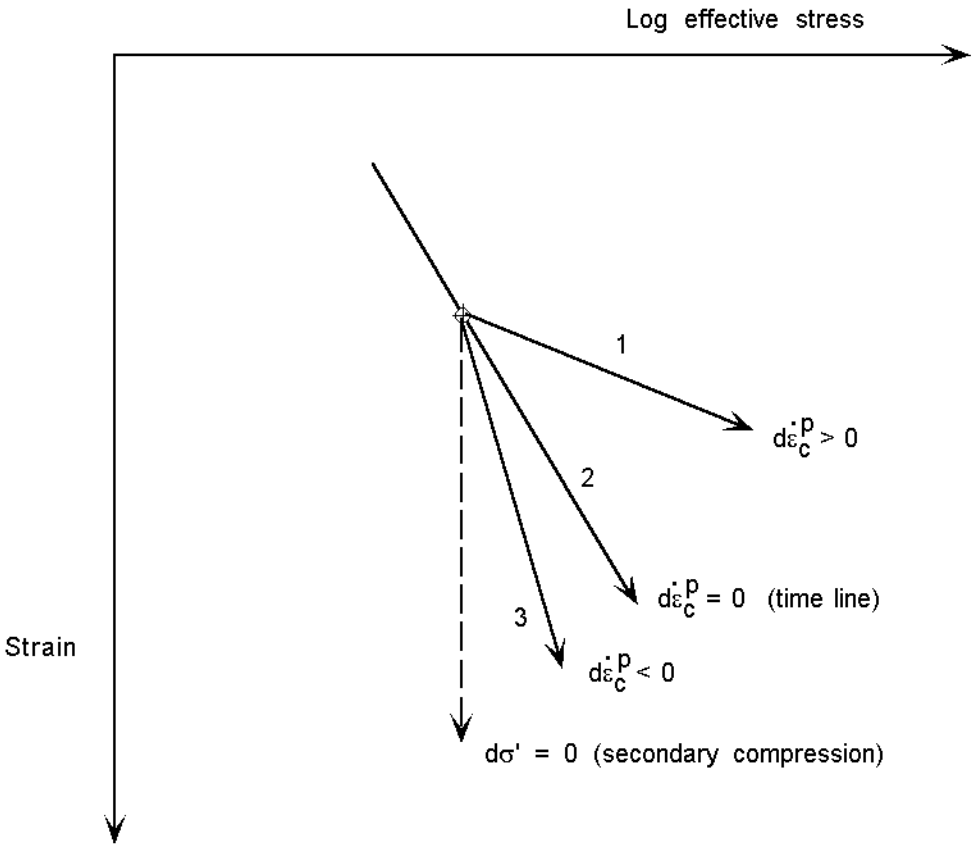

Figure 3.4: Effect of creep rate change on stress-strain paths

defining the time-line through the point corresponding to the current values of effective stress and void ratio.

3.1.2 Secondary Compression

Secondary compression in incremental oedometer tests is a major source of information about the creep component of compression. This compression (secondary compression) can be represented by the C_α-relationship:

$$\varepsilon = \varepsilon_{eop} + C_\alpha \log\left(\frac{t}{t_{eop}}\right), \quad t > t_{eop} \tag{3.6}$$

The parameters of this relationship are the rate of secondary compression, C_α, and the time to the end of primary consolidation, t_{eop}. The values of t and t_{eop} are measured from beginning of the last load increment. This relationship is difficult to apply in some situations and limits the usefulness of Type I instant time line models (see chapter 2.3.1). When fill placement or other load changes occur over a period of time, the origin of time and thus the values of t and t_{eop} are not well defined.

Fundamentally the C_α-relationship is concerned with the rate of creep compression, not the amount of creep compression. Differentiating equation 3.6 twice, Rajot showed that the C_α-relationship describes the way in which the rate of creep compression decreases with time when effective stress becomes constant:

$$\ddot{\varepsilon} + \frac{2.3}{C_\alpha}\left(\dot{\varepsilon}_c^p\right)^2 = 0, \quad t > t_{eop} \tag{3.7}$$

The solution to equation 3.7 for the case of a single load applied at t = 0 is equation 3.6, in which ε_{eop} and t_{eop} are integration constants. For other conditions also, if equation 3.7 is satisfied when effective stress becomes constant, creep compression will increase linearly with the logarithm of time, and this condition will continue indefinitely. Although the integration constants for other conditions will depend on the loading conditions and the loading history, the rate of creep compression will not depend on these loading conditions. Equation 3.7 complies with the rheological principles of determinism and objectivity.

Rajot hypothesized that the C_α-relationship describes asymptotic secondary compression behavior represented by the following relationship:

$$\ddot{\varepsilon}_c^p \approx -\frac{2.3}{C_\alpha}\left(\dot{\varepsilon}_c^p\right)^2, \quad \text{when } \dot{\sigma} \to 0 \tag{3.8}$$

During secondary compression, $\ddot{\varepsilon}_c^p$ and $\left(\dot{\varepsilon}_c^p\right)^2$ are of the same order, decreasing to zero in proportion to $1/t^2$.

Rajot simulated this type of behavior with an extended Kelvin element including a non-linear spring and a non-linear dashpot. The following expressions were derived for the tangent stiffness of the spring (k_c^p) and the viscosity of the dashpot (η), which together satisfy equation 3.8 and insures asymptotic convergence to the C_α-relationship during secondary compression:

$$k_c^p = \frac{2.3}{C_\alpha}\eta\dot{\varepsilon}_c^p \tag{3.9}$$

and

$$\eta = \eta^{tl}\exp\left\{\frac{2.3}{C_\alpha}\left(\varepsilon_c^p - \varepsilon_c^{p(t)l}\right)\right\}\frac{\dot{\varepsilon}_c^p}{\dot{\varepsilon}_c^{p-tl}} \tag{3.10}$$

in which the superscript (tl) designates values when convergence to the C_α-relationship begins.

When the rate of compression is increasing, Rajot found that the following expression produced appropriate values of viscosity to represent the behavior of the creep component of compression:

$$\eta = A\frac{\sigma'}{\dot{\varepsilon}} + \eta_o \tag{3.11}$$

in which σ' is the effective stress and $\dot{\varepsilon}$ is the sum of the instant and the creep rates of compression. The dimensionless constant, A, and viscosity, η_o, are sub-parameters of the model. These values are constant, independent of soil properties and physical scale. They serve only to facilitate numerical computations at the first instants after a new load is applied.

The value of the constant A is most important at low strain rates, while the constant, η_o, extends the applicability of the model to large compression rates which occur near drainage boundaries at the early stages of consolidation. For simulation of the consolidation of thick clay layers, where only the value of A is important, Rajot found that A = 1.00 is an appropriate value. The value of η_o is set equal to 10^5 kPa minutes for all analysis conditions.

The variation of viscosity during consolidation depends on the loading conditions. The expression for the viscosity during primary consolidation is given by equation 3.11, and during secondary compression by equation 3.10. As a consequence, the transition in the value of viscosity must be appropriate to model this transition in behavior from primary to secondary compression. Rajot found it convenient to define this transition by the following condition:

$$\ddot{\varepsilon}_c^p < 0 \qquad (3.12)$$

According to this criterion, viscosity is defined by equation 3.11 if the compression rate is increasing and by equation 3.10 if the compression rate is decreasing. When the compression rate is decreasing, the value of stiffness and viscosity from equations 3.9 and 3.10 insures progressive convergence to the C_α-relationship.

3.1.3 Capabilities of Rajot's Model

Secondary compression

To illustrate the capabilities of Rajot's model, a standard oedometer test of a 2.5 cm thick sample of San Francisco Bay Mud with drainage at both top and bottom was simulated using Rajot's computer program CS1. The calculations were performed using properties representative of San Francisco Bay Mud: $C_{\varepsilon c}$= 0.35; $C_{\varepsilon r}$ = 0.03; C_α= 0.008; c_v = 1.39 m^2/year. The initial preconsolidation pressure, $\sigma'^{(o)}_{pref}$, was 70 kPa. Beginning with an initial effective stress equal to 25 kPa throughout the specimen, loads were applied to increase the stress to 50 kPa, 100 kPa, and 200 kPa in three successive steps.

Computed variations of strain with time are shown in Figure 3.5. The second and third load increments, both with final stresses larger than the initial preconsolidation pressure, caused significant amounts of secondary compression. In both cases the strain-log time curves reached a

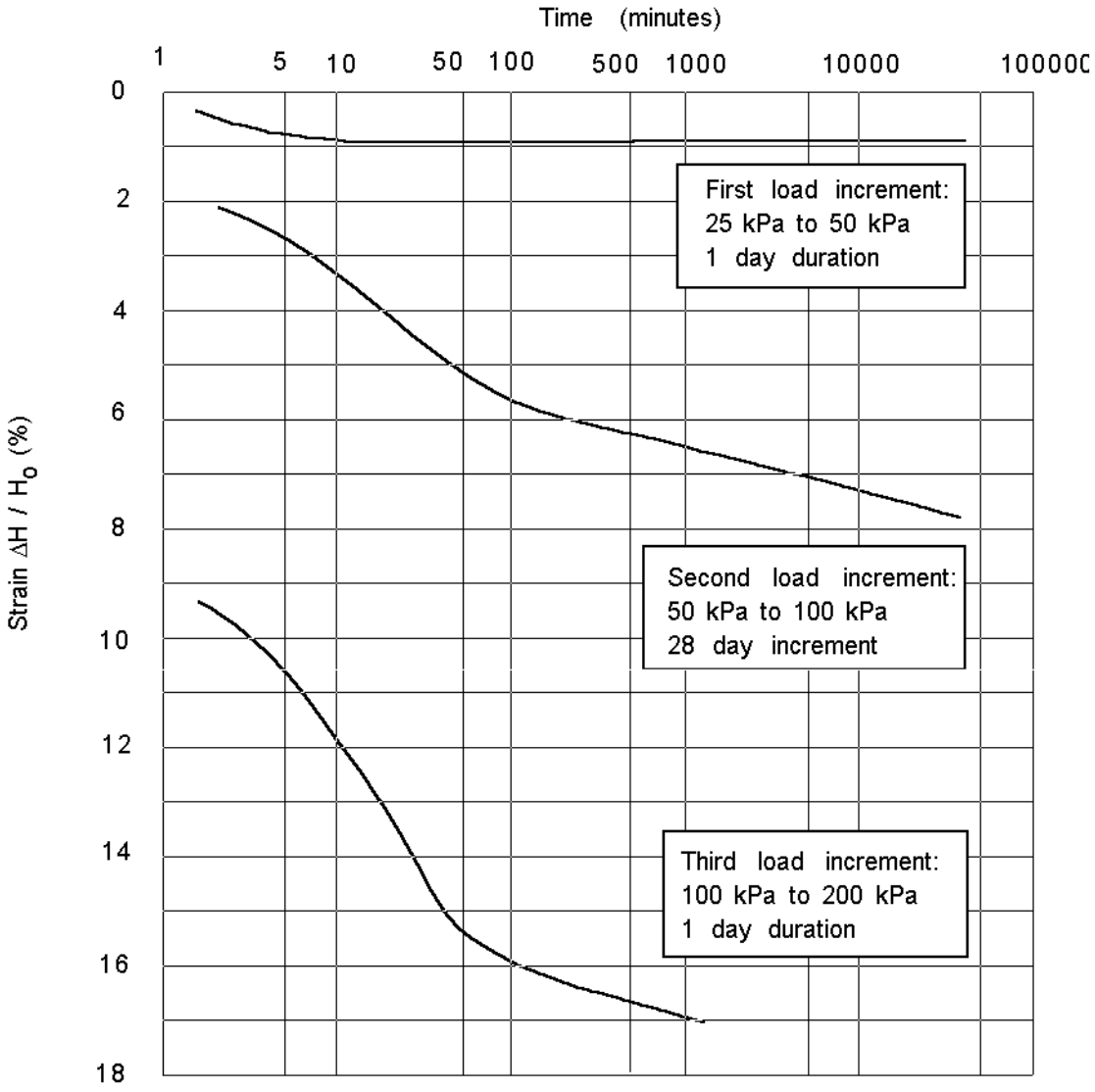

Notes:

1. Intial value of reference preconsolidation stress, $\sigma^{o}_{p\text{-}ref}$ = 70 kPa
2. Test specimen thickness = 2.5 cm. with drainage at top and bottom

Figure 3.5: Calculated time curves for incrementally loaded oedometer tests using Rajot's time-dependent theory

final slope of 0.8 percent per log cycle consistent with C_α= 0.008. For the second load increment this slope remained constant from the end of primary to 28 days, when the third load increment was applied.

The model simulates the behavior often observed in incrementally loaded oedometer tests: little or no secondary compression for stresses smaller than the preconsolidation stress, secondary compression strains increasing linearly with log time after the end of primary consolidation, and coefficients of secondary compression that are constant for stress increments above the preconsolidation stress.

Time Lines and Aging

Figure 3.6 illustrates time lines that were simulated for four different load durations. The same values of applied stress were used in each analysis (σ' = 60, 90, 130, 160, 190, 220 and 250 kPa) and the load durations were 1 hour for the first analysis, 5 hours for the second, 1 day for the third, and 4 days for the fourth analysis. Each analysis produced a different stress-strain curve, or time line, corresponding to the load duration. The soil properties used in the analyses were characteristic of the plastic clay from Drammen, Norway (Bjerrum, 1967): $C_{\varepsilon c}$= 0.24; $C_{\varepsilon r}$ = 0.024; C_α= 0.012; c_v = 1.86 m^2/year.

The results of a computer simulation of the laboratory test used by Bjerrum (1967) to investigate the effect of prolonged load application on preconsolidation stress is also shown in Figure 3.6. The plotted values represent the calculated strain at mid-height of the Drammen plastic clay specimen. Bjerrum applied stresses of 60, 90, 130, 160, 190, 220, and 250 kPa. All of the loads were maintained for one day, except the 130 kPa load, which was applied for 28 days.

The calculated results in Figure 3.6 are the same as Bjerrum's: the final (one-day) strain for the 90 kPa load is located on the one-day time line, as are the final strains for 160, 190, 220, and 250 kPa

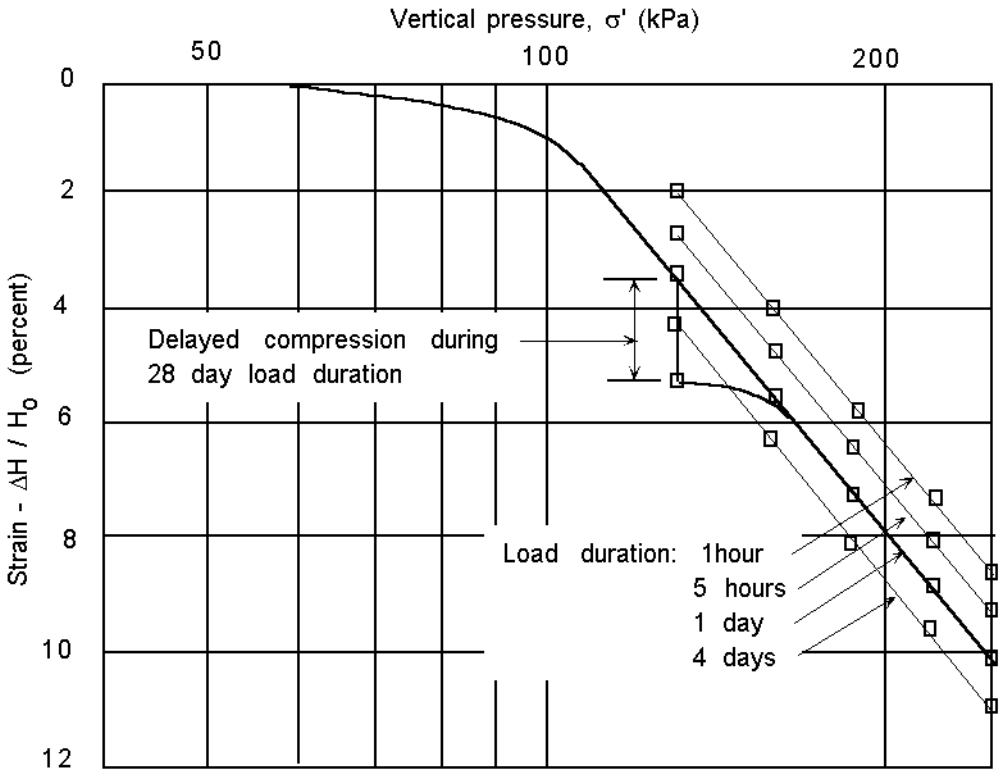

Figure 3.6: Time lines and incremental loading test results calculated using Rajot's theory, with one load increment lasting 28 days

loads, which were maintained for one day. The final (28-day) strain for the 130 kPa load falls below the 4-day time line; the point would fall on the 28-day time line if one had been established. Due to the prolonged loading at 130 kPa, the value of the preconsolidation pressure increased to about 160 kPa, essentially the same magnitude of the aging effect found in Bjerrum's experiment.

Effect of Strain Rate on Preconsolidation Pressure

Rajot's computer program CS1 was also used to simulate constant rate of strain consolidation tests on a Bay Mud specimen using strain rates of 8.3 x 10-7, 1.6 x 10-6, and 4.0 x 10-6 sec-1. The strain-log stress curves calculated in these analyses were plotted, and values of preconsolidation pressure were determined using Casagrande's construction. Figure 3.7 shows the apparent preconsolidation pressure normalized with respect to the initial reference preconsolidation pressure for one-day incremental loading ($P'_p / \sigma'^{(o)}_{pref}$). The results indicate that the normalized preconsolidation pressure increases as the rate of strain increases. This is the same type of behavior that Leroueil et al. (1985) observed in their CRS tests which are illustrated in Figure 2.7.

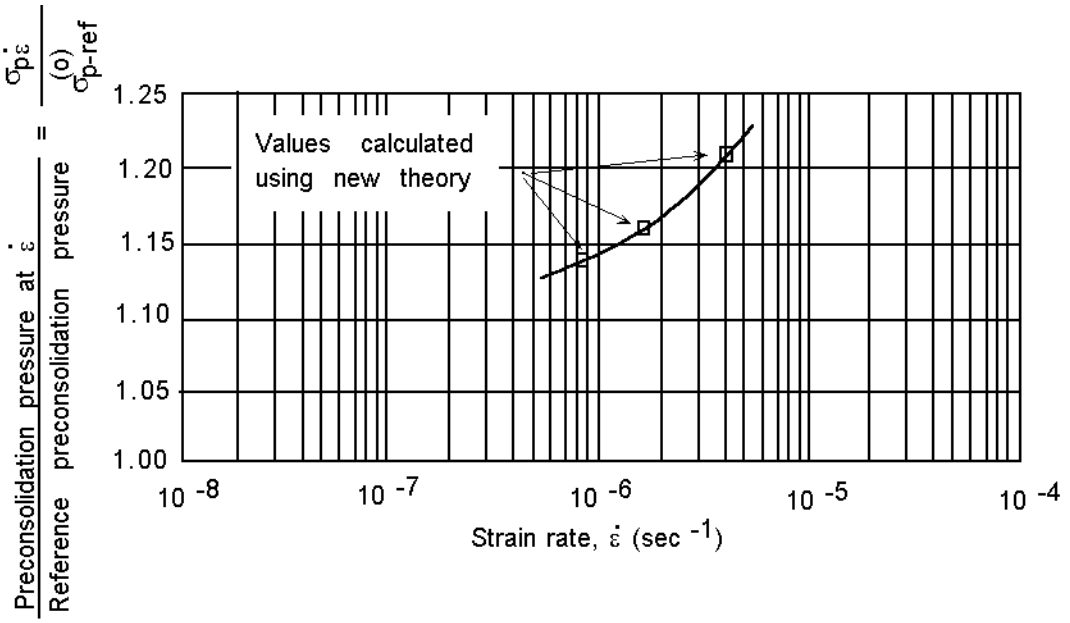

Figure 3.7: Calculated variation of preconsolidation pressures with strain rate

Effect of Layer Thickness

To illustrate the effects of layer thickness on rate and amount of consolidation predicted by the theory, analyses were performed to compare consolidation of a 2-cm thick specimen of San Francisco Bay Mud, drained at the top and bottom, and a one meter thick layer of Bay Mud drained at the top only. The Bay Mud properties used in the analyses were the same as listed previously, and are shown in Figure 3.8. The initial effective stresses, initial reference preconsolidation pressures ($\sigma'^{(o)}_{pref}$) and the final effective stresses are illustrated in Figure 3.8. The initial effective stress and preconsolidation pressure in the 2-cm thick test specimen were equal to the values at the center of the one meter thick layer (σ' = 25 kPa, $\sigma'^{(o)}_{pref}$ = 45 kPa). Both the test specimen and the one-meter thick layer were subjected to a uniform 50 kPa increase in stress throughout the thicknesses of the specimen and the layer.

The calculated strain-log time curves are shown in Figure 3.9. The average strain at the end of primary consolidation in the one-meter thick layer is larger than the average strain in the 2-cm thick test specimen at the end of primary and after 24 hours. Larger strains occurred in the one-meter thick layer because the longer drainage distance slows consolidation and allows greater amounts of time-delayed compression (creep). The average strain at the end of primary consolidation was 7.0% for the 2-cm specimen and 9.5% for the one-meter thick layer.

The secondary compression curves are linear and have the same slope. A linear projection of the secondary compression curve for the 2-cm thick test specimen is also shown in Figure 3.9. The strains calculated for the one-meter thick layer are above the dotted line and therefore less than the extrapolated lab strains at any time. Rajot's theory and CS1 predict average strains that are between those corresponding to Hypothesis A and Hypothesis B (Jamiolkowski et al., Figure 2.1).

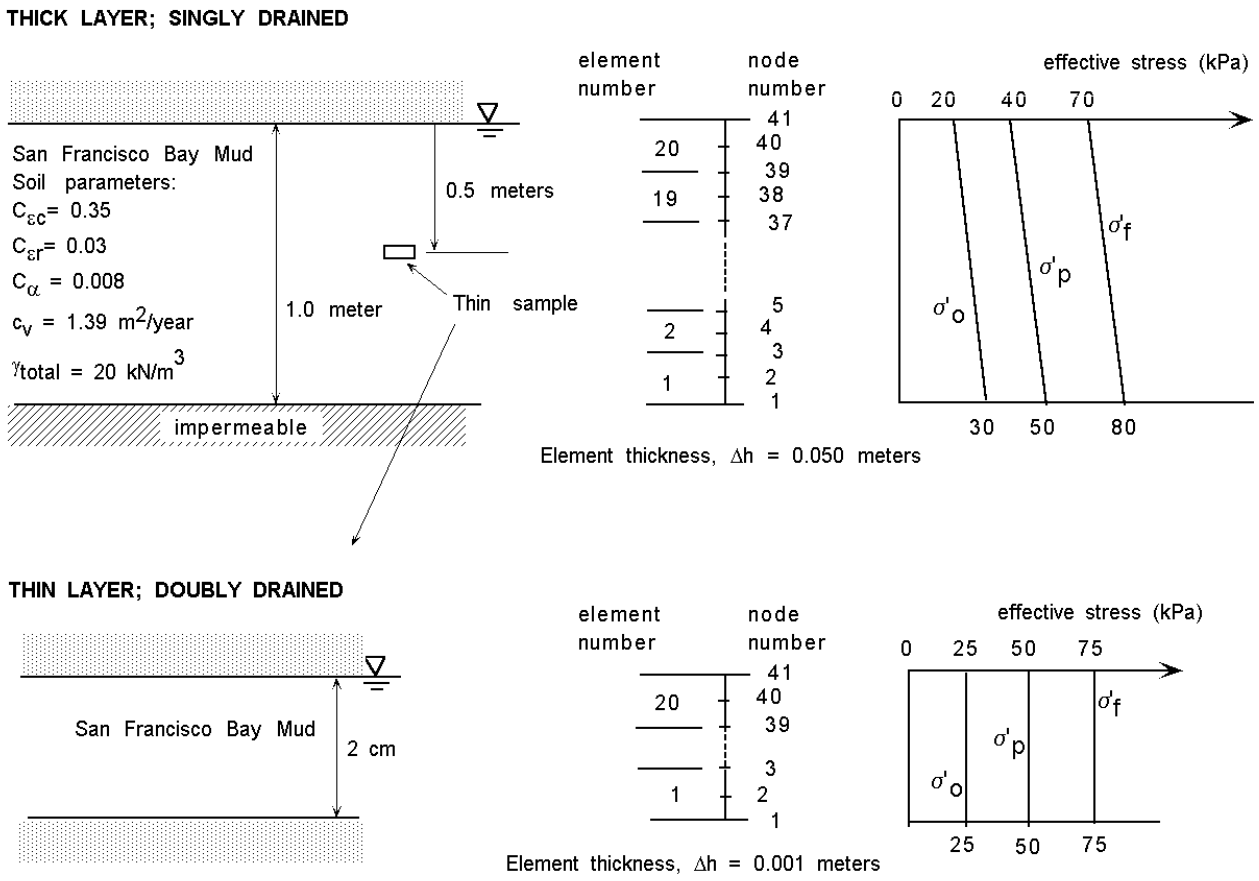

Figure 3.8: Thin and thick layer profiles and soil properties

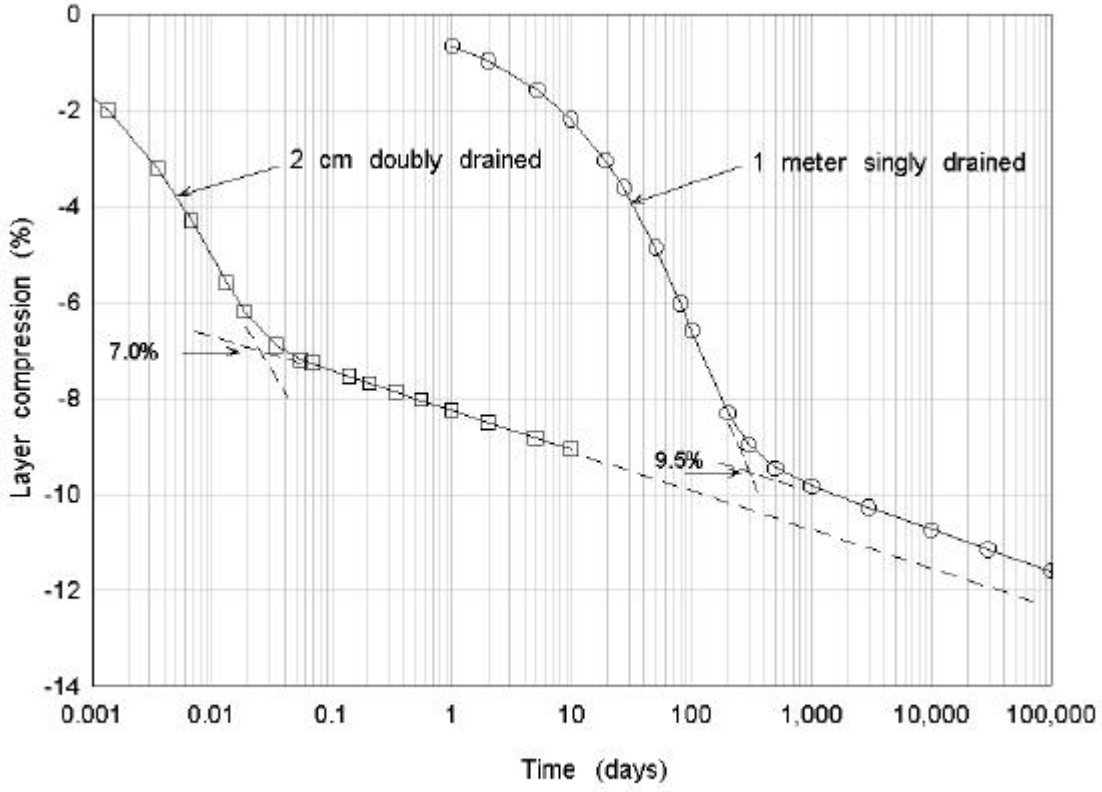

Figure 3.9: Calculated strain-log time curves for thin and thick layers

3.2 PROCEDURE FOR SIMULTANEOUS ANALYSIS OF CONSOLIDATION AND SECONDARY COMPRESSION

Analysis of consolidation involves coupling the stress-strain-time relationships of a constitutive model with the hydraulic and continuity conditions for flow of water through soil. The basic equations that govern one dimensional consolidation are as follows:

1. Stress equilibrium.

$$\frac{\partial \sigma_z}{\partial z} + f_z = 0 \qquad (3.14)$$

where: σ_z = total vertical stress; f_z = unit body force; z = depth.

2. Flow continuity of a compressible fluid through a deforming porous media:

$$\frac{\partial \varepsilon_v}{\partial t} + \frac{n}{Q}\frac{\partial u}{\partial t} - \frac{\partial}{\partial z}\left[k_z\left(1 + \frac{1}{\gamma_w}\frac{\partial u}{\partial z}\right)\right] = 0 \qquad (3.15)$$

where: k_z = vertical permeability; ε_v = volumetric strain = ε_z = vertical strain; γ_w = unit weight of water; u = pore pressure; n = porosity; Q = bulk modulus of the fluid; and *t* = time.

3. Effective stress principle:

$$\sigma_z = \sigma'_z + u \qquad (3.16)$$

where: σ'_z = effective vertical stress; u = pore pressure.

4. Effective stress-strain relationship (constitutive equation):

$$d\sigma'_z = C \cdot d\varepsilon_z \qquad (3.17)$$

where C is the tangent modulus that relates effective stress and strain.

The differences in governing equations for conventional and time-dependent analyses arise from the selection of the stress-strain relationship (equation 3.17).

For conventional analyses, the constitutive equation is time-independent and given by:

$$d\varepsilon_z = m_v \cdot d\sigma'_z \qquad (3.18)$$

where: $m_v = \frac{\partial \varepsilon_z}{\partial \sigma'_z} = \frac{C_c}{2.3 \cdot (1 + e_o) \cdot \sigma'_z}$, or $\frac{C_r}{2.3 \cdot (1 + e_o) \cdot \sigma'_z}$, (3.19)

Combining equations 3.14 through 3.18 and assuming that the pore fluid is incompressible and total stress is constant in time, leads to Terzaghi's basic differential equation for one-dimensional consolidation:

$$\frac{k}{m_v \cdot \gamma_w} \cdot \frac{\partial^2 u_e}{\partial z^2} = \frac{\partial u_e}{\partial t} \qquad (3.20)$$

where u_e = excess pore pressure = $u - u_o$ and u_o = initial pore pressure.

The time-dependent model includes both instant and creep (delayed) strain. At any time, $t^{(n)}$, the total strain increment is:

$$\Delta\varepsilon^{(n)} = \Delta\varepsilon_i^{(n)} + \Delta\varepsilon_d^{(n)} \tag{3.21}$$

Rajot (1992) found that the incremental form of the stress-strain relationship for either the elastic or plastic domains can be generally stated as:

$$\Delta\varepsilon^{(n)} = D\Delta\sigma'^{(n)} + \Delta\tilde{\varepsilon}^{(n)} \tag{3.22}$$

The expressions for D and $\Delta\tilde{\varepsilon}^{(n)}$ are derived from constitutive equation 3.3 when the current effective stress is less than the critical stress ($\sigma' < \sigma'_c$) and from equation 3.4 when the current effective stress is greater than or equal to the critical stress ($\sigma' \geq \sigma'_c$). The expression for the critical stress, σ'_c, is given by equation 3.2. As with the numerical analysis with conventional (time-independent) theory, these equations are solved for displacements and pore pressures, and the permeability is updated at each time step. However, the displacements now consist of instant and creep components and the reference preconsolidation pressure must be recomputed at each time step to reflect the current creep strain rate.

In the elastic domain, the instant elastic and creep strain increments for the physical model (Figure 3.1) are given by:

$$\Delta\varepsilon_i^{(n)} = \frac{1}{k_i^e}\Delta\sigma'^{(n)} = \frac{C_{\varepsilon r}}{2.3\sigma'}\Delta\sigma'^{(n)} \tag{3.23}$$

$$\Delta\varepsilon_c^{p(n)} = \frac{1}{k_c^p}\Delta\sigma'^{(n)} \tag{3.24}$$

The creep strain at time, t, is:

$$\varepsilon_c^p = \varepsilon_c^{p(n)} + \frac{1}{k_c^p}\left(\sigma'_c - \sigma'^{(n)}_c\right) \tag{3.25}$$

The constitutive relationship for the creep part of the model, illustrated in Figure 3.1, can be expressed by:

$$\sigma' = \sigma'_c + \eta\frac{d\varepsilon_d}{dt} \tag{3.26}$$

Solving equation 3.25 for σ'_c and substituting in equation 3.26 gives:

$$\eta \frac{d\varepsilon_d}{dt} + k_c^p \varepsilon_c = \sigma' + \left(k_c^p \varepsilon_c^{p(n)} - \sigma_c'^{(n)} \right) \tag{3.27}$$

Rajot (1992) assumed a linear variation of effective stress, $\sigma'(t)$, over each time step increment and integrated equation 3.27 to derive the creep strain increment, $\Delta\varepsilon_c^{p(n)}$:

$$\Delta\varepsilon_c^{p(n)} = \frac{\alpha}{k_c^p}\left(\sigma'^{(n)} - \sigma_c'^{(n)} \right) + \frac{\Delta\sigma'^{(n)}}{k_c^p}\left[1 - \alpha \frac{\eta}{k_c^p \Delta t^{(n)}} \right] \tag{3.28}$$

where:

$$\alpha = 1 - \exp\left\{ - \frac{k_c^p \Delta t^{(n)}}{\eta} \right\} \tag{3.29}$$

Combining equations 3.24 and equation 3.28 in equation 3.23 and rearranging terms produces an expression for the incremental strain in the elastic domain which has the same form as equation 3.22:

$$\Delta\varepsilon^{(n)} = D^e \Delta\sigma'^{(n)} + \Delta\tilde{\varepsilon}^{e(n)} \tag{3.30}$$

$$D^e = \frac{1}{k_i^e} + \frac{1}{k_c^p} - \alpha \frac{\eta}{k_c^{p\,2} \Delta t^{(n)}} \tag{3.31}$$

$$\Delta\tilde{\varepsilon}^{e(n)} = \frac{\alpha}{k_c^p}\left(\sigma'^{(n)} - \sigma_c'^{(n)} \right) \tag{3.32}$$

where α is given by equation 3.29 and:

When the soil skeleton is yielding ($\sigma' \geq \sigma'_c$), the stress-strain relationship is given by equation 3.4 . Integrating equation 3.4 and assuming linear behavior for each time step, Rajot (1992) arrived at the following equation for incremental strain, $\Delta\varepsilon^{(n)}$:

$$\Delta\varepsilon^{(n)} = \frac{C_{\varepsilon c}}{2.3} \frac{\Delta\sigma'^{(n)}}{\sigma'^{(n)}} - \frac{C_\alpha}{2.3} \frac{\Delta\dot{\varepsilon}_c^{p(n)}}{\dot{\varepsilon}_c^{p(n)}} \tag{3.33}$$

Using equation 3.28 and 3.33, Rajot showed that the incremental strain formulation during yielding has the form of equation 3.22:

$$\Delta\varepsilon^{(n)} = D^{p}\Delta\sigma'^{(n)} + \Delta\tilde{\varepsilon}_c^{p(n)} \tag{3.34}$$

where:

$$D^{p} = \frac{C_{\varepsilon c}}{2.3\sigma'^{(n)}} - \alpha\frac{C_\alpha}{2.3}\frac{1}{k_c^{p}\Delta t^{(n)}\dot{\varepsilon}_c^{p(n)}} \tag{3.34}$$

$$\Delta\tilde{\varepsilon}_c^{p(n)} = \alpha\frac{C_\alpha}{2.3} \tag{3.35}$$

and α is given by equation 3.29.

The incremental form of equation 3.22 may be rewritten with strain as the independent variable:

$$\Delta\sigma'^{(n)} = C\Delta\varepsilon^{(n)} + \Delta\tilde{\sigma}'^{(n)} \tag{3.36}$$

where C=1/ D and $\Delta\tilde{\sigma}'^{(n)} = -\frac{1}{D}\Delta\tilde{\varepsilon}^{(n)}$.

The soil stiffness, C, and the permeability, k, of each sublayer is recomputed at each time step. A linear relationship is assumed between the log of permeability and void ratio. The change in permeability is computed from the slope of the reference time line, $C_{\varepsilon c}$, and the input value of coefficient of consolidation, c_v. The assumptions involved in this method of evaluating permeability are illustrated in Figure 3.10. From Terzaghi's consolidation theory:

$$k = c_v \cdot m_v \cdot \gamma_w \tag{3.37}$$

Substituting Equation 3.19 we have:

$$k = \frac{c_v \cdot C_c \cdot \gamma_w}{2.3\cdot(1+e_o)\cdot\sigma'_z} \tag{3.38}$$

Since c_v remains essentially constant in the normally consolidated range of stresses and permeability varies only with void ratio, the permeability in the recompression and the virgin compression stress range may be recomputed using equation 3.38. The value of c_v is from the virgin compression stress range, and s'_v is the effective stress. If the current stress is less than the reference preconsolidation stress, $\sigma'^{(o)}_{pref}$, then s'_v is the value of effective stress corresponding to the current void ratio on the reference virgin compression curve:

$$\sigma'_v = \sigma'^{(o)}_{pref} \cdot \exp\left[\left(\frac{2.3}{C_{\varepsilon c}}\right)\cdot\left(\varepsilon_t - \varepsilon_e\right)\right] \qquad (3.39)$$

where: $\sigma'^{(o)}_{pref}$ = preconsolidation stress, $C_{\varepsilon c}$ = virgin compression index, ε_t = total strain, ε_e = elastic recompression strain from the initial overburden stress to the preconsolidation stress, $\sigma'^{(o)}_{pref}$.

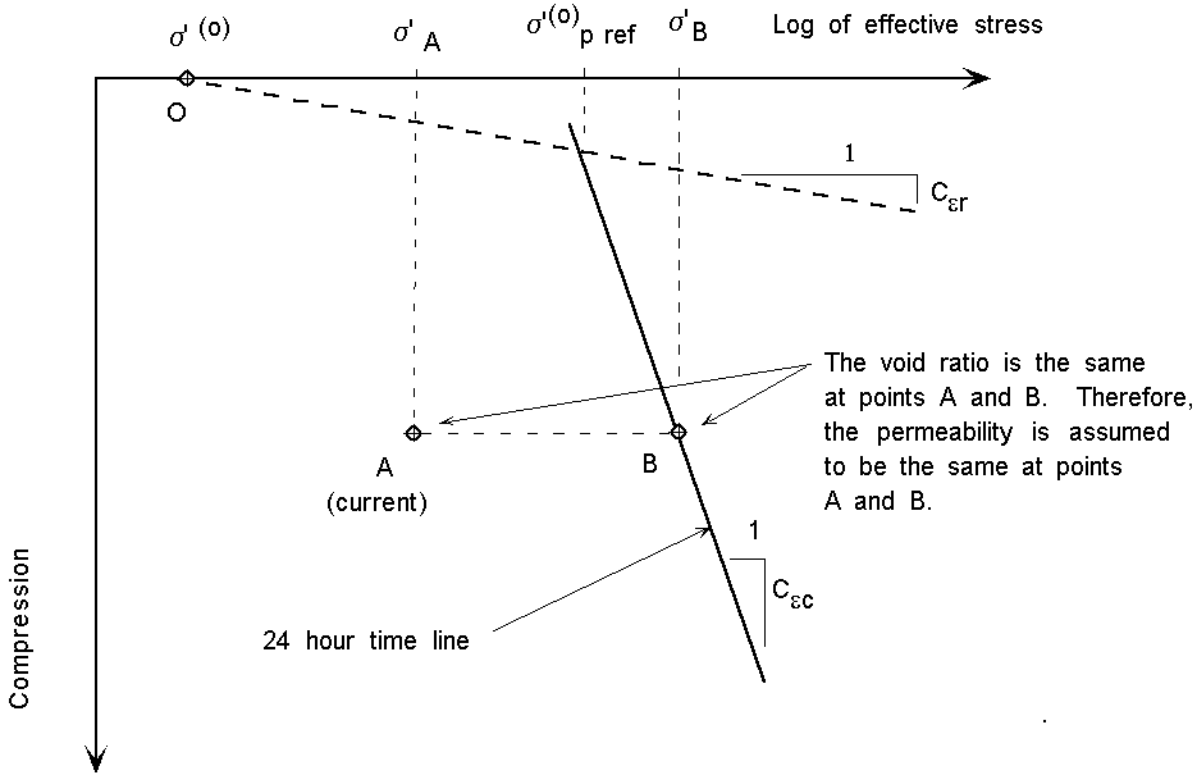

Figure 3.10: Permeability-strain-effective stress relationship

3.3 RAJOT'S COMPUTER PROGRAM, CS1

The computer program CS1 uses the finite element method to compute displacements and pore water pressures at prescribed locations within the soil mass during the consolidation process. The subsurface profile (domain Ω) is represented by discrete elements and the loads and drainage conditions are specified on the boundaries (Γ_j). The incremental form of the time-dependent constitutive model and the flow equations are used to formulate the element stiffness matrices. Rajot used an infinitesimal strain solution based on the results of a comparative study by Meijer (1984) which found little difference between finite strain and infinitesimal strain solutions for clay soils.

The two governing differential equations for deformation and continuity of flow through a porous medium are derived from the basic equations 3.14 to 3.17. The first equation for deformation of a solid in the space domain Ω, with boundaries, Γ_j, and subjected to external forces is obtained by substituting equations 3.16 and 3.36 in equation 3.14:

$$C\frac{\partial^2 v}{\partial z^2}+\frac{\partial \tilde{\sigma}'}{\partial z}+\frac{\partial u_z}{\partial z}+f_z=0 \qquad (3.40)$$

where $\tilde{\sigma}'$ is the time-dependent component of the stress-strain behavior and *v* is the displacement. The second equation is the flow continuity condition given by equation 3.15:

$$\frac{\partial \varepsilon_v}{\partial t}+\frac{n}{Q}\frac{\partial u}{\partial t}-\frac{\partial}{\partial z}\left[k(1+\frac{1}{\gamma_w}\frac{\partial u}{\partial z})\right]=0 \qquad (3.41)$$

The element stiffness matrices used in CS1 were derived by applying Galerkin's method of weighted residuals and Green's theorem to rewrite these governing equations in integral form. Green's theorem was used to transfer differentiation from the independent variables to the weighting functions over the element, and to generate boundary terms. In the Galerkin method, the trial functions (shape functions) and weighting functions are the same. The CS1 program

interpolates the displacements and pore pressures using either linear trial functions or using parabolic trial functions for both variables. Equations 3.40 and 3.41 may now be rewritten in incremental form as:

$$\int_\Omega \left(C\frac{\partial(\Delta v)}{\partial z} - \Delta\tilde{\sigma}' - \Delta u \right)\frac{\partial}{\partial z}\left(\delta(\Delta v)\right)d\Omega - \int_\Omega \Delta f_z \delta(\Delta v)d\Omega - \int_\Gamma \Delta T_z \delta(\Delta v)d\Gamma = 0 \qquad (3.42)$$

$$\int_\Omega \left\{ \left(\frac{\partial \dot{v}}{\partial z} + \frac{n}{Q}\dot{u} \right)\delta u + k\left(1 + \frac{1}{\gamma_w}\frac{\partial u}{\partial z} \right)\frac{\partial}{\partial z}(\delta u) \right\} d\Omega - \int_\Gamma q\delta u d\Gamma = 0 \qquad (3.43)$$

In these equations the volumetric strain is negative in compression, pore pressure is positive in compression, and q is positive if fluid is flowing out of the element.

The displacements and pore pressures in the domain Ω are interpolated over each element using the following interpolation functions:

$$\Delta v = \sum_{j=1}^{NPE} \Delta v_j \psi_j \qquad (3.44a)$$

$$\delta(\Delta v) = \sum_{i=1}^{NPE} \delta(\Delta v_i \psi_i) \qquad (3.44b)$$

$$\Delta u = \sum_{j=1}^{NPE} \Delta u_j \psi_j \qquad (3.44c)$$

$$v(z,t) = \sum_{j=1}^{NPE} v_j(t)\psi_j(z) \qquad (3.44d)$$

$$\dot{v}(z,t) = \sum_{j=1}^{NPE} \dot{v}_j(t)\psi_j(z) \qquad (3.44e)$$

$$u(z,t) = \sum_{j=1}^{NPE} u_j(t)\psi_j(z) \qquad (3.44f)$$

$$\dot{u}(z,t) = \sum_{j=1}^{NPE} \dot{u}_j(t)\psi_j(z) \qquad (3.44g)$$

where NPE is the number of nodes per element, and ψ_j are the interpolation (shape) functions which are continuous over the element.

Substituting the interpolation functions (equations 3.44a to 3.44g) in equations 3.43 and 3.44 produces the following system of equations, expressed in matrix form, for the set of elements in the domain, Ω:

$$\begin{bmatrix} [K_{ij}^{11}] & [K_{ij}^{12}] \\ \end{bmatrix} \begin{bmatrix} [\Delta v_j] \\ [\Delta u_j] \end{bmatrix} = [F_i^1] \tag{3.45}$$

and

$$\begin{bmatrix} [M_{ij}^{21}] & [M_{ij}^{22}] \end{bmatrix} \begin{bmatrix} [\dot{v}_j] \\ [\dot{u}_j] \end{bmatrix} + \begin{bmatrix} [K_{ij}^{21}] & [K_{ij}^{22}] \end{bmatrix} \begin{bmatrix} [v_j] \\ [u_j] \end{bmatrix} = [F_i^2] \tag{3.46}$$

in which:

$$K_{ij}^{11} = \int_{\Omega^e} C \frac{\partial \psi_i}{\partial z} \frac{\partial \psi_j}{\partial z} d\Omega^e \tag{3.47}$$

$$K_{ij}^{12} = \int_{\Omega^e} \frac{\partial \psi_i}{\partial z} \Psi_j d\Omega^e \tag{3.48}$$

$$F_i^1 = \int_{\Omega^e} \left\{ \Delta\tilde{\sigma}' \frac{\partial \psi_i}{\partial z} + \Delta f_z \psi_i \right\} d\Omega^e + \left[\Delta T_z \Psi_i \right]_{z_a}^{z_b} \tag{3.49}$$

$$M_{ij}^{21} = \int_{\Omega_e} \psi_i \frac{\partial \psi_j}{\partial z} d\Omega^e \tag{3.50}$$

$$M_{ij}^{22} = \int_{\Omega_e} \psi_i \frac{n}{Q} \psi_j d\Omega^e \tag{3.51}$$

$$K_{ij}^{21} = 0 \tag{3.52}$$

$$K_{ij}^{22} = \int_{\Omega_e} \frac{\partial \psi_i}{\partial z} \frac{k}{\gamma_w} \frac{\partial \psi_j}{\partial z} d\Omega^e \tag{3.53}$$

$$F_i^2 = \int_{\Omega_e} -k\frac{\partial \psi_i}{\partial z} d\Omega^e + \left[\psi_i q\right]_{z_A}^{z_B} \tag{3.54}$$

This system of equations for time-dependent consolidation analysis is nearly the same as the system of equations for conventional analyses that use time-independent soil behavior. Removing the first term in the brackets in equation 3.49 reduces this formulation to that for conventional analyses with time-independent stress-strain behavior.

The time derivatives, $\dot{v}$ and $\dot{u}$ in equations 3.44e, 3.44g, and 3.46 can be approximated using the θ-method:

$$\theta\dot{v}^{(n+1)} + (1-\theta)\dot{v}^{(n)} = \frac{\Delta v^{(n)}}{\Delta t^{(n)}} \tag{3.55a}$$

$$\theta\dot{u}^{(n+1)} + (1-\theta)\dot{u}^{(n)} = \frac{\Delta u^{(n)}}{\Delta t^{(n)}} \tag{3.55b}$$

where θ is a coefficient which varies from 0 to 1. Substituting these equations in equation 3.46 and integrating produces a new matrix:

$$\left[\left[\bar{K}_{ij}^{21}\right]\ \left[\bar{K}_{ij}^{22}\right]\right]\begin{bmatrix}[v_j]\\ [u_j]\end{bmatrix} = \left[\bar{F}_i^2\right] \tag{3.56}$$

in which:

$$\bar{K}_{ij}^{21} = \int_{\Omega_e} -\frac{\partial \psi_i}{\partial z}\psi_j d\Omega^e \tag{3.57}$$

$$\bar{K}_{ij}^{22} = \left(\frac{n}{Q}\right)^{(t)}\int_{\Omega_e}\psi_i\psi_j d\Omega^e + \theta\Delta t\left(\frac{k}{\gamma_w}\right)^{(n+1)}\int_{\Omega_e}\frac{\partial \psi_i}{\partial z}\frac{\partial \psi_j}{\partial z}d\Omega^e \tag{3.58}$$

$$\bar{F}_i^2 = -\Delta t^{(n)}\left\{\theta k^{(n+1)} + (1-\theta)k^{(n)}\right\}\int_{\Omega_e}\frac{\partial \psi_i}{\partial z}d\Omega^e + \left[\psi_i \Delta t^{(n)}\left\{\theta q^{(n+1)} + (1-\theta)q^{(n)}\right\}\right]_{z_A}^{z_B} +$$
$$\int_{\Omega_e}\psi_i\frac{\partial \psi_i}{\partial z}d\Omega^e v_k^{(n)} + \left[\left(\frac{n}{Q}\right)^{(t)}\left\{\int_{\Omega_e}\psi_i\psi_k d\Omega^e\right\} - (1-\theta)\Delta t^{(n)}\left(\frac{k}{\gamma_w}\right)^{(n)}\int_{\Omega_e}\frac{\partial \psi_i}{\partial z}\frac{\partial \psi_k}{\partial z}d\Omega^e\right]u_k^{(n)} \tag{3.59}$$

Assembling equations 3.45 and 3.56, we now have the complete set of equations in matrix form:

$$\begin{bmatrix} [K_{ij}^{11}] & [K_{ij}^{12}] \\ [\bar{K}_{ij}^{21}] & [\bar{K}_{ij}^{22}] \end{bmatrix} \begin{bmatrix} [\Delta v_j] \\ [\Delta u_j] \end{bmatrix} = \begin{bmatrix} [F_i^1] \\ [\bar{F}_i^2] \end{bmatrix} \qquad (3.60)$$

Displacements and pore pressures are calculated incrementally for each time step in CS1. At the start of the computations, it is assumed that the soil profile has achieved secondary compression and the viscosity, η, in the delayed component of the model is defined by equation 3.10. However, the parameters, η^{tl}, $\varepsilon_c^{p(tl)}$, and $\dot{\varepsilon}_c^{p(tl)}$ in equation 3.10 are unknown. It is therefore assumed that effective stresses are increasing and that the soil skeleton behaves elastically for the first three time steps. Thereafter the strain rate may be calculated and used to determine the viscosity, $\eta = \sigma'/\dot{\varepsilon}$.

The non-linearity of the stress-strain behavior and the change from instant elastic to instant plastic behavior at the critical stress level is accommodated through the use of convergence criteria, and by providing an automatic time stepping routine. If one of the convergence criteria is not satisfied for a time step, the time step size is halved and the computation is repeated. After convergence, the value of the next time step is anticipated based on previous values. Figure 3.11 illustrates the general computational procedure involved in CS1 which is summarized here:

1. Compute the initial effective stress and pore pressure conditions for static equilibrium and hydrostatic conditions prior to load application.

2. Set the initial values of the reference preconsolidation pressure and compute the creep rate of the reference time line based on laboratory test results.

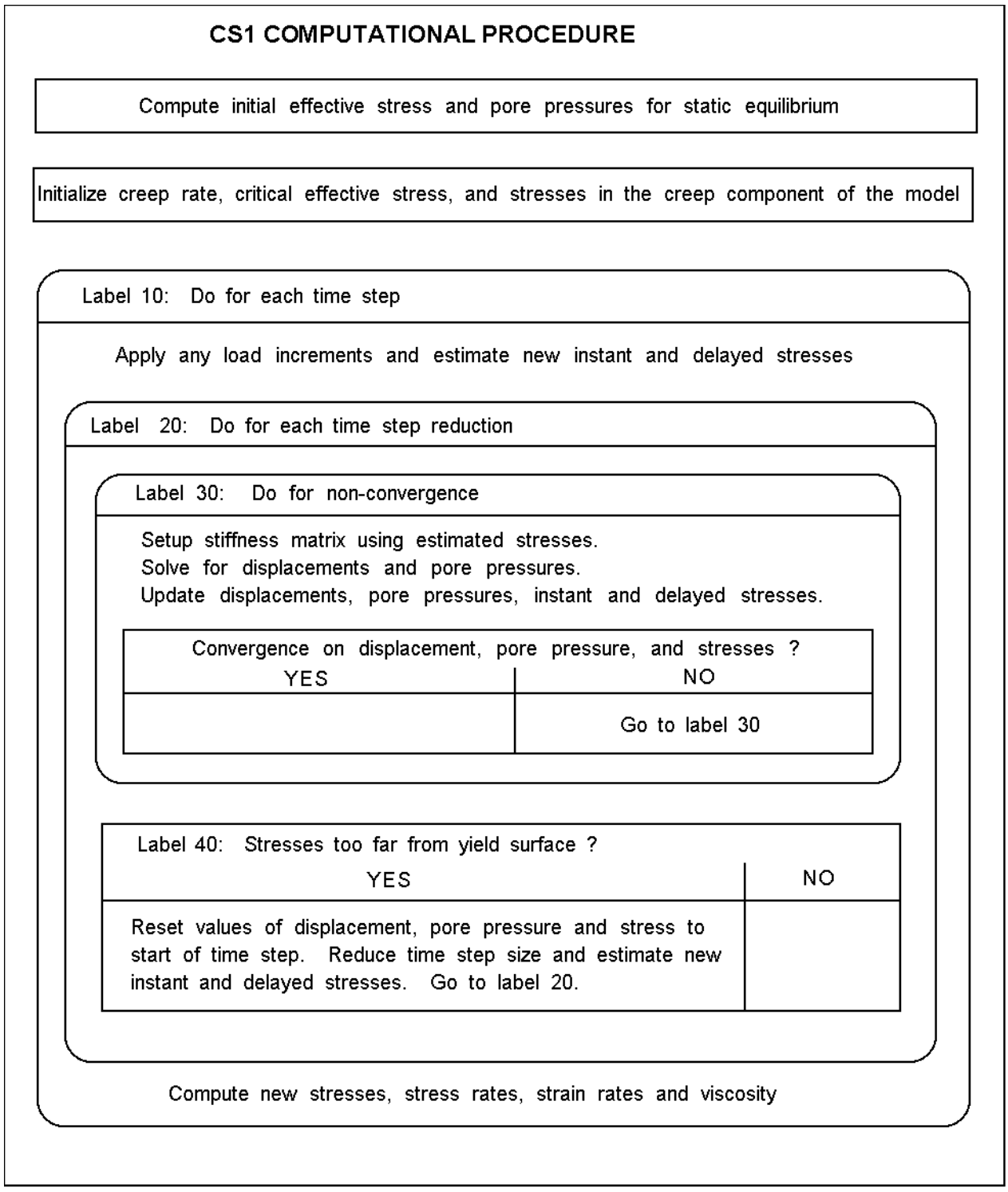

Figure 3.11: CS1 computational procedures

3. Set the initial values of critical stress corresponding to the initial creep rate. It is assumed that the current effective overburden pressure is the initial critical stress and calculates the corresponding creep rate.

4. Initialize the stresses in the creep component of the model.

5. For a time step increment, Δt, apply any load increments and compute displacements and pore pressures

6. Check for convergence of displacements, pore pressures, and stresses. If converged, update stresses and strains. If not converged, return to step 5 and repeat the computation using new stiffness values for the instant and delayed components of the model.

7. Compute the critical effective stresses for each element.

8. For each element, compare the current effective stress with the critical effective stress. If the current stress does not exceed the critical stress by the specified tolerable value, then update the critical stress values and continue. Otherwise, reduce the time step size and return to step 5.

Element stresses are computed using full integration in which the number of Gauss points equals the number of nodal points. Convergence of the computed displacements, pore pressures, and stresses are based upon the following criteria:

Criterion 1: Nodal Displacement Convergence

The change in displacements from one iteration to the next (between time *t* and *t+Dt*) :

$$\sum_{1}^{n}\left[(w_{t+\Delta t)} - w_t)^2 \Big/ (w_t)^2\right] \le 1.0E-6 \qquad (3.61)$$

where: n = number of nodal points or sublayer boundaries in the problem, w_t = displacement at each node at time *t* or *t+Dt*.

Criterion 2: Nodal Pore Pressure Convergence

The global change in pore pressures from one iteration to the next (between time t and *t+Dt*):

$$\sum_{1}^{n}\left[(u_{t+\Delta t)}-u_t)^2 \Big/ (u_t)^2\right] \le 1.0E-6 \qquad (3.62)$$

where: n = number of nodal points or sublayer boundaries in the problem, u_t = pore pressure at each node at time *t* or *t+Dt*.

Criterion 3: Element Stress Convergence

The global change in the effective initial and delayed stresses from one iteration to the next (between time *t* and *t+Dt*):

$$\sum_{1}^{nel}\left[(\sigma'_{t+\Delta t}-\sigma'_t)^2 \Big/ (\sigma'_t)^2\right] \le 1.0E-6 \qquad (3.63)$$

where: nel = number of elements or sublayers in the problem, s'_t = effective stress at each element or sublayer at time *t* or *t+Dt*. Both the initial and delayed effective stresses are checked for convergence.

Criterion 4: Yield Surface Convergence

The effective stress in any sublayer after each time step increment does not exceed:

$$(1.0+Tol)\cdot\sigma'_p \qquad (3.64)$$

where: *Tol* is the yield tolerance (time-dependent analyses use *Tol* = 0.10), σ'_p is the current preconsolidation or critical stress. The value of σ'_p is updated after criteria 1 through 3 are satisfied at each time step.

Chapter 4

CONSOL97 COMPUTER PROGRAM

Rajot's CS1 computer program was developed as a research tool to implement his elasto-visco-plastic theory and to examine some basic implications of the new theory. CS1 was not developed as a general-purpose, user friendly tool for analysis of the wide variety of one-dimensional consolidation problems encountered in consulting practice. Due to a lack of such a computer program, geotechnical engineers have ignored the effects of strain rate and creep on consolidation behavior. This chapter describes the changes made to CS1 to develop a general-purpose computer program named CONSOL97. This chapter also includes a description of input data required to use CONSOL97, and the numerical performance of CONSOL97 as compared to actual laboratory oedometer test data.

4.1 PRACTICAL IMPLEMENTATION OF RAJOT'S THEORY

The CS1 finite element program is limited to elasto-visco-plastic settlement analysis of only one soil layer with drainage at the top, the bottom, or both, and a continuous preconsolidation stress profile. The layer must consist of only one soil type with compressibility that conforms to a linear relationship between strain and log of effective stress. Practical situations may involve multiple soil layers, some of which are free draining, and organic and sensitive clays that are often characterized by nonlinear variations of strain with the log of effective stress (curved virgin compression curves). In addition, the stress history of soil profiles may be better represented by discontinuous preconsolidation stress profiles.

CONSOL97 can accommodate multiple layers of cohesive or granular soils, any preconsolidation stress profile, and any type of one-dimensional, stress-strain behavior. In addition, CONSOL97 can accommodate virgin compression values of c_v and C_α that vary with effective stress. For each soil type, the user can indicate whether or not to include elasto-visco-plastic creep behavior. If the elasto-visco-plastic model is selected for a soil type, then the user specifies a value of C_α. To perform a conventional analysis without creep, the elasto-plastic soil model is specified for all of the soil layers. In this case, CONSOL97 is essentially equivalent to the earlier program CONSOL (Duncan et al 1988).

CONSOL97 can be used to evaluate a wide range of loading conditions. If the loading does not correspond to a large area load, with uniform stress changes throughout the layer, the user selects a loading geometry from a list of options and CONSOL97 calculates the new stresses in each sublayer. The loading options are similar to those found in CONSOL (Duncan et al. 1988): strip, circular, and large area loads; specified stress changes in each sublayer; specified initial and final stresses in each sublayer; and stresses due to changes in the groundwater level. If the existing soil profile has not fully consolidated, the user may specify the "underconsolidated" loading option which determines the excess pore pressure profile for use in the settlement analysis. Changes in loading due to submergence of the soil profile and any newly placed fill are also considered in the analyses.

CS1 analyses of thick, slightly overconsolidated clay layers revealed an inconsistency between the assumed in-situ creep rate based on lab values of C_α and the in-situ creep rate based upon the lab measured preconsolidation stress. Extremely slow rates of consolidation in soil elements located away from drainage boundaries were accompanied by excessive hardening (increase in preconsolidation stress) of the soil even while the effective stress remained less than the initial preconsolidation stress. To correct this problem, CONSOL97 computes values of $C_{\alpha\ field}$ that are consistent with measured preconsolidation stresses and the age of the deposit, as explained in section 4.1.1.

The accuracy and efficiency of the numerical computations are affected by time step size, thickness of the finite elements used to model the soil layers, the specified convergence criteria (section 3.3) and the selection of interpolation functions. These computational control parameters have been studied so that CONSOL97 selects them automatically based on problem geometry and soil properties. A mesh generator has also been added to allow the user to construct elements of uniform thickness or geometrically varying thickness.

4.1.1 In-situ Secondary Compression

At the start of loading, the CS1 model assumes that the soil layer has reached secondary compression and the in-situ creep rate corresponds to the creep rate line at this in-situ effective stress. The relationship between in-situ creep rate, OCR, and reference creep rate used in the CS1 model is illustrated in Figure 4.1. Point "O" represents an element of soil with an existing effective overburden stress, σ'_o, and an in-situ creep rate , $\dot{\varepsilon}^p_{c-age}$. If a load, $\sigma_{p\,ref}$ is applied at the current strain rate $\dot{\varepsilon}^p_{c-age}$, the stress-strain path would follow O-B. The plastic strain increment is given by:

$$\varepsilon^p = \left(C_{\varepsilon c} - C_{\varepsilon r}\right) \log\left(\frac{\sigma_{p-ref}}{\sigma_o}\right) \qquad (4.1)$$

If the load were applied to instantaneously increase the strain rate from $\dot{\varepsilon}^p_{c-age}$ to $\dot{\varepsilon}^p_{c-ref}$, the stress-strain path would follow O-A-B and produce the plastic strain increment, ε^p:

$$\varepsilon^p = C_\alpha \log\left(\frac{\dot{\varepsilon}^p_{c-ref}}{\dot{\varepsilon}^p_{c-age}}\right) \qquad (4.2)$$

Equating 4.1 and 4.2 and substituting OCR = $\sigma_{p\text{-}ref}$ / σ_o produces an expression for OCR as a function of in-situ creep rate, $\dot{\varepsilon}^p_{c-age}$ and the reference creep rate:

$$OCR = \left(\frac{\dot{\varepsilon}^p_{c-ref}}{\dot{\varepsilon}^p_{c-age}}\right)^{C\alpha / \left(C\varepsilon c - C\varepsilon r\right)} \qquad (4.3)$$

Since $\dot{\varepsilon}^{p}_{c-age} = C_{\alpha} \big/ \left(2.3 \cdot t_{age}\right)$, equation 4.3 can be written in terms of time, t_{age} and t_{ref}:

$$OCR = \left(\frac{t_{age}}{t_{ref}}\right)^{C\alpha/(C\varepsilon c - C\varepsilon r)} \qquad (4.4)$$

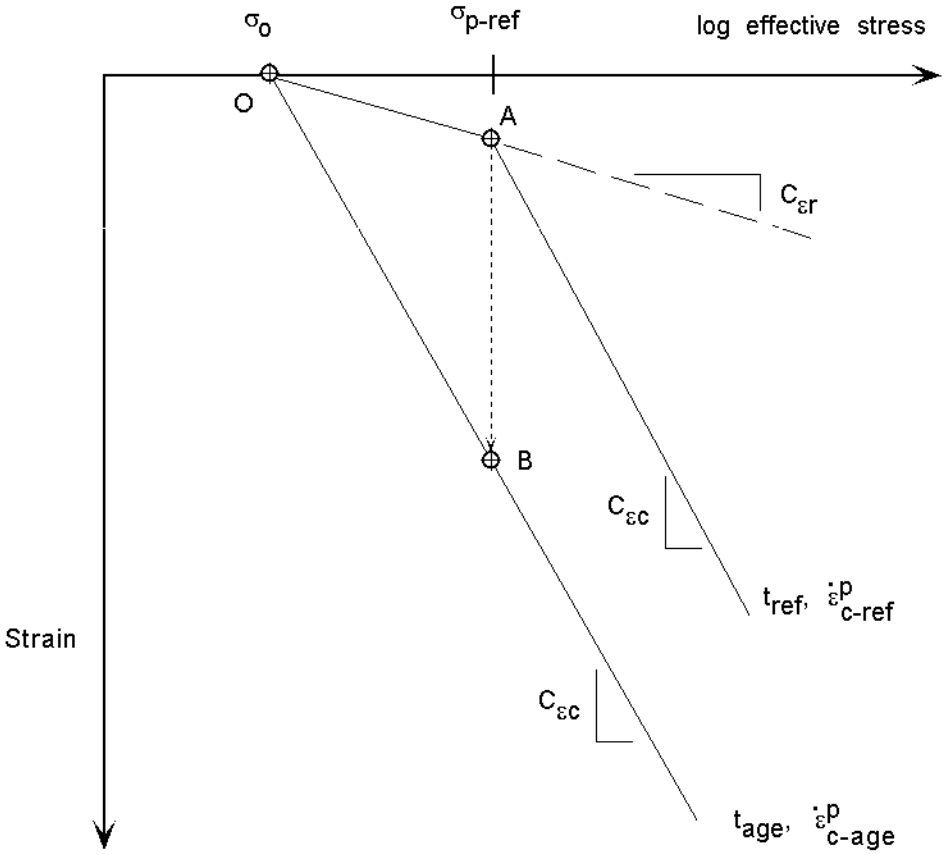

FIGURE 4.1: Relationship between OCR, in-situ creep rate and reference creep rate

Consider a 30 meter thick layer of San Francisco Bay Mud with the soil properties illustrated in Figure 4.2. The layer is drained at the top and the value of OCR varies from 2.0 at the top to

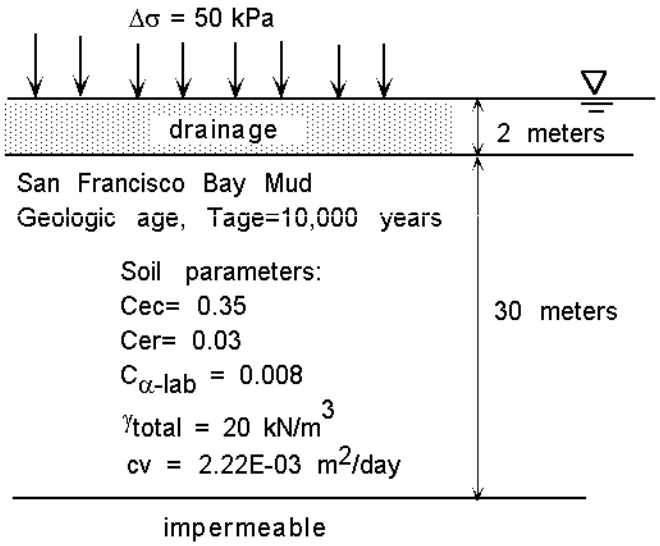

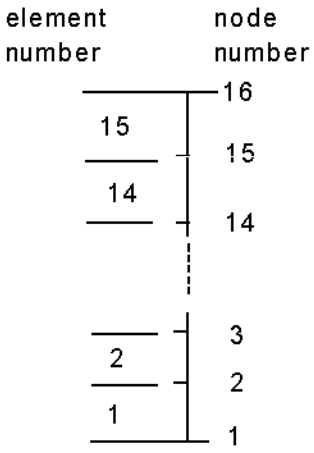

Element thickness, Δh= 2 meters

Other model parameters:

viscosity, η_o = 1.0 E+06 kPa-minute

Yield tolerance, tol = 0.1

γ_{water} = 10 N/m^3 γ_{fill} = 20 N/m^3

Bulk modulus of water = 2.0E+06 kPa

(a) Problem geometry

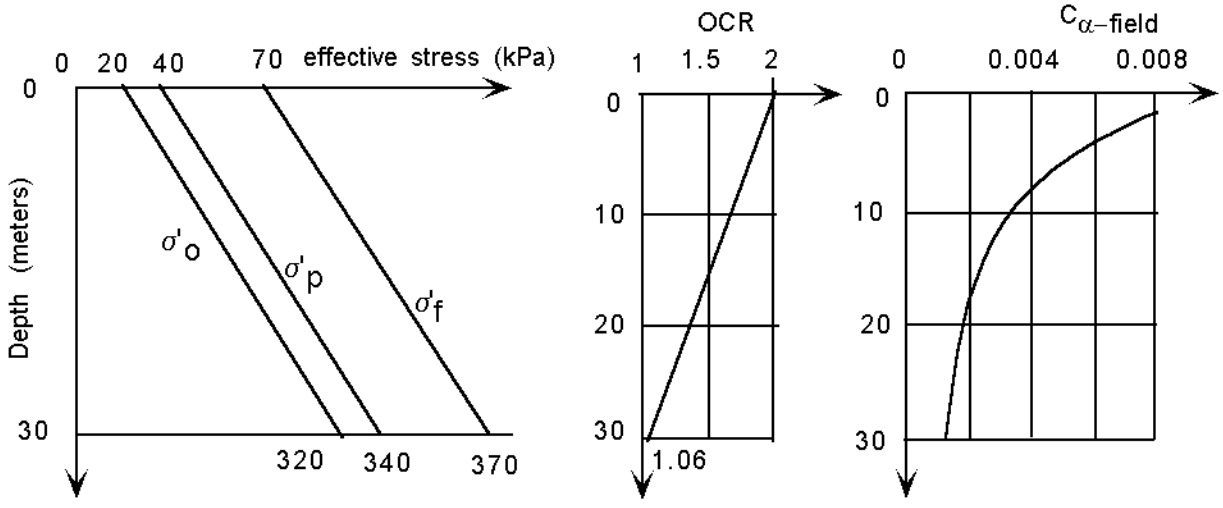

(b) Stress, OCR and field C_α profiles

Figure 4.2: Finite element model for in-situ creep rate study

1.06 at the bottom of the layer. Applying equation 4.4 with t_{ref} = 1 day, and the geologic age of the deposit is estimated at 10,000 years (Trask, P. D. and Rolston, J. W., 1961), the CS1 model would be consistent with an OCR of about 1.45 throughout the clay layer, which would not be consistent with laboratory measurements of preconsolidation pressure on undisturbed specimens. Thick deposits of geologically recent clay may have an overconsolidated crust near the surface, but at increasing depths, values of OCR typically decrease to values slightly greater than one. This contradiction between OCR values from laboratory test data and from CS1 computations indicates that the initial creep rate used by the original CS1 model was inconsistent with actual in-situ conditions defined by OCR, age of the deposit and, $C_{\alpha lab}$.

An examination of the reliability of using laboratory measured preconsolidation pressures and C_α values indicated that using $\sigma^o_{p\ ref}$ values determined from lab tests may be more reliable than using C_α values determined from lab tests. Field settlement measurements of relatively thin layers of clay confirm that lab determined $\sigma^o_{p\ ref}$ values are reasonably accurate. Long term field values of C_α are less reliable because secondary compression that occurs after 20 years or more of primary consolidation settlement is rarely measured. Using constant C_α values determined from a relatively short duration laboratory test (typically 24 hours for each load increment) to model much longer geologic time periods does not acknowledge the influence of other non-mechanical effects on soil behavior such as thixotropy or chemical bonding.

Therefore, the CS1 program was modified to compute values of $C_{\alpha\ field}$ that are consistent with measured preconsolidation pressures and the age of the deposit. The in-situ creep rate, $\dot{\varepsilon}^p_{c-age}$ for a soil deposit with a geologic age, t_{age} is given by:

$$\dot{\varepsilon}^p_{c-age} = C_{\alpha field} \Big/ \left(2.3\, t_{age}\right) \qquad (4.5)$$

The in-situ creep rate consistent with OCR and t_{age} is obtained from equation 4.3 by substituting $C_{\alpha\text{-field}}$ for C_α , and solving for $\dot{\varepsilon}^p_{c-age}$:

$$\dot{\varepsilon}^{p}_{c-age} = \left(\frac{C_{\alpha field}}{2.3t_{ref}}\right)\left(\frac{1}{OCR}\right)^{(C\varepsilon c - C\varepsilon r)/C\alpha field} \tag{4.6}$$

Equating 4.5 and 4.6 and solving for $C_{\alpha field}$:

$$C_{\alpha field}\Big/\left(2.3\,t_{age}\right) = \left(\frac{C_{\alpha field}}{2.3t_{ref}}\right)\left(\frac{1}{OCR}\right)^{(C\varepsilon c - C\varepsilon r)/C\alpha field} \tag{4.7}$$

$$t_{ref}\Big/t_{age} = \left(1/OCR\right)^{(C\varepsilon c - C\varepsilon r)/C\alpha field} \tag{4.8}$$

$$\ln\left(t_{ref}/t_{age}\right) = \left(\frac{C_{\varepsilon c} - C_{\varepsilon r}}{C_{\alpha field}}\right)\ln\left(\frac{1}{OCR}\right) \tag{4.9}$$

$$\left(\frac{C_{\varepsilon c} - C_{\varepsilon r}}{C_{\alpha field}}\right) = \frac{\ln\left(t_{ref}/t_{age}\right)}{\ln\left(1/OCR\right)} \tag{4.10}$$

$$C_{\alpha field} = \left(C_{\varepsilon c} - C_{\varepsilon r}\right)\left(\frac{\ln\left(OCR\right)}{\ln\left(t_{age}/t_{ref}\right)}\right) \tag{4.11}$$

The value of C_α used in the analyses varies between $C_{\alpha field}$ and $C_{\alpha\,lab}$. The value of C_α is adjusted continuously until the computed effective stress σ'_v becomes equal to σ'^{o}_{p-ref} using the following parabolic equation:

$$C_\alpha = C_{\alpha lab} - \left(C_{\alpha lab} - C_{\alpha field}\right)\left(\frac{\left(\sigma^{o}_{p-ref}/\sigma'_v\right)-1}{\left(\sigma^{o}_{p-ref}/\sigma'^{o}_{v}\right)-1}\right)^{1/2} \tag{4.12}$$

The rate of delayed compression and the yield computations are based upon C_α from equation 4.12. If the soil deposit has been mechanically over-consolidated and the C_α computations indicate that $C_{\alpha\,field}$ exceeds $C_{\alpha\,lab}$, then $C_{\alpha\,field}$ is set equal to $C_{\alpha\,lab}$.

The relationship between the CS1 creep rate lines and CONSOL97 creep rate lines are shown in Figure 4.3. For the given initial effective overburden stress, σ'_o, preconsolidation stress, σ^{o}_{p-ref} , and geologic age, the in-situ creep rate line, represented by the line labeled "$C_{\alpha lab}$ creep rate line", does not pass through the initial effective stress-strain state. The modified value of C_α

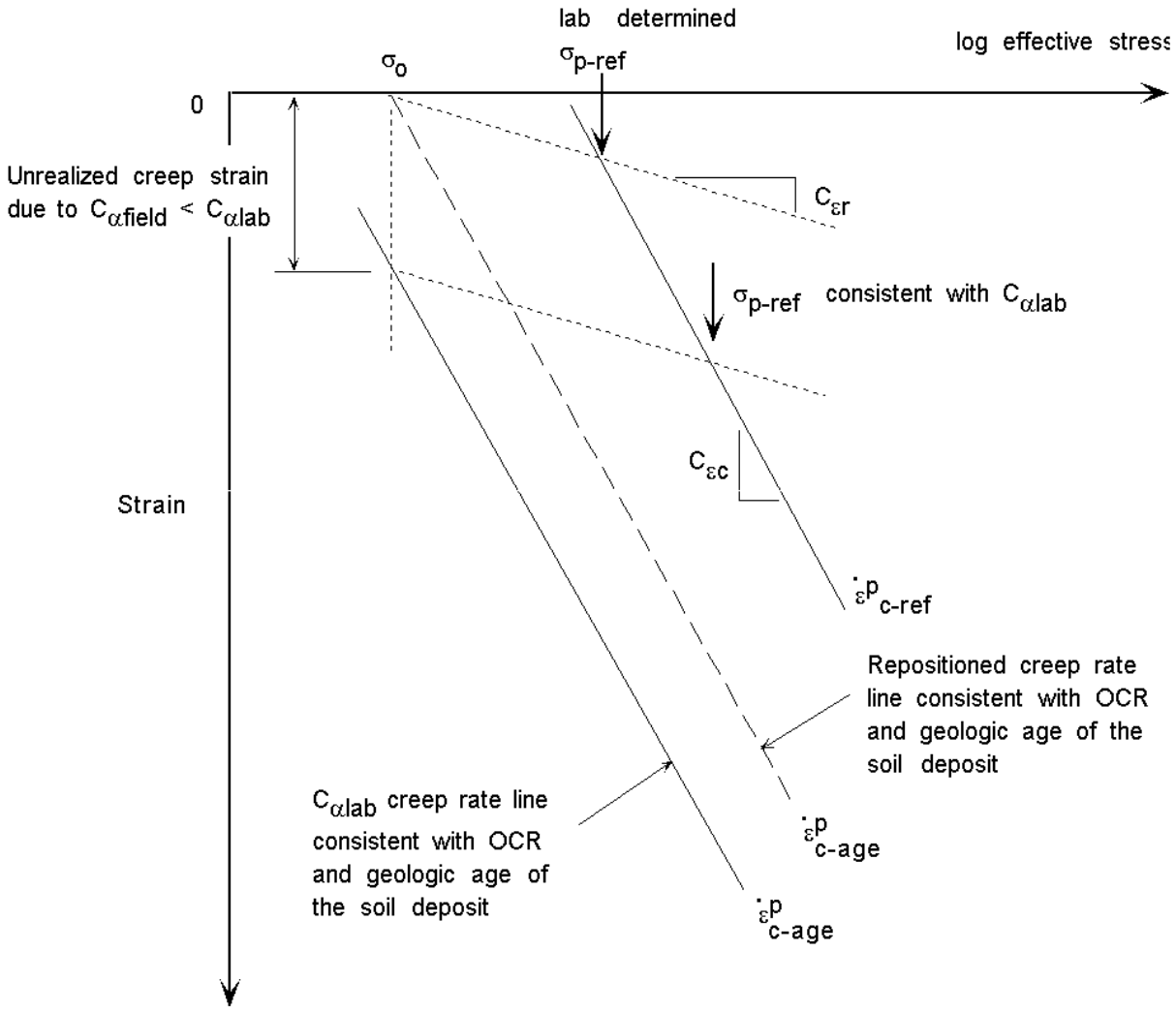

Figure 4.3: Relationship between CS1 creep rate lines and CONSOL97 creep rate lines

compresses the time lines and repositions the "$C_{\alpha lab}$ creep rate line" to pass through the initial effective stress-strain state. In essence decreasint the value of C_α to $C_{\alpha\,field}$ reduces the amount of creep strain to values consistent with the age and OCR of the deposit.

The revised CS1 model was used to analyze the 30 meter thick layer of San Francisco Bay Mud illustrated in Figure 4.2a. The computed values of $C_{\alpha field}$ that are consistent with OCR and the geologic age of the deposit are shown in Figure 4.2b. $C_{\alpha\,field}$ values equal $C_{\alpha\,lab}$ values (0.008) in the top 2 meters of the soil profile where the values of OCR exceeded 1.46. Below a depth of about 2 meters, the computed $C_{\alpha\,field}$ values decreased to reflect slower in-situ creep rates consistent with OCR and geologic age of the deposit.

The CONSOL97 strain-log time results in Figure 4.4 indicate about 7% more layer compression at the end of primary consolidation than CS1. The additional layer compression occurred after the average degree of consolidation exceeded about 50%. As expected, both the CS1 and CONSOL97 results indicate faster rates of consolidation and 28% to 35% more layer compression at the end of primary consolidation than conventional CONSOL results.

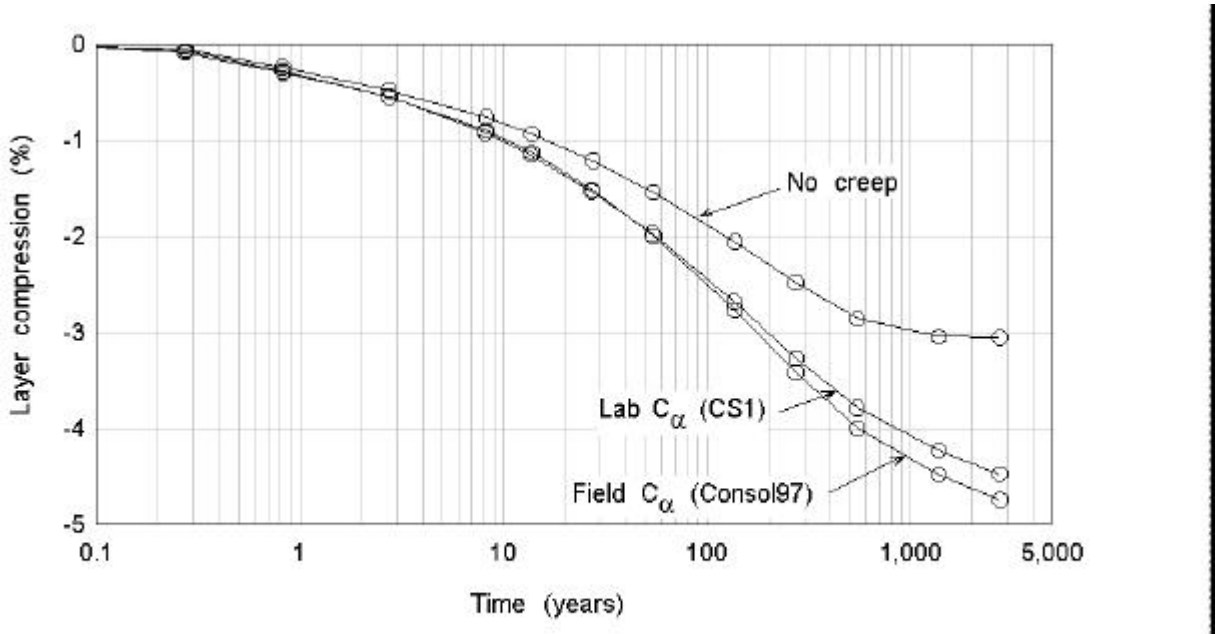

Figure 4.4: Layer compression vs. log time for 30 meter thick layer of San Francisco Bay Mud

The strains computed by CONSOL97 for each sublayer were larger than the strains computed by CS1 when the in-situ creep rates were slower than those computed CS1. An additional 5% strain was computed for a soil element at a depth of 5 meters and an additional 19% strain was computed for a soil element at a depth of 29 meters. The creep, instant and total strains during consolidation at a depth of 29 meters are shown in Figure 4.5. The results indicate that most of the additional strain computed by CONSOL97 is attributable to the instant strain component.

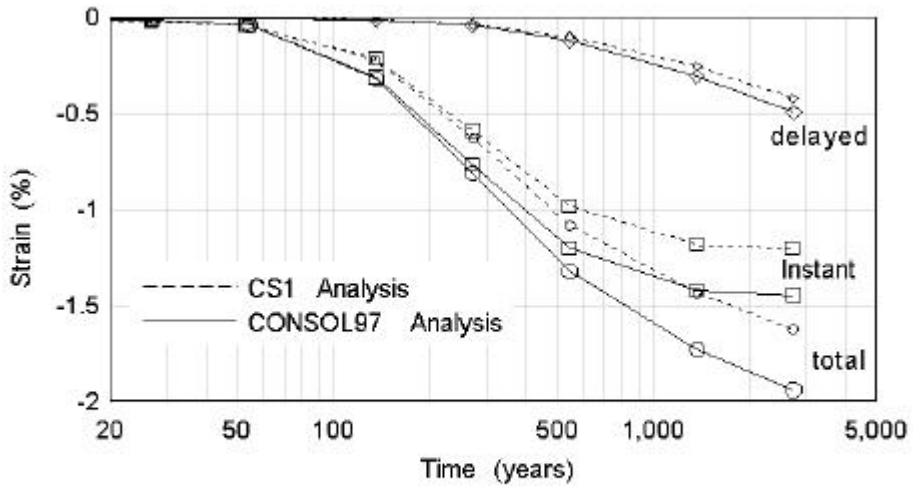

Figure 4.5: Strain components vs. log time at a depth of 29 meters

The computed stress-strain and OCR-log time behavior at a depth of 29 meters is shown in Figures 4.6 and 4.7. Both plots indicate that yielding occurs more quickly and at lower effective stresses in the CONSOL97 computations than for the CS1 computations. The CONSOL97 stress-strain path follows a slower creep rate line than CS1 does and therefore, produces more compression.

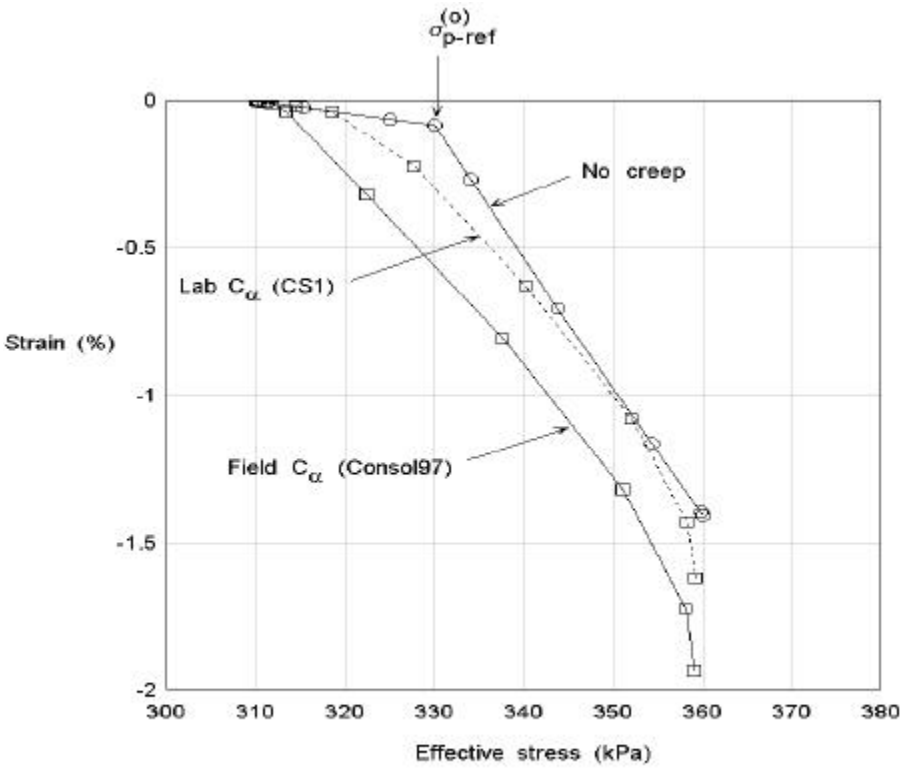

Figure 4.6: Stress-strain behavior at a depth of 29 meters

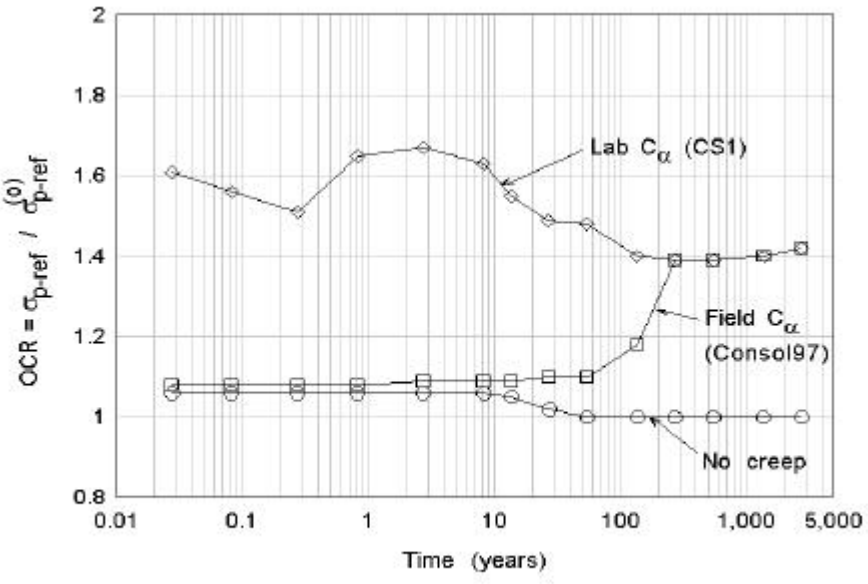

Figure 4.7: OCR vs log time at a depth of 29 meters

At the start of loading, the rate of consolidation calculated by CS1 is much slower than the assumed in-situ rate of creep compression and the soil hardens (yield stress increases), which seems illogical. Compression strains consist of instant elastic and creep until the rate of consolidation "catches up" with the creep rate to produce yielding and instant plastic compression strain. In contrast, the CONSOL97 in-situ creep rate at the start of loading is close to the rate of consolidation and the soil element quickly yields and produces instant plastic compression strains.

During the consolidation process, the CS1 program calculated unusually large values of preconsolidation stress, $\sigma_{p\,ref}$ at the bottom of the layer. The initial input value of the preconsolidation stress ($\sigma^{(o)}_{p-ref}$) was 340 kPa at a depth of 29 meters, corresponding to an OCR of 1.06. After 2.7 years of consolidation CS1 predicted $\sigma_{p\,ref}$ = 519 kPa. At the end of pore pressure dissipation after about 1400 years, $\sigma_{p\,ref}$ decreased to a value of 503 kPa corresponding to an OCR value of 1.4 ($OCR = \sigma_{p-ref}/\sigma'_v$). The CONSOL97 results appear more reasonable because they show less hardening at the bottom of a thick singly drained layer. The reference preconsolidation stress, $\sigma_{p\,ref}$, remained nearly constant at 340 kPa while the effective stress, σ'_v, remained less than $\sigma^{(o)}_{p-ref}$. When σ'_v exceeded $\sigma^{(o)}_{p-ref}$ after about 110 years, $\sigma_{p\,ref}$ increased to about 450 kPa (OCR=1.2). At the end of consolidation, the computed preconsolidation stress was 501 kPa (OCR=1.4).

CONSOL97 models in-situ conditions which are affected by non-mechanical processes such as thixotropy or chemical bonding, more consistently than does CS1. For thick clay layers, CONSOL97 predicts more layer compression and it better represents the creep rates and corresponding preconsolidation stresses during consolidation.

4.1.2 Loading Options

CONSOL97 sets the initial excess pore pressures equal to the changes in vertical stress ($\Delta u = \Delta\sigma$) throughout the depth of the stratum at the beginning of the analysis. The values of change in vertical stress can be defined by the user at each sublayer boundary (finite element node) or they

can be calculated by CONSOL97. For loads of infinite lateral extent, such as placement or removal of large areal fills, the change in vertical stress is constant over the depth of the stratum:

$$\Delta\sigma_v = \Delta h \cdot \gamma_f \qquad (4.13)$$

where: $\Delta\sigma_v$ is the change in vertical stress, Δh is the thickness of fill added or removed, γ_f is the unit weight of the fill. The change in vertical stress due to a change in water level is:

$$\Delta\sigma_v = \Delta h_w \cdot \gamma_w \qquad (4.14)$$

where: Δh_w is the change in water level, γ_w is the unit weight of water.

For loads acting over areas of finite lateral extent, such as strip loads, or circular loads, the change in stress are not constant over the depth of the layer. CONSOL97 calculates stress influence factors (I_z) at each node based on equations from Boussinesq's elastic theory. The changes in vertical stress due to a surface load, q, are given by:

$$\Delta\sigma_v = q \cdot I_z \qquad (4.15)$$

Stress influence factors and equations for a uniform strip load of infinite length are shown in Figure 4.8. The equations can be used to calculate the change in vertical stress at any position for a strip of any width. The graph in the lower part of Figure 4.8 shows how the value of I_z changes with depth (z), strip width (b), and distance (x) from the center of the strip.

Stress influence factors beneath the center and the edge of circular loaded areas are shown in Figures 4.9 and 4.10. Boussinesq's equation for I_z beneath the center of the load is shown in the upper part of Figure 4.9, and the variation of I_z with Z/R is shown in the lower portion. There is no closed form expression for I_z at other locations beneath circular loaded area. However, approximate values of I_z for stresses beneath the edge of the loaded area are shown by the plotted points in the lower part of Figure 4.10. These were obtained from a chart published in NAVFAC DM 7.1 (198??). The numerical approximation of these values of I_z used in CONSOL97 are shown by the line in the lower part of Figure 4.10.

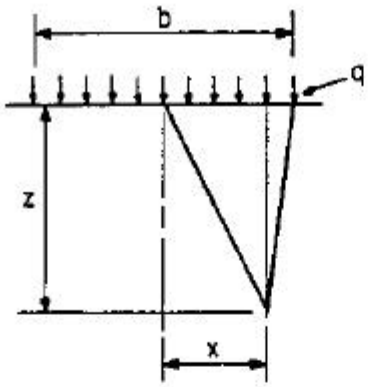

b = width of strip

x = distance from of strip

The equations for the Boussinewq Stress Influence Factor, I:

$$\alpha = \tan^{-1} [(x - b/2)/z] \quad \ldots(1)$$

$$\beta = \tan^{-1} [(x + b2)/z] - \alpha \quad \ldots(2)$$

$$I = 1/\pi [\beta + \sin(\beta) \cos(\beta + 2\alpha)] \quad \ldots(3)$$

The change in vertical stress is then given by:

$$\Delta\sigma = I \cdot q \quad \ldots(4)$$

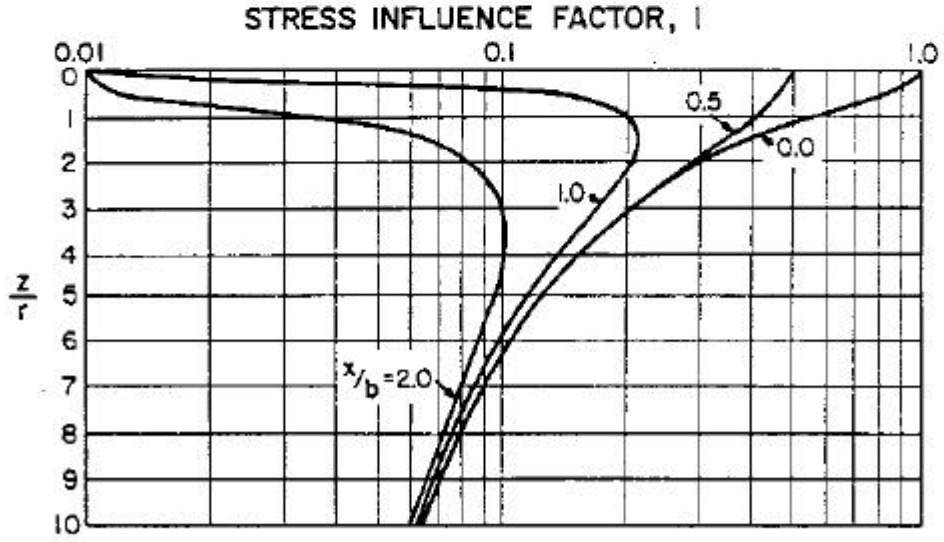

Figure 4.8: Boussinesq stress influence factors for an infintely long strip load (from Duncan et al. 1988)

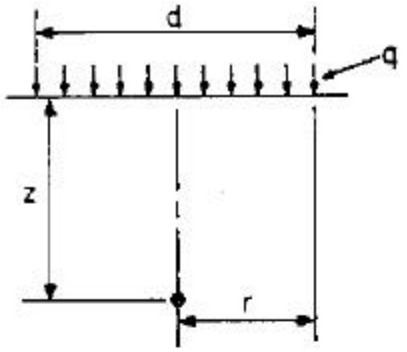

z = depth

r = radius = d/2

The equation for the Boussinesq Stress Influence Factor, I:

$$I = 1.0 - \frac{1}{(r/z)^4 + 1}^{1.5} \qquad \ldots(1)$$

The change in vertical stress is then given by:

$$\Delta\sigma = I.q \qquad \ldots(2)$$

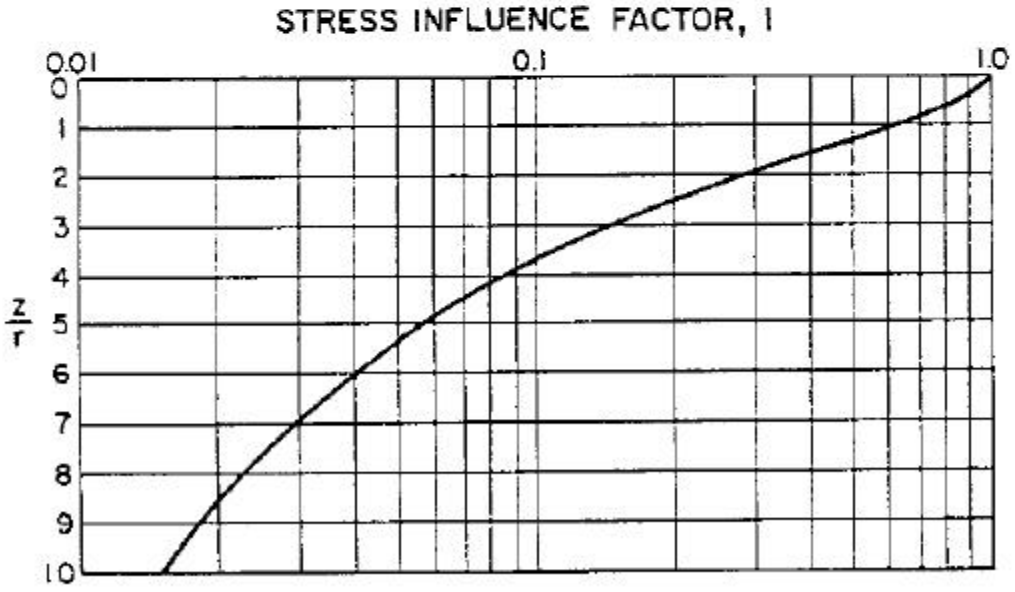

Figure 4.9: Boussinesq stress influence factors for stresses beneath the center of a circular loaded area (from Duncan et al. 1988)

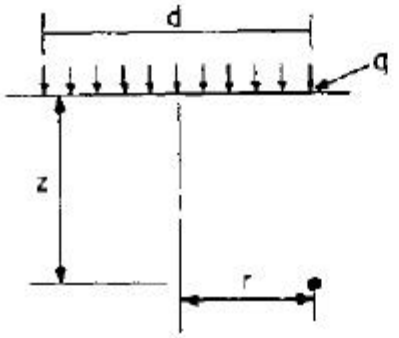

z = depth

r = radius = d/2

The equation for the Boussinesq Stress Influence Factor, I:

for z/r ≤ 0.5:	$\alpha = -0.3010 - 0.1412*z/r$	...(1)
for 0.5 ≤ z/r < 1.0:	$\alpha = -0.2617 - 0.2197*z/r$	...(2)
for 1.0 ≤ z/r < 1.5:	$\alpha = -0.2403 - 0.2411*z/r$	...(3)
for 1.5 ≤ z/r < 4.0:	$\alpha = -0.2883 - 0.2092*z/r$	...(4)
for 4.0 ≤ z/r < 7.0:	$\alpha = -0.4888 - 0.1590*z/r$	...(5)
for 7.0 ≤ z/r:	$\alpha = -1.0844 - 0.0739*z/r$	...(6)

The stress influence factor is given by:

$I = 10^{\alpha}$ ...(7)

The change in vertical stress is then given by:

$\Delta\sigma = I \cdot q$ ...(8)

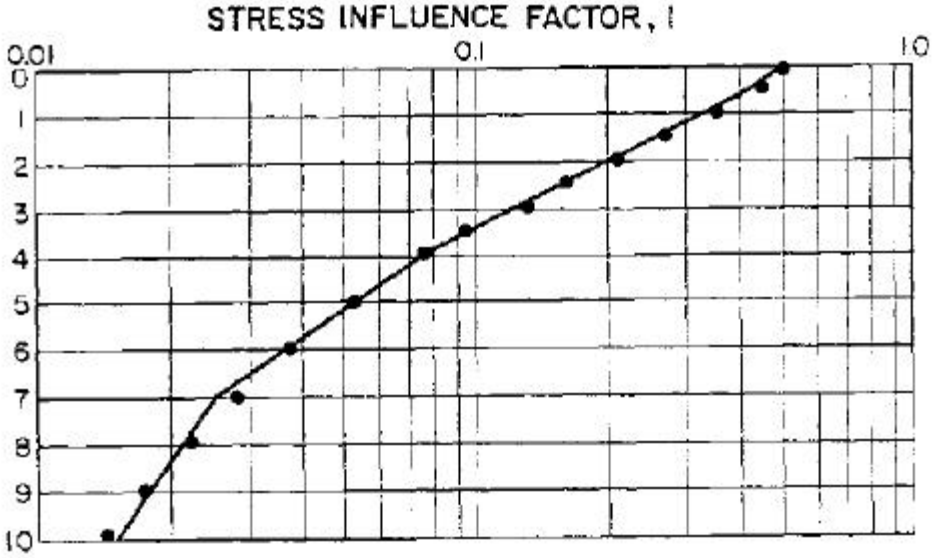

Figure 4.10: Boussinesq stress influence factors for stresses beneath the edge of a circular loaded area (from Duncan et al 1988)

For an under-consolidated soil profile, the reference preconsolidation stresses are less than the computed initial effective stresses, σ'_{vo}, based on hydrostatic pore pressure conditions. CONSOL97 first computes the magnitude of excess pore pressures at each node:

$$\Delta u = \sigma'_{vo} - \sigma'_{p-ref} \tag{4.16}$$

and then redefines the values of initial effective stresses in the under-consolidated sublayers so that they are equal to the preconsolidation stresses.

4.1.3 Fill Submergence and Unsaturated Soil Zones

Settlement of the ground surface during consolidation can cause submergence of existing newly placed fill soils. A buoyancy correction is required to account for the resulting changes in excess pore pressure. Figure 4.11 illustrates the correction used in CONSOL97. If the loads are of finite lateral extent, the settlement will not be uniform, and the change in vertical stress due to buoyancy effects will not be uniform across the loaded area. CONSOL97 has two options to account for these effects. The first option approximates these buoyancy effects by adjusting the excess pore pressures at each sublayer as if the fill were of infinite lateral extent. The second option adjusts the excess pore pressures by an amount that is equal to the correction shown in Figure 4.11, multiplied by the stress influence factors computed for each sublayer.

For unsaturated materials, a portion of the compression occurs instantaneously upon application of the load, and Δu may be appreciably smaller than $\Delta\sigma_v$. For these conditions, the assumptions used in CONSOL97 will lead to higher-than-actual pore pressures and slower-than-actual settlement rates.

When field piezometric levels indicate that the groundwater surface is located below the top of the soil profile, the pore water pressure distribution above the groundwater table cannot be easily determined. CONSOL97 was formulated based on hydrostatic groundwater conditions (total

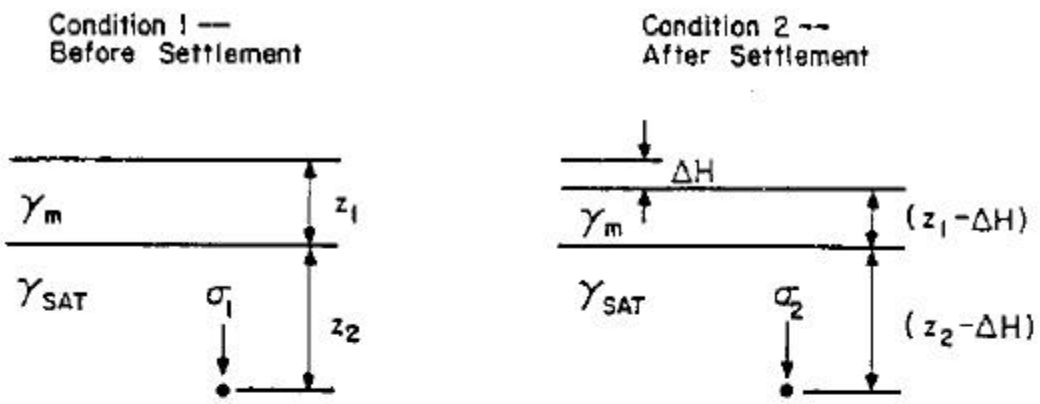

$\sigma_1' = z_1\ \gamma_m + z_2\ (\gamma_{sat} - \gamma_w)$ $\sigma_2' = (z_1-\Delta H)\ \gamma_m + (z_2+\Delta H)(\gamma_{sat} - \gamma_w)$

The change in equilibrium effective stress (after all excess pore pressure has dissipated) due to submergence of a layer of fill thickness, ΔH, can be expressed as:

$$\Delta\sigma' = \sigma_2' - \sigma_1' \qquad \ldots(1)$$

$$\Delta\sigma' = (z_1-\Delta H)\ \gamma_m + (z_2+\Delta H)(\gamma_{sat} - \gamma_w) - z_1\ \gamma_m + z_2(\gamma_{sat} - \gamma_w) \qquad \ldots(2)$$

$$\Delta\sigma' = -\Delta H\gamma_m + \Delta H(\gamma_{sat} - \gamma_w) \qquad \ldots(3)$$

$$\Delta\sigma' = -\Delta H(\gamma_m + \gamma_w - \gamma_{sat}) \qquad \ldots(4)$$

The change in excess spore pressure (before any drainage or dissipation) is equal to the long term change in effective stress:

$$\Delta_u = \Delta\sigma' \qquad \ldots(5)$$

$$\Delta_u = -\Delta H(\gamma_m + \gamma_w - \gamma_{sat}) \qquad \ldots(6)$$

Figure 4.11: Derivation of correction for buoyancy effect (from Duncan et al 1988)

head is constant) throughout the soil profile prior to application of any loads except the under-consolidated case. Therefore, the piezometric head is negative in the unsaturated zone and positive in the saturated zone, as illustrated in Figure 4.12.

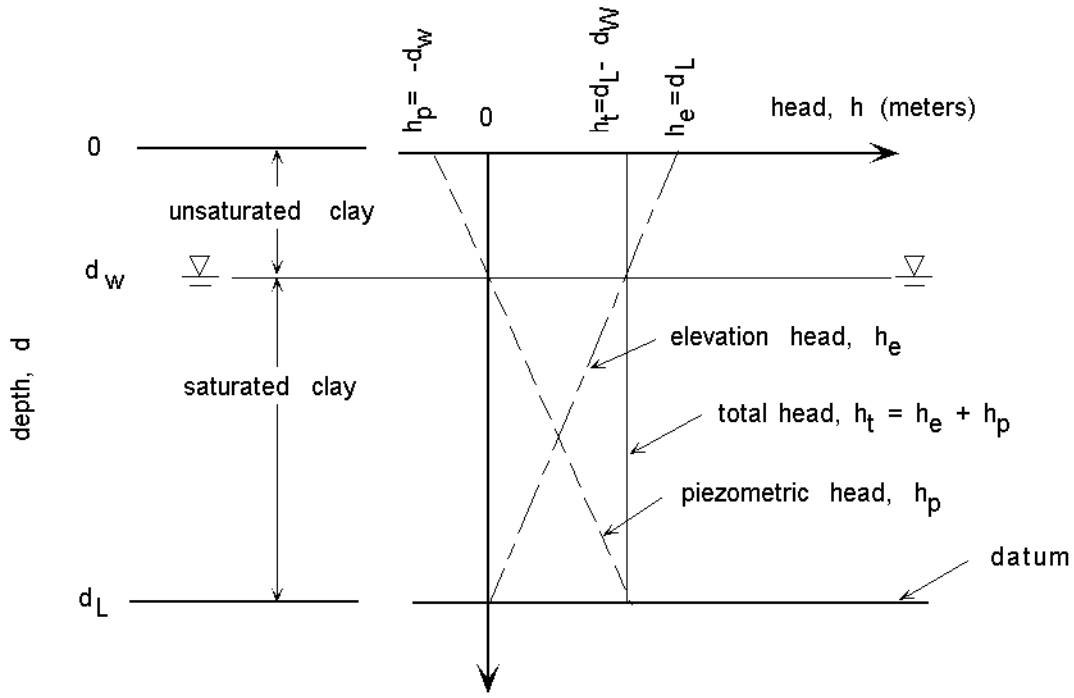

Figure 4.12: Long-term steady state head profile used by CONSOL97 for unsaturated clay profiles

4.1.4 Stress Dependent Compression Ratio, Coefficient of Secondary Compression, and Consolidation Coefficient

Figure 4.13 illustrates soil behavior typical of sensitive or organic clays. The strain vs. log effective stress behavior in Figure 4.13a is nonlinear in the virgin stress range. The slope of the virgin compression curve, $C_{\varepsilon c}$, decreases with increasing effective stress. The coefficients of consolidation, cv, and secondary compression, C_α, shown in Figures 4.13b and 4.13c also vary with effective stress.

Mesri and Godlewski (1977) have reported that secondary compression behavior is related to soil compressibility during primary consolidation and they proposed that $C_\alpha/C_{\varepsilon c}$ is constant for most

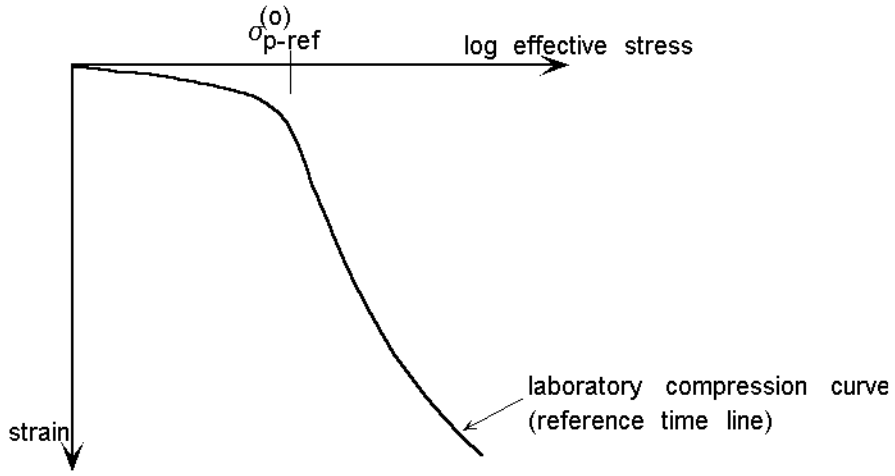

(a) Strain vs effective stress

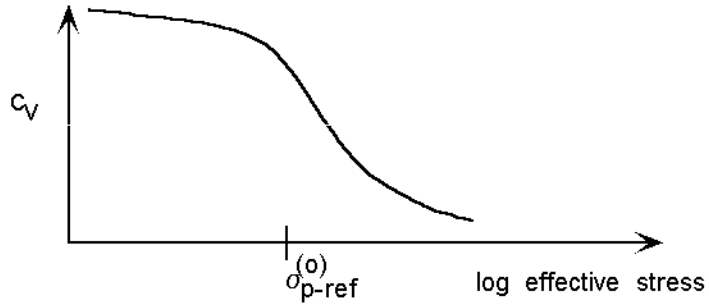

(b) Coefficient of consolidation vs. effective stress

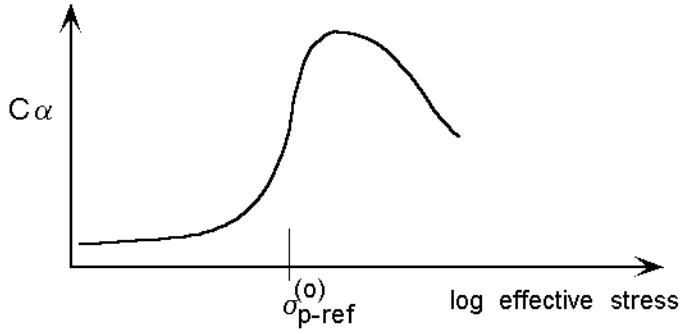

(c) Secondary compression coefficient vs. effective stress

Figure 4.13: Typical behavior of sensitive or organic clays

soils. For a non-linear strain vs log stress relationship in which $C_{\varepsilon c}$ varies, the secondary compression coefficient, C_α must also change if $C_\alpha/C_{\varepsilon c}$ is constant. In this case, the creep rate of the reference time line or any of the other parallel time lines is not constant. Figure 4.14a illustrates a set of non-linear time lines. Creep rate isograms can be determined from the information in Figure 4.14a. A schematic representation of one creep rate isogram is given in Figure 4.14b.

CONSOL97 can model stress-dependent $C_{\varepsilon c}$, c_v and C_α values. The non-linear strain vs. log stress relationship is approximated by linear segments, as illustrated in Figure 4.14a. Each segment number, j, is defined by a value of effective stress, $\sigma_{(j)}$ at the start of the segment, a value of $C_{\varepsilon c(j)}$, and a value of $C_{\alpha(j)}$. For the first segment (j=1), σ_1 equals the value of the initial reference preconsolidation stress, $\sigma^{(o)}_{p-ref}$. CONSOL97 uses this information to compute creep rates and permeabilities that conform to the nonlinear time lines at each time step.

As described in Chapter 3, the creep rate depends on the computed values of critical stress, and reference preconsolidation stress; changes in permeability depend on the computed equivalent stress. The following sections describe the derivation of the expressions for critical stress, reference preconsolidation stress, and equivalent stress for stress-dependent soil behavior.

Critical stress

The relationship between critical stress, σ_p, and the reference preconsolidation stress, σ_{p-ref}, for non-linear strain vs. log effective stress is shown in Figure 4.15. If the soil skeleton is yielding at point A, the current stress equals the critical stress, σ_p. An expression for the critical stress at point A can be derived by considering two stress-strain paths due to loading from σ_p to σ_{p-ref}: path A-C in which the soil skeleton continues to yield and path A-B-C in which the soil

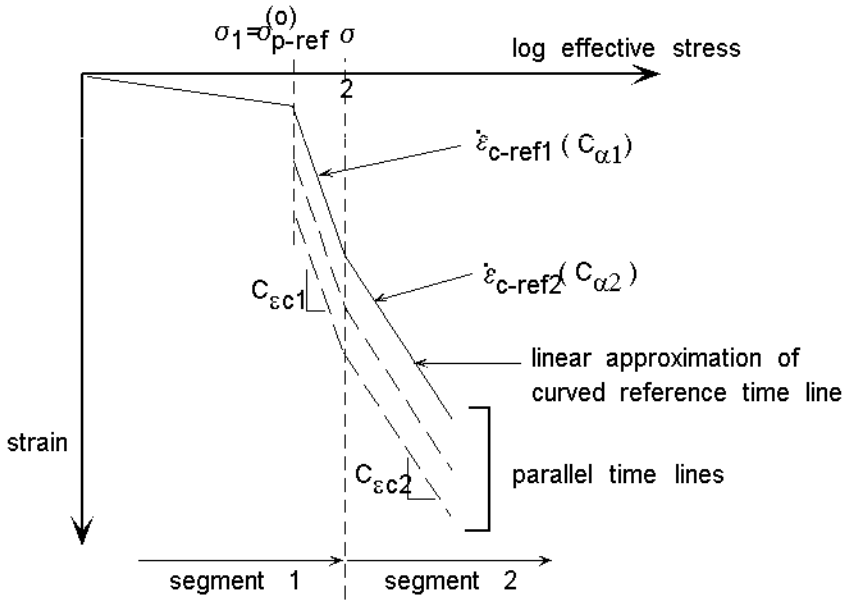

(a) CONSOL97 time line approximations for non-linear strain vs. log effective stress

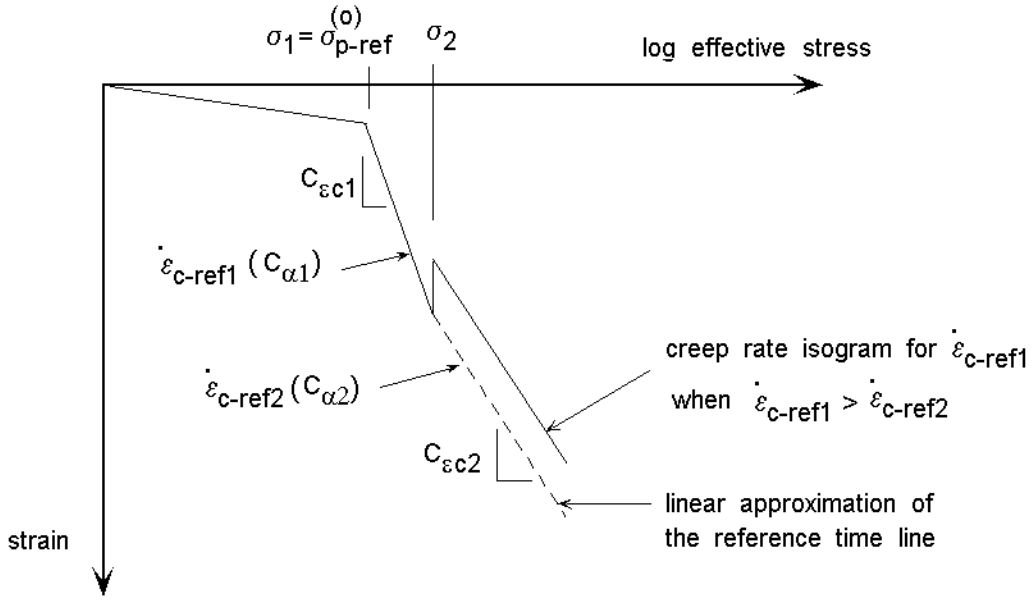

(b) Creep rate isogram when C_α varies with effective stress

Figure 4.14: CONSOL97 nonlinear time lines

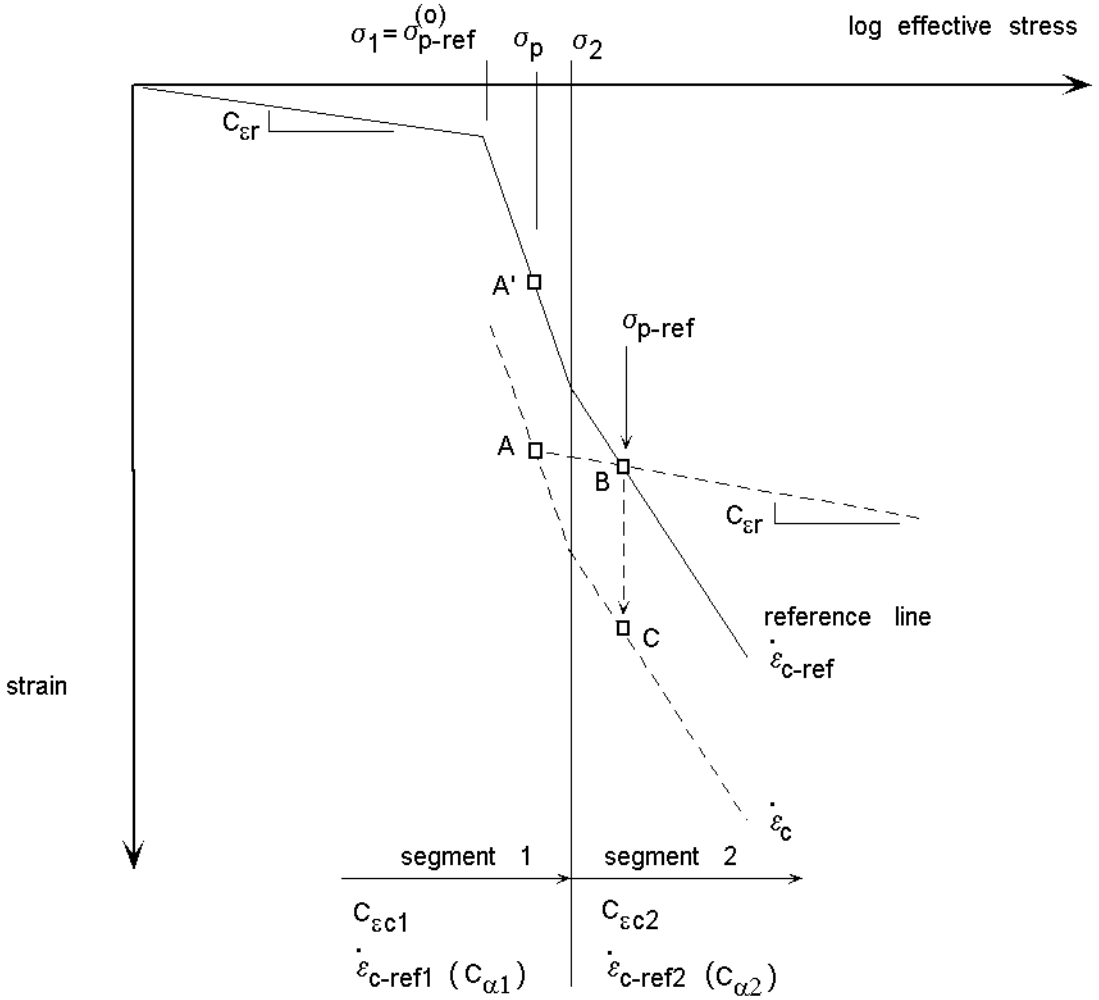

Figure 4.15: Relationship between critical stress, σ_p, and refererence preconsolidation stress, $\sigma_{p\text{-}ref}$, for non-linear strain vs. log stress

instantaneously compresses elastically from point A to B followed by creep compression from B to C. The strain increment, $d\varepsilon_{a\text{-}c}$, is the same magnitude as $d\varepsilon_{a\text{-}b} + d\varepsilon_{b\text{-}c}$. The plastic strain component, $d\varepsilon^p$, is:

$$d\varepsilon^p = d\varepsilon_{b-c} = d\varepsilon_{a-c} - d\varepsilon_{a-b} \qquad (4.17)$$

and

$$d\varepsilon_{b-c} = C_{\alpha 2} \log\left(\frac{\dot{\varepsilon}_{c-ref}}{\dot{\varepsilon}_c}\right) \tag{4.18}$$

$$d\varepsilon_{a-c} = C_{\varepsilon c1} \log\left(\frac{\sigma'_2}{\sigma'_p}\right) + C_{\varepsilon c2} \log\left(\frac{\sigma_{p-ref}}{\sigma'_2}\right) \tag{4.19}$$

$$d\varepsilon_{a-b} = C_{\varepsilon r} \log\left(\frac{\sigma'_2}{\sigma_p}\right) + C_{\varepsilon r} \log\left(\frac{\sigma_{p-ref}}{\sigma'_2}\right) \tag{4.20}$$

Substituting equations 4.18, 4.19, and 4.20 in equation 4.17 and solving for the critical stress σ_p:

$$\sigma_p = \sigma'_2 \left[\left(\frac{\sigma_{p-ref}}{\sigma'_2}\right)^{\frac{C_{\varepsilon c2} - C_{\varepsilon r}}{C\varepsilon c1 - C\varepsilon r}} \Big/ \left(\frac{\dot{\varepsilon}_{c-ref2}}{\dot{\varepsilon}_{c2}}\right)^{\frac{C\alpha 2}{C\varepsilon c1 - C\varepsilon r}} \right] \tag{4.21}$$

Reference Preconsolidation Stress

An expression for the reference preconsolidation stress, σ_{p-ref} in equation 4.21 may be derived in terms of the initial reference preconsolidation stress, $\sigma^{(o)}_{p-ref}$, and the total plastic creep strain. Consider recompression loading in Figure 4.16 from the initial effective stress at point O to the current effective stress, $\sigma_{current}$, at point D. The total amount of plastic creep strain, $\varepsilon^p_c - \varepsilon^{p(o)}_c$, along path O-D is the same as the amount of plastic strain, $\varepsilon^p - \varepsilon^{p(o)}$, along the path O-A-B-C:

$$\varepsilon^p_c - \varepsilon^{p(o)}_c = \left(C_{\varepsilon c1} - C_{\varepsilon r}\right) \log\left(\frac{\sigma'_2}{\sigma^{(o)}_{p-ref}}\right) + \left(C_{\varepsilon c2} - C_{\varepsilon r}\right) \log\left(\frac{\sigma_{p-ref}}{\sigma'_2}\right) \tag{4.22}$$

Solving for the reference preconsolidation stress, σ_{p-ref}:

$$\sigma_{p-ref} = \sigma'_2 \exp\left[\frac{2.3\left(\varepsilon^p_c - \varepsilon^{p(o)}_c\right)}{C_{\varepsilon c2} - C_{\varepsilon r}} - \frac{C_{\varepsilon c1} - C_{\varepsilon r}}{C_{\varepsilon c2} - C_{\varepsilon r}} \ln\left(\frac{\sigma'_2}{\sigma^{(o)}_{p-ref}}\right)\right] \tag{4.23}$$

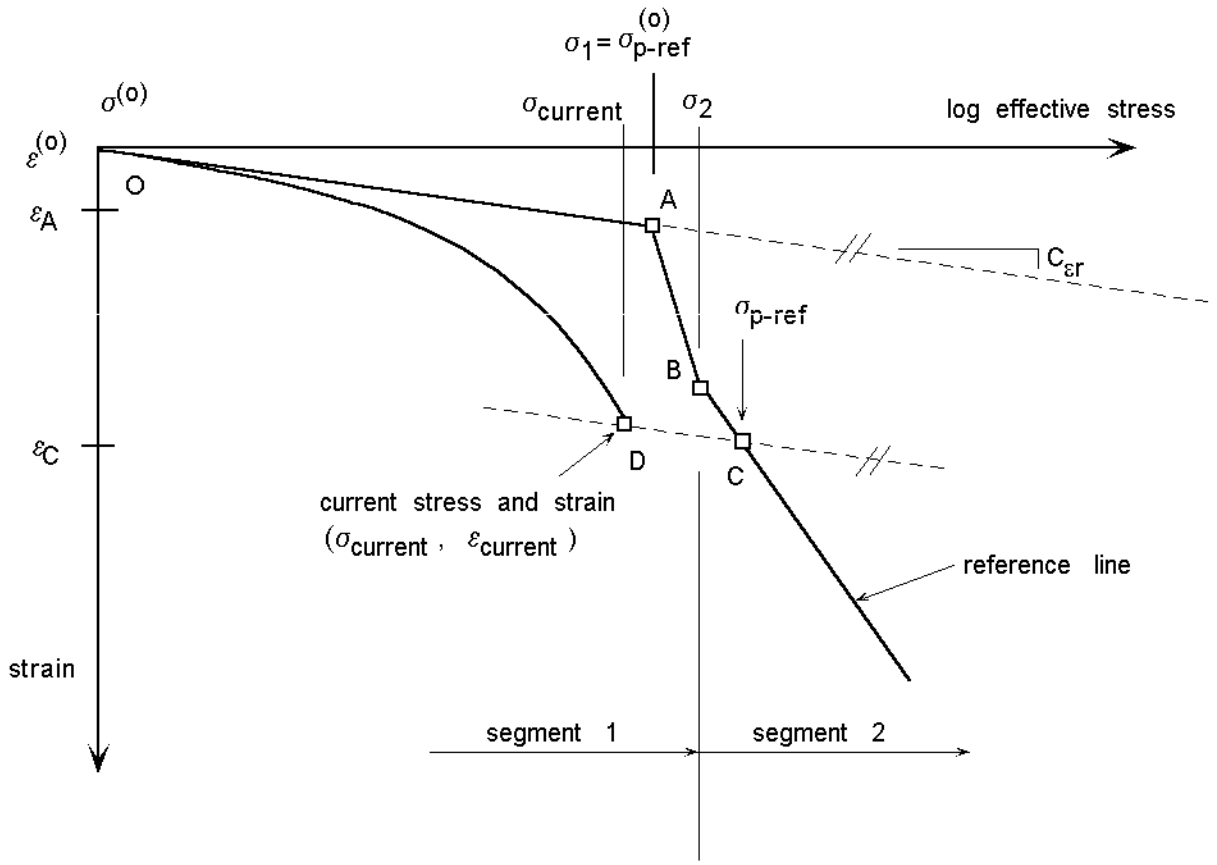

Figure 4.16: Influence of creep during recompression on the reference preconsolidation stress, $\sigma_{p\text{-}ref}$, for non-linear strain vs. log effective stress

Equivalent Stress for Permeability Computations

The equation for computing new permeabilities during consolidation:

$$k = \frac{c_v \cdot C_c \cdot \gamma_w}{2.3 \cdot (1 + e_o) \cdot \sigma'_v} \qquad (3.38)$$

requires an effective stress, σ'_v, on the reference time line or an equivalent effective stress, σ'_{equiv}, that produces the current void ratio on the reference virgin compression curve. The equivalent

effective stress on the non-linear strain vs effective stress line is illustrated in Figure 4.17 and can be expressed as follows:

$$\sigma'_{equiv} = \sigma'_2 \exp\left[\frac{2.3}{C_{\varepsilon c2}}\left\{\varepsilon_A - \frac{C_{\varepsilon r}}{2.3}\ln\left(\frac{\sigma^{(o)}_{p-ref}}{\sigma'_o}\right) - \frac{C_{\varepsilon c1}}{2.3}\ln\left(\frac{\sigma'_2}{\sigma^{(o)}_{p-ref}}\right)\right\}\right] \qquad (4.24)$$

The value of c_v in equation 3.38 corresponds to the effective stress, σ'_{equiv} .

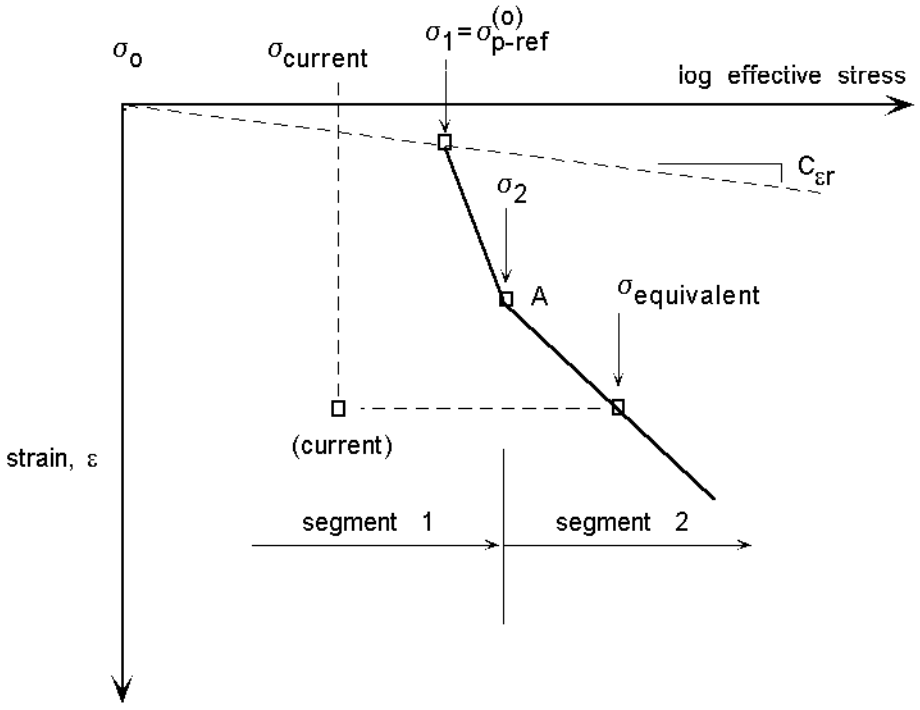

Figure 4.17: Relationship between permeability and nonlinear strain-log effective stress

Generalized Formulations

Equations 4.21 and 4.23 and 4.24 can be generalized for any number of stress-strain segments. The reference preconsolidation stress (equation 4.23):

$$\sigma_{p-ref} = \sigma_k \exp \frac{\left[2.3\left(\varepsilon_c^p - \varepsilon_c^{p(o)}\right) - \sum_{j=(ns0+1)}^{j=k} 2.3\left(C_{\varepsilon c(j)} - C_{\varepsilon r}\right) \ln\left(\frac{\sigma_{(j)}}{\sigma_{(j-1)}}\right)\right]}{\left(C_{\varepsilon c(k)} - C_{\varepsilon r}\right)} \qquad (4.25)$$

where ns0 is the segment number of the strain-log stress curve that contains the initial reference preconsolidation stress, $\sigma_{p-ref}^{(o)}$, and the index k varies from (ns0+1) to (ns-1). CONSOL97 calculates $\sigma_{p\text{-}ref}$ for the smallest value of *k*, compares $\sigma_{p\text{-}ref}$ and the effective stress σ_{k+1} that defines the next stress-strain segment. If $\sigma_{p\text{-}ref}$ is less than σ_{k+1}, then k=k+1 and a new value of $\sigma_{p\text{-}ref}$ is computed. The desired value of $\sigma_{p\text{-}ref}$ corresponds to the largest value of *k* in which $\sigma_{p\text{-}ref}$ is less than or equal to σ_{k+1}. Using the this value of *k*, the critical stress (equation 4.21) is:

$$\sigma_p = \sigma_{ns} \left[\prod_{j=(ns+1)}^{j=k} \left(\frac{\sigma_j}{\sigma_{j-1}}\right)^{\frac{C\varepsilon c(j) - C\varepsilon r}{C\varepsilon c(ns) - C\varepsilon r}} \Bigg/ \left(\frac{\dot{\varepsilon}_{c-ref(ns)}}{\dot{\varepsilon}_{c(ns)}}\right)^{\frac{C\alpha(ns)}{C\varepsilon c(ns) - C\varepsilon r}} \right] \qquad (4.26)$$

where *ns* is the segment number corresponding to the current effective stress and $\sigma_k = \sigma_{p\text{-}ref}$.

The equivalent stress (equation 4.24) is:

$$\sigma'_{equiv} = \sigma'_k \exp\left[\frac{2.3}{C_{\varepsilon c(k)}} \left\{ \varepsilon - \frac{C_{\varepsilon r}}{2.3} \ln\left(\frac{\sigma_{p-ref}^{(o)}}{\sigma'_o}\right) - \sum_{j=ns0}^{j=k} \frac{C_{\varepsilon c(j)}}{2.3} \ln\left(\frac{\sigma'_j}{\sigma_{(j-1)}}\right) \right\} \right] \qquad (4.27)$$

where $\sigma_k = \sigma_{p\text{-}ref}$.

4.1.5 Numerical Accuracy and Stability

Numerical approximations inherent in the finite element method affect the accuracy of the solutions and the stability of the computations. Errors arise due to discretization of the soil continuum and the time domain. Instability can occur due to oscillations in values of pore pressure, and ill-conditioning of the element stiffness matrices. CS1 performance depends on control parameters such as: element thickness, Δh (number of elements); type of element (two-

noded linear elements or three-noded quadratic elements); time step size, Δt; time derivative coefficient, θ; yield tolerance, tol; convergence criteria on non-linear stress-strain behavior, eps; and the viscosity parameter, η_o, used in Rajot's model to initiate the numerical computations.

The author's familiarity with the performance characteristics of the CS1 computer program was acquired by running several hundred analyses over a period of 3 years. Although the basic algorithm is sound, the program's complexity can result in unsuccessful program executions or inaccurate results. The most significant characteristics of CS1 performance are summarized here:

- Computational times for CS1 elasto-visco-plastic analyses were much longer than conventional elasto-plastic analyses with the CONSOL program. For example, a conventional (elasto-plastic) CONSOL analysis of fill placement on a 3 meter thick clay layer represented by 20 linear elements requires less than 5 seconds on a 120 Mhz computer whereas a CS1 elasto-visco-plastic analysis requires about 40 seconds of computing time.

- Two-noded elements produce results that were as accurate and that require 25 % less computational time than three-noded elements.

- Oscillations in pore pressures and displacements occurred throughout the finite element mesh during load application and for a short time after loading. The magnitude of the oscillations depended on the magnitude and the rate of loading. During the times when oscillations occurred, computed nodal displacements and pore pressures are inaccurate. When oscillations subside, the computations become accurate.

- The CS1 automatic time-stepping routine produced accurate results when appropriate minimum and maximum time step size limits were used. However, accurate results and successful program executions depended on the selection of the correct time step sizes for a

specific loading, subsurface profile, soil properties, finite element mesh and yield tolerance values, which an inexperienced user would find difficult.

- The yield tolerance and convergence criteria values affected the accuracy and the success or failure of program execution. The time-stepping routine and convergence criteria were restrictive and resulted in many unsuccessful executions.

- Numerical convergence to a solution was affected more by time step size than by the number of elements. If the time step size was small enough, the yield tolerance and convergence criteria were not important factors in producing accurate computations.

- Unsuccessful computer runs generally failed during application of the load or during the early stages of consolidation, because the effective stresses in some of the elements exceeded the tolerable critical stress value.

- The automatic time-stepping routine significantly reduced the computational time, without significantly reducing computational accuracy.

- Increasing η_o from 10^4 to 10^7 kPa-minute, increased the computed strains and reduced the error in computed strain from about -3.5% to about -0.5%. However, when $\eta_o = 10^7$, the computed strain log time behavior of a lab specimen during secondary compression was found to be non-linear and C_α was found to be about 16% too small. A viscosity value of 10^6 kPa-minute produced results that closely matched all of the exact solutions so that values of ε, $C_{\varepsilon c}$, C_α, and σ'_{p-ref} were very close to the ideal theoretical values.

To illustrate the importance of time step size, Δt, on the performance characteristics of CS1, an incrementally loaded laboratory oedometer test was simulated, in which each of two load increments were applied for one day. The specimen (2.54 cm thickness) was represented by 4, 8,

16, 32 or 64 linear elements of equal thickness. The soil properties, model parameters, initial stresses, preconsolidation stress, finite element mesh and loading schedule are shown in Figure 4.18. The convergence and yield tolerance criteria were not used in these analyses. The time step size, Δt, was held constant for 400 minutes after each load application (the end of primary consolidation was about 180 minutes after load application). Analyses were performed using initial time step sizes of 0.01, 0.05, 0.1, 0.5, and 1.0 minutes. After 400 minutes, the time step size was increased to 5.0 minutes in all analyses.

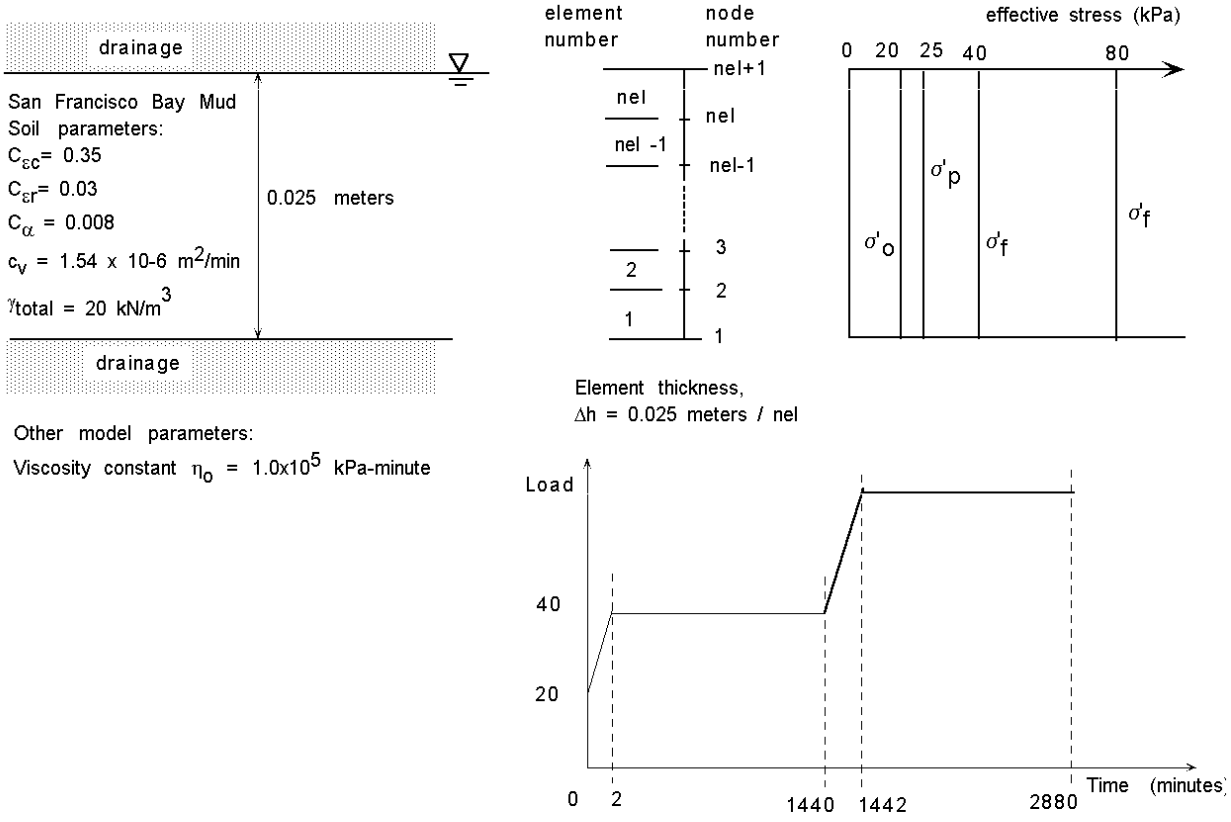

Figure 4.18: Problem geometry and loading for time step stability study

The effect of Δt on computed strains are summarized in Figure 4.19. The results indicate that time step size is more important in producing strain convergence than the number of elements.

With decreasing time step size, the strains increase and, at a time step size of 0.01 minutes, converge to the same value, ε_{con} for all element thickesses. A mesh size $\Delta h/H_o \leq 0.2$ and a time step size less than about 0.05 minutes would provide good accuracy and computational efficiency in this case.

The computational time for the 32 element model and a time step size of 0.01 minutes was about 13 minutes on a 120 Mhz computer. Using the automatic time-stepping routine in CS1 in which the time step size could vary from 0.01 minutes to 1.0 minutes, the computation time was reduced to about 1-1/4 minutes and the accuracy was only slightly diminished (about a 1% change).

These performance characteristics were the basis for changes made to CS1 and incorporated in CONSOL97. The changes were designed to improve computational stability and efficiency without sacrificing significant accuracy. The following changes were incorporated in CONSOL97 to simplify and improve computational performance of the CS1 program:

- The sublayers are represented by two-noded elements (linear interpolation functions).

- The yield tolerance has been removed from the computations and the convergence criteria (eps) for non-linear stress-strain behavior has been relaxed from 10^{-6} to 10^{-2}. Computational accuracy is controlled by proper selection of mesh thickness and an internally determined time step size based on mesh size, c_v, and layer thickness.

- The time step size, Δt, during loading and for a short time after loading, is set equal to a minimum value Δt_{min} that is determined by CONSOL97. Subsequently, CONSOL97

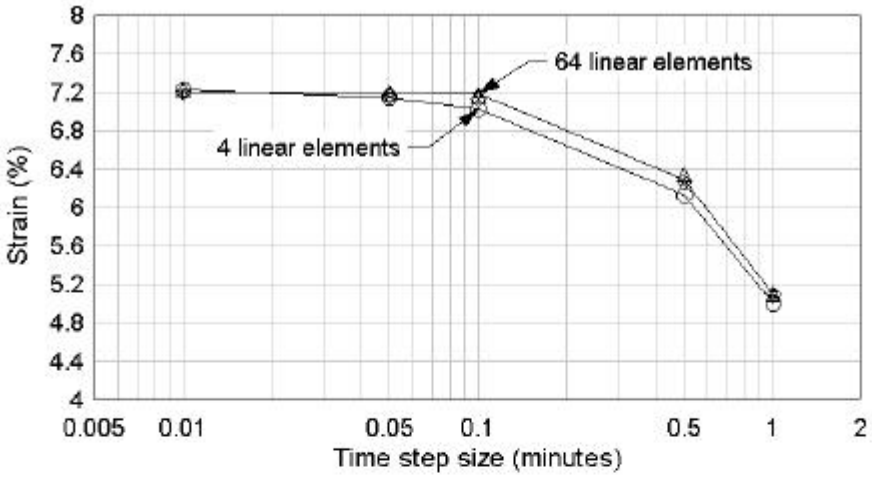

(a) Load increment from 20 kPa to 40 kPa

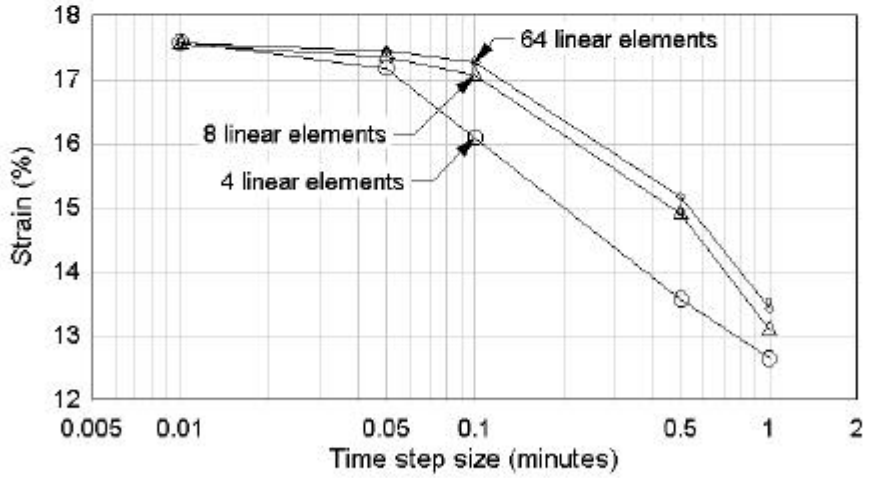

(b) Load increment from 40 kPa to 80 kPa

Figure 4.19: CS1 time step size convergence study for an oedometer test simulation.

- computes a maximum time step, Δt_{max}, and automatically selects Δt within the range of Δt_{min} and Δt_{max}.

- The user must specify the number of time steps to use between two specified output times. This provides the user with some control over the duration of the computations. Fewer time increments will reduce computational time but may decrease computational accuracy.

The minimum time step value, Δt_{min}, corresponds to the value Δt that produces numerical convergence when it is used for the full duration of the analysis. Based on numerous CS1 analyses of lab test and field loading simulations, the relationship between coefficient of consolidation (c_v), element thickness (Δh), and Δt_{min} that was found to work well is given by:

$$\Delta t_{min} = 10^{-2} \cdot \frac{\Delta h^2}{c_v} \qquad (4.29)$$

CONSOL97 uses the following procedure to select a suitable time step size during the computations:

1. Use equation 4.29 to compute Δt_{min} for each element. Select the smallest value for use in the analysis.
2. Compute Δt_{max} by dividing each time period between two consecutive output times into equal time step intervals. A single value for the number of intervals is specified by the user. The following equation can be used to estimate Δt_{max}:

   $$\Delta t_{max} = 0.1 \cdot \frac{\left(H_k / nel\right)^2}{c_v} \qquad (4.30)$$

   where H_k is the longest drainage distance for layer k and nel is the number of elements in the layer.
3. During application of the load and for a duration equal to $100 \cdot \Delta t_{min}$ after the full load application, use the time step Δt_{min}, and remove the convergence and yield tolerance criteria.

4. Subsequent time step sizes are automatically selected such that (a) $\Delta t_{min} \le \Delta t \le \Delta t_{max}$, (b) the criteria for convergence equal 10^{-2} is satisfied, and (c) and a yield tolerance is satisfied. A yield tolerance of 0.1 is internally prescribed for elasto-visco-plastic analyses and 0.01 for conventional analyses.

In any finite element analysis, the user should verify that the solution has converged to within an acceptable range of the numerically correct solution. This can be accomplished by increasing the number of elements and/or decreasing the time step increment (increasing the number of time step increments): if the solution has converged, the new solution should be very close to the previous solution. For some elasto-visco-plastic analyses, the user may encounter a combination of subsurface profile, loading, and soil properties that produces computational failure. In such cases, the user should consider using a refined finite element mesh, or using CONSOL97 to perform a elasto-plastic analysis.

4.1.6 Mesh Design

The selection of an appropriate number of sublayers for each soil layer depends on the drainage boundary conditions, soil properties, specified convergence tolerance, and the type of analysis. A conventional consolidation analysis requires fewer sublayers than a elasto-visco-plastic analysis to achieve accurate results. Thinner sublayers near drainage boundaries (where hydraulic gradients are largest), and thicker sublayers near the center of a soil layer and near impermeable drainage boundaries, will provide more accurate results and efficient analyses.

The user should model the least permeable soil layer such that the sublayers near the drainage boundaries are thinner than $0.2H_o$. Other sublayers should be modeled such that the sublayer thicknesses at the drainage boundaries are proportional to $\sqrt{c_v}$ for each layer. However, if the layers are made too thin for a elasto-visco-plastic analysis, computational difficulties may occur due to machine precision limitations.

To accommodate these guidelines, CONSOL97 includes a mesh generation subroutine that can sub-divide each soil layer to produce the following mesh geometries: 1. uniformly thick elements; 2. increasing element thickness with increasing depth; 3. decreasing element thickness with increasing depth; 4. increasing element thickness followed by decreasing element thickness with depth. The user specifies the desired number of sub-layers and the type of mesh geometry for each layer. If a non-uniform mesh geometry is selected, CONSOL97 sizes the adjacent elements so each larger element is twice as thick as the adjacent smaller element.

4.2 CONSOL97 INPUT DATA

The data file required to operate CONSOL97 is created from information provided by the user in a series of data input screens. This user friendly interface operates in a Windows environment with several tools to assist the user. This chapter describes the general type of data that the user must provide in the input screens. A description of specific data input procedures and variables may be found in Appendix A, "CONSOL97 User's Manual."

The CONSOL97 input file consists of five types of data: 1. control data to specify the type of output file, number of time steps, and output times; 2. subsurface data to define the subsurface profile and the finite element mesh that will be used to model the subsurface profile; 3. soil property data for each soil type including the existing stress state (normally consolidated, overconsolidated, or underconsolidated); 4. boundary data that identifies free draining layers within the soil profile; 5. load data that specifies the magnitude and schedule of each load application.

This data generally consists of familiar soil properties obtained from standard incremental oedometer tests, and other easily determined information based upon the specific problem

geometry. To simplify the operation of CONSOL97, some of the required data has been pre-programmed.

4.2.1 Problem Description and Control

The user has options for specifying the type of analysis (elasto-visco-plastic or conventional elasto-plastic), type of output file, the specific times at which computational results should be provided, and the set of dimensional units (force, length, and time).

Several control parameters have been prescribed in CONSOL97. However, the user can control the numerical computations by changing the number and thickness of the finite element mesh and the number of time steps between the specified output times. The user can significantly affect the computational accuracy by increasing the number of time steps, which decreases the time step size.

4.2.2 Subsurface Profile and Finite Element Mesh

A soil layer is a portion of the soil profile that contains one soil type, one type of stress state or preconsolidation profile (underconsolidated, normally consolidated, or overconsolidated) and in which the σ^{o}_{p-ref} profile is constant or linearly varying with depth. Drainage boundaries must coincide with the top or bottom of a soil layer. Figure 4.20 illustrates two soil profiles divided into appropriate soil layers based on soil types, σ^{o}_{p-ref} profile, and drainage conditions.

The selection of an appropriate number of sub-layers for each soil layer will depend on the drainage boundary conditions, soil properties, and the type of analysis. A conventional consolidation analysis will require fewer layers than a time dependent CONSOL97 analysis.

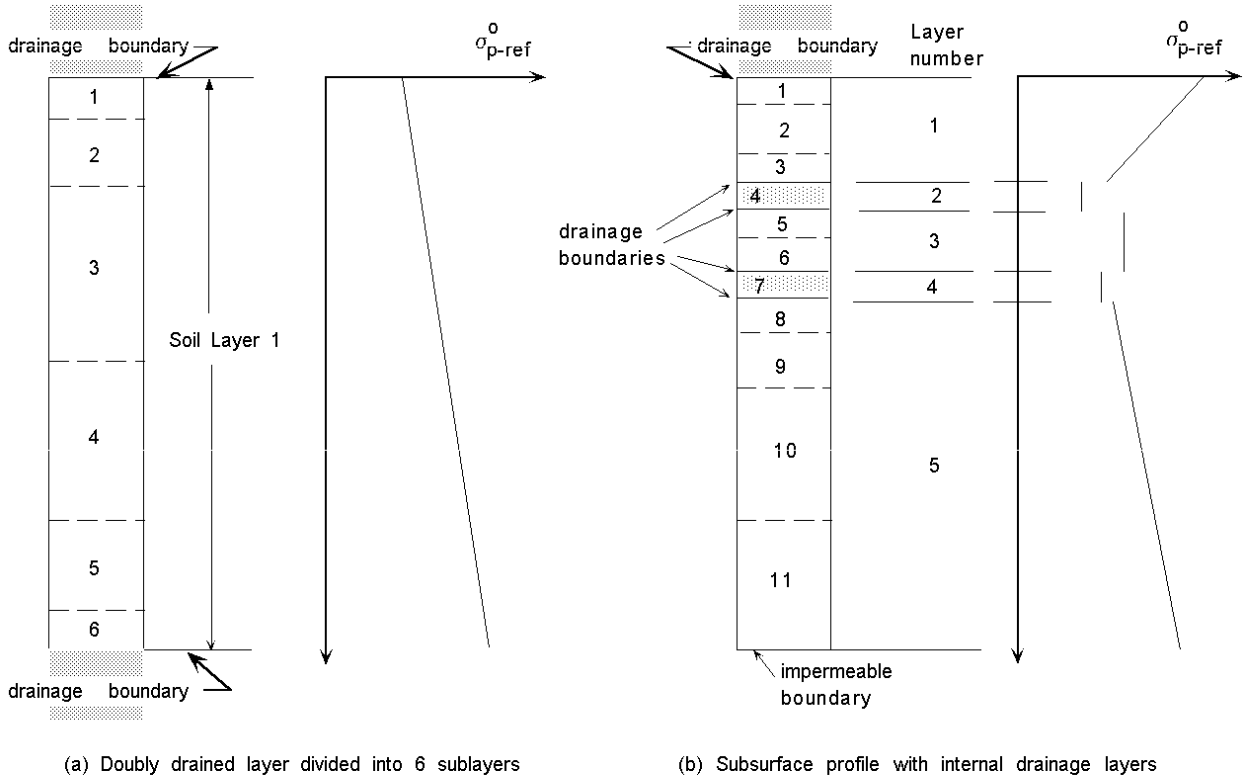

(a) Doubly drained layer divided into 6 sublayers

(b) Subsurface profile with internal drainage layers

Figure 4.20: Divison of a subsurface profile into layers and sublayers

4.2.3 Soil Properties

All of the soil properties needed to perform a conventional or elasto-visco-plastic analysis can be determined from a standard incremental oedometer test. A elasto-visco-plastic analysis uses all of the soil properties required for a conventional analysis plus two additional soil parameters: the coefficient of secondary compression C_α and the estimated geologic age of the soil deposit.

The values of in-situ void ratio (e), virgin compression index (C_c), recompression index (C_r), coefficient of consolidation (c_v), secondary compression coefficient (C_α) , and preconsolidation pressure (σ^o_{p-ref}) are determined from laboratory test results using conventional procedures. Multiple values of C_c, C_α, and c_v are used for each soil type if the behavior is stress dependent. If

the soil profile has more than one soil type, different values of C_c, C_r, c_v, C_α, T_{age} are used for each soil type. The geologic age (T_{age}) of the deposit is usually estimated from published information about the specific geologic unit identified on the site.

A standard 24 hour oedometer test (ASTM 2435) is typically used to determine the stress - strain relationships at the end of primary or at 24 hours. The 24 hour strains will include some secondary compression strain but several investigators (Leroueil et al, 1985) have determined that the value of C_c for both end of primary and 24 hour strain values are the same but σ^o_{p-ref} can be about 10 to 20% larger and C_r can be smaller for end of primary strains. For time dependent analyses, the user specifies both σ^o_{p-ref} and the reference time at which the measured strains occurred. For a conventional test in which each load is applied for 24 hours, the reference time is 24 hours. The reference time for σ^o_{p-ref} values determined from the end of primary consolidation strains is the time to end of primary, t_{eop}.

As illustrated in Figure 4.21, the values of C_r and σ^o_{p-ref} depend on the duration of loading used in the laboratory tests. The reference preconsolidation stress is determined by Casagrande's graphical procedure. CONSOL97 assumes that the value of C_r represents elastic behavior without creep compression and the location of the reference time line is defined by the intersection of the elastic recompression line and the reference preconsolidation stress. Since creep compression occurs at all stress levels, it is not possible to obtain the true elastic recompression line. However, the amount of creep strain can be minimized by using the portion of the recompression curve corresponding to an overconsolidation ratio greater than 2 to obtain a revised recompression ratio, C_r.

For San Francisco Bay mud with C_α = 0.008, C_c = 0.9, and c_v = 1.54E-06 m^2/minute, the revised recompression ratio, C_r = 0.052 whereas the conventional C_r = 0.09. Using C_r = 0.052 changes the value of σ^o_{p-ref} on the reference time line. The revised σ^o_{p-ref} (σ_1 in Figure 4.21) value would

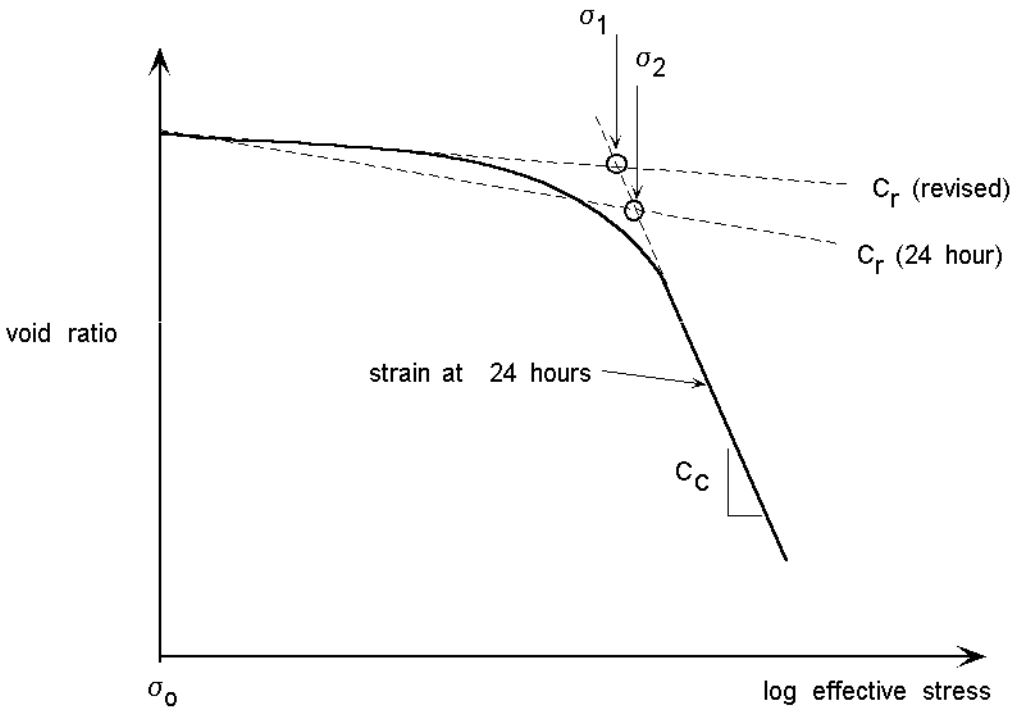

Definitions:

σ_o Initial effective overburden stress

σ_1 Revised reference preconsolidation stress for time-dependent analyses

σ_2 Reference preconsolidation stress for 24 hour loading

Figure 4.21: Definition of soil parameters

thus be less than the value of σ^{o}_{p-ref} determined from the one day (σ_2 in Figure 4.21) loading curve. The effect of these parameter modifications were examined by simulating an incremental oedometer test on a doubly drained 2.54 cm thick sample of San Francisco Bay Mud. The initial overburden stress was 20 kPa, σ^{o}_{p-ref} = 40 kPa and the applied loads were 40, 80 and 160 kPa. Using conventional C_r and σ^{o}_{p-ref} values, CONSOL97 results indicate about 22% more strain during recompression than the theoretical values (1.1% vs. 0.9%) and a correspondingly larger value of C_r. The revised parameters resulted in displacements and strains that match theoretical values for stress levels less than the preconsolidation stress. At larger stresses, the displacements and strains were the same for the revised and the conventional parameters.

If the proposed loading results in final stresses close to the preconsolidation stress, the revised value of C_r and σ^{o}_{p-ref} will provide more accurate results. For all other loading conditions, the user can select values of C_r and σ^{o}_{p-ref} that are consistent with the Casagrande method of construction.

The preconsolidation stress profile is determined from consolidation tests done on samples obtained from various depths in the soil profile. For each consolidatoin test, a range of values of σ^{o}_{p-ref} should be found and plotted on a graph simlar to those shown in Figure 4.22, where the bars indicate the possible range of values of σ^{o}_{p-ref} consistent with the test data. The profile line is a “best fit” curve through the ranges of σ^{o}_{p-ref} values. A simlar procedure should be used to evaluate the “best fit” void ratio curve. The stress state at any depth in the subsurface profiel will either be underconsolidated (UC), normally consolidated (NC), or overconsolidated (OC). Each of these stress states is illstrated in Figure 4.22.

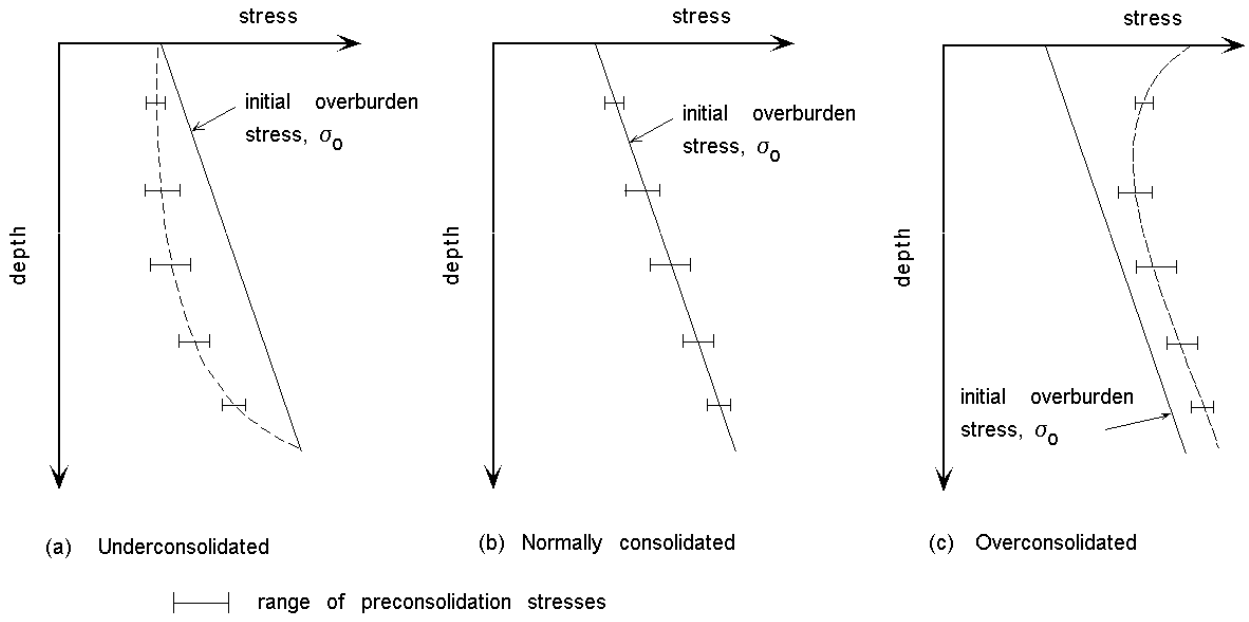

Figure 4.22: Preconsolidation stress profiles

4.2.4 Boundary Conditions

CONSOL97 numerically solves for displacements and pore pressures at each sublayer boundary except at drainage boundaries which have known boundary conditions. CONSOL97 assumes no displacement at the bottom of the soil profile. However, the user must specify the location of drainage boundaries so that CONSOL97 can calculate the hydrostatic pore pressures at these locations. During the computations, the boundary pore pressures are updated after each time step to account for settlement or changes in the groundwater level.

4.2.5 Loading Conditions

The change in vertical stress for each layer is computed based on the loading option specified by the user. With a minimum amount of data input CONSOL97 computes the new stresses at each sublayer boundary due to an applied surface load, or change in groundwater level. If the existing

soil profile has not fully consolidated, the user may specify the "underconsolidated" loading option which determines the excess pore pressure profile for use in the settlement analysis.

CONSOL97 provides the following load options:

Load Option 1: Specified Change in Stress

This load option is used when the other load options cannot adequately describe the loading. The user specifies the change in vertical stress for each layer, and enters these values into the appropriate screen.

Load Option 2: Change in Water Level

CONSOL97 calculates the change in vertical stress due to a specified change in the water level. If the water level drops below the top of the compressible layer, the pore water pressure above the new water level becomes negative and the change in stress is uniform throughout the compressible layer.

Load Option 3: Large Areal Load

Simulates the placement or removal of a uniform thickness of fill over a large area. The program calculates a uniform change in stress for each layer.

Load Option 4: Infinitely Long Strip

CONSOL97 calculates the change in vertical stress for each layer when a strip load of infinite length is applied on the surface. A strip footing load can be simulated by choosing appropriate values of strip width, fill thickness and unit weight.

Load Option 5: Circular Areal Load

CONSOL97 calculates the change in stress for each layer due to the placement or removal of a circular load on the surface. The load due to a circular or square spread footing can be simulated by choosing appropriate values of diameter, fill thickness and unit weight.

Load Option 6: Specified Stresses

The user specifies the initial pressure, final pressure, and preconsolidation pressure to calculate settlements. This load option is different from load option 1 through 5 because it over-rides the values of σ'_{vo}, σ'_{f}, $\sigma'^{(o)}_{p-ref}$ initially calculated by CONSOL97. This load option may only be specified at time t=0.

Load Option 7: No External Applied Load (Under-Consolidated Profile)

This load option is used to compute settlements that occur with no additional load, as a result of incomplete consolidation under a previous loading. At the start of the analysis the soil profile will have excess pore pressures which are dissipating and causing additional settlements. CONSOL97 analyzes the dissipation of excess pore pressures and the time rate of settlement. The excess pore pressures are equal to the final effective overburden pressure (at hydrostatic water pressures) minus the preconsolidation pressures specified for each layer. This load option may only be used at time t=0.

For each loading the user indicates the time at the beginning of load application and the length of time required to complete the full load application. Each load must have a ramp time greater than zero. CONSOL97 determines the minimum allowable loading duration based on the sublayer thicknesses and c_v. If the input ramp time is too small, CONSOL97 increases the value. If shorter ramp times are desired, the user should decrease the layer thickness near drainage boundaries

CONSOL97 will compute the settlement and pore pressure results at the output times specified by the user. Internally, CONSOL97 computes the results for small time step increments that insure numerical accuracy.

4.3 CONSOL97 PERFORMANCE

The performance of CONSOL97 has been examined in several hundred analyses. Its operation is shown in this section by simulating a standard oedometer test on a one inch thick specimen of San Francisco Bay Mud, and comparing the results with the original laboratory test data. The relatively undisturbed specimen was obtained from a depth of 17.5 feet at Hamilton Air Force Base in Marin County, California. Each load was applied for 24 hours, and settlement readings were obtained at frequent intervals during each load application. The laboratory stress-strain curve and the soil parameters used in the CONSOL97 simulation are illustrated in Figure 4.23. The finite element mesh and initial stress conditions are shown in Figure 4.24.

The laboratory data for the nonlinear virgin compression curve shown in Figure 4.23 have been connected by straight line segments. The slope of each line segment ($C_{\varepsilon c}$) decreases with increasing stress and $C_{\varepsilon c}$ varies from a value of 0.36 near the preconsolidation stress to 0.16 for the last load increment. The recompression ratio was obtained from the flattest portion of the unloading curve since it more closely represents elastic behavior without significant creep compression.

The preconsolidation stress was established at the intersection of the elastic recompression slope, $C_{\varepsilon r}$ and the slope of the first segment of the virgin compression curve (see Figure 4.23). A value of 950 psf was determined using this procedure.

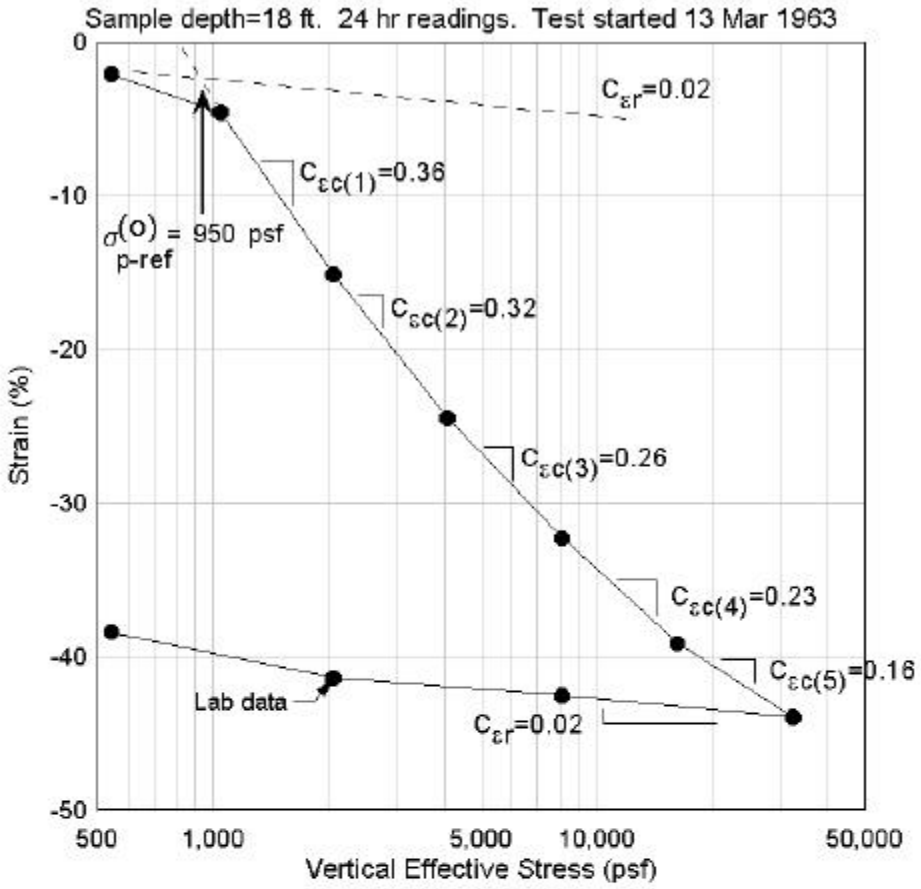

Soil properties from laboratory test data

Effective stress interval (psf)	Segment number	$C_{\varepsilon c}$	C_{α}	$c_v \times 10^{-5}$ (ft^2/minute)
950 to 2046	1	0.36	0.012	1.4
2046 to 4075	2	0.32	0.011	2.4
4075 to 8111	3	0.26	0.010	3.1
8111 to 16185	4	0.23	0.008	5.3
16185 to 32331	5	0.16	0.004	6.3

Figure 4.23: Laboratory stress-strain curve and summary of San Francisco Bay Mud properties

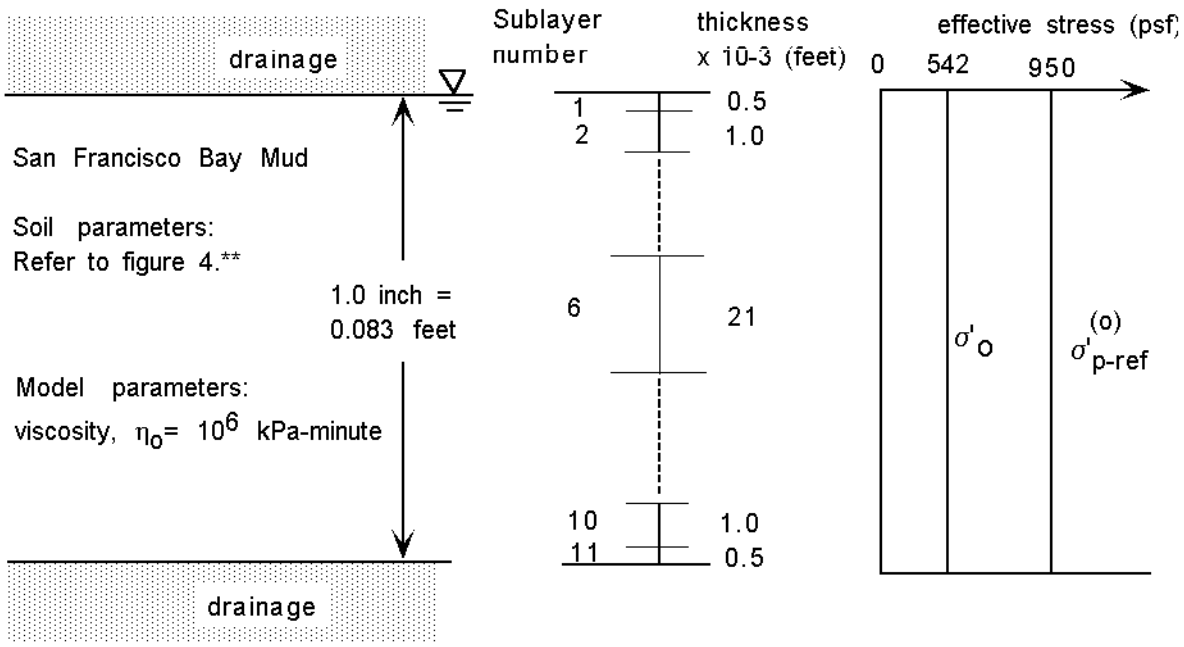

Figure 4.24: Finite element model of San Francisco Bay Mud specimen

The laboratory strain vs. log time plots indicated that with increasing effective stress, C_α decreased from 0.012 to 0.004 and c_v increased from 1.4×10^{-5} ft^2/minute to 6.3×10^{-5} ft^2/minute for stresses larger than the preconsolidation stress.

4.3.1 Stress-strain

The stress-strain results of the elasto-visco-plastic CONSOL97 simulation are illustrated in Figure 4.25 along with the lab data and a conventional, elasto-plastic CONSOL97 analysis. The elasto-visco-plastic CONSOL97 results closely match the lab curve during loading although the computed strains are about 3% smaller than the lab strains. This same inaccuracy has been noted

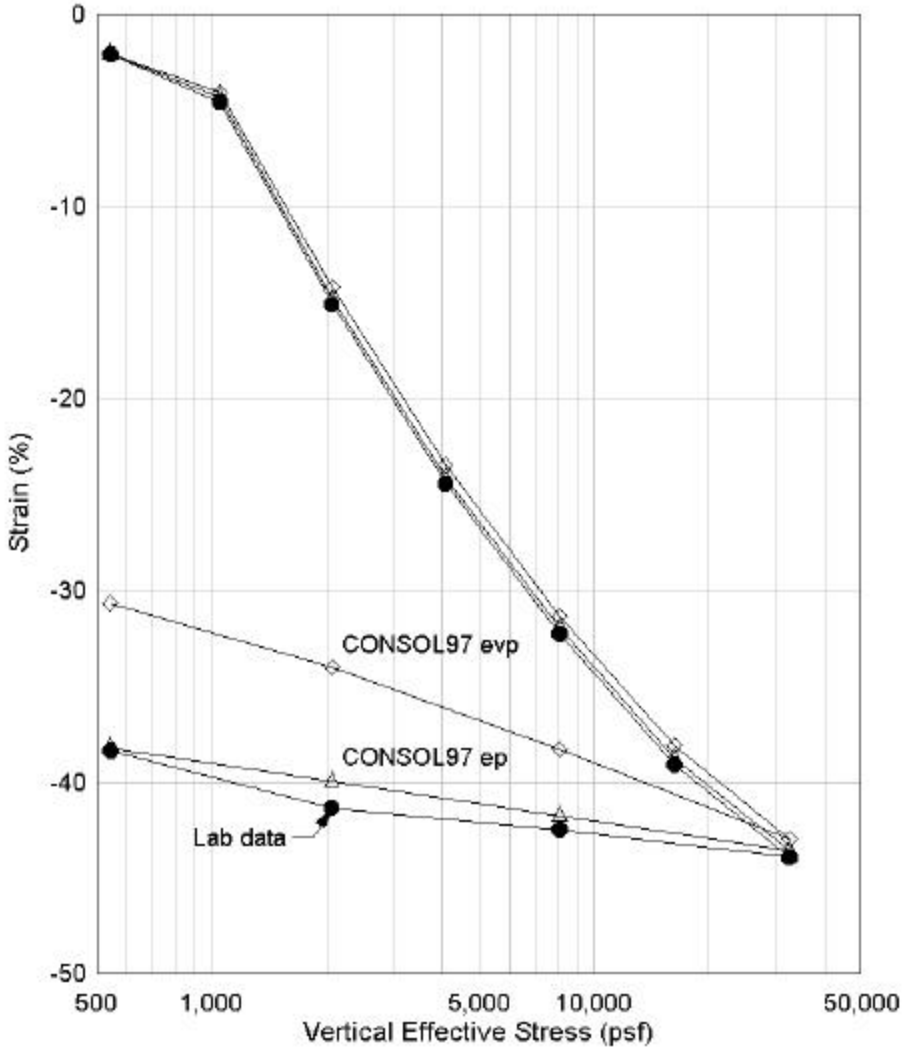

Figure 4.25: San Francisco Bay Mud strain vs. log effective stress curves from laboratory data and CONSOL97 simulation

previously. It can be reduced by decreasing the allowable convergence error, decreasing the yield tolerance, reducing the time step size, and increasing the number of sublayers. The computational time increases in proportion to the number of time steps, number of elements, and the number of iterations required to achieve convergence and yield tolerance criteria. The current analysis with nine load increments was completed in about 1-1/2 minutes on a 120 Mhz computer.

During unloading, the CONSOL97 elasto-visco-plastic analysis predicts much larger rebound than the lab results. This excessive rebound occurs because Rajot's model assumes visco-elastic unloading behavior. Since the lab results indicate elastic behavior rather than visco-elastic behavior during unloading, it may be more appropriate to use the conventional elasto-plastic soil model to simulate unloading situations. This may be accomplished by performing a separate CONSOL97 analysis to simulate unloading, or by performing only a elasto-plastic analysis. using information at the last load increment. The data input for the second analysis could be obtained by making the following changes to the first data input file:

1. Select elasto-plastic for the method of analysis;
2. Specify a new sample height by subtracting the calculated compression from the original specimen height;
3. Select load option 6 (specifed stresses) and provide the initial effective stresses and preconsolidation stresses from the first analysis. Input the final stresses.

4.3.2 Strain-time

Figures 4.25 to 4.29 present a comparison of laboratory and CONSOL97 strain vs. log time values. In order to compare results clearly, the CONSOL97 curves were adjusted to remove the 3% strain error at the start of each load increment. The curves show close agreement during loading even though the CONSOL97 simulation approximates the lab parameters by using constant values of $C_{\varepsilon c}$, c_v and C_α for each load increment.

The unloading curves were also adjusted at the start of each unloading increment. For the first two unloading increments, CONSOL97 predicts larger and faster rates of swelling than the lab

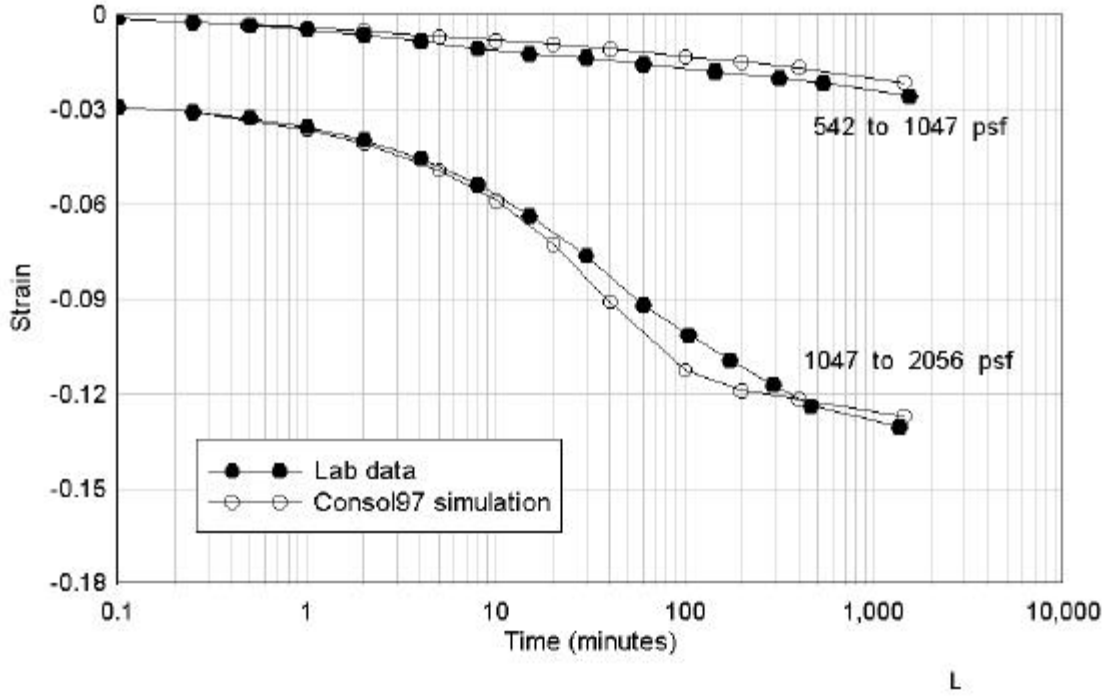

Figure 4.26: San Francisco Bay Mud strain vs. log time at stresses equal to 1047 psf and 2056 psf.

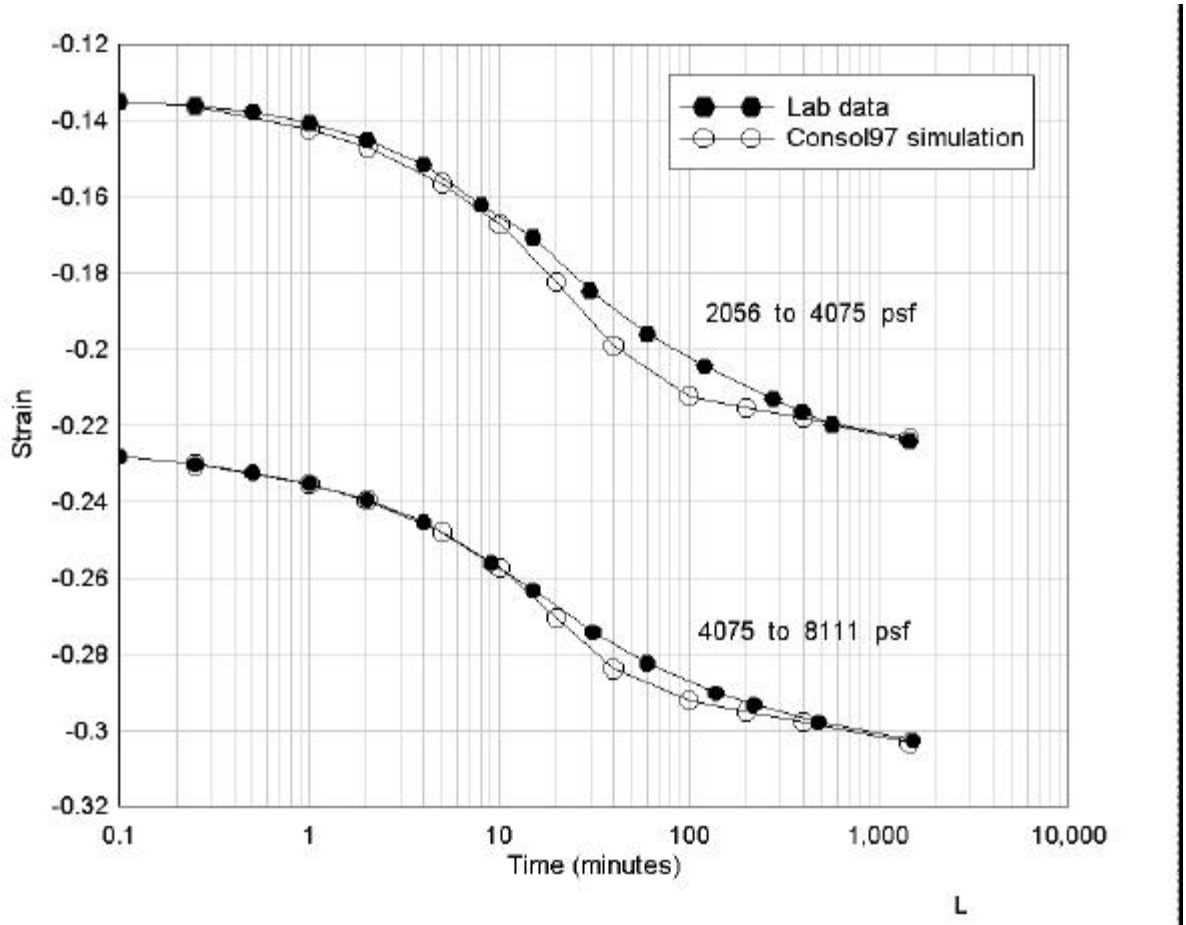

Figure 4.27: San Francisco Bay Mud strain vs. log time at stresses equal to 4075 psf and 8111 psf

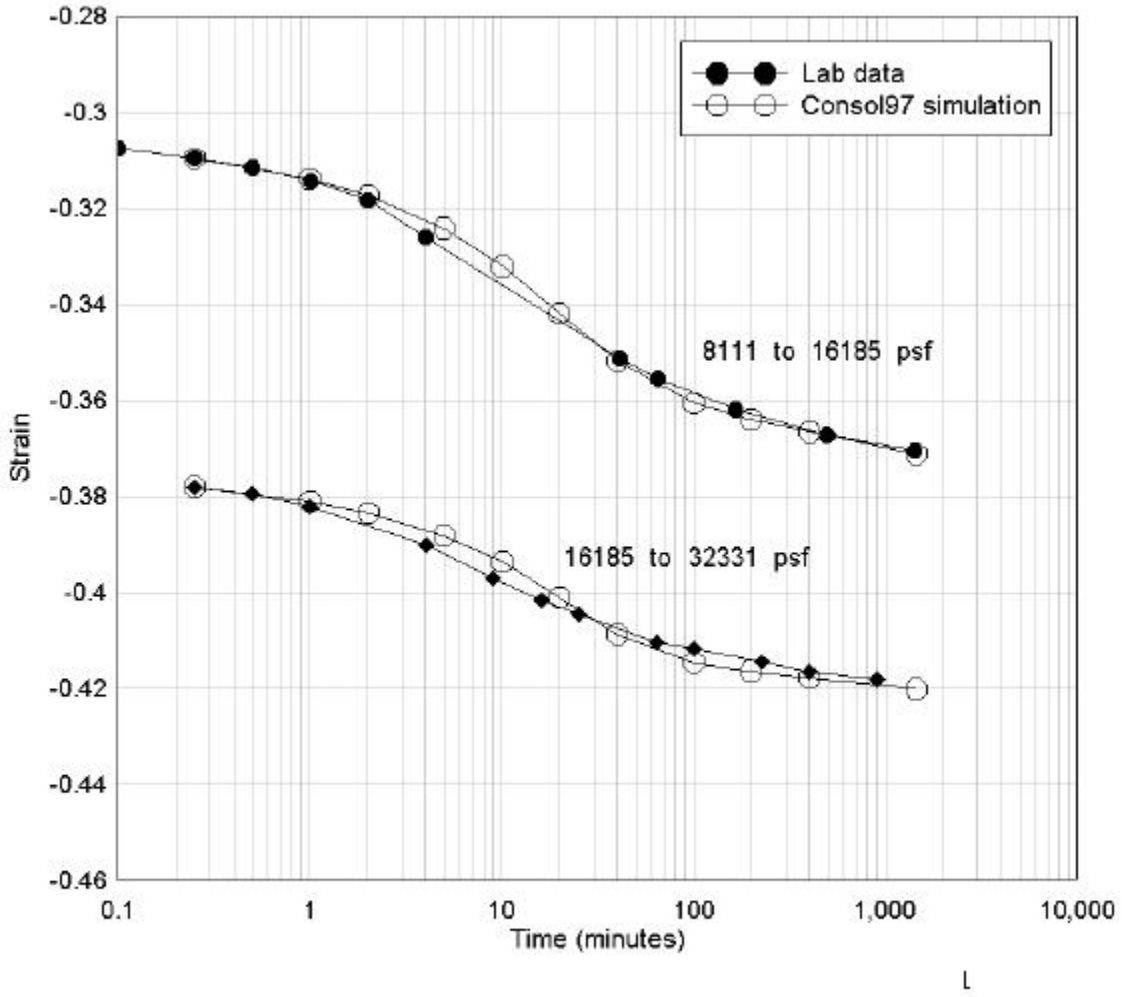

Figure 4.28: San Francisco Bay Mud strain vs. log time at stresses equal to 16185 psf and 32331 psf.

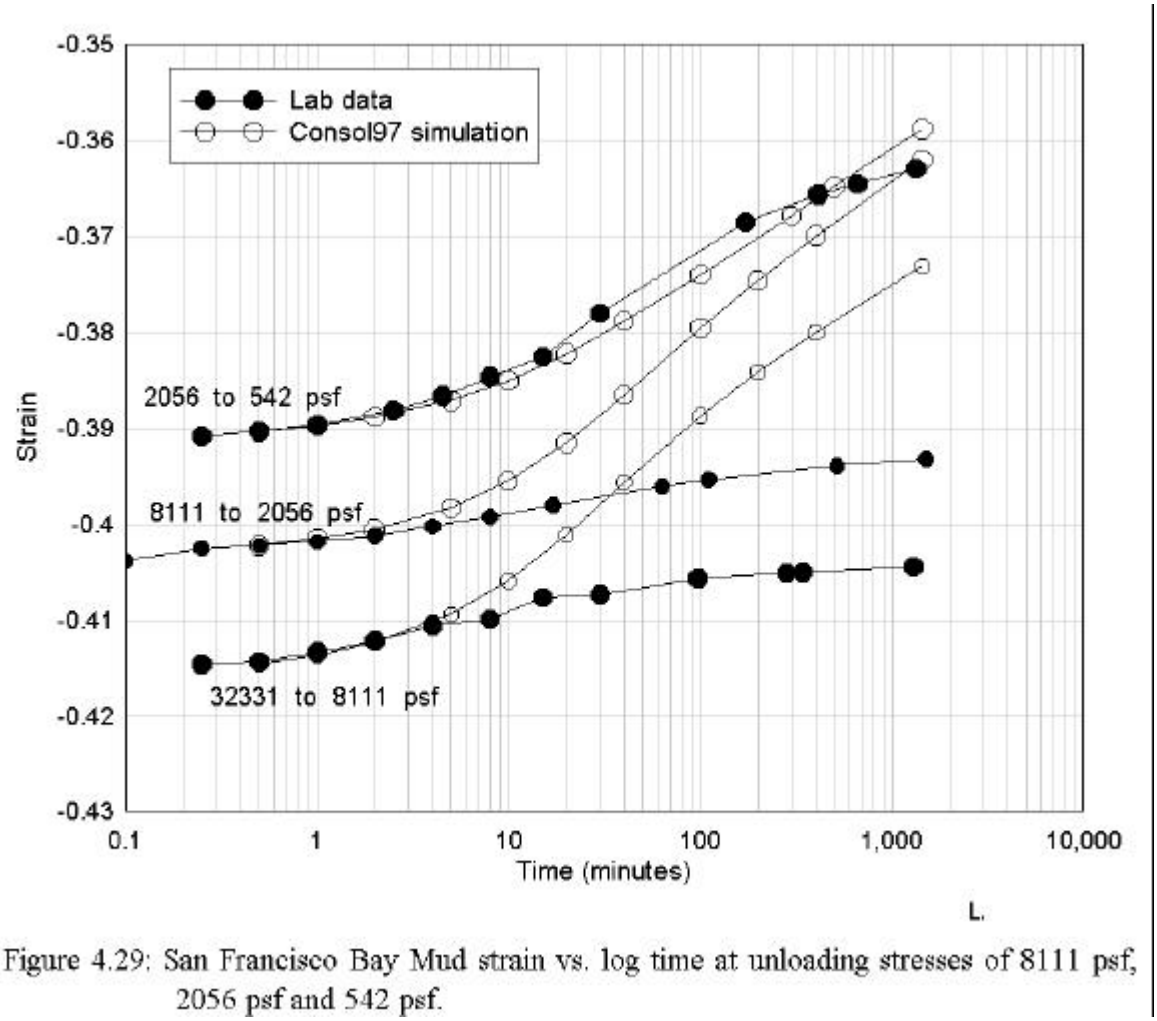

Figure 4.29: San Francisco Bay Mud strain vs. log time at unloading stresses of 8111 psf, 2056 psf and 542 psf.

test data. This divergence is due to the large amount of computed creep strain. The third and final set of unloading curves demonstrate very close agreement.

4.3.3. Coefficient of Secondary Compression

A comparison of secondary compression behavior is shown in Figure 4.30. The coefficients of secondary compression determined from lab data and CONSOL97 computations generally match very closely except at stresses of 2045 psf and 4056 psf. At these stresses the computed C_α

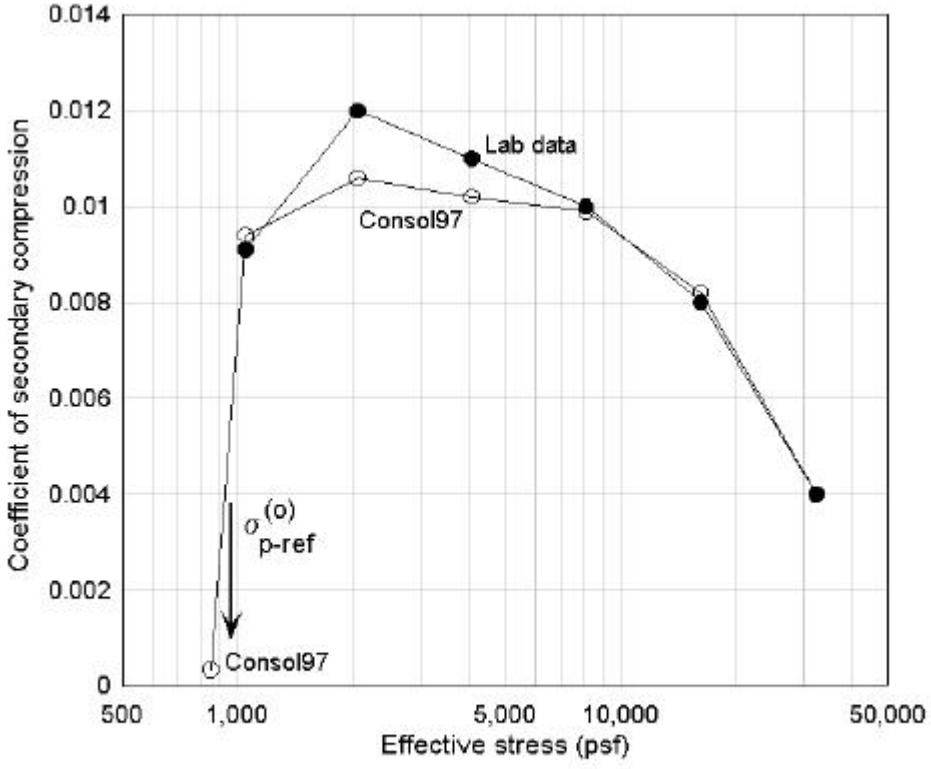

Figure 4.30: Secondary compression coefficient vs. effective stress

values deviate by 5% to 10% from the corresponding lab values. Insufficient lab data was available to compare C_α values at stresses less than the preconsolidation stress; CONSOL97 computations predicted significantly lower values of C_α at these low stresses, as shown in Figure 4.30. These small values of C_α at stresses below the preconsolidation stresses are typical of many test results on overconsolidated clays (Larsson 1981; Ladd 1973; Mesri and Godlewski 1977)

Chapter 5

COMPARISONS OF CONSOL97 RESULTS AND FIELD TEST MEASUREMENTS

This chapter examines the usefulness of CONSOL97 in predicting measured field behavior. Although the accuracy of Rajot's model has been verified by simulating lab tests (Chapter 4), this fact does not confirm its applicability for predicting field performance where strain rates may be many orders of magnitude slower than in the lab. Even if Rajot's theory, as implemented in CONSOL97, is capable of accurately representing time-dependent phenomena for a wide range of strain rates, the true capabilities of the model will depend on its ability to accurately simulate in situ behavior from laboratory tests. For example, lab determined preconsolidation stresses may not represent in situ preconsolidation stresses because the test results are affected by sample disturbance. In addition, the time-dependent model simulates "mechanical" aging of the soil (decrease in void ratio due to creep), but it does not consider cementation or interparticle bonding that hardens the soil and which are different than "mechanical" aging.

CONSOL97 was used to simulate one-dimensional consolidation of three well-instrumented and documented full scale test fills: Väsby, Sweden (Chang, 1969; Chang, 1981); Skå-Edeby, Sweden (Hansbo, 1960; Holtz and Broms, 1972) and; Berthierville, Canada (Kabbaj et al, 1988). Soil properties determined from standard incremental oedometer tests were used in the CONSOL97 simulations and the computed strains and pore pressures were compared to measured values. The objective of these comparisons was to determine the general validity of using time-dependent theory to predict field performance.

5.1 *VÄSBY TEST FILL*

5.1.1 Project Description

The Väsby test fill is located near the village of Uplands Väsby, 30 km north of Stockholm on the east coast of Sweden. The Swedish Geotechnical Institute (SGI) designed and constructed the test in 1945 to study the long-term behavior of Swedish clays and the suitability of the site for construction of an airport. The Väsby tests constitute the longest, continuously monitored and most complete set of pore pressure and deep settlement data of any field consolidation test.

One drained test and two "undrained" tests were constructed at the locations illustrated in Figure 5.1. The drained test consisted of installing paper drains in the clay soils and placing fill to a height of 2.5 meters in 1945. The "undrained" tests were constructed without paper drains. The first "undrained" test was constructed in 1947 with same dimensions as the drained test to determine the effectiveness of the paper drains. A second "undrained" test fill, constructed in 1948, had the same plan dimensions but the height of fill was only 0.3 meters. Only the "undrained", 2.5 meter high, test fill will be discussed here, and since drainage and consolidation are synonymous, the descriptive term "undrained", which refers to the absence of paper drains, will be omitted to avoid confusion.

Before the test fill was constructed, a 0.3 m thick layer of topsoil was scraped off the ground surface to elevation 6.85 m. Gravel fill was placed with side slopes of 1.5H:1V and a height of 2.5 meters in 25 days. The produced an applied stress of 40.6 kPa at the ground surface and about 28.2 kPa at the bottom of the clay layer at a depth of 13.5 meters below the ground surface. The dry unit weight of the fill was 16.24 kN/m^3, and the saturated unit weight of the fill was estimated to be about 17.18 kN/m^3. Based on these values, a stress reduction of 9.8 kPa would occur for each foot of fill submergence below the groundwater table (Chang, 1969).

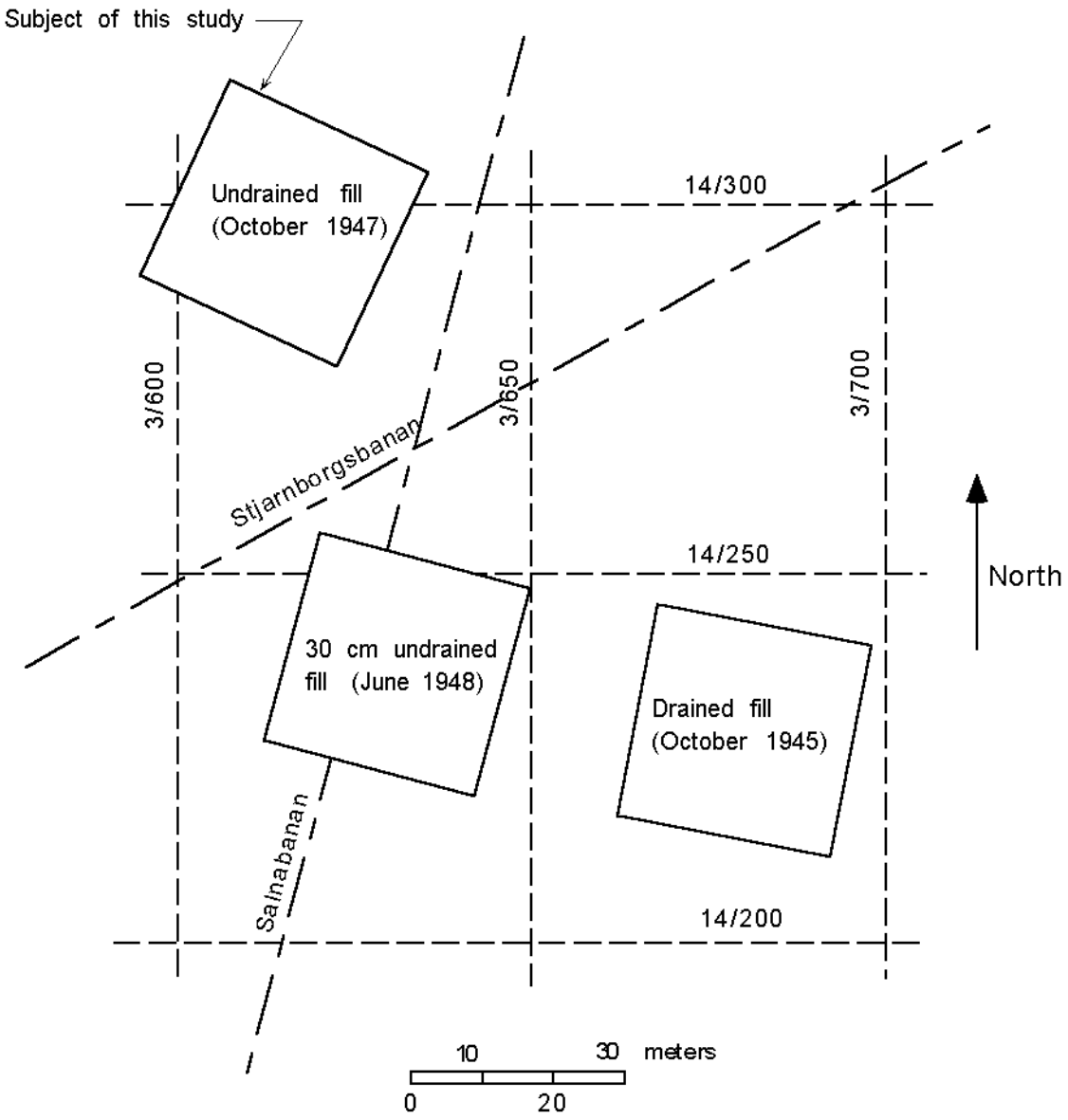

Figure 5.1: Test fill locations at Väsby, Sweden (from Chang, 1981)

Instrumentation was installed before the fill was constructed, and consisted of surface settlement platforms, deep settlement gauges, and piezometers. Many of the original instruments stopped functioning and new instruments were installed at later dates. The instrumentation layout and installation dates are illustrated in Figure 5.2. In general, the deep settlement gauges were

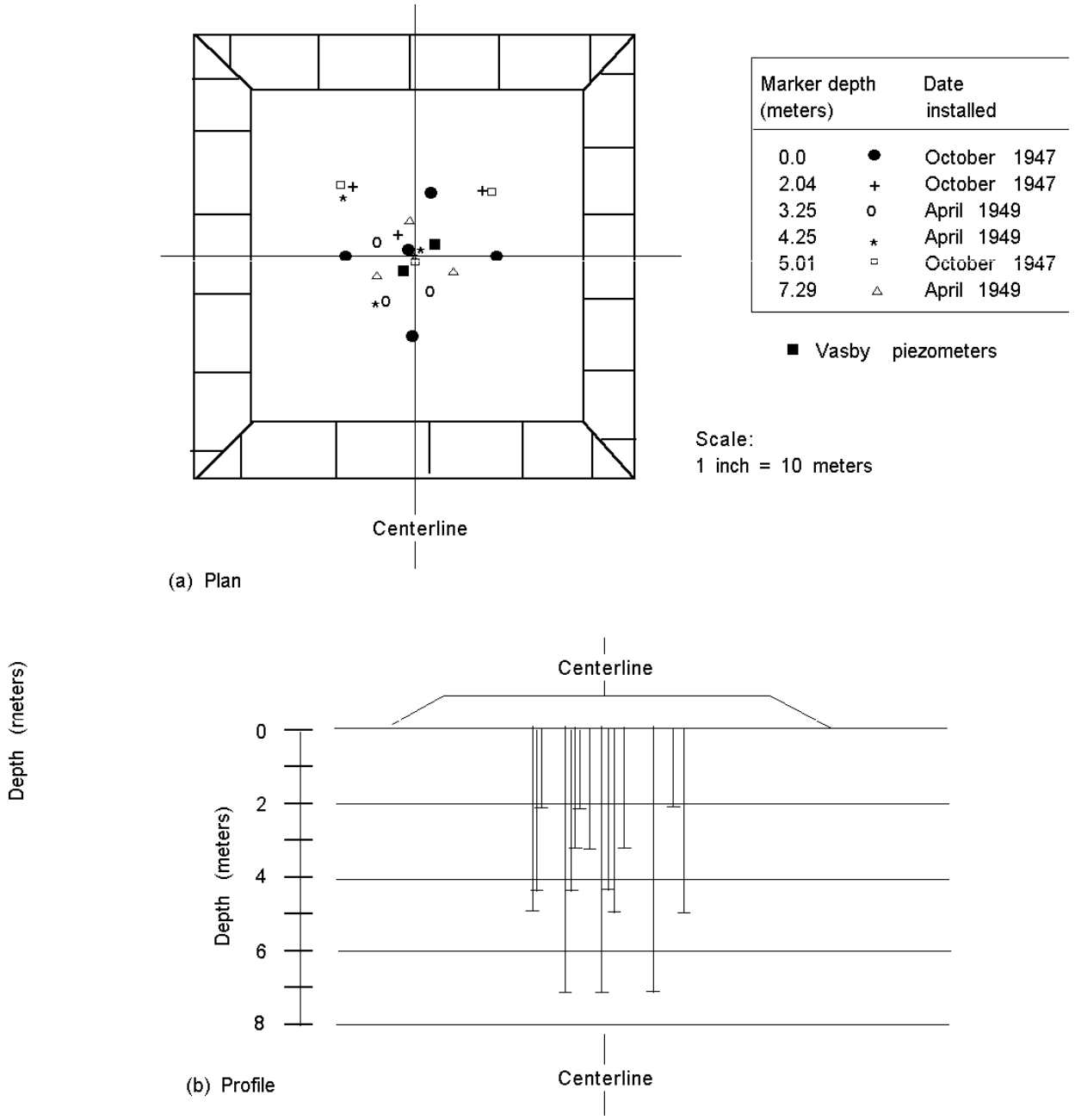

Figure 5.2: Instrumentation layout at the Vasby test fill (from Chang, 1981)

installed at about 2 meter intervals in the top half of the soil profile. Pore pressure devices were installed for the full depth of the soil profile.

Test measurements were made regularly until the mid 1950's. Subsequent measurements were somewhat incomplete until an intensive investigation was started in 1966 (Chang, 1969) under the direction of Professor Ralph B. Peck and Dr. Bengt Broms. Measurements were made again in 1968 (Chang, 1969), and regularly until 1980 (Chang 1981).

The original settlement markers in the clay became inoperative during the investigation. Newer models were installed but they also malfunctioned with time. Therefore, the settlement distribution with depth has been mainly deduced from changes in water content. New piezometers were installed in 1968 and the pore pressures in 1979 were measured by retractable piezometers.

5.1.2 Site Geology and Subsurface Conditions

The soils at the site are of glacial and post glacial origins. During the last glacial epoch, the Baltic Sea to the east of the site was periodically blocked from the Atlantic Ocean. The salinity of the Baltic Sea changed dramatically until the final retreat and melting of the last glaciers during the Pleistocene era. As the glaciers retreated northward, the meltwater deposited post glacial sediments on the underlying Precambrian Age bedrock.

The Väsby test site is very flat, and about 7 meters above sea level. The subsurface profile, illustrated in Figure 5.3, consists of bedrock at an elevation of -7.0 m overlain by about 14 meters of post glacial soil deposits that are predominantly clay. The bedrock surface is covered by 2.5 cm to several meters of medium gray sand. The lower portion of the clay deposit is a glacial clay deposited by meltwater. The upper portion of the clay deposit is a post-glacial clay comprised of the lower clay that was redeposited more recently. The profile in Figure 5.4 summarizes soil strength and index properties before placement of the fill. Although the post glacial clay profile has been subdivided, the layers are very similar except that the colors gradually change shades

(Chang 1981).

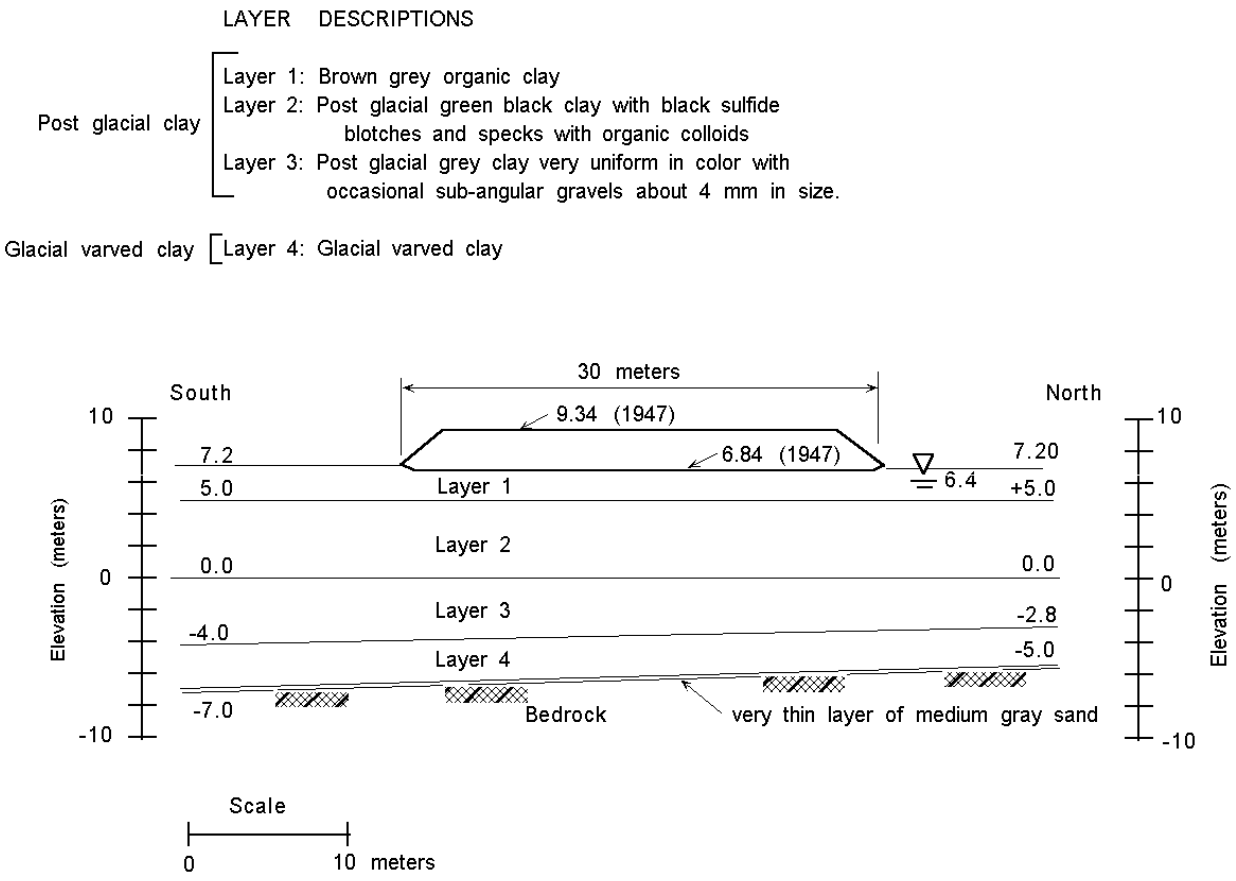

Figure 5.3: Soil profile beneath the Väsby test fill (after Chang, 1981)

The site is covered by about a 0.5 m thick dry crust of organic soil. The underlying post glacial soil is soft and primarily a sulfide-rich deposit of highly plastic clay containing as much as 5.4% organic material. With increasing depth, the organic content decreases to less than 2% at a depth of about 7 meters. The natural water content also decreases from about 130% at the top of the soft clay to about 80% at the bottom of the soft post glacial clay. With increasing depth, the liquidity index increases from about 1.0 to 1.2, sensitivity increases from about 2 to 7 and bulk density increases from about 1.3 t/m^3 to about 1.7 t/m^3.

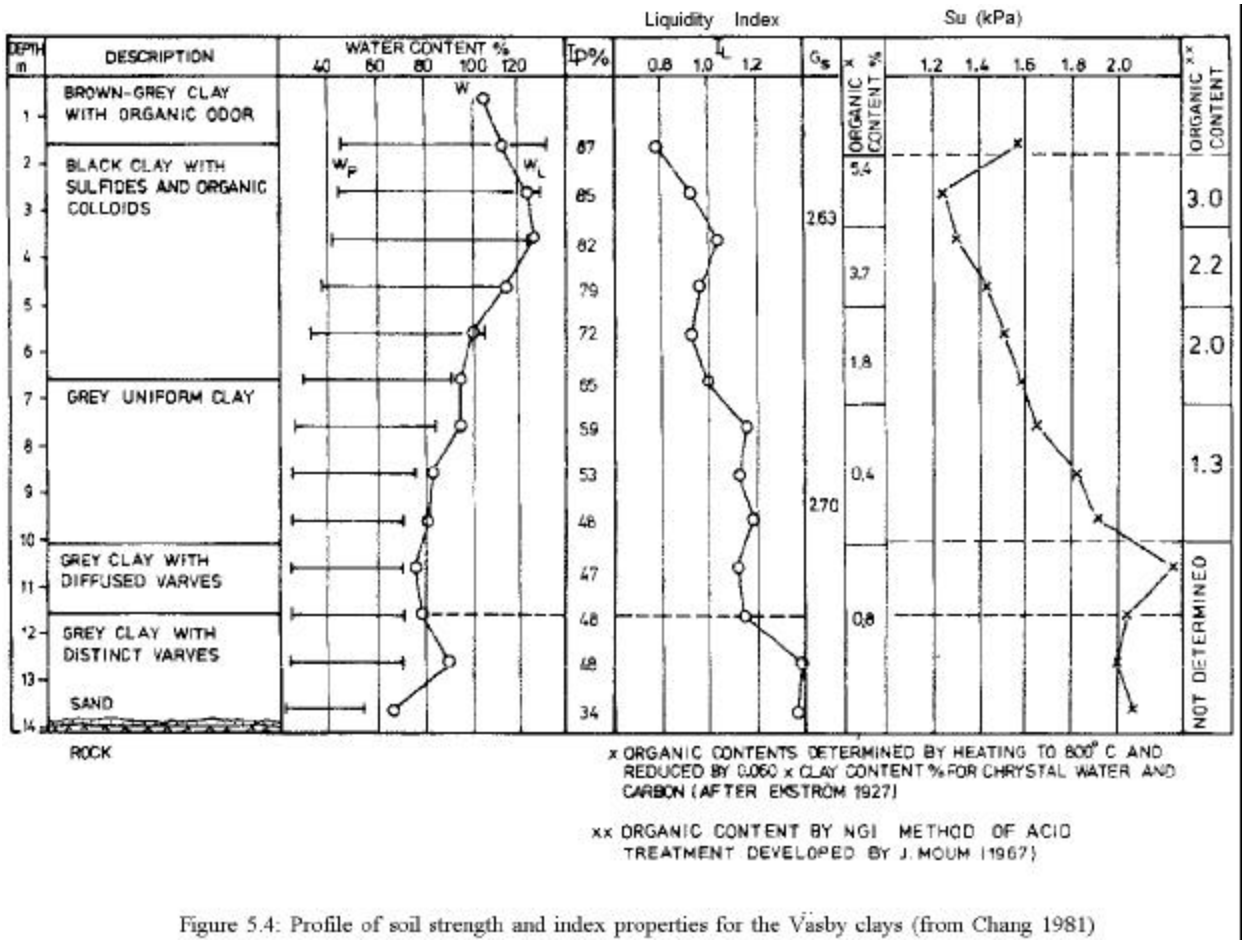

Figure 5.4: Profile of soil strength and index properties for the Väsby clays (from Chang 1981)

The glacial varved clay beneath the post glacial clay has less than about 1% organic content. The clay is highly plastic with a liquid limit of about 70 and natural water contents that indicate liquidity indexes of 1.2 to 1.3.

Except for seasonal fluctuations of ±0.2 m, the mean groundwater level outside the loaded area is generally located at a depth of 0.8 m below the natural ground surface (elevation 6.4 m). The pore pressures outside the loaded area are hydrostatic.

5.1.3 Soil Properties

A geotechnical profile of clay compressibility, consolidation coefficients and stress history is shown in Figure 5.5. The soil properties are based upon laboratory oedometer testing by Chang (1969, 1981), Larsson (1977, 1981) and Leroueil (1987). The majority of the tests were performed by Chang and consisted of conventional incremental laboratory oedometer tests performed on samples taken with the SGI sampler. Each load was applied for one day and then doubled (load increment ratio, LIR=1). Some of the test results were corrected for friction that developed between the soil sample and the oedometer ring. Larsson and Leroueil performed a limited number of CRS and creep oedometer tests.

The preconsolidation stresses plotted in Figure 5.5 were estimated from Chang's 24 hour and end of primary test data using Casagrande's method. The 24 hour friction corrected values are slightly smaller than the uncorrected values and, in some cases, the 24 hour values are less than the original effective overburden stress. As expected the end of primary values determined by Chang are significantly larger than the 24 hour values.

The 24-hour lab test results were used in the CONSOL97 analysis. An interpreted preconsolidation stress profile is presented in Figure 5.5. The clay is slightly overconsolidated for the full depth except for about a one to 2 meter thick heavily overconsolidated crust at the ground surface. The preconsolidation stresses beneath the crust are about 5 to 10 kPa larger than the effective overburden stress.

Summary plots of void ratio vs. logarithm of effective stress for 24-hour load increments, and sample compression vs. logarithm of time are included in Appendix A. The laboratory strain vs. log effective stress curves exhibit some non-linearity in the virgin compression range of stresses. Virgin compression ratio values computed from the 24- hour oedometer test results in the stress range appropriate for this loading situation vary from about 0.35 to 0.6.

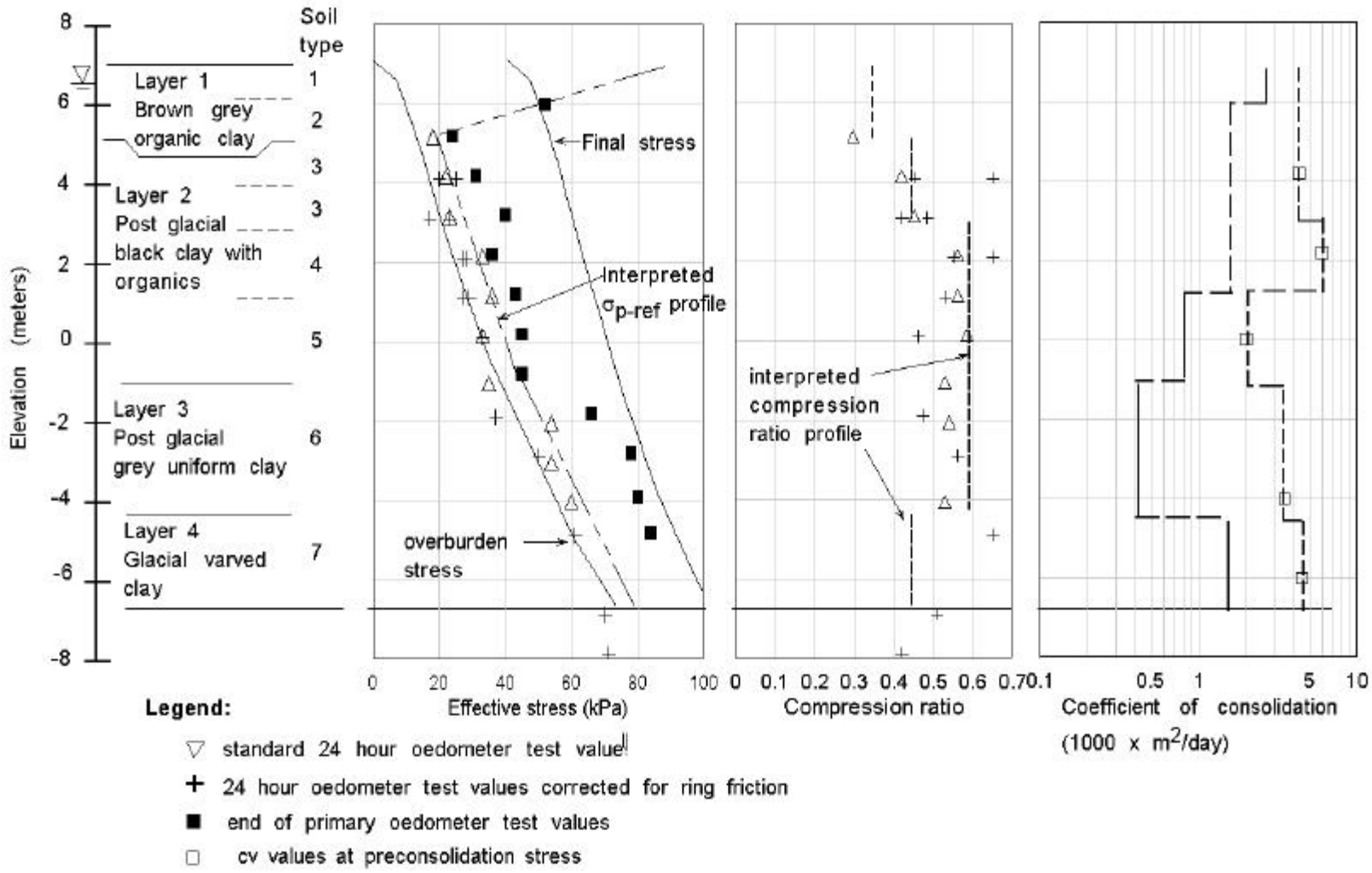

Figure 5.5: Geotechnical profile beneath the Vasby test fill

Values of consolidation coefficients were determined from oedometer tests on five samples. Two sets of values are shown: one at the preconsolidation stress and another at stresses greater than the preconsolidation stress. The results summarized in Figure 5.6 indicate that c_v values at the preconsolidation stress are about five times larger than the minimum c_v values at stress levels that are about 20 to 40 kPa larger than the preconsolidation stress. The c_v values were in the range of about $1x10^{-3}$ to $8x10^{-3}$ m^2/day at the preconsolidation stress and minimum c_v values were in the range of $0.3x10^{-3}$ to $1.0x10^{-3}$ m^2/day.

Secondary compression values were determined from the results of the oedometer test data shown in Figure 5.7 from a test performed on a sample taken from a depth of 5.0 meters. C_α values decreased from about 0.037 at an effective stress of about 50 kPa to a value of about 0.020 at effective stresses greater than about 100 kPa. The ratio, $C_\alpha/C_{\varepsilon c}$, for 24-hour lab data is about 0.06. Mesri and Choi (1985) and Larsson (1986) reported similar values for the clay at this test site.

5.1.4 CONSOL97 Input and Results

The soil properties used in the CONSOL97 analysis are summarized in Figure 5.5 and Table 5.1. The clay layer was divided into 7 layers and 28 sublayers of varying thickness. The sublayers at the drainage boundaries were about 0.02 meters thick and the sublayers at the center of the clay layer were about 1.5 meters thick. Seven different sets of soil parameters were used to characterize the range of soil properties throughout the clay profile. Each soil type was defined by a single value of $C_{\varepsilon c}$ and $C_\alpha = 0.06 \cdot C_{\varepsilon c}$. The coefficient of consolidation was specified for each 10 kPa increase in effective stress. Figure 5.5 illustrates the range of c_v values used in each sublayer based on the range of initial and final effective stresses.

TABLE 5.1
Summary of Laboratory Determined Soil Properties
Väsby Test Fill

Refer to Figure 5.5, Geotechnical profile beneath Väsby test fill

Soil Number	Layer elevation (m)	Unit weight (kN/m3)	$C_{\varepsilon c}$	C_{α}	$C_{\varepsilon r}$	Coefficient of consolidation c_v (m^2/day)	
						at $\sigma_{p\text{-}ref}$	at σ_{final}
1	7.10 to 6.00	14.00	0.40	0.024	0.04	0.0043	0.0026
2	6.00 to 5.06	14.00	0.40	0.024	0.04	0.0043	0.0015
3	5.06 to 2.85	13.40	0.40	0.024	0.04	0.0043	0.0015
4	2.85 to 1.15	13.90	0.60	0.036	0.05	0.0060	0.0015
5	1.15 to -1.00	14.40	0.60	0.036	0.05	0.0020	0.0007
6	1.00 to -4.25	15.40	0.60	0.036	0.05	0.0035	0.0004
7	-4.25 to -6.40	17.20	0.55	0.034	0.04	0.0045	0.0015

The results of the CONSOL97 analysis using the EVP model are illustrated in Figures 5.8 and 5.9. Initial undrained settlements of 0.06 m have been added to the computed results since CONSOL97 does not compute them. This value represents the measured initial settlement less the computed consolidation settlement of 0.005 m after 25 days. As shown in Figure 5.8, the computed rate of fill settlement in the years after load application is much slower than the measured rate of settlement. After 30 years of consolidation, the computed settlement was 0.8 m as compared to a measured settlement of 1.5 m.

The computed and measured excess pore pressures after 21 and 30 years are shown in Figure 5.9. After 21 years, the computed pore pressures from the ground surface to a depth of 5 meters (elevation 2.1) are as much as twice the measured values. Below a depth of 5 meters, the computed excess pore pressures are in good agreement with measured values. Nine years later, computed excess pore pressures are still as much as twice the measured values but the zone of overprediction has deepened to about 8 meters (elevation -1).

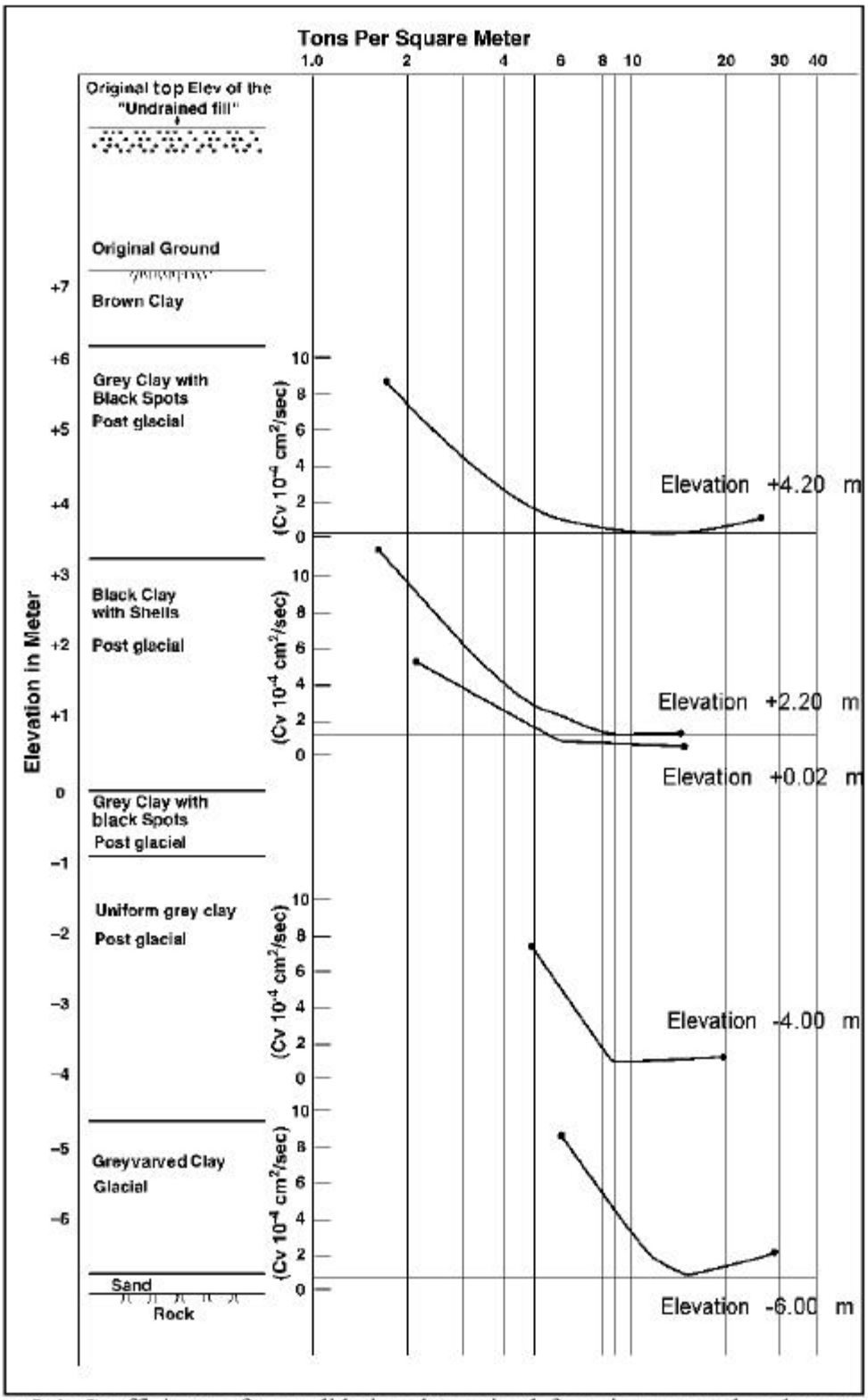

Figure 5.6: Coefficients of consolidation determined from incremental oedometer tests on Vasby clay (from Chang 1969)

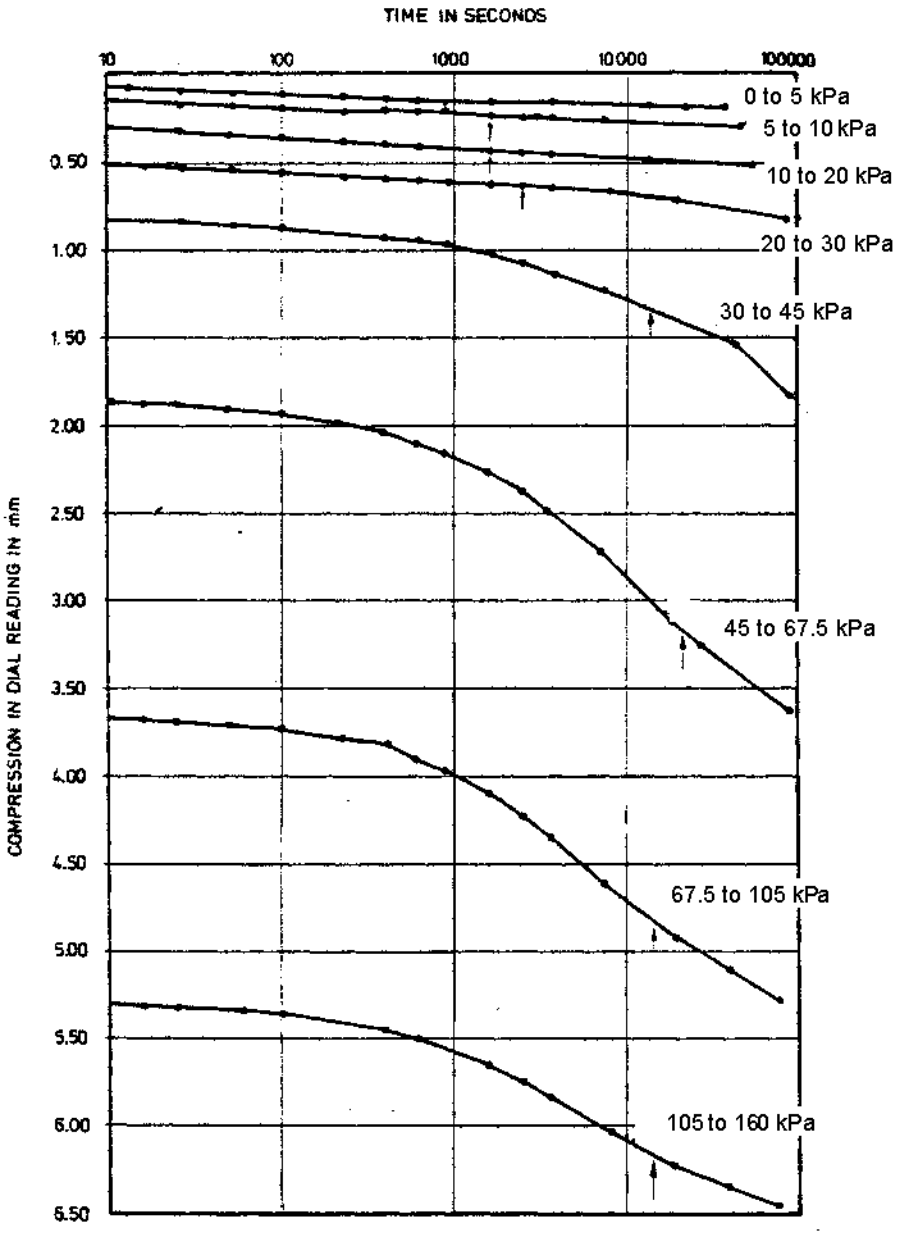

Figure 5.7: Typical oedometer compression vs. logarithm time for Vasby clay (from Chang 1981)

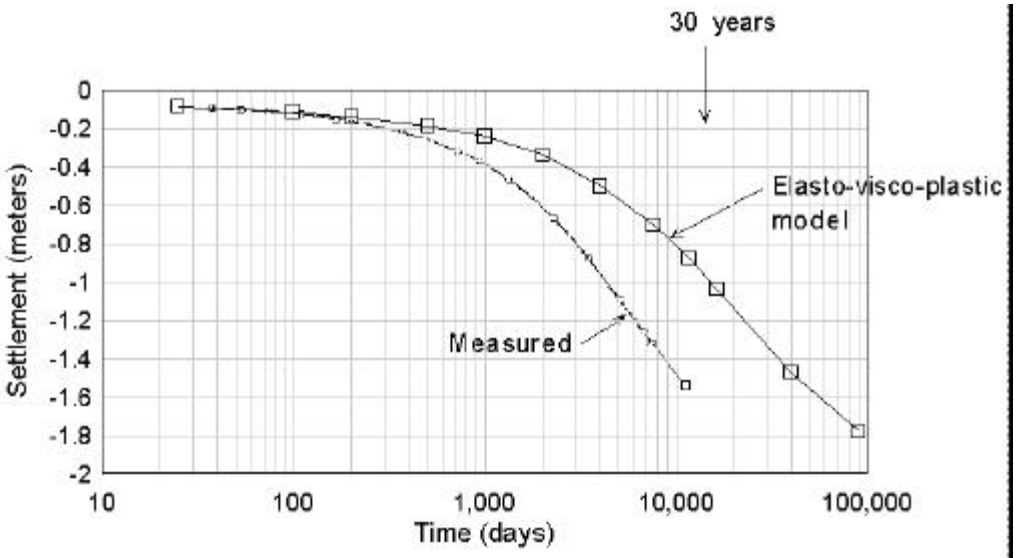

Figure 5.8: Measured and computed settlement of the Vasby test fill

The computed results indicate that the coefficient of consolidation for the top portion of the clay profile is much larger than assumed in the analysis. Lacking lab test data for the brown weathered clay crust to a depth of 2 meters, it was incorrectly assumed that c_v values for the shallowest test sample at a depth of 4.2 meters would be representative of the clay crust. However, the black unweathered organic clays at a depth of 4.2 m are distinctly different than the overlying clay crust. Therefore, additional analyses were performed to determine c_v values in the top two meters of the clay profile (layers 1 and 2) that would produce excess pore pressures in these layers that more closely agree with measured excess pore pressures. It was found that c_v values in sublayer one (1.0 m thick) equal to 10 times the original assumed values and c_v values in sublayer two (1.0 m thick) equal to 5 times the original assumed values produced good agreement with measured pore pressures.

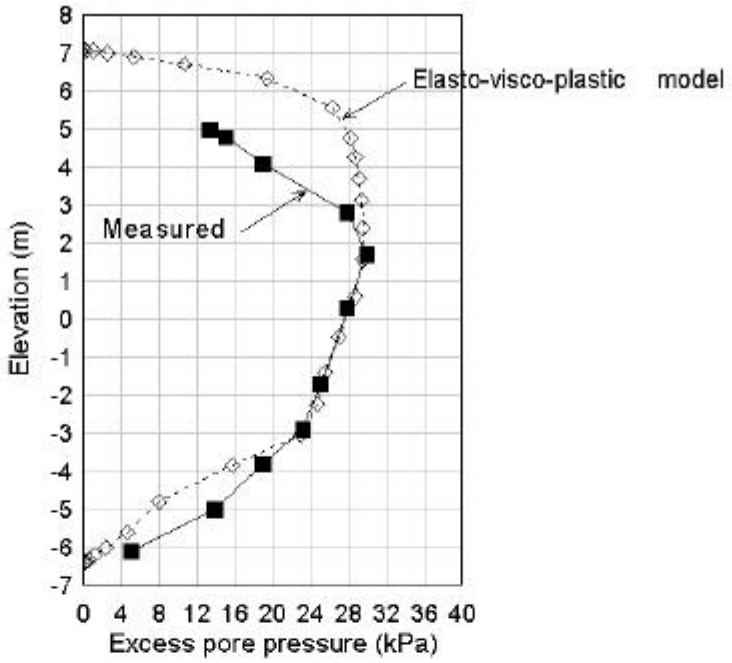

(a) Excess pore pressures after 21 years

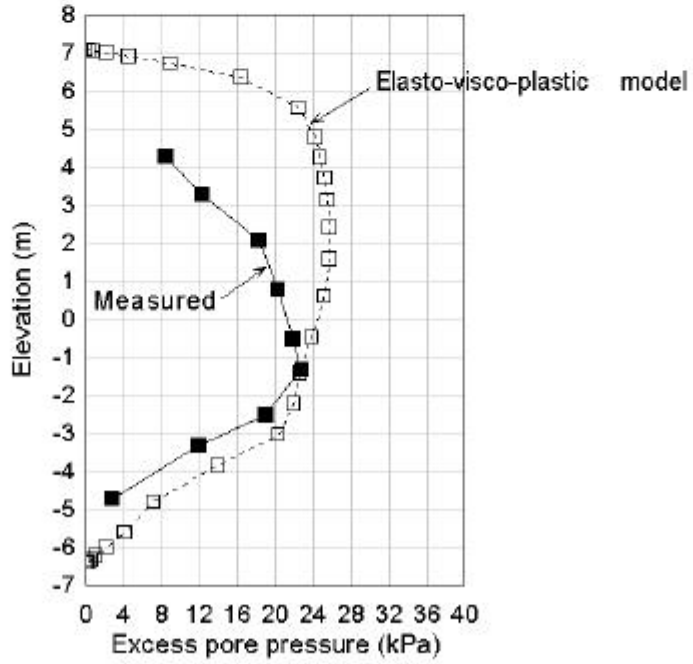

(b) Excess pore pressures after 30 years

Figure 5.9: Measured and computed excess pore pressures beneath the Vasby test fill

The results of the revised EVP analysis are shown in Figures 5.10 to 5.13. The computed magnitude and rate of fill settlement (Figure 5.10) has increased due to the increase in the value of c_v in the permeable crust, but they are still significantly less than the measured settlement magnitude and rates. After 30 years (approximately 11000 days) of consolidation, the computed fill settlement is about 0.4 m less than the measured settlement of 1.6 m. The computed settlement profile after 21 years of consolidation (Figure 5.11a) matches the field measurements below elevation -1. Above elevation -1, the computed settlements are about 20 to 30% less than measured values. There is very little difference between the computed EVP and EP settlements.

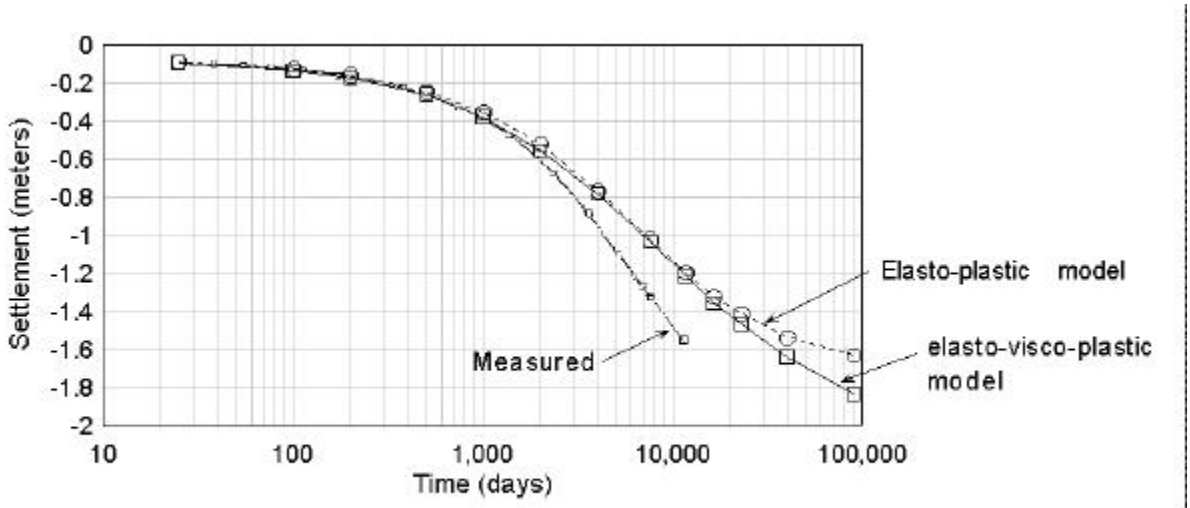

Figure 5.10: Measured and computed settlement of the Vasby test fill assuming a permeable crust

Comparisons of measured and computed strains in the top three soil zones to a depth of 7.29 meters are shown in Figure 5.12. The computed EVP magnitudes and rates of strain in zone one (depth 0 to 2.04 m), zone 2 (depth 2.04 to 5.01 m) and zone 3 (depth 4. 25 to 7.29 m) agree reasonably well with measurements although the rate of compression in zone 3 is slower than measured. In zones one and two, the field measurements indicate that the rate of strain has

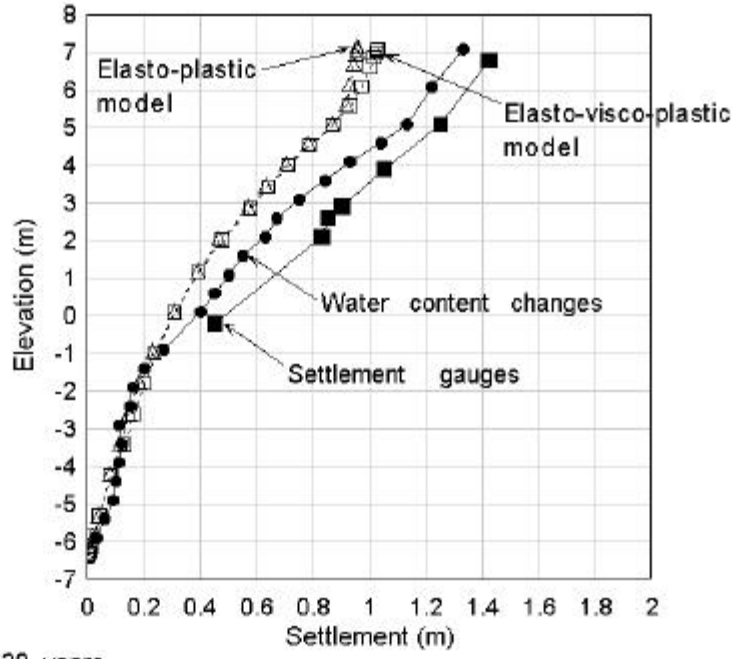

(a) Settlement profile after 20 years

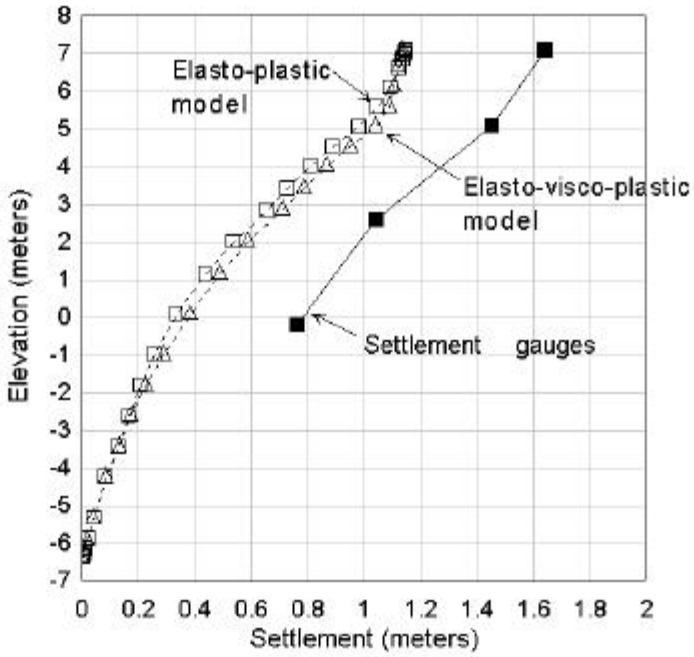

(b) Settlement profile after 30 years

Figure 5.11: Measured and computed setttlement profiles beneath the Vasby test fill assuming a permeable crust

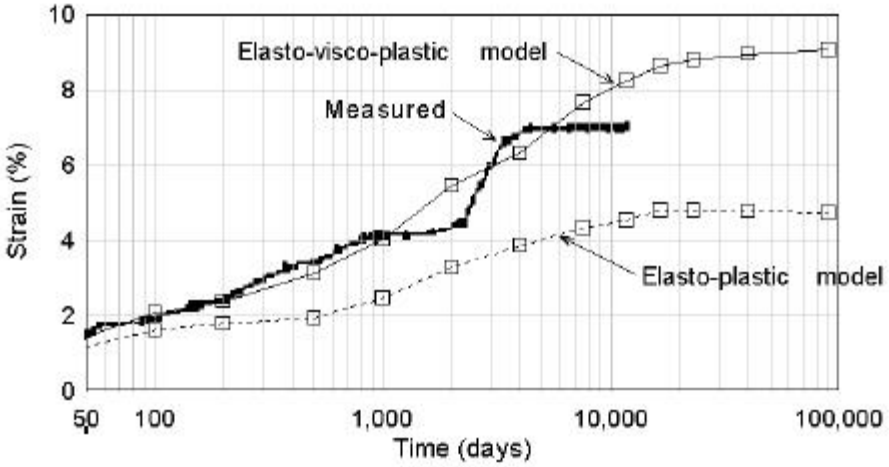

(a) Compression of the clay layer between 0 and 2.04 meters below the original ground surface.

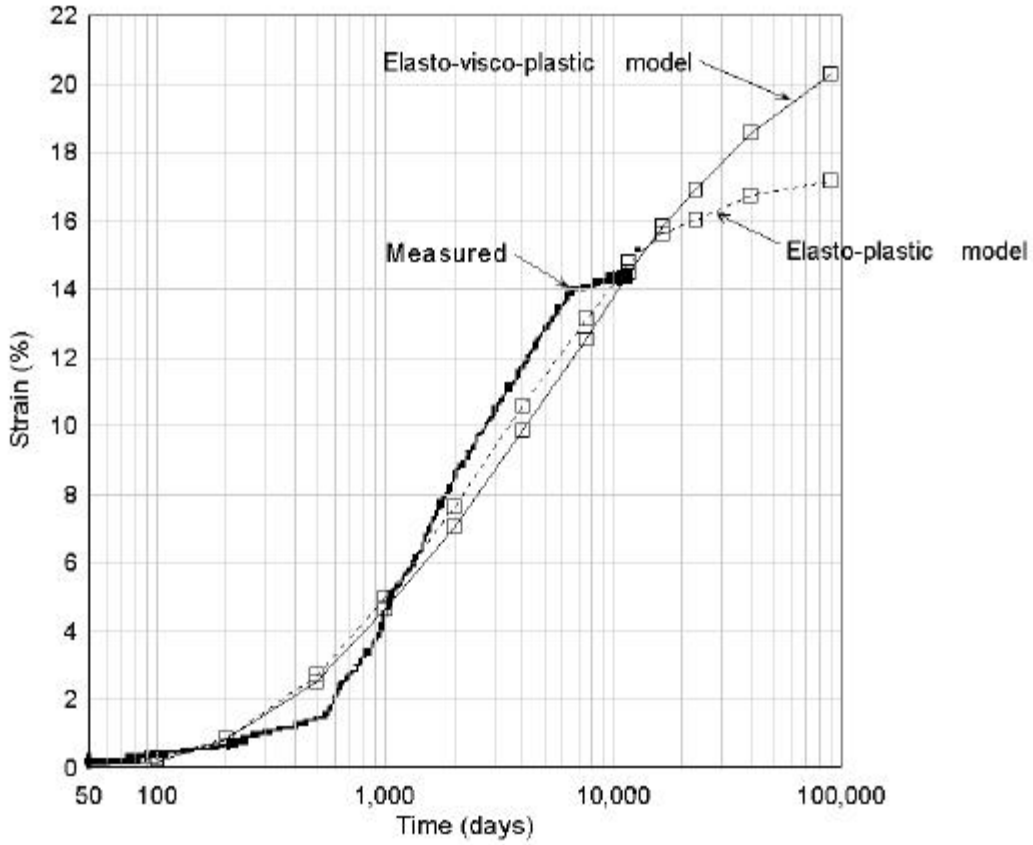

(b) Compression of the clay layer between 2.04 and 5.01 meters below the original ground surface

Figure 5.12: Measured and computed Vasby clay compression vs. logarithm of time assuming a permeable crust

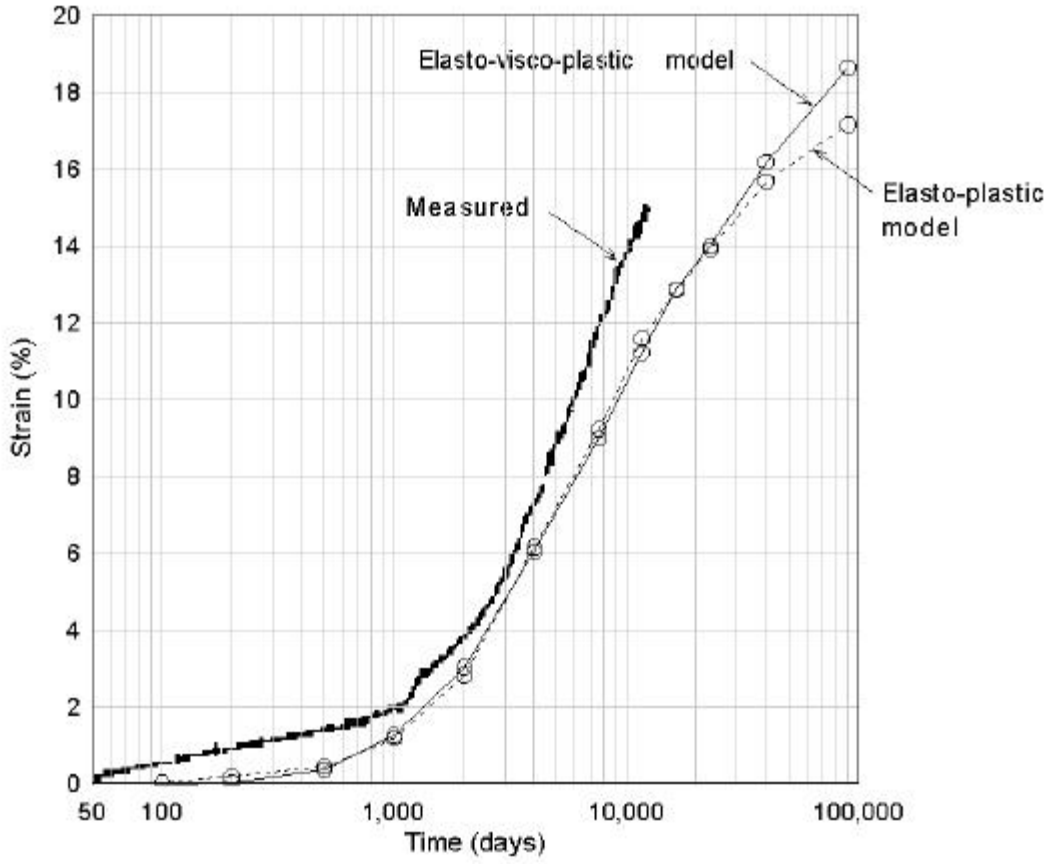

(c) Compression of the clay layer between 4.25 and 7.29 meters below the original ground surface

Figure 5.12 (continued): Measured and computed Vasby clay compression vs. logarithm of time assuming a permeable crust

slowed and that consolidation is complete, whereas, the CONSOL97 results indicate that an additional 50% more compression will occur in the next 50 years.

Measured and computed excess pore pressure profiles for 1968 (21 years) and 1977 (30 years) are shown in Figure 5.13. After 21 years, the CONSOL97 analysis underestimates excess pore pressures below elevation 4 and, after 30 years, the computed excess pore pressures are generally larger than measured values except in the middle of the clay layer. Computations using the EP

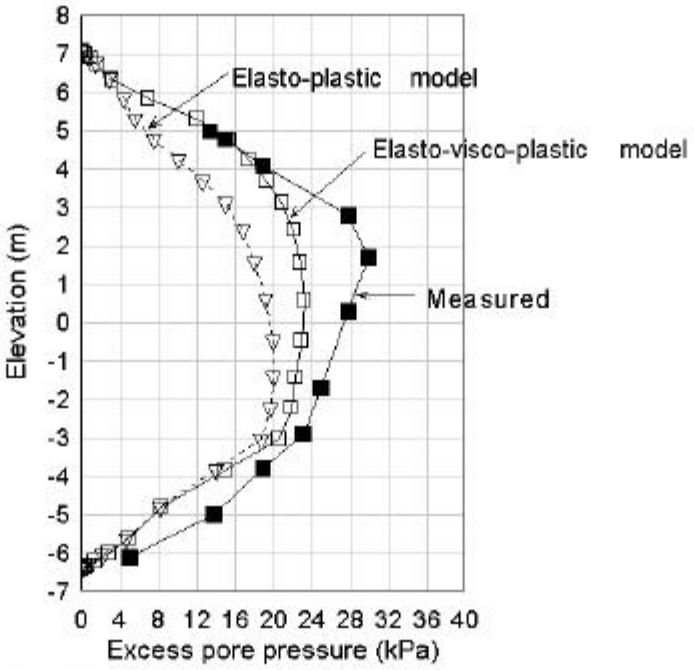

(a) Excess pore pressures after 21 years

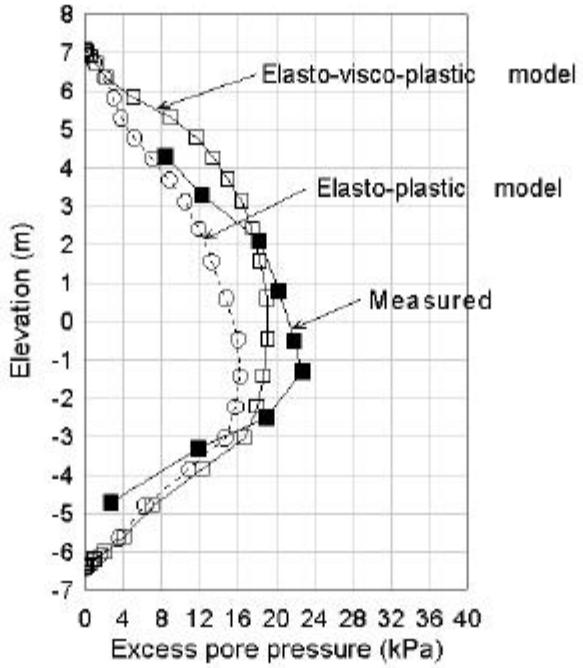

(b) Excess pore pressures after 30 years

Figure 5.13: Measured and computed excess pore pressures beneath the Vasby test fill assuming a permeable crust

model generally indicate excess pore pressures that are significantly smaller than measured values after 21 and 30 years of consolidation.

The large differences in measured and computed excess pore pressures suggest that the input parameters derived from the lab tests may not accurately represent in situ behavior. Leroueil and Kabbaj (1987) and Lacasse et al (1985) have shown that sample disturbance can significantly affect laboratory measured values of preconsolidation stress, coefficient of consolidation and compression ratios of Swedish sensitive clays. Chang (1969) reported that the coefficient of consolidation for a sample taken at a depth of 3.5 m and tested at NGI in an 80 mm diameter oedometer were about 2.3 times the values obtained from tests on 50 mm diameter samples.

Void ratio vs. logarithm effective stress curves shown in Figure 5.14 illustrate the effects of sample disturbance on the stress-strain behavior of Väsby clay. Both curves were obtained from 24 hour incremental oedometer tests (LIR=1) on samples taken from a depth of 4.3 m. The test results for the 50 mm diameter SGI sample were obtained in 1967 and reported by Chang (1981). The 200 mm diameter sample was obtained with a Laval sampler, trimmed to 50 mm diameter, and tested at Laval University (Leroueil and Kabbaj, 1987). The curve for the less disturbed Laval sample has a sharper break and is much steeper for stresses exceeding the preconsolidation stress than the curve for the SGI sample. The "undisturbed" compressibility ratio, $C_{\varepsilon c}$, is 0.74 (compared to 0.47) and the preconsolidation stress is 35 kPa (compared to 23 kPa). Leroueil and Kabbaj (1987) have reported that the end of primary preconsolidation stresses at depths of 3 m to 10 m are about 20 kPa larger than the effective overburden stresses.

Undisturbed soil properties were estimated from this additional test data on high quality samples and used in another CONSOL97 analysis. The profile of "undisturbed" soil properties is shown in Figure 5.15 and summarized in Table 5.2. The 24-hour preconsolidation stresses below the heavily over consolidated crust were increased by about 5 to 10 kPa (about 15 to 20 kPa greater than the effective overburden stress). Laboratory c_v values (Figure 5.7) at the larger undisturbed"

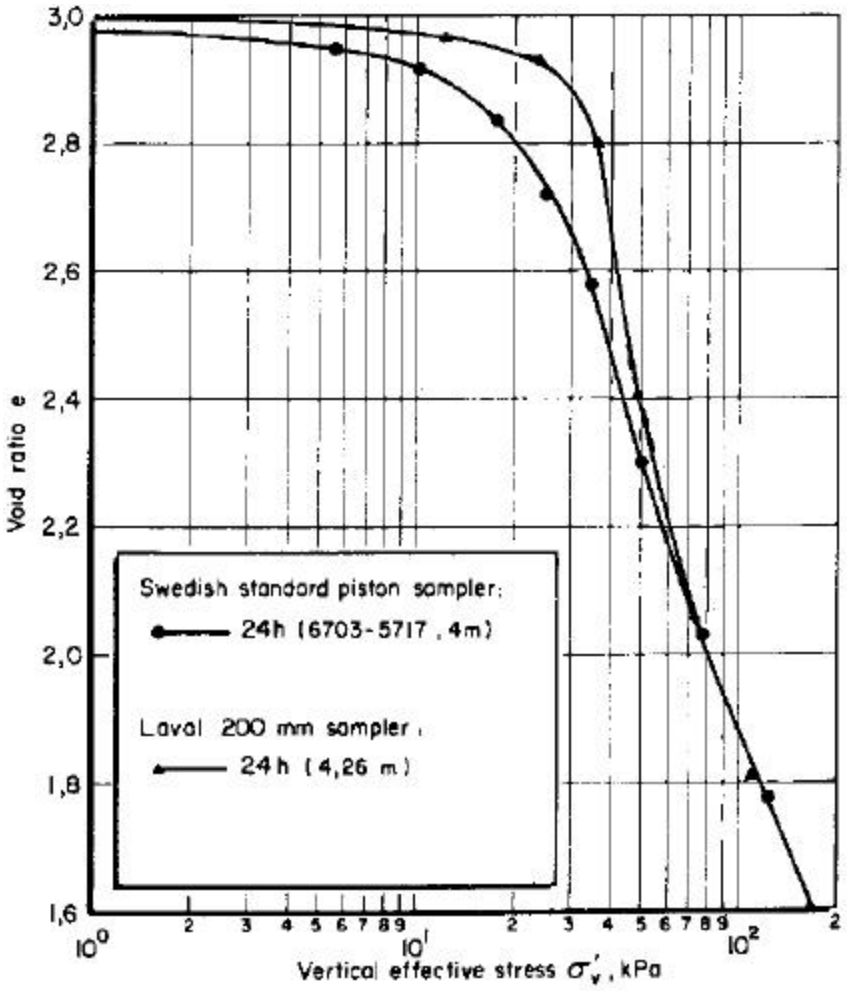

Figure 5.14: Effect of sample disturbance on Vasby clay compressibility (from Leroueil and Kabbaj, 1987)

preconsolidation stresses were close to minimum values. In order to account for sample disturbance effects measured by Chang (1969), the laboratory c_v values and the assumed c_v values in the dry crust were doubled.

The void ratio vs. log effective stress curve from Leroueil and Kabbaj (1987) was used to characterize stress dependent values of $C_{\varepsilon c}$ and $C_\alpha = 0.06 \cdot C_{\varepsilon c}$. For stresses less than 50 kPa the original $C_{\varepsilon c}$ value increased from a maximum value of 0.6 to an undisturbed $C_{\varepsilon c}$ value equal to 0.74. However, since $C_{\varepsilon c}$ and C_α values are stress-dependent, the initial values of $C_{\varepsilon c}$ and C_α used in the revised analysis actually decrease with depth: from the ground surface to about 9 m $C_{\varepsilon c}$ = 0.74 and C_α=0.044; from 9 m to the bottom of the profile, $C_{\varepsilon c}$ = 0.54 and C_α= 0.032. As consolidation progresses and the effective stresses below a depth of about 10 meters increase and exceed about 75 kPa, $C_{\varepsilon c}$ decreases to 0.36 and C_α decreases to 0.022.

TABLE 5.2
Summary of Estimated "Undisturbed" Soil Properties
Väsby Test Fill

Refer to Figure 5.15, "Undisturbed" geotechnical profile beneath Väsby test fill

Soil Number	Layer elevation (m)	Unit weight (kN/m3)	$C_{\varepsilon c}$		C_α		$C_{\varepsilon r}$	c_v (m^2/day)	
			at $\sigma_{p\text{-}ref}$	at σ_{final}	at $\sigma_{p\text{-}ref}$	at σ_{final}		at $\sigma_{p\text{-}ref}$	at σ_{final}
1	7.10 to 6.00	14.00	0.74	0.51	0.044	0.031	0.04	0.043	0.026
2	6.00 to 5.06	14.00	0.74	0.51	0.044	0.031	0.04	0.026	0.015
3	5.06 to 2.85	13.40	0.74	0.51	0.044	0.031	0.04	0.0086	0.003
4	2.85 to 1.15	13.90	0.74	0.51	0.044	0.031	0.05	0.012	0.003
5	1.15 to -1.00	14.40	0.74	0.36	0.044	0.022	0.05	0.004	0.0014
6	1.00 to -4.25	15.40	0.51	0.36	0.031	0.022	0.05	0.007	0.0008
7	-4.25 to -6.40	17.20	0.36	0.36	0.022	0.022	0.04	0.009	0.003

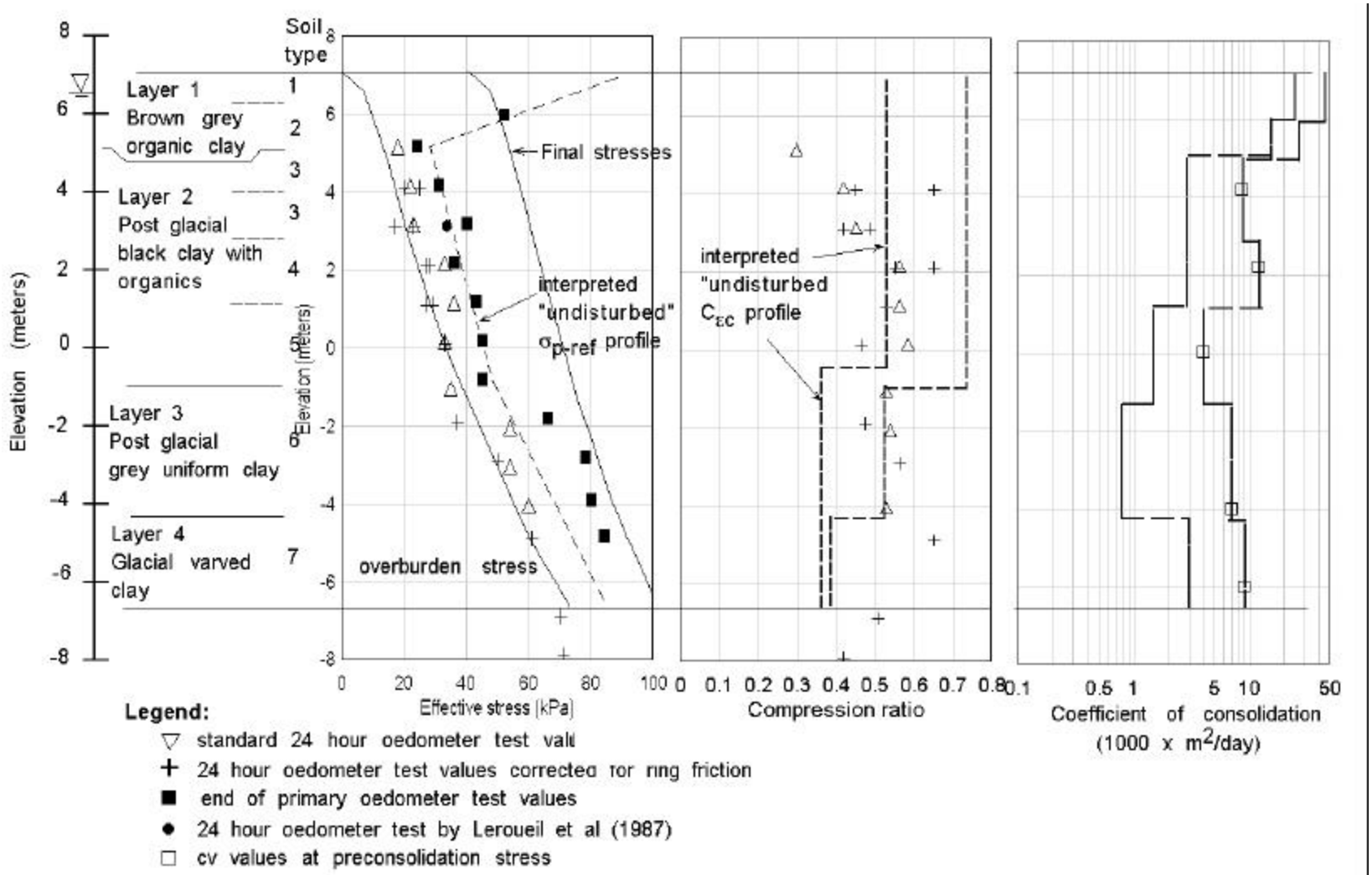

Figure 5.15: "Undisturbed" geotechnical profile beneath the Vasby test fill

Results of the CONSOL97 “undisturbed” analyses are summarized in Figure 5.16 to 5.19. Increasing the preconsolidation stress, compressibility, and coefficient of consolidation resulted in an increase in computed settlement magnitudes, settlement rates and excess pore pressure dissipation and better agreement with field measurements. The differences between EVP and EP model computations are also more significant. The EVP model predicts about 2 meters of settlement at the end of pore pressure dissipation after about 120 years (calendar year 2067) of loading whereas the EP model predicts about 1.4 meters of settlement.

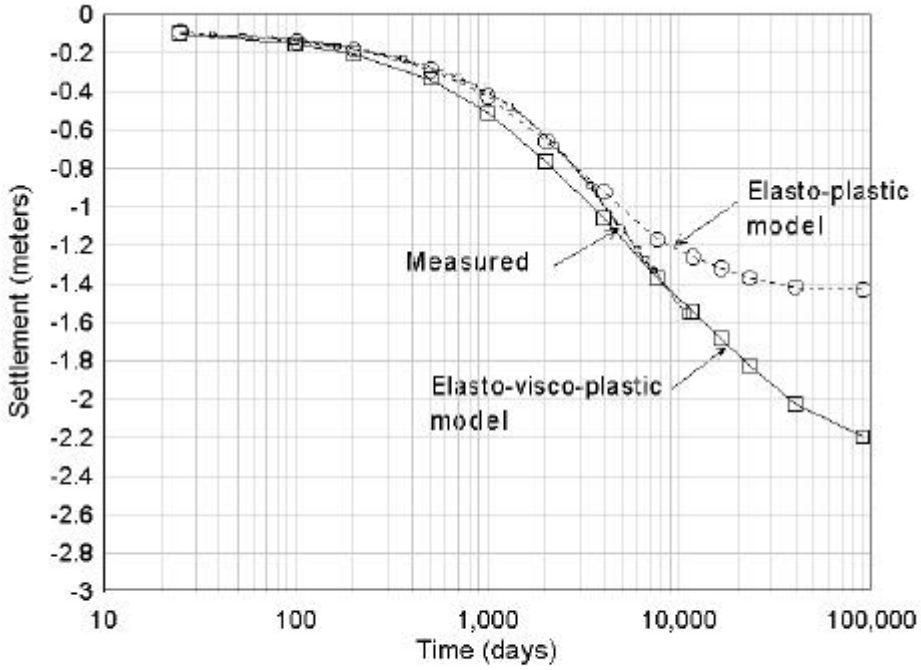

Figure 5.16: Measured settlement of the Väsby test fill and values computed using "undisturbed properties."

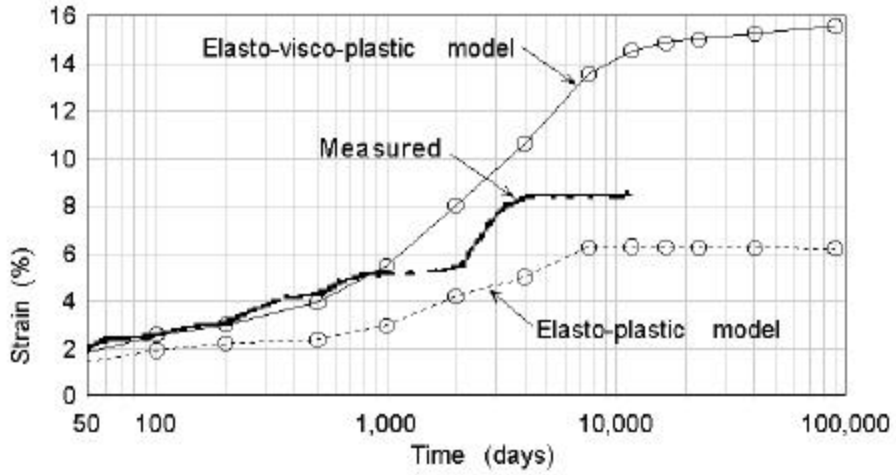

(a) Compression of the clay layer between 0 and 2.04 meters below the original ground surface

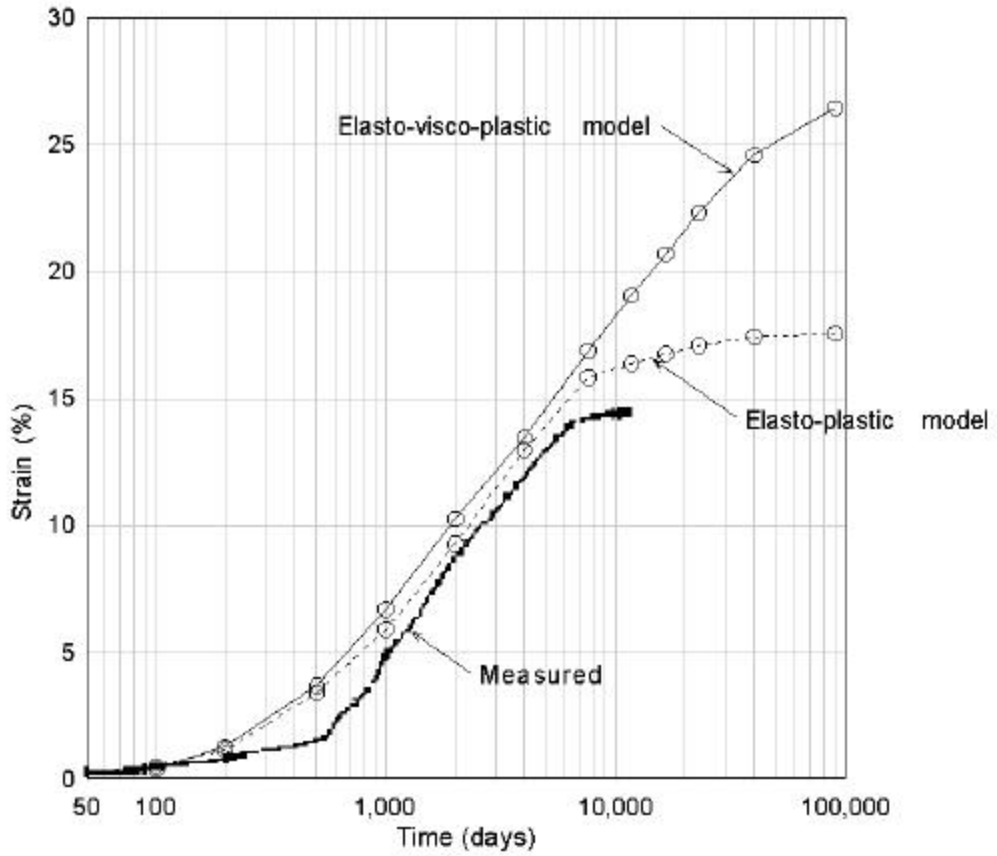

(b) Compression of the clay layer between 2.04 and 5.01 meters below the original ground surface

Figure 5.17: Measured compression vs. logarithm of time and values computed using "undisturbed" Vasby clay properties

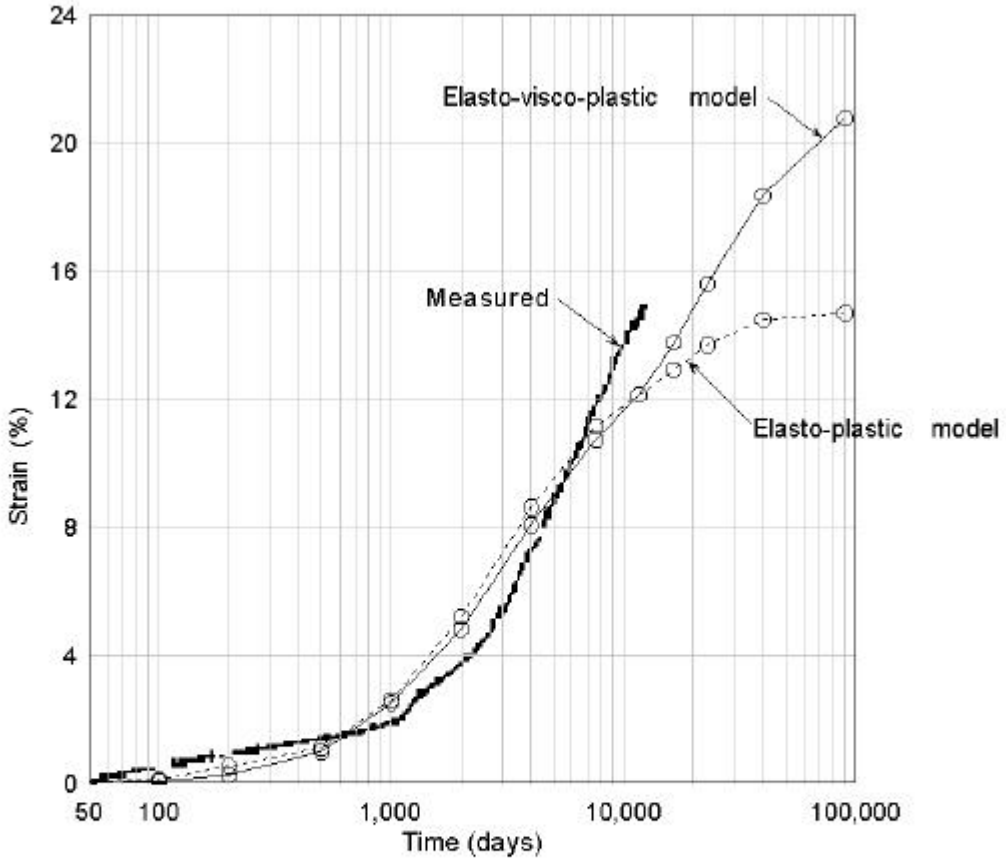

(c) Compression of the clay layer between 4.25 and 7.29 meters below the original ground surface

Figure 5.17 (continued): Measured compression vs. logarithm of time and values computed using "undisturbed" Vasby clay properties

Computed fill settlements (Figure 5.16) using the EVP model are in good agreement with 30 years of field measurements although the computed rate of settlement during the first 3 years is slightly faster than measured. Similar to the previous CONSOL97 analysis, the computations predict continued consolidation in clay zones one and two (Figures 5.17a and 5.17b) whereas the measurements indicate compression rates and magnitudes that are less than would be expected for secondary compression. The CONSOL97 analyses predict a doubling of the measured layer one

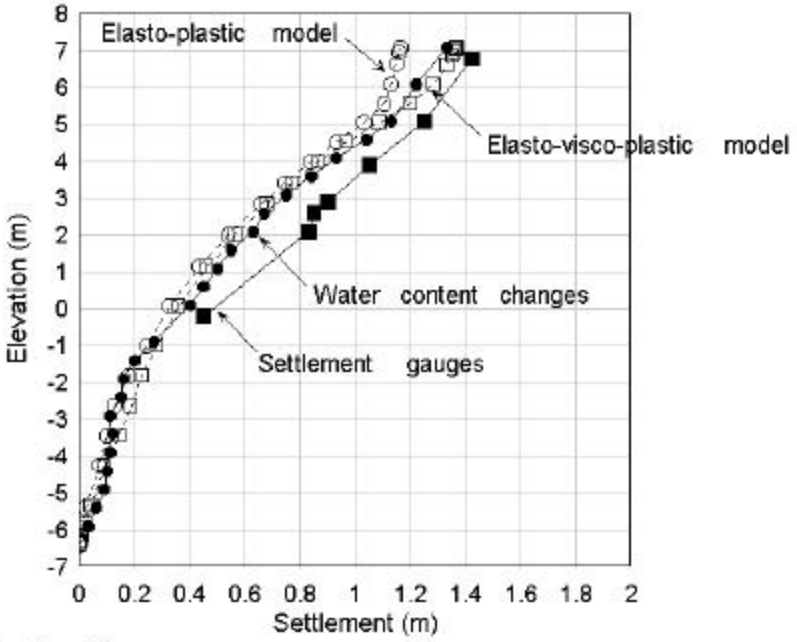

(a) Settlement profile after 20 years

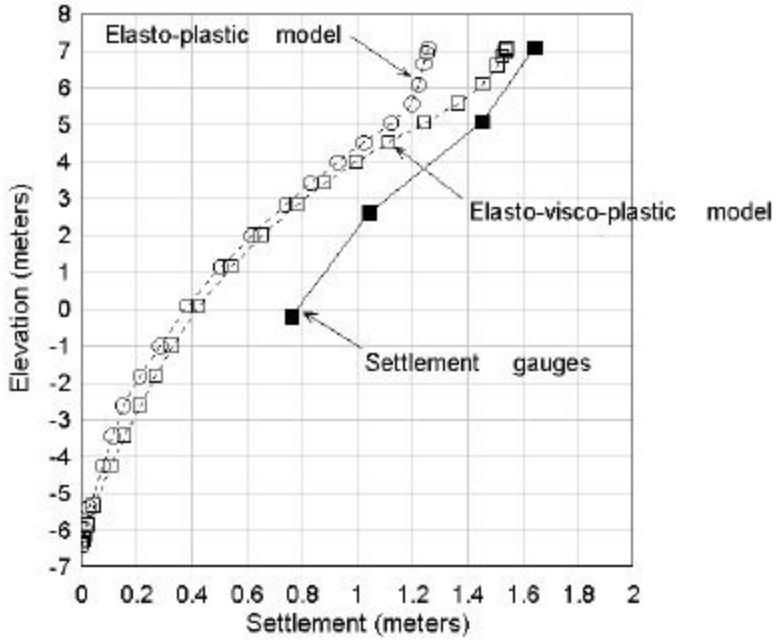

(b) Settlement profile after 30 years

Figure 5.18: Measured settlement profiles and values computed using "undisturbed" properties beneath the Vasby test fill

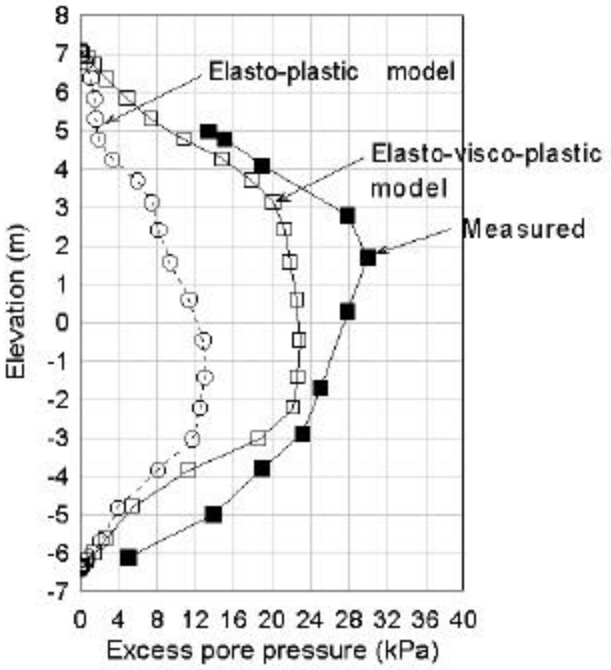

(a) Excess pore pressures after 20 years

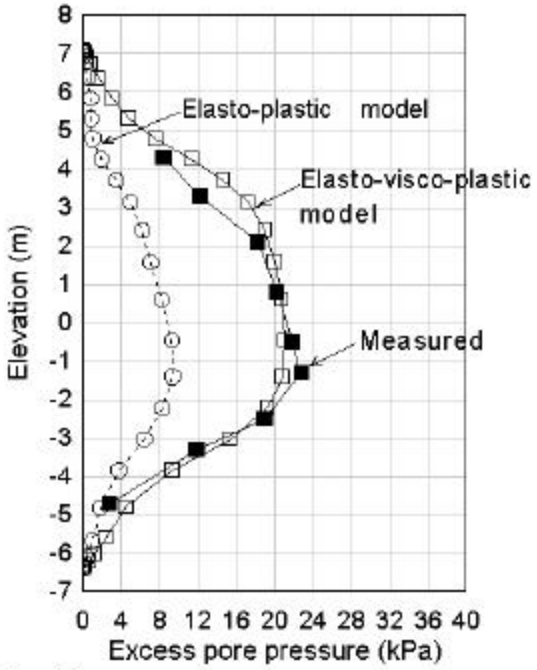

(b) Excess pore pressures after 30 years

Figure 5.19: Measured excess pore pressures and values computed using "undisturbed" properties beneath the Vasby test fill

and layer two strains in the next 50 years. In zone 3, the computed rate of strain is slower than measured (Figure 5.17c).

Measured settlement profiles and values computed using "undisturbed" properties for 1968 and 1977 are presented in Figure 5.18. The computed settlements for 1968 are in excellent agreement with the settlements determined from measured water content changes, but they are about 0.05 to 0.2 meters less than settlement gauge measurements in the upper 7.29 meters of the clay deposit. The computed settlements for 1977 are about 0.1 to 0.4 m less than the settlement gauge measurements. The EP model significantly underestimates settlement in the overconsolidated crust.

Figure 5.19 illustrates measured and computed excess pore pressure profiles after 20 and 30 years of consolidation. The computed EVP excess pore pressures in 1967 are less than measured values as would be expected based upon the predicted faster rates of settlements. Measured excess pore pressures are as much as 8 kPa larger than computed values. By 1977 the measured and computed excess pore pressures are in good agreement. Excess pore pressures computed using the EP model are about 50% less than excess pore pressures measured in 1967 and 1977.

5.1.5 Discussion

The measured strains and excess pore pressures in zone one (depth 0 to 2.04 m) and zone two (2.04 to 5.01 m) appear inconsistent. In 1969, the settlement gauges indicated strain rates much smaller than the rate of secondary compression, although the measured excess pore pressures in these zones were as large as 16 kPa. Also, from 1969 to 1979, the excess pore pressures decreased from about 30 kPa to 20 kPa but the gauges indicate no settlement in the upper 6 meters of the clay profile. The pore pressure data appears more reliable because new retractable piezometers were installed during test fill observations in 1969 and pore pressure readings were taken beneath the fill and in natural ground. The natural ground water level was 0.8 m below the

ground surface (elevation 6.4 m). The piezometers were re-installed and measurements were made again in 1979. Since pore pressure measurements do not rely upon initial readings and the accuracy of the instruments has been verified (Chang 1998), it appears that the inconsistent strain and pore pressure measurements were caused by settlement gauges that have once again malfunctioned.

The results of these CONSOL97 analyses indicate the effect of clay crust layers on consolidation and the importance of using high quality test data to realize the full predictive capabilities of the more sophisticated CONSOL97 EVP model. The analyses show that the clay crust permeability can be as much as 5 times higher than the underlying saturated soils and a significant factor in estimating rates of settlement and excess pore pressure dissipation. Soil parameters derived from standard sampling and laboratory testing procedures have produced computed settlements and rates of settlement that are much less than measured.

Of all the laboratory input parameters required to perform a CONSOL97 analysis, c_v (or permeability) is the most unreliable. Better agreement between measured and computed settlement and excess pore pressures could be obtained by further modification of the input parameters. However, without more reliable data, such an exercise would do little to validate the suitability of the CONSOL97 model in predicting long-term field consolidation. Although the Väsby test fill represents some of the most extensive field test data available, it unfortunately involves sensitive clays which suffers more adversely from sample disturbance. This added complexity makes it more difficult to assess the suitability of the CONSOL97 computer program. However, the measurements and CONSOL97 analyses with estimated “undisturbed” soil parameters clearly indicate that time dependent soil behavior increases the magnitude and rate of settlement and excess pore pressure dissipation as compared to conventional time-independent soil models.

The importance of creep compression on field behavior is clearly evident by examining Kabbaj et

al (1988) comparison of in situ stress-strain curves in zone three (depth 4.25 to 7.29 m) with laboratory stress-strain curves determined from tests on high quality samples obtained with the Laval sampler. The results summarized in Figure 5.20 indicate that the in situ strains are much larger than predicted by the laboratory stress-strain curve. The 1979 in situ strains are larger than predicted by the laboratory curves although the in situ effective stress is about 24 kPa less than the final effective stress.

The magnitude of the creep strain component from 1960 to 1968 was estimated from the in situ and lab curves. In this time interval the effective stresses increased from about 42.7 to 44.6 kPa and the strains increased from 9.0 to 12.3%. Using a lab value $C_{\varepsilon c} = 0.94$ to compute the instant strain component, the average coefficient of secondary compression from 1960 to 1968 was estimated to be about 0.075 and $\frac{C_\alpha}{C_{\varepsilon c}} = 0.080$, somewhat larger than the values used in the CONSOL97 analyses ($C_{\varepsilon c} = 0.74$ and $\frac{C_\alpha}{C_{\varepsilon c}} = 0.060$).

5.2 *SKÅ-EDEBY TEST FILL*

5.2.1 Project Description

The Skå-Edeby test fill is located on an island about 25 kilometers west of Stockholm, Sweden. The Swedish Geotechnical Institute and the Swedish Road Board designed and constructed the test field in 1957 to study the consolidation behavior of the soft clays, and to obtian information for construction of a new airfield. The test field consists of four circular test fills located as shown in Figure 5.21. Sand drains were installed at three of the fill sites and one test fill was "undrained" (no sand drains). This study will only address the performance of the "undrained" test fill, which will be subsequently referred to as the Skå-Edeby test fill.

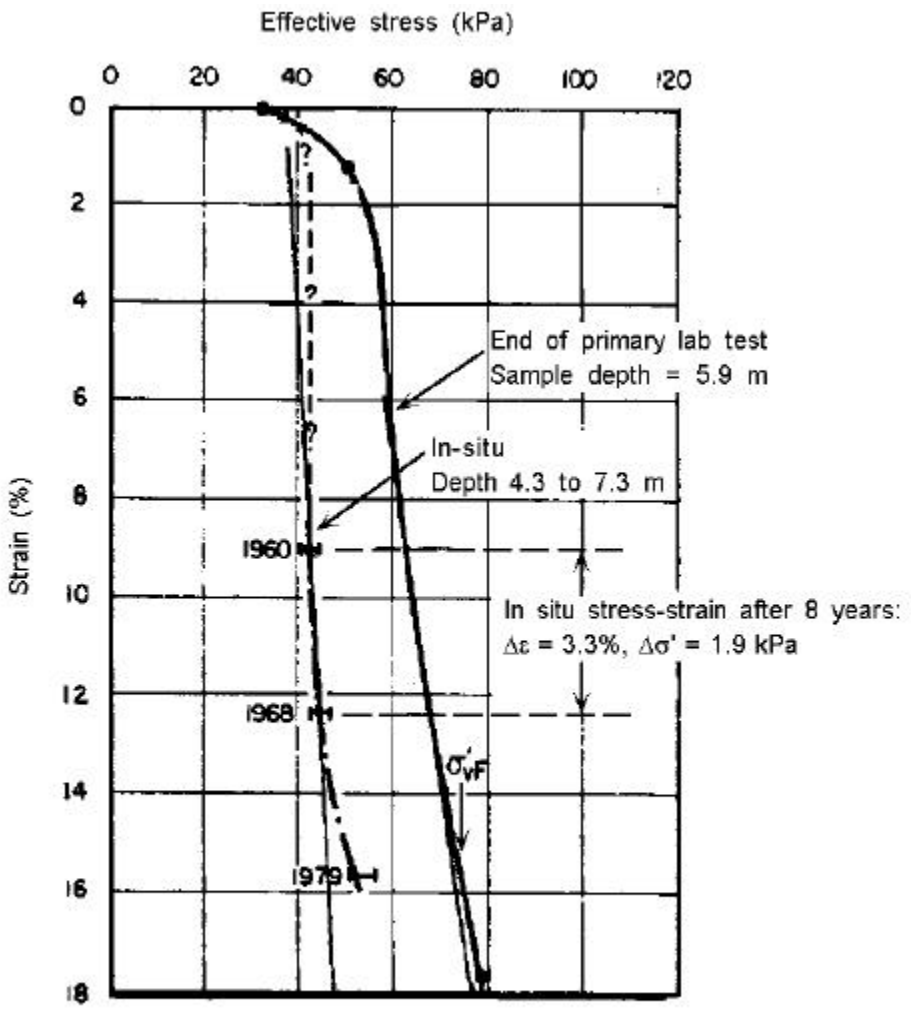

Figure 5.20: Comparison of laboratory end-of primary and in situ stress-strain curves beneath the Vasby test fill (after Kabbaj et al 1988)

The test fill was constructed in June and July of 1957, with a bottom diameter of 35 meters, slopes of 1.5H.1V, and a height of 1.5 meters. The gravel fill had an average bulk density of 1.79 t/m^3, and the applied stress increase was 27 kN/m^2. Surface and subsurface settlement gauges, and SGI hydraulic piezometers for measuring pore water pressures were installed at locations illustrated in Figure 5.22 prior to placing the test fill. Instrument readings were taken periodically,

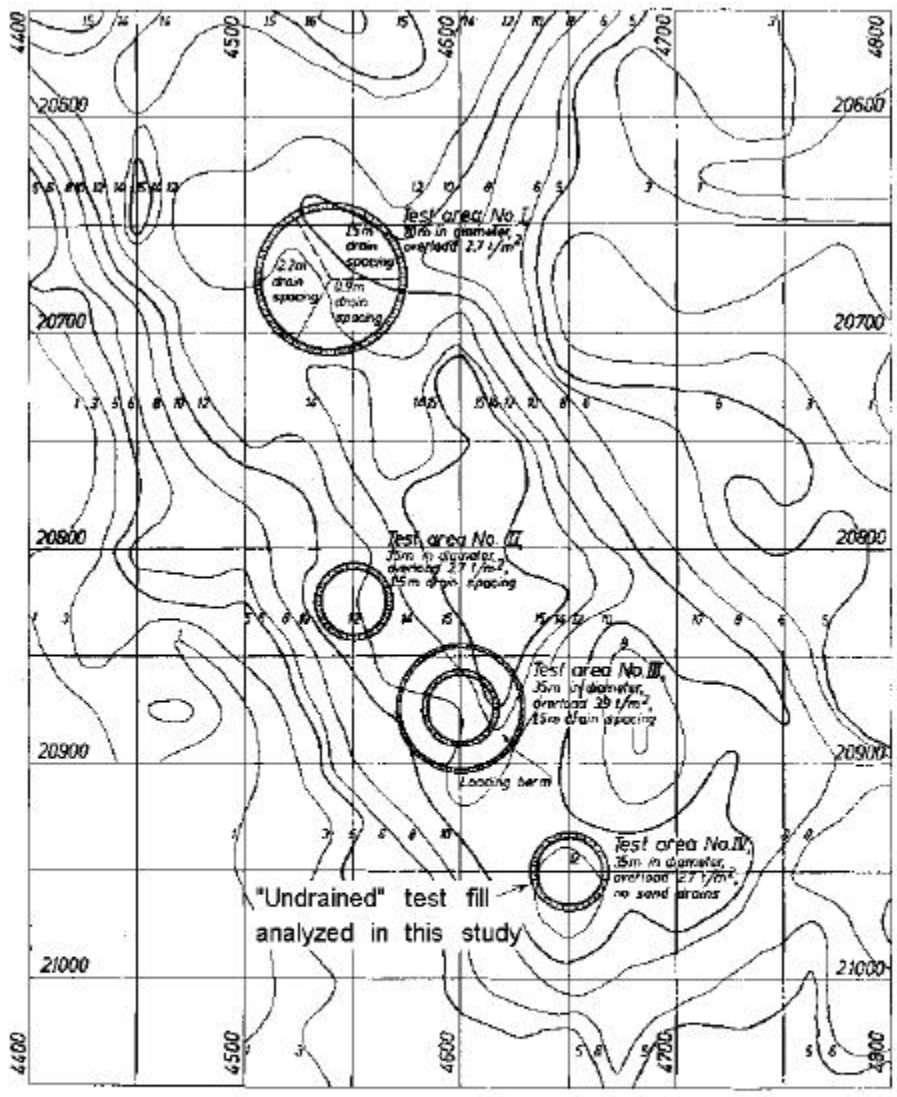

Notes:
1. Isopach lines of clay thickness in meters
2. Horizontal distances in meters

Figure 5.21: Skå-Edeby test fills and depth from ground surface to firm bottom (from Hansbo, 1960)

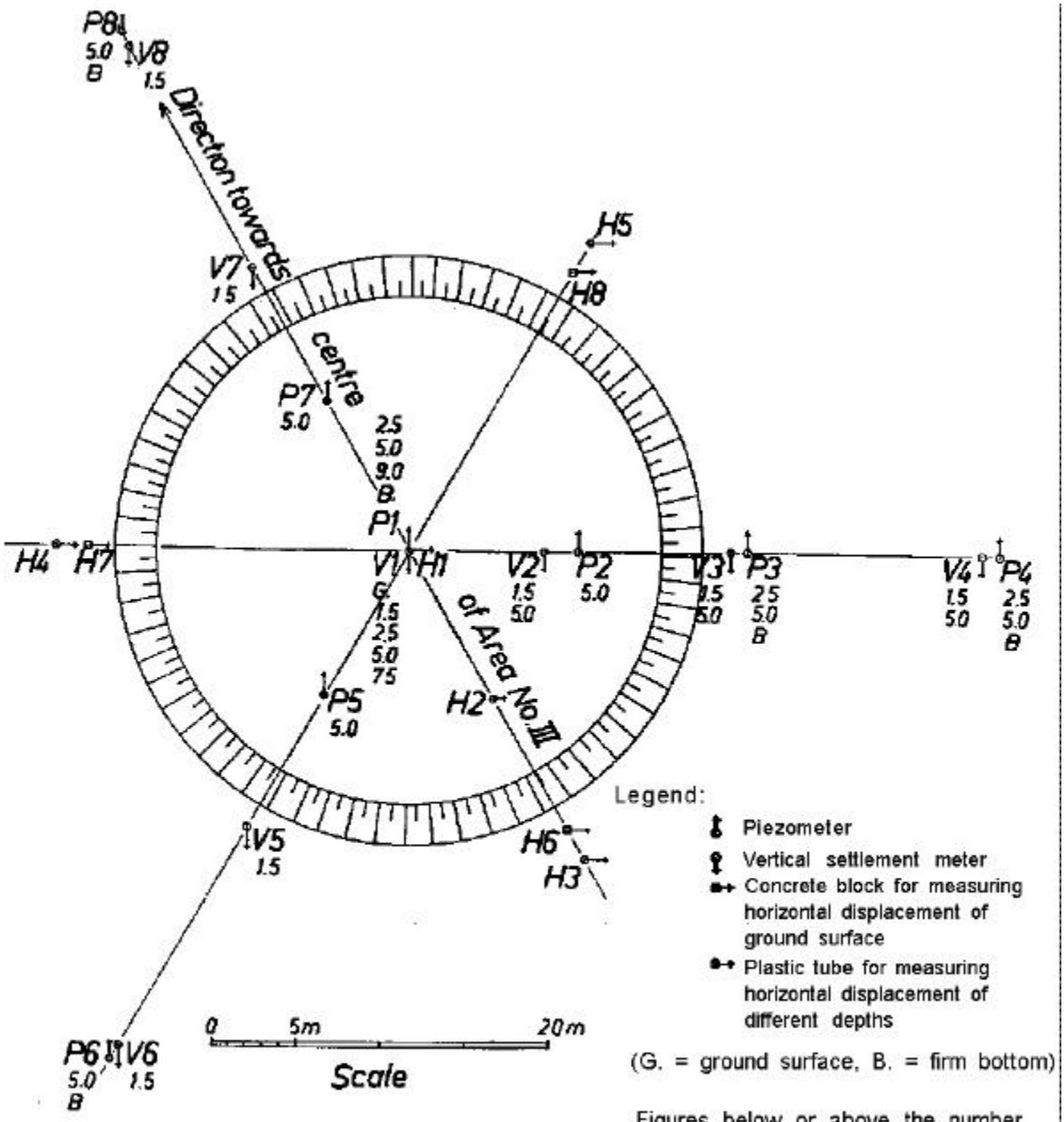

Figure 5.22: Instrumentation layout at Skå-Edeby test fill (from Hansbo, 1960)

even though the site had been abandoned for economic reasons. Hansbo (1960) published the first full report of the original site investigations and two years of instrument measurements.

Another detailed study of the test fills was undertaken in 1970 by Holtz, and included the installation of newer NGI piezometers due to some erratic results obtained from the original SGI piezometers. The results were reported at the Purdue conference in 1972 (Osterman and Lindskog, 1963, Holtz and Lindskog 1972, Holtz and Broms, 1972). Subsequent instrumentation measurements were obtained regularly, and the most recent results were published in connection with site studies by Larsson (1986). The site was also used to study the effects of piston sampler size on the quality of samples (Holtz and Holm, 1972).

5.2.2 Site Geology and Subsurface Conditions

The geologic conditions at Skå-Edeby are very similar to those at the Väsby test fill site, and typical of recent, post glacial and glacial clay deposits of central Sweden (Holtz and Broms, 1972). The site probably emerged from the Baltic Sea about 500 years ago, and is only about 2.5 m above sea level. The deepest sediments consist of glacial clays which are about 7500 years old. The upper, more recent post glacial soils were deposited within the last 4500 years. Both the glacial and post glacial deposits are predominantly soft, normally consolidated clays of moderate sensitivity, which are rich in iron sulfides and contain about 0.4% organic material. Salinity measurements of the glacial and post glacial clays indicate that some leaching has occurred because the pore water contains only about 0.5% salt.

A profile of subsurface conditions, soil strength and index properties is shown in Figure 5.23. The site is underlain by bedrock or very dense glacial moraine deposits at a depth of 12 meters. Bedrock is overlain by about 9 meters of glacial deposits consisting of soft “varved” clay. The “varves” consist of clay bands of different colors, and not alternating bands of clay and silt that is typically associated with the word varves. Post glacial deposits comprise the upper portion of the

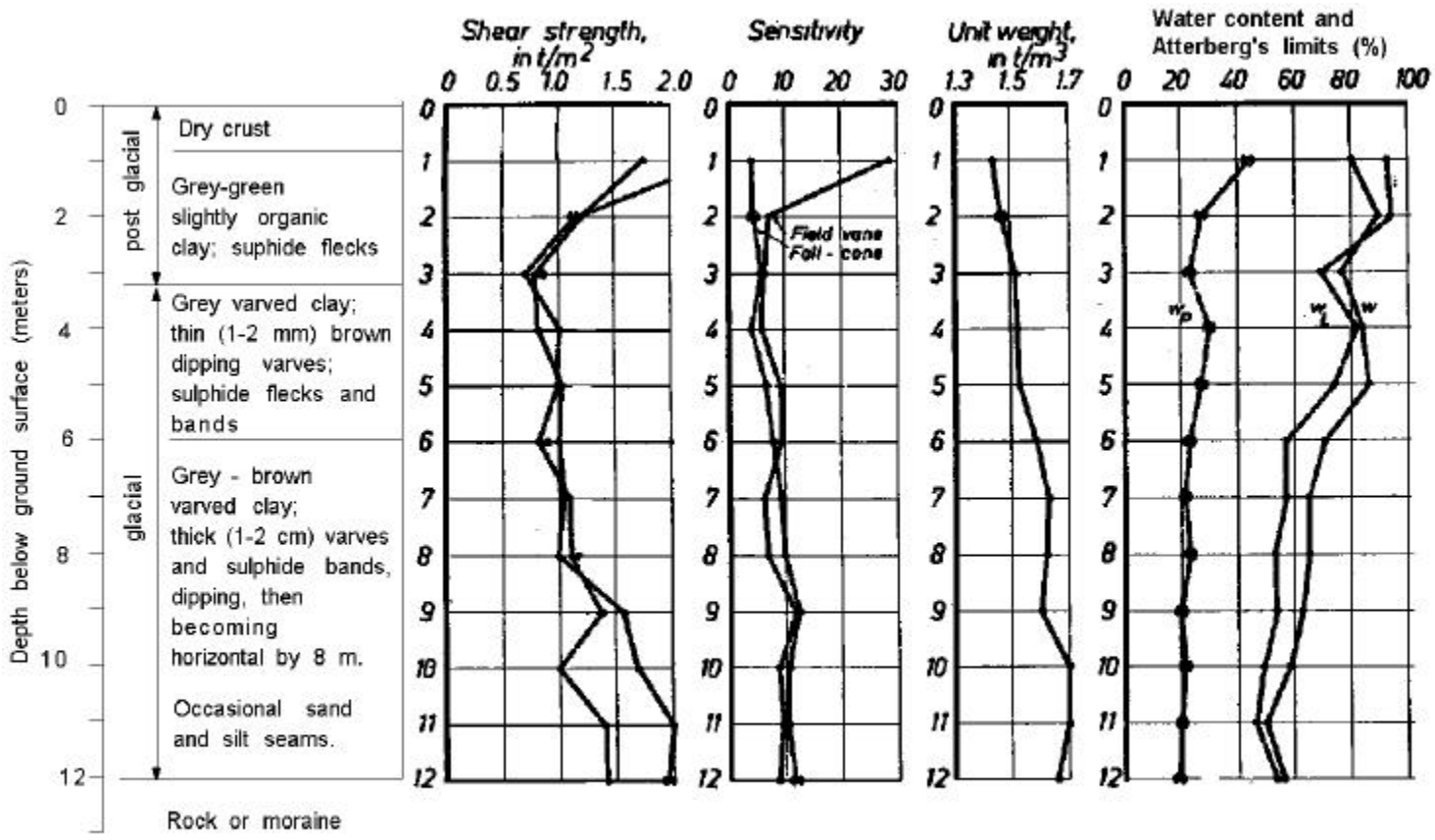

Figure 5.23: Profile of soil strength and index properties beneath the test fill at Ska-Edeby (from Hansbo, 1960)

soil profile, which consists of soft, slightly organic clay. The top of the post glacial soil profile, to a depth of 0.7 meters below the ground surface, consists of a dry, clay crust.

The groundwater table is usually about 0.5 m below the ground surface. Measurements indicate that the groundwater levels vary seasonally with a maximum variation of ±0.5 m. The pore pressures in natural ground are hydrostatic, corresponding to an average water table elevation.

5.2.3 Soil Properties

The index properties shown in Figure 5.23 were measured prior to placement of the test fill. The natural water contents are high and typically exceeded the liquid limit, except within two meters of the ground surface where the natural water contents were slightly less than the liquid limit. The highest water contents of about 100% were measured in the glacial clays at a depth of about 3 to 6 meters. Bulk densities generally increased from about 1.5 t/m^3 near the ground surface to about 1.7 t/m^3 at the bottom of the soil profile. Clay sensitivity increased from about 4 at the ground surface to about 10 to 12 near the bottom of the soil profile.

Consolidation properties were measured in four studies performed at the site. Incremental oedometer tests were performed in the original 1957 study (Hansbo, 1960), in 1971 (Holtz and Broms, 1972) and in 1977 (Holms and Holtz, 1977). CRS tests were performed by Larsson (1986). The SGI IV sampler was used in the original site investigation to obtain clay samples for the strain vs. logarithm effective stress and c_v vs. logarithm effective stress curves shown in Figure 5.24. Each load was applied to the 60.5 mm diameter by 20 mm thick samples for about 3 days and then doubled (LIR=1). Additional samples were obtained with the SGI VIII sampler which reportedly provided higher quality clay specimens (Hansbo, 1960). Strain vs. log effective stress curves for these samples, which were loaded for one day, are presented in Figure 5.25.

The strain vs log effective stress curves for the SGI IV and SGI VIII test results indicate that the

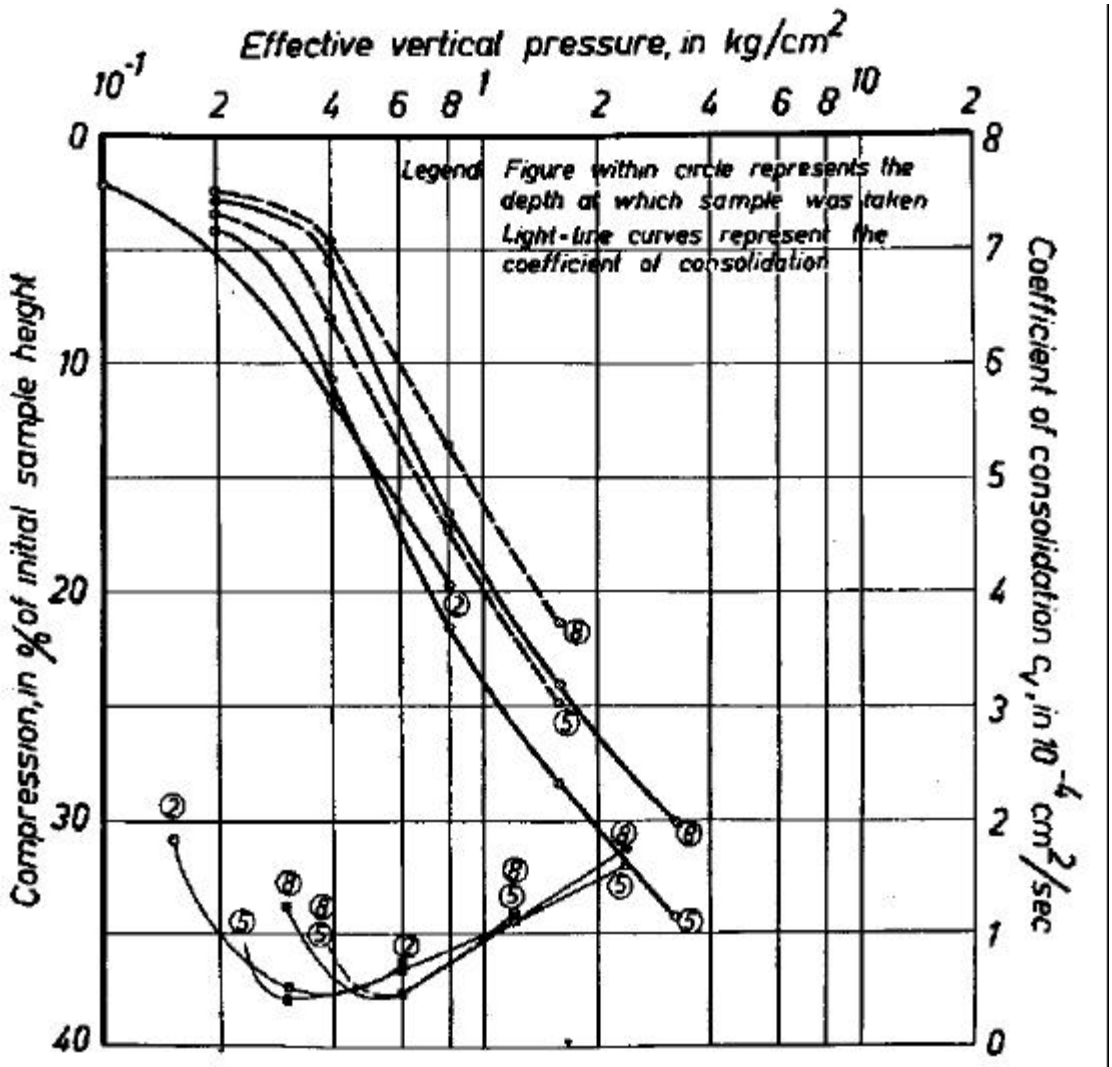

Figure 5.24: Incremental oedometer test results on samples obtained with the SGI IV sampler at the Ska Edeby test fill (from Hansbo, 1960)

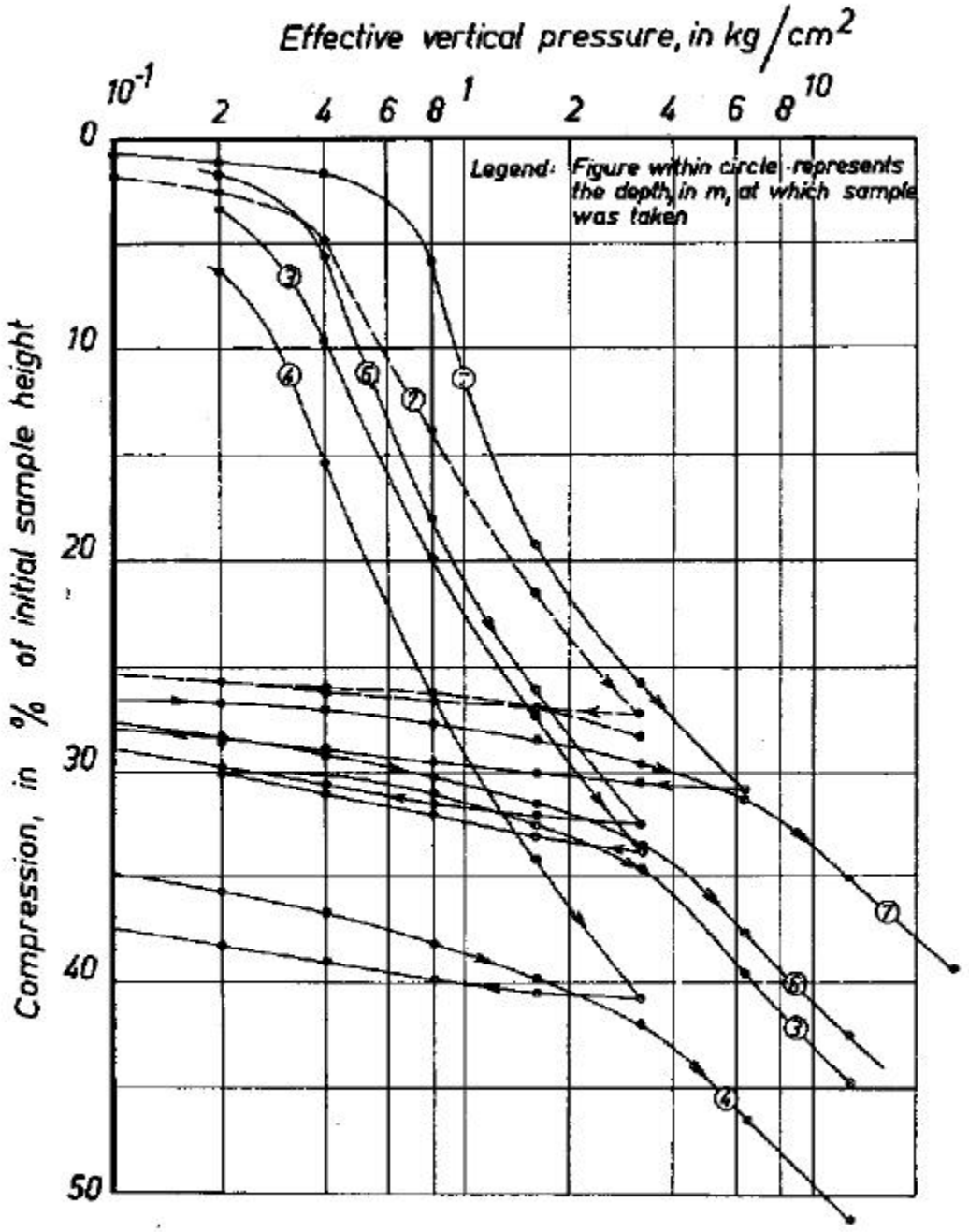

Figure 5.25: Incremental oedometer test results on samples obtained with the SGI VIII sampler at the Ska Edeby test site (from Hansbo, 1960)

SGI VIII samples are less disturbed than the SGI IV samples. The SGI VIII sample data shown in Figure 5.26 exhibit larger compressibility and more non-linear behavior than the SGI IV test results in Figure 5.24. The lab compression ratios summarized in the geotechnical profile (Figure 5.25) for the more disturbed samples were about 20% to 40% less than values for the less disturbed samples. Compression ratios for the less disturbed samples varied from about 0.52 at stresses less than about 50 kPa to a minimum value of about 0.35 at stresses in the range of 80 to 100 kPa.

As expected, the preconsolidation stresses estimated from one day loading curves (Figure 5.25) are larger than the preconsolidation stresses from 3 day loadings (Figure 5.24). In most cases the 3 day preconsolidation stresses are less than the initial effective overburden stress. The one day test results and other data (Holms and Holtz, 1977; Larsson, 1986) generally indicate that below a depth of about 2 or 3 meters, the soil profile is essentially normally consolidated for a groundwater level one meter below the ground surface.

Secondary compression data from the original site investigations was not reported. The only available secondary compression values were reported by Larsson (1986). The ratio $C_\alpha/C_{\varepsilon c}$ was expected to be about 0.04.

Laboratory values of consolidation coefficient are shown in Figure 5.24 and on the geotechnical profile (Figure 5.26). For each of the five specimens tested in the original SGI study, c_v values were smallest near the estimated preconsolidation stress, and increased with increasing effective stress. The measured minimum values were about 0.0005 m^2/day. Larsson's (1986) interpretation of c_v values measured in CRS tests are also shown in Figure 5.26. These values are typically about 2 to 3 times as high as the SGI values, which were determined from tests on samples obtained with the older SGI IV sampler. No data was reported for the higher quality samples obtained with the SGI VIII sampler.

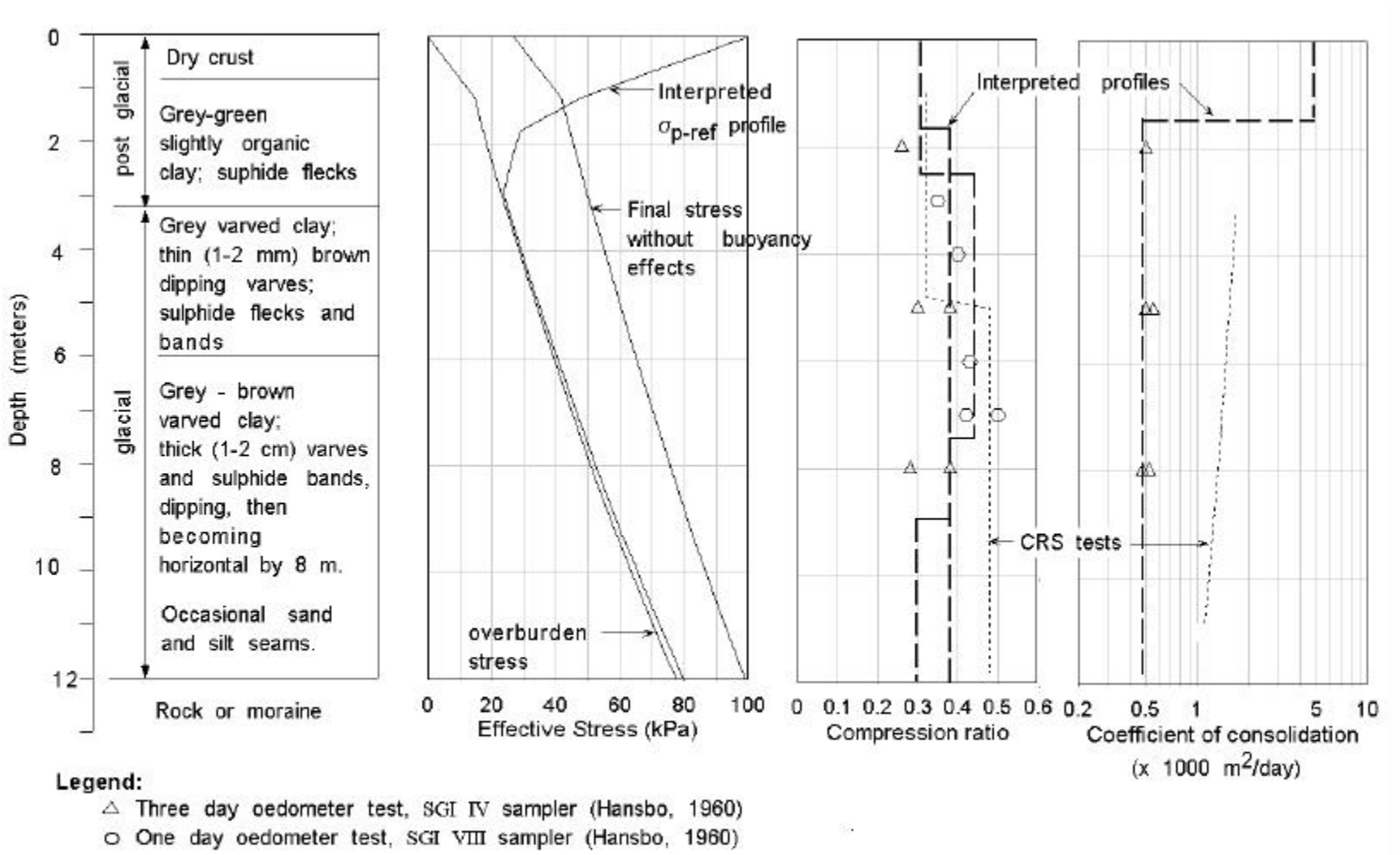

Figure 5.26: Geotechnical profile beneath the Ska-Edeby test fill

5.2.4 CONSOL97 Input and Results

Two CONSOL97 analyses of the Skå-Edeby test fill were performed. The first analysis was based on the incremental oedometer test data from the original SGI study. It is believed that the quality of this test data is typical of most standard sampling and testing procedures. A second analysis was performed using all the published test data and engineering judgment to estimate "undisturbed" soil properties.

The interpreted standard lab test soil properties used in the CONSOL97 analysis of the Skå-Edeby test fill are summarized in Figure 5.26 and Table 5.3. The clay layer was divided into 7 layers and 23 sublayers of varying thickness. The sublayers at the drainage boundaries were about 0.02 meters thick and the sublayers at the center of the clay layer were about 1.2 meters thick. Seven different soil types were used to characterize the range of soil properties throughout the clay profile. Stress-dependent soil properties, $C_{\varepsilon c}$, and $C_\alpha = 0.04 \cdot C_{\varepsilon c}$, for each soil type were defined by three values for the range of stresses in this problem. For an applied stress of 27 kPa, the increase in laboratory values of c_v were insignificant and appeared to justify the use of a single value for each soil type. Hansbo (1960) reported that the upper one meter of the clay deposit had "frequent fissures." Lacking laboratory test data for the crust soils, c_v values in sublayer one (1.5 m thick) and two (1.0 m thick) were assumed equal to 10 and 5 times laboratory values measured in CRS tests by Larsson (1986).

The results of the CONSOL97 analysis using the EVP model are illustrated in Figures 5.27 to Figure 5.30. As shown in Figure 5.27, the computed rate of fill settlement is much slower than the measured rate of settlement. The most recent settlement measurements, after 25 years (1982), are more than twice computed settlements, and are also greater than the computed ultimate settlements which are predicted to occur after about 90 years. Settlements measured at depths of 1.5, 2.5, 5.0 and 7.5 meters (Figures 5.28 and 5.29) were also about 2 to 3 times the computed settlements. Computed excess pore pressures after 14 years (1971) and 25 years (1982) are

shown in Figure 5.30. They generally exceed the measured values by about 30% to 50%.

TABLE 5.3
Summary of Laboratory Determined Soil Properties
Skå-Edeby Test Fill

Refer to Figure 5.26, Geotechnical profile beneath Skå-Edeby test fill

Soil Number	Layer depth (m)	Unit weight (kN/m3)	$C_{\varepsilon c}$		C_{α}		$C_{\varepsilon r}$	c_v (m^2/day) from $\sigma_{p\text{-}ref}$ to σ_{final}
			at $\sigma_{p\text{-}ref}$	at σ_{final}	at $\sigma_{p\text{-}ref}$	at σ_{final}		
1	0.0 to 1.5	14.00	0.30	0.30	0.012	0.012	0.03	0.005
2	1.5 to 2.5	14.50	0.38	0.38	0.015	0.015	0.03	0.0005
3	2.5 to 5.0	14.90	0.45	0.38	0.018	0.015	0.03	0.0005
4	5.0 to 7.5	15.50	0.45	0.45	0.018	0.018	0.03	0.0005
5	7.5 to 9.0	16.00	0.38	0.38	0.015	0.015	0.03	0.0005
6	9.0 to 10.5	16.40	0.30	0.38	0.012	0.015	0.03	0.0005
7	10.5 to 12.0	17.00	0.30	0.38	0.012	0.015	0.03	0.0005

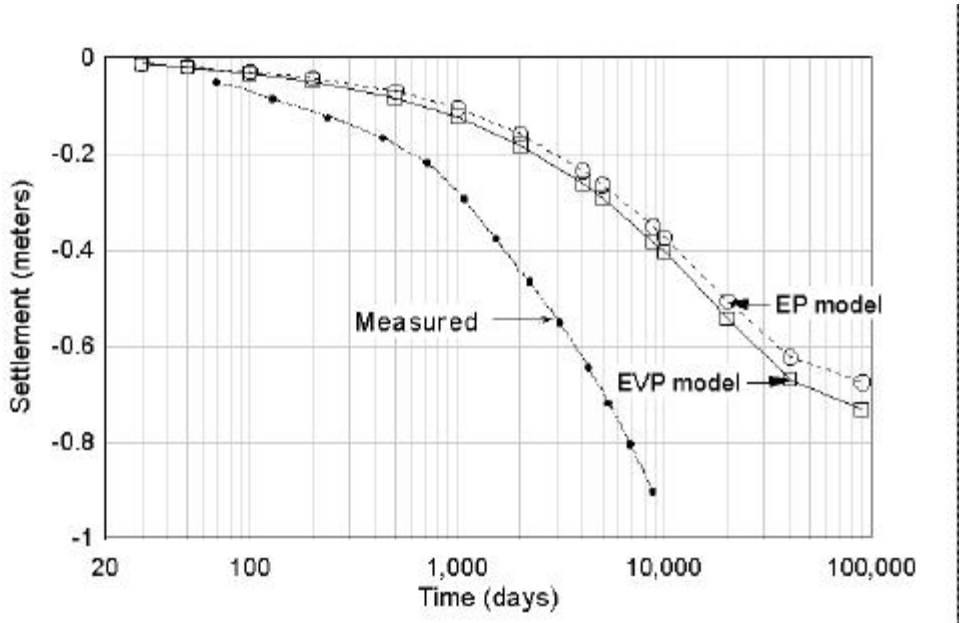

Figure 5.27: Measured and computed settlement of the Skå Edeby test fill

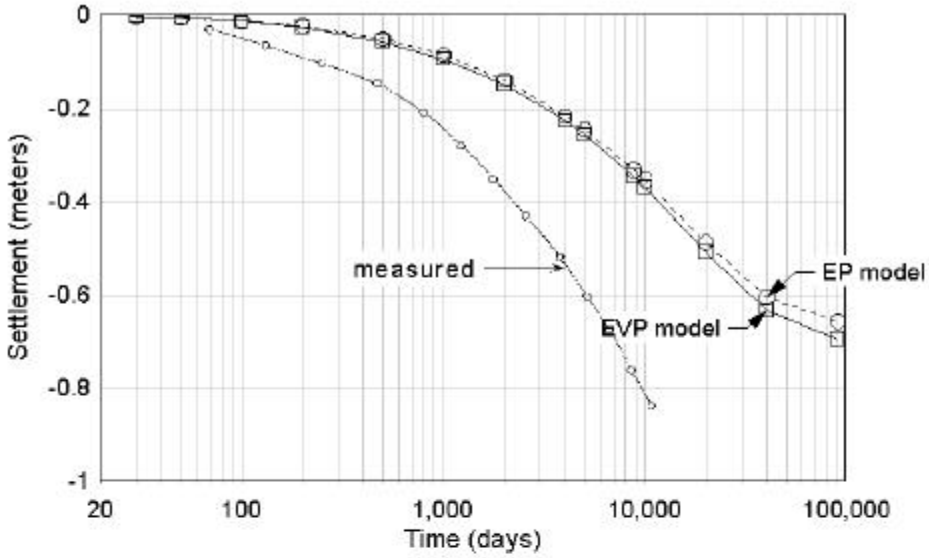

(a) Settlements at a depth of 1.5 meters

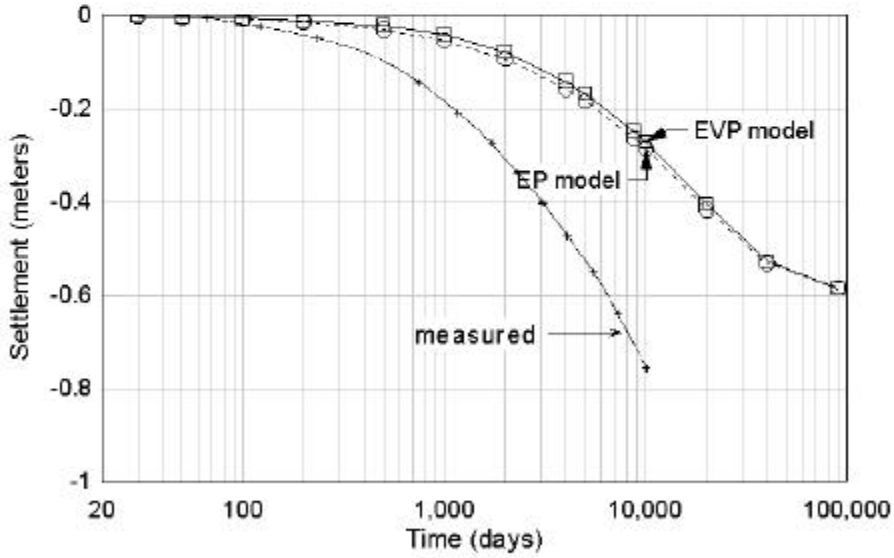

(b) Settlements at a depth of 2.5 meters

Figure 5.28: Measured and computed settlements at 1.5 and 2.5 meters below the Ska Edeby test fill

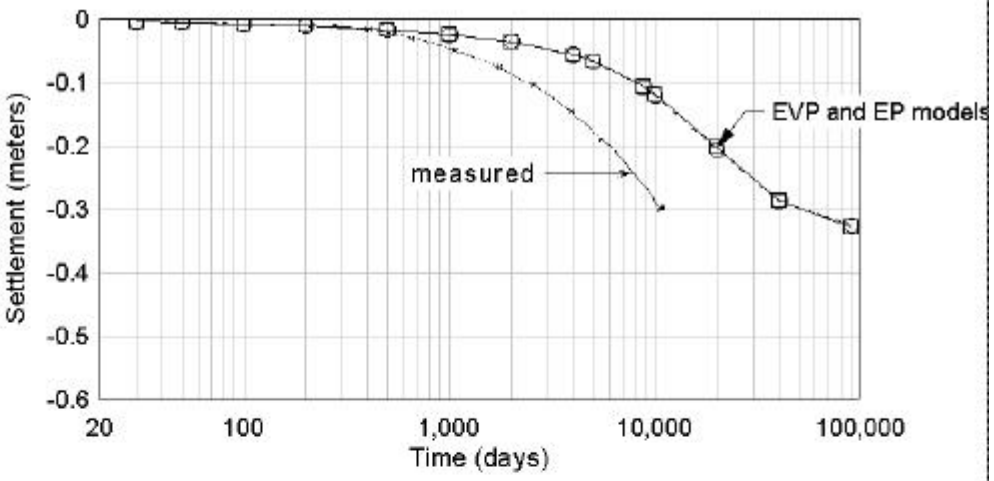

(a) Settlements at a depth of 5.0 meters

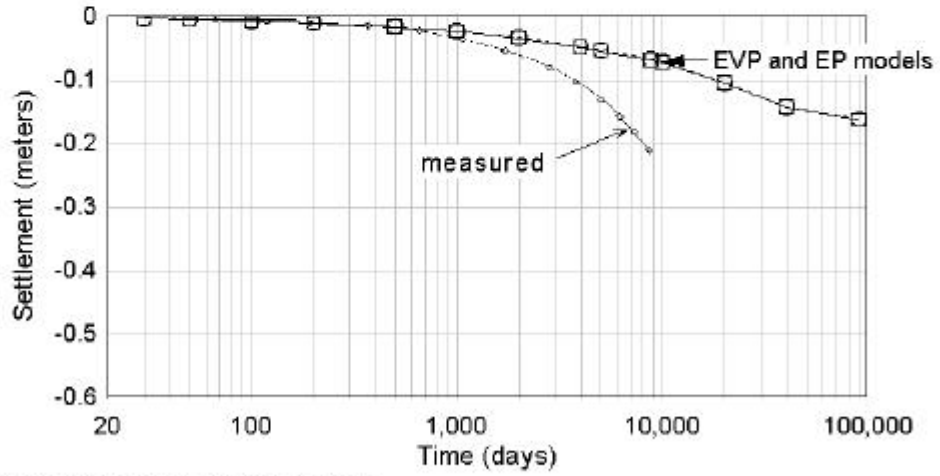

(b) Settlements at a depth of 7.5 meters

Figure 5.29: Measured and computed settlements at 5.0 and 7.5 meters below the Ska Edeby test fill

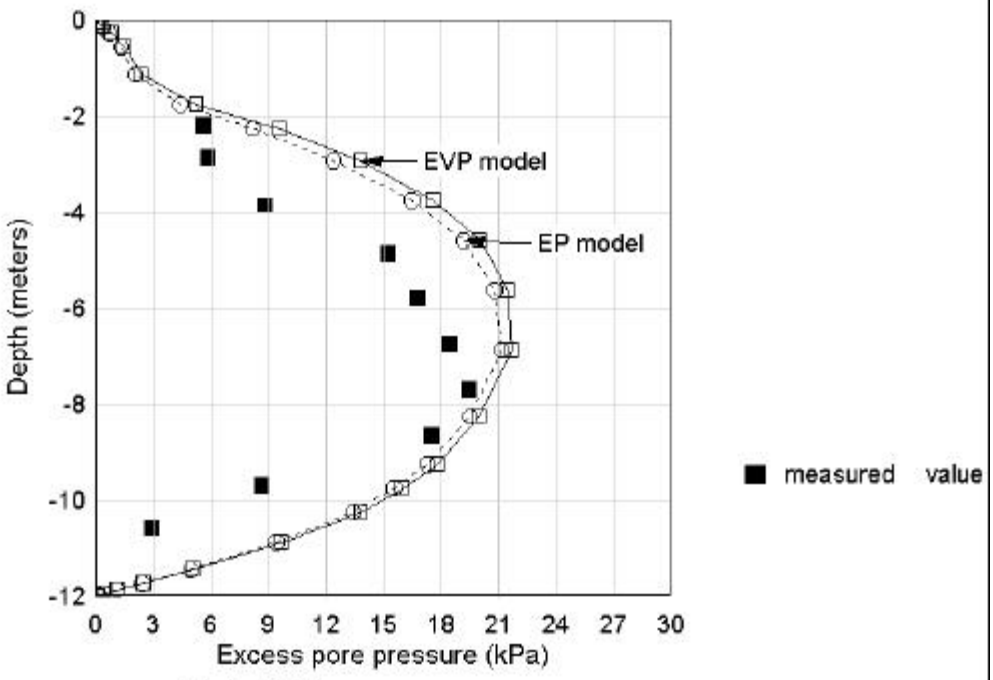

(a) Excess pore pressure profile in 1971

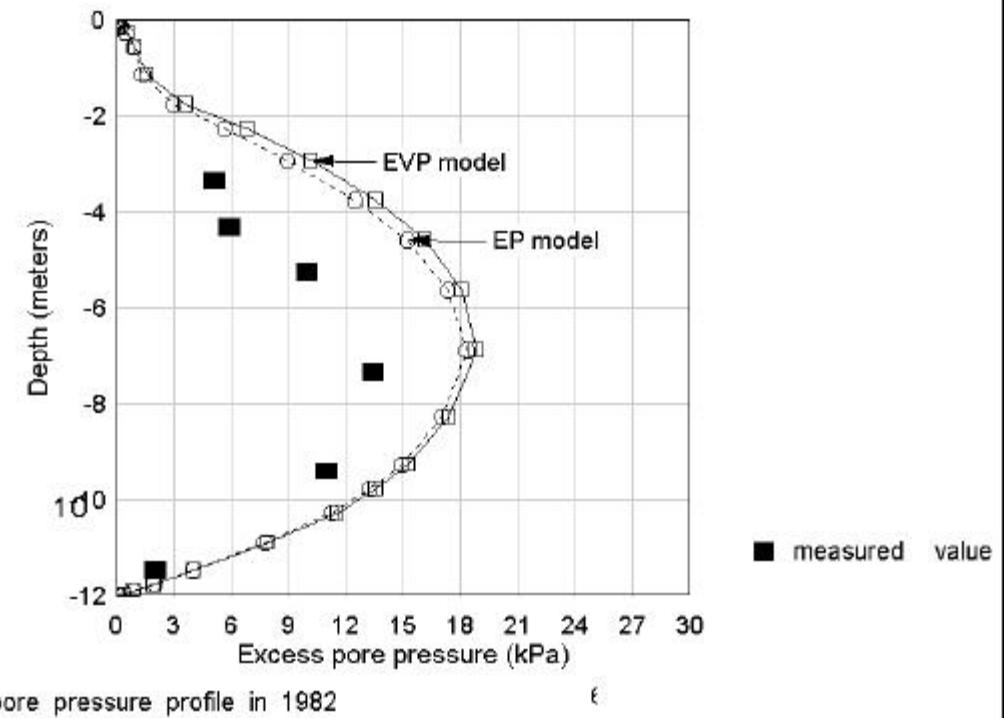

(b) Excess pore pressure profile in 1982

Figure 5.30: Measured and computed excess pore pressure profiles beneath the Ska Edeby test fill

These results suggest that the coefficients of consolidation and compressibility parameters measured in the original laboratory investigations are smaller than in situ values. In a study of the permeability of sensitive clays from Canada, USA and Sweden, Tavenas et al (1983) have shown that permeabilities back calculated from incremental oedometer tests consistently under-estimate in situ permeability, and that the values could differ by as much as one order of magnitude. Therefore, Larsson's (1986) c_v values from CRS tests on better quality samples, which were about 2 to 3 times larger than the original laboratory values, were considered to be more representative of "undisturbed" in situ soil properties. C_v values for the crust soils in sublayer one (1.5 m thick) and two (1.0 m thick) were assumed equal to 10 and 5 times the estimated "undisturbed" c_v values.

Compressibility parameters were also increased to account for sample disturbance effects in the original tests. The less disturbed test results for SGI VIII samples were considered more representative of "undisturbed" properties. These values are about 20% larger than the original lab values. The ratio $C_\alpha = 0.04 \cdot C_{\varepsilon c}$ were not changed. The "undisturbed" profile of soil properties is shown in Figure 5.31, and is summarized in Table 5.4.

TABLE 5.4
Summary of Estimated "Undisturbed" Soil Properties
Skå-Edeby Test Fill

Refer to Figure 5.31, "Undisturbed" geotechnical profile beneath Skå-Edeby test fill

Soil Number	Layer depth (m)	Unit weight (kN/m3)	$C_{\varepsilon c}$		C_α		$C_{\varepsilon r}$	c_v (m^2/day) from $\sigma_{p\text{-}ref}$ to σ_{final}
			at $\sigma_{p\text{-}ref}$	at σ_{final}	at $\sigma_{p\text{-}ref}$	at σ_{final}		
1	0.0 to 1.5	14.00	0.35	0.35	0.014	0.014	0.03	0.015
2	1.5 to 2.5	14.50	0.52	0.52	0.021	0.021	0.03	0.0075
3	2.5 to 5.0	14.90	0.52	0.46	0.021	0.018	0.03	0.0015
4	5.0 to 7.5	15.50	0.52	0.46	0.021	0.018	0.03	0.0015
5	7.5 to 9.0	16.00	0.46	0.46	0.018	0.018	0.03	0.0015
6	9.0 to 10.5	16.40	0.52	0.46	0.021	0.018	0.03	0.0015
7	10.5 to 12.0	17.00	0.52	0.46	0.021	0.018	0.03	0.0015

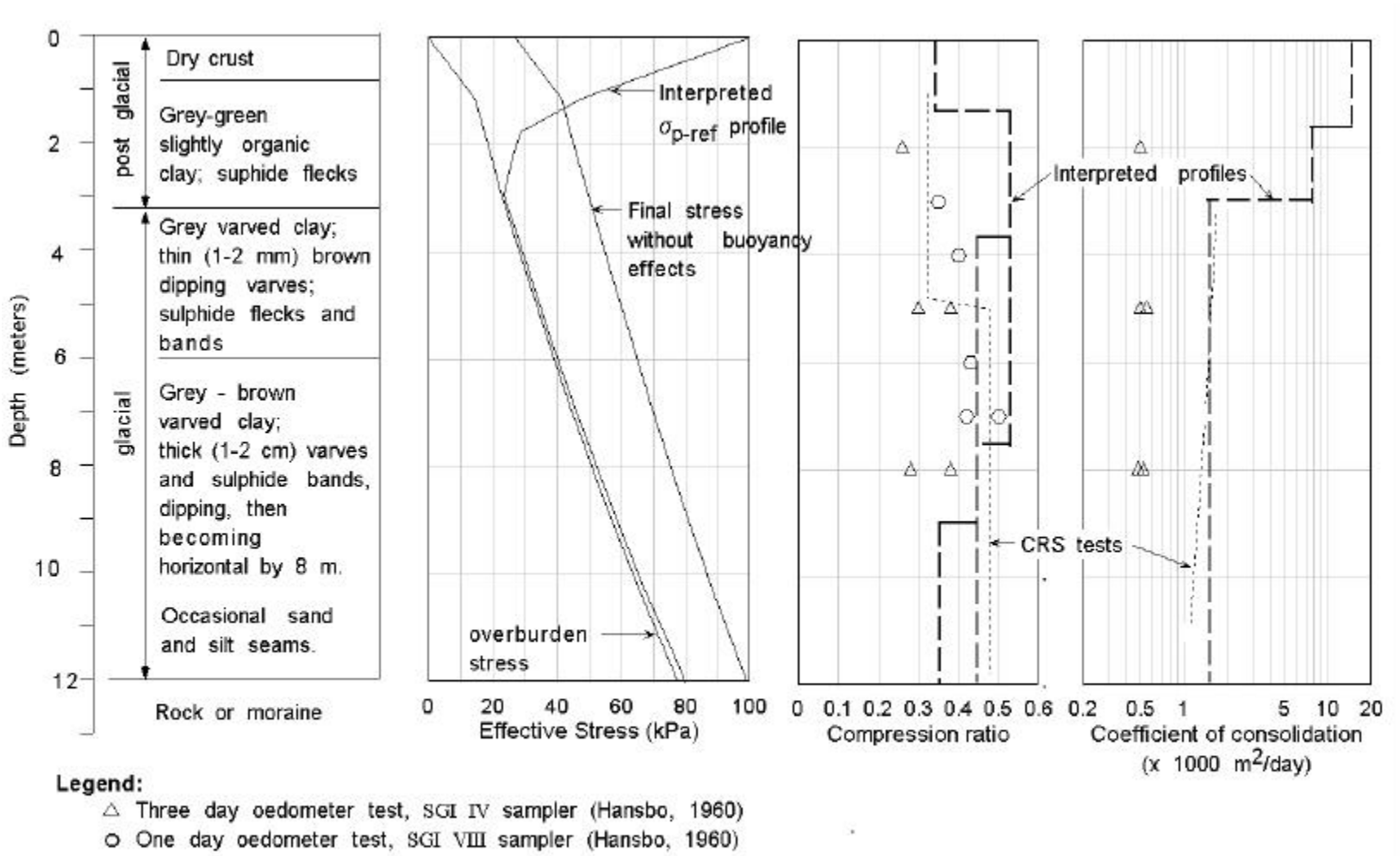

Figure 5.31: "Undisturbed" geotechnical profile beneath the Ska-Edeby test fill

The calculated rate and magnitude of fill settlement (Figure 5.32) and settlements at depth (Figures 5.33 and 5.34) are in good agreement with measured results for about 1000 days. Subsequently, the measured settlement rates are significantly faster than computed. The most recent fill settlement measurement, after 25 years (about 8000 days), is about 30% greater than the computed settlement, and is also larger than the computed settlement at the end of pore pressure dissipation, which is predicted to occur after about 60 years.

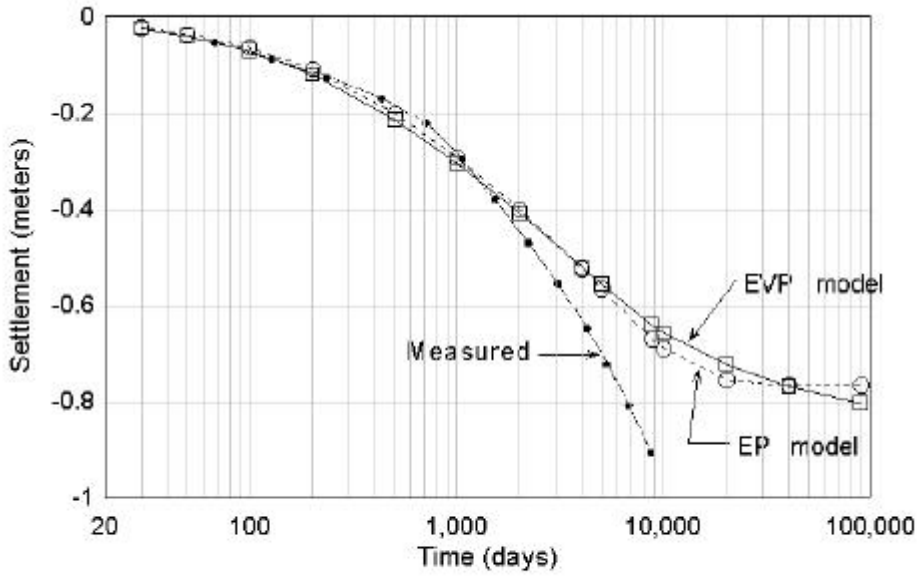

Figure 5.32: Measured settlement and values computed using "undisturbed" soil properties beneath the Ska Edeby test fill

Settlements measured at depths of 1.5, 2.5, 5.0 and 7.5 meters (Figures 5.33 and 5.34) were about 30% to 50% larger than the computed settlements. Measured and computed settlement profiles in 1981, after 24 years of consolidation, are shwon in Figure 5.35. The EVP model settlements are less than measured settlements throughout the full depth of the clay layer. Near the center of the clay layer, the computed settlements are as much as 50% less than measured settlements.

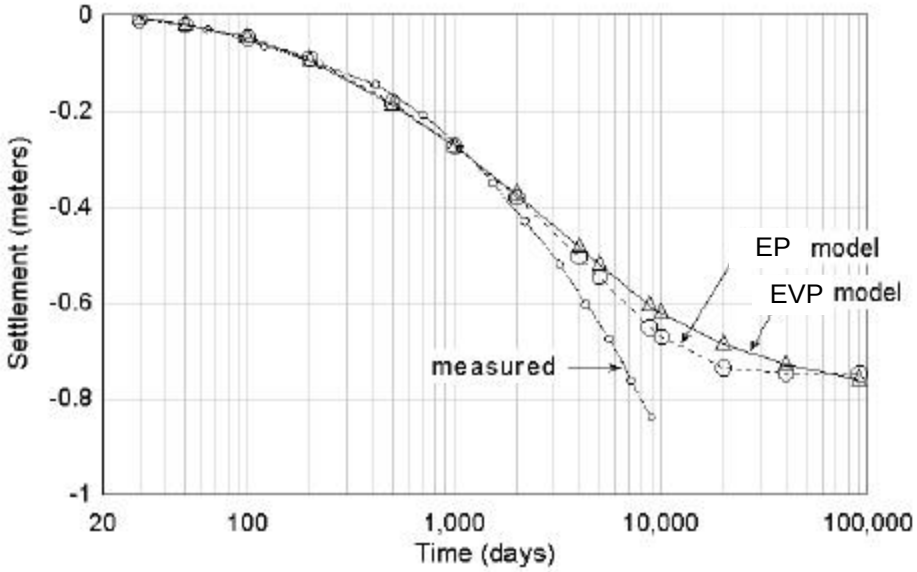

(a) Settlements at a depth of 1.5 meters

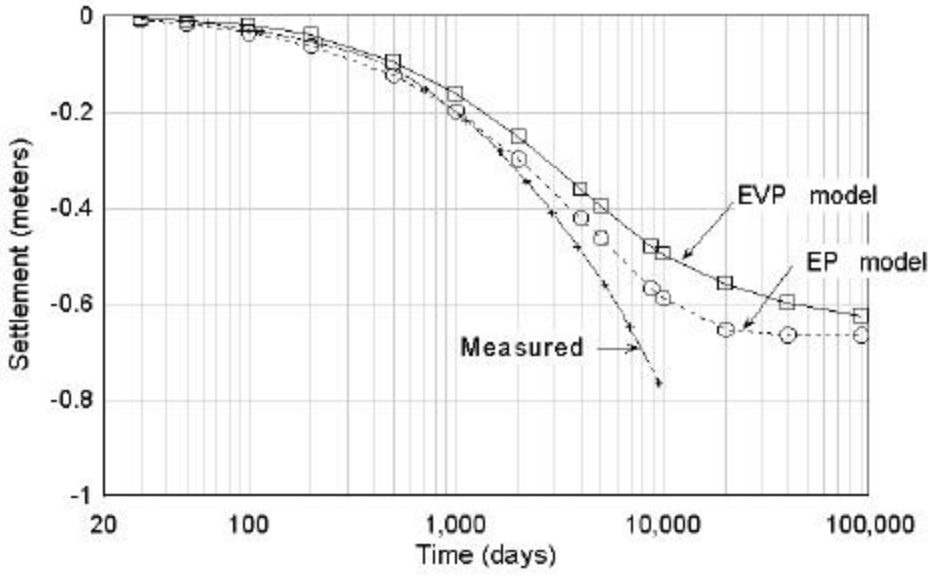

(b) Settlements at a depth of 2.5 meters

Figure 5.33: Measured settlements at 1.5 and 2.5 meters below the Skå Edeby test fill and values computed using "undisturbed" soil properties

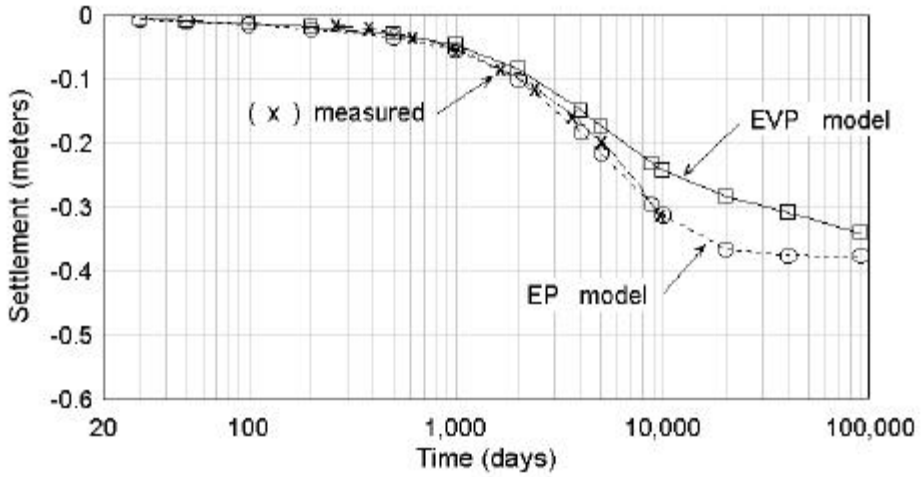

(a) Settlements at a depth of 5.0 meters

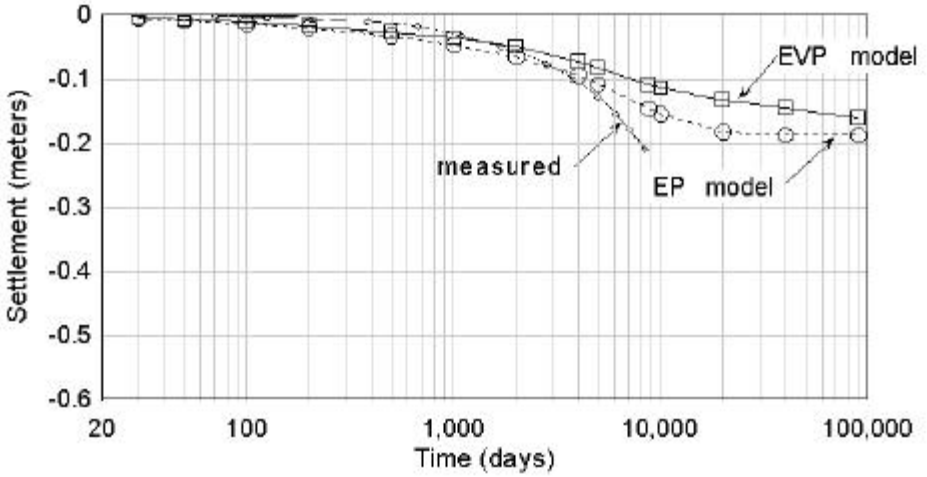

(b) Settlements at a depth of 7.5 meters

Figure 5.34: Measured settlements at 5.0 and 7.5 meters below the Skå Edeby test fill and values computed using "undisturbed" soil properties

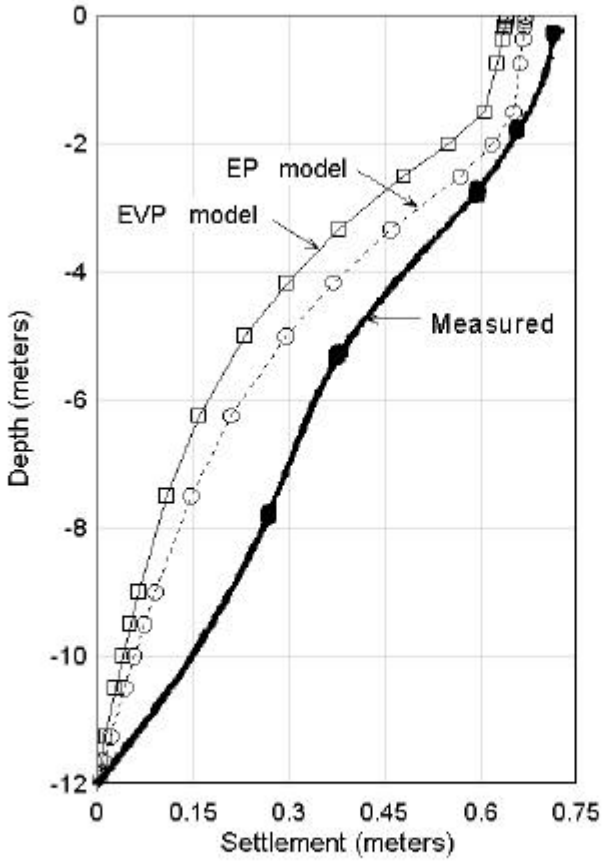

Figure 5.35: Measured settlement profile in 1981 and values computed using "undisturbed" soil properties beneath the Ska°Edeby test fill

Computed excess pore pressures after 14 and 25 years (Figure 5.36) are significantly less than measured values throughout the soil profile. Computed and measured excess pore pressures are greatest at a depth of 7 or 8 meters, but the computed excess pore pressures are only about 50% of measured values.

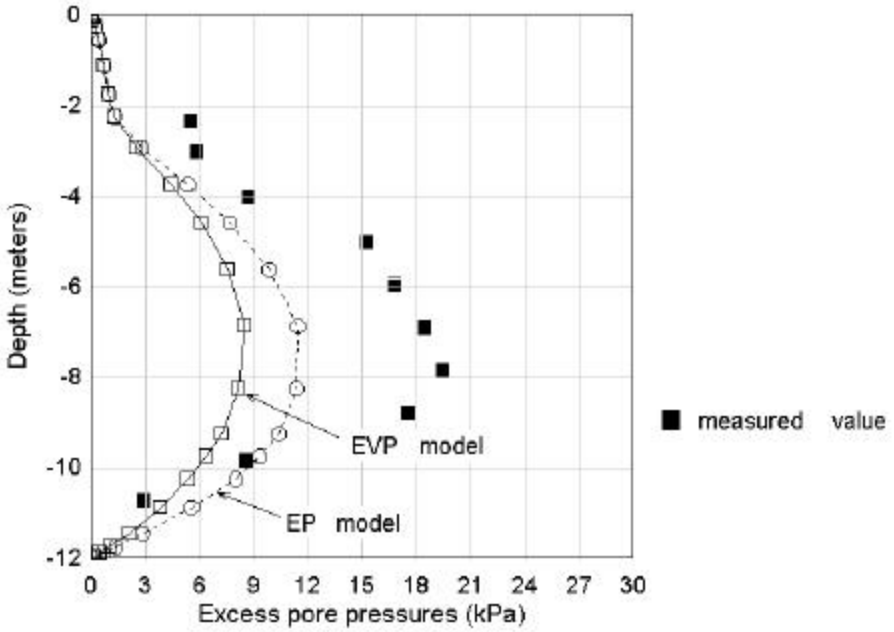

(a) Excess pore pressure profile in 1971

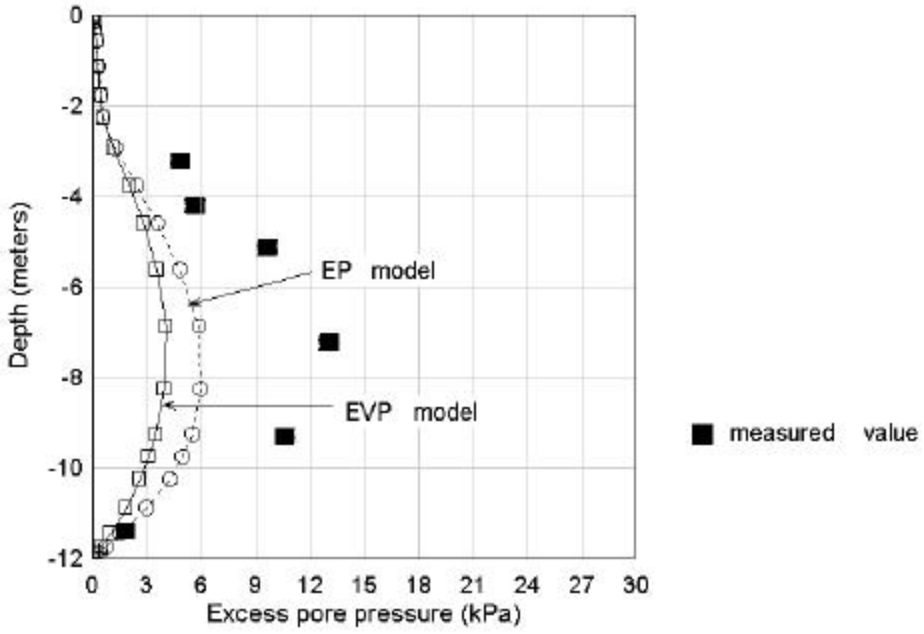

(b) Excess pore pressure profile in 1982

Figure 5.36: Measured excess pore pressure profiles and values computed using "undisturbed" soil properties beneath the Skå Edeby test fill

5.2.5 Discussion

CONSOL97 analyses of the nearly normally consolidated soils beneath the Skå-Edeby test fill significantly underestimated settlement and excess pore pressures. The latest measurements of excess pore pressures (1982) indicate that much more settlement can be expected, whereas CONSOL97 analyses with estimated "undisturbed" soil parameters indicate that excess pore pressure dissipation and settlement are nearly complete. There appear to be inaccuracies associated with both the soil properties (probably due to disturbance effects) and CONSOL97 (due to numerical problems).

It can be seen in figure 5.32 through 5.36 that the settlements and excess pore pressures computed with the EP model are larger than those computed with the EVP model. However, this behavior is inconsistent with the assumptions used to derive the model. Including secondary compression in the analysis should produce larger strains, rather than smaller. Figure 5.37 shows the computed strain vs. log effective stress for a soil element located at the center of the clay layer. The EP model curve represents the reference time line which has a reference creep rate of 7.8×10^{-3} day^{-1}. The computed creep rate for the EVP model curve is about 10^{-6} day^{-1}. Since the EVP model creep rate is less than the reference time line creep rate, it should be located to the left of the reference time line.

The source of this inconsistency is errors associated with the numerical procedures, related to the very small strain rates and effective stress rates, and numerical oscillations during the early stages of consolidation. For a small time step increment, $\Delta t^{(n)}$, the yield strain is given by:

$$\Delta\varepsilon^{(n)} = \frac{C_{\varepsilon c}}{2.3}\frac{\Delta\sigma'^{(n)}}{\sigma'^{(n)}} - \frac{C_{\alpha}}{2.3}\frac{\Delta\dot{\varepsilon}_c^{p(n)}}{\dot{\varepsilon}_c^{p(n)}} \qquad (5.1)$$

In this case, the initial creep strain rate, $\dot{\varepsilon}_c^{p(n)}$, is about 10^{-11} day^{-1} and $\Delta\sigma'^{(n)}$ is essentially equal to zero at the center of the clay layer. In order to avoid numerical difficulties when the effective stresses are nearly constant, Rajot (1992) imposed bounds on the tangent compressibility.

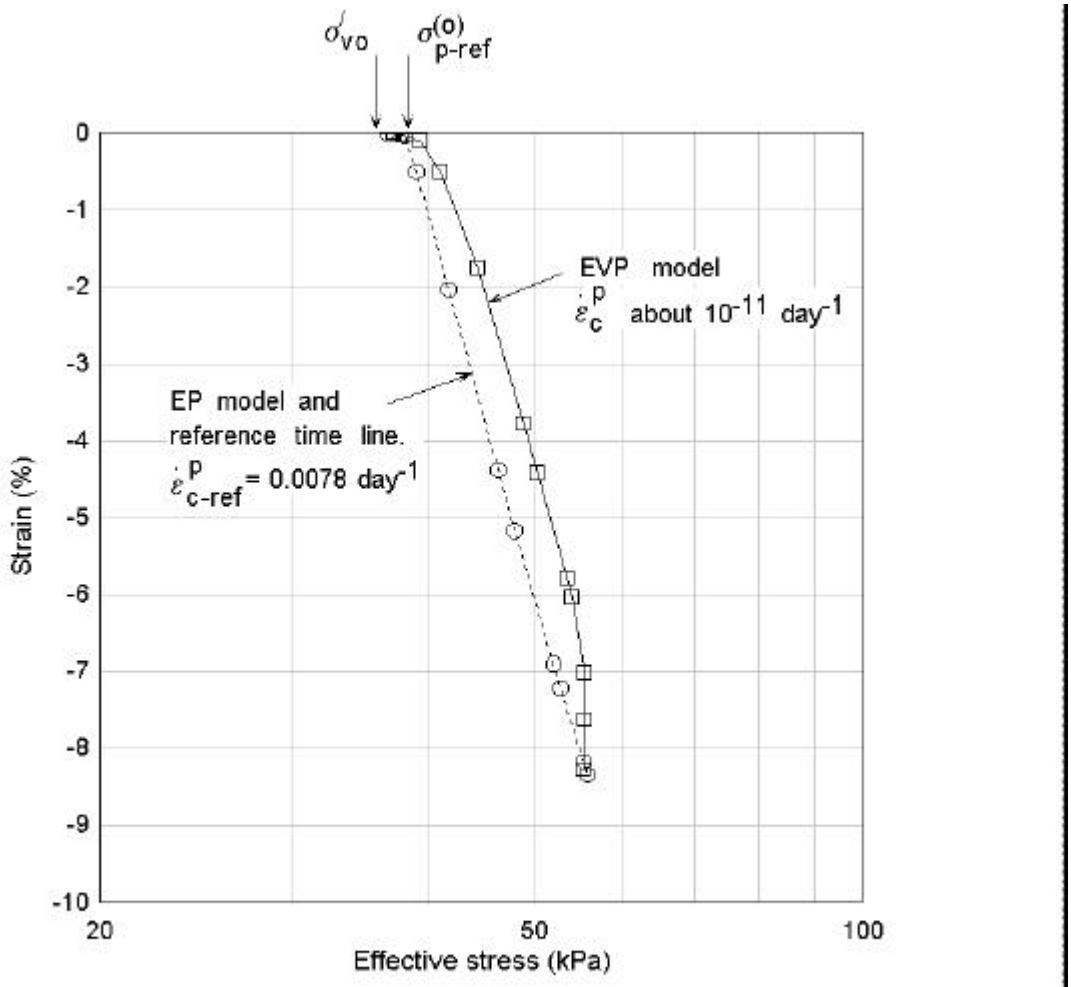

Figure 5.37: Effective stress - strain path for a soil element at the center of the clay layer beneath the Ska Edeby test fill

Removing these constraints produces fatal “divide by zero” or “floating point” errors during execution. However, these constraints result in the physically unreasonable behavior shown in figures 5.31 through 5.37.

5.3 BERTHIERVILLE TEST FILL

5.3.1 Project Description

The Berthierville site is located on the north shore of the St. Laurent River between Quebec City and Montreal, Canada at the intersection of highway routes 40 and 158. The site is relatively level at an elevation of 9.5 m. The test fill was constructed to study the behavior of a 3.2 meter thick layer of soft clay located at a depth of about 5 meters between an upper and a lower sand layer.

The test fill consisted of constructing a 2.4 meter high circular embankment with a diameter of 24 meters at the crest, and 1V:2H slopes. Embankment construction began on 25 October 1983 with the placement of 0.6 meters of sand each day for four days. The top 0.1 meters of the embankment material consisted of gravel. The embankment produced an applied stress of 39 kPa at the ground surface.

Surface settlement plates, deep electrical settlement gauges, and electrical, pneumatic, and hydraulic piezometers were installed prior to placing the fill. All of the deep settlement gauges and piezometers were installed within a circle with a radius of 3.5 m around the center of the fill as shown in Figure 5.38. The piezometers were installed on two circles of radii 2 m and 3.5 m and included four electrical, six pneumatic, and six hydraulic piezometers. A few hydraulic piezometers were placed about 20 m from the toe of the embankment to measure natural groundwater conditions during the test.

Two sets of deep settlement gauges were installed: one set at the center of the embankment and another set 3.5 m apart. As shown on the instrumentation profile, Figure 5.39, the gauges were installed within the clay deposit and in the sand layers above and below the clay. The eight electrical gauges divided the deposit into sublayers approximately 90 cm thick. Seven surface

settlement plates were installed across the fill.

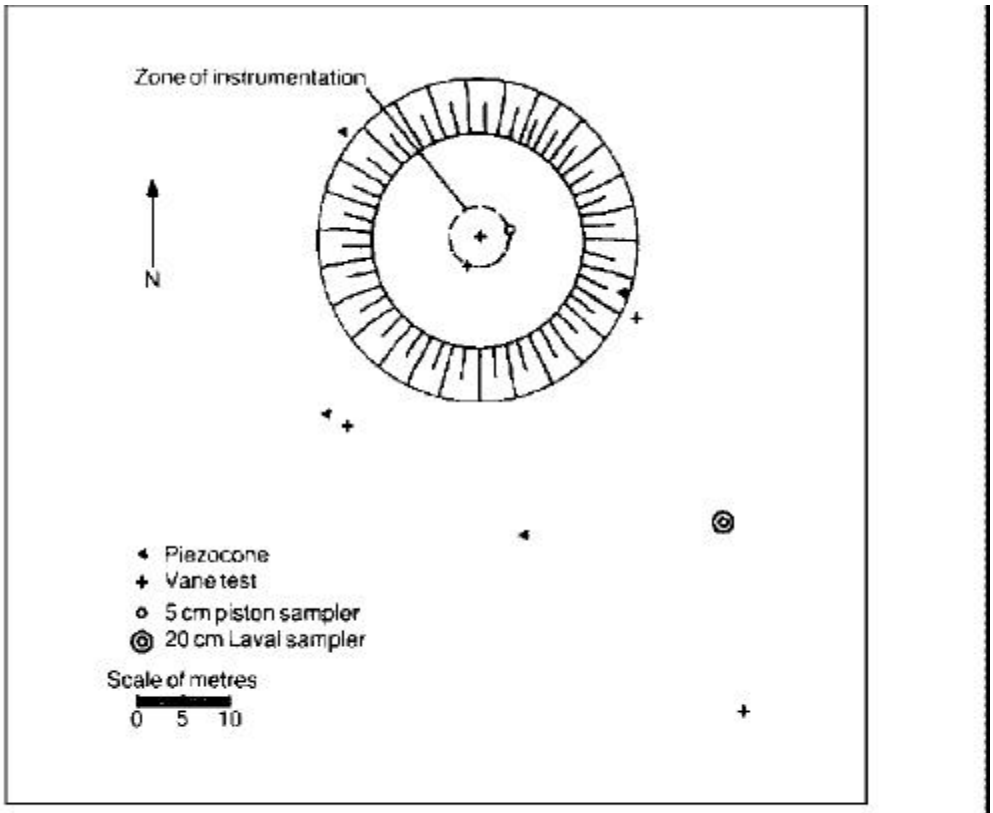

Figure 5.38: Instrumentation and geotechnical exploration layout at the Berthierville test fill (from Kabbaj et al, 1988)

5.3.2 Site Geology and Subsurface Profile

The area is underlain by as much as 70 meters of clay, which was deposited in the Champlain Sea between 12,000 and 8,500 years Before Present (Samson and Garneau, 1973). The clay is underlain by bedrock or a thin layer of glacial till, and is covered by about 10 to 15 m of more recent soils, which were deposited in the Lampsilis lake (Quigley, 1980). Close to the ground

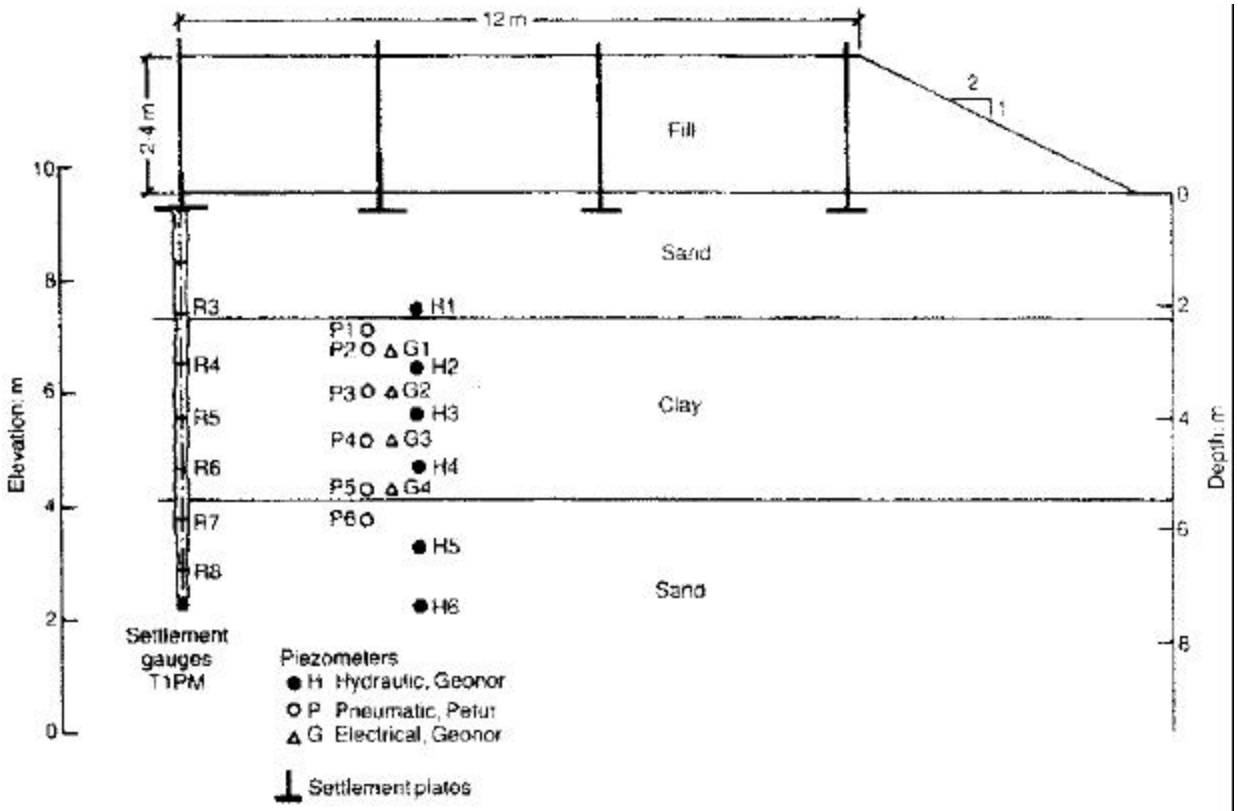

Figure 5.39: Instrumentation profile beneath the Berthierville test fill (from Kabbaj et al., 1988)

surface, the stratigraphy consists of 3 to 5 meters of silty clay covered by a few meters of sand and underlain by successive layers of sand and sandy silt, and stratified silt and silty clay. The three to 5 m thick upper clay layer was the subject of this field test.

Subsurface exploration of the upper clay consisted of completing five vane test profiles, four piezocone profiles, one borehole with a stationary piston sampler (5 cm diameter) and two boreholes with a 200 mm diameter Laval sampler. The exploration locations are shown in Figure 5.38, and the subsurface conditions to a depth of 6 meters are shown in Figure 5.40. Below the top 10 to 20 cm of topsoil, the site is underlain by a 2.15 m thick layer (elevation 9.5 to 7.35 m) of fine to medium sand and an 3.2 m thick (elevation 7.35 to 4.15 m) layer of clay. The upper

clay layer is relatively homogeneous and is saturated. Fine sand lies below elevation 4.15 m, and below this are deeper clay deposits with an overstress ($\sigma'^{o}_{p-ref} - \sigma'_{vo}$) of about 80 kPa (Samson and Garneau, 1973).

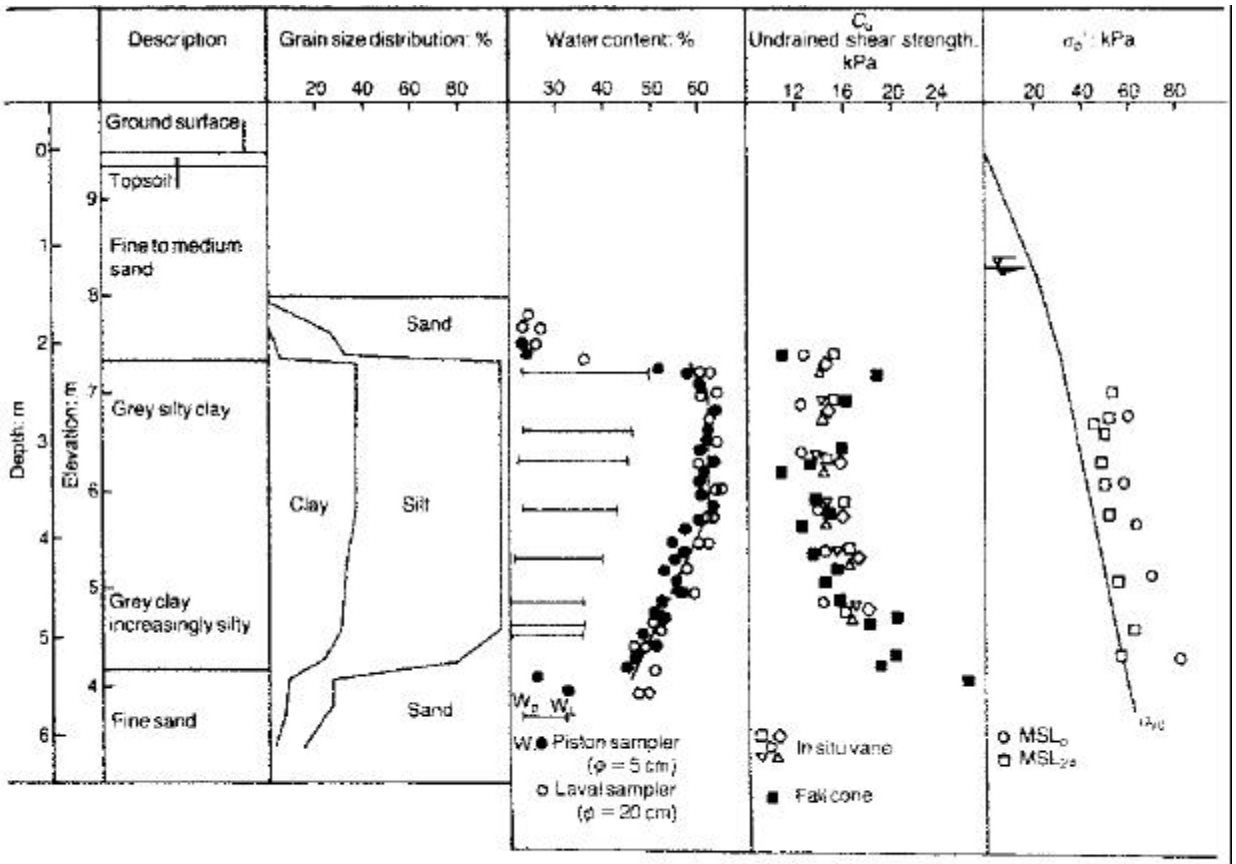

Figure 5.40: Geotechnical profile beneath the Berthierville test fill (from Kabbaj et al., 1988)

Groundwater measurements made in the upper and lower sand layers during the test are shown in Figure 5.41. At the start of fill construction, the groundwater table was at elevation 8.2 m in the upper sand and at elevation 7.5 m in the lower sand, indicating a downward hydraulic gradient of about 0.22. Upon completion of the fill in 4.5 days, the upper piezometric level increased to

elevation 8.4 m and continued rising for the next month to elevation 9.6 m. The upper and lower piezometric levels fluctuate seasonally by as much as one meter. The average seasonal piezometric level in the upper sand during the 3- year test was about elevation 9.0 m.

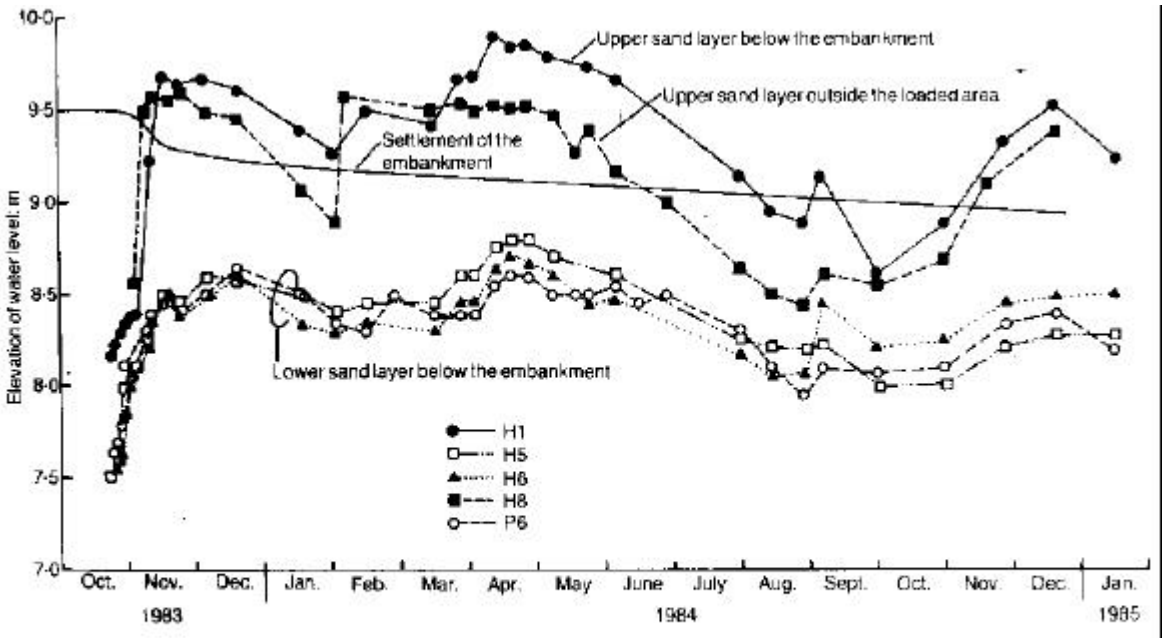

Figure 5.41: Groundwater conditions at Berthierville test site (from Kabbaj et al., 1988)

5.3.3 Soil Properties

A geotechnical profile of upper clay index properties and in-situ stresses is shown in Figure 5.40. The plasticity index decreases with depth from 25 to 16. The water content is 62% in the upper half of the clay, and decreases linearly to 47% at the bottom of the layer at elevation 4.15 m. The liquidity index is typically 1.8. The 24- hour preconsolidation stresses indicate that the clay is overconsolidated, with an OCR of about 1.4 at the top, and about 1.1 at the bottom.

The saturated unit weight of the upper sand was reported to be 19.7 kN/m^3 (Leroueil et al, 1988).

The saturated unit weight of the clay used in the analysis was back calculated from the specified initial effective stresses, and includes the effect of the downward hydraulic gradient, i, estimated to be about 0.22 in the clay layer. The gradient effectively increases the saturated unit weight by $\Delta\gamma_{sat} = i \cdot \gamma_{water} = 2.16\ kN/m^3$ to a total value of 18.4 kN/m^3.

The compressibility properties of the upper clay layer were determined from laboratory tests. Both conventional incremental and constant rate of strain tests were performed on specimens obtained with a 5 cm diameter piston sampler. The specimens were trimmed to 19 mm diameter by 50.8 mm thickness. The incremental or "multiple stage load" (MSL) tests were performed by loading the specimen every 24 hours (MSL_{24}) using a load increment ratio, $\Delta\sigma'/\sigma'$, equal to 0.5, or by reloading as soon as the excess pore pressures were essentially equal to zero (MSL_p). The strain-log of effective stress curves for two samples taken from elevations 5.1 and 6.1 m are shown in Figure 5.42 (Leroueil et al 1988). The curves are nonlinear and the compressibility varies from about 0.6 for stresses less than about 60 kPa to about 0.3 for stresses that exceed 100 kPa.

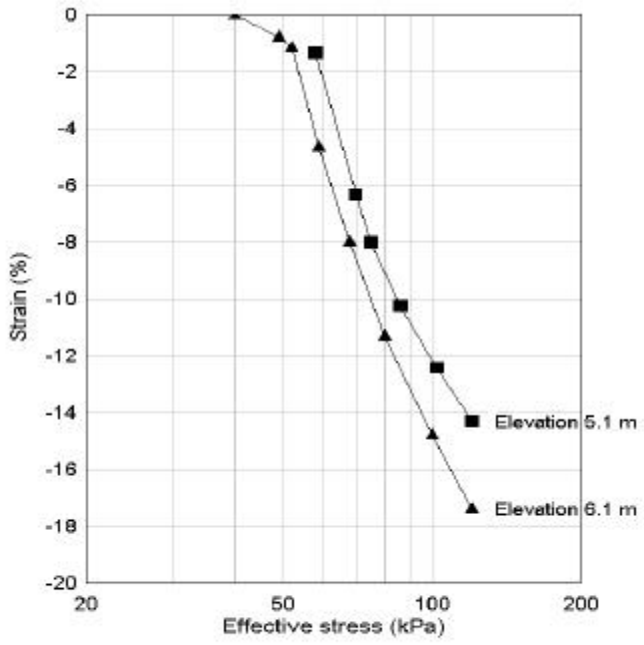

Figure 5.42: Berthierville clay stress-strain behavior from incremental 24 hour oedometer tests (after Leroueil et al., 1988).

The coefficients of secondary compression, C_α , were based upon one set of "typical" strain-log time test results on a sample from the upper portion of the clay layer (Kabbaj et al 1988). The data, shown in Figure 5.43, was obtained from long term creep tests in which a single load increment was applied to 50 mm thick, singly drained specimens for one year. The ratio $C_\alpha / C_{\varepsilon c}$ was found to vary between 0.027 and 0.030.

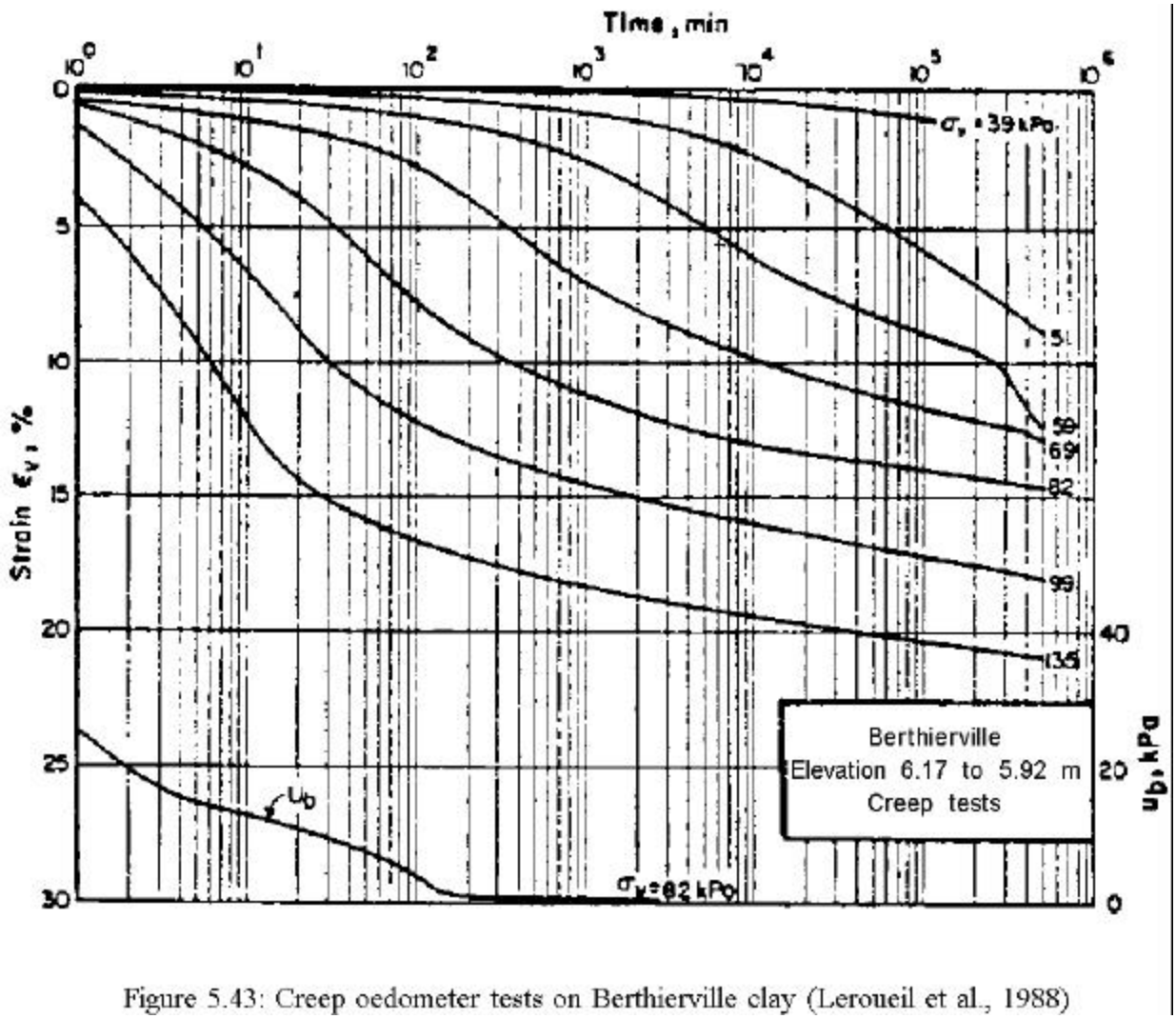

Figure 5.43: Creep oedometer tests on Berthierville clay (Leroueil et al., 1988)

The coefficients of consolidation at different effective stresses were determined by back calculation from lab falling head permeability tests on samples taken from the top, middle and bottom of the clay layer (Leroueil et al. 1988). The test data shown in Figure 5.43 was used to determine lab c_v values. Only the c_v value for the 39 to 82 kPa load increment (LIR=1) was evaluated because the data for this larger load increment were easier to interpret. The oedometer c_v value was about 50% of the c_v value calculated from permeability tests. Due to an insufficient amount of lab c_v data, the c_v values calculated from permeability tests were used in the analyses.

Back calculated coefficients of consolidation for three clay sublayers are summarized in Figure 5.44. The coefficient of consolidation at the preconsolidation stress was estimated to vary from about 3.4×10^{-3} m^2/day at the top of the clay to about 7.2×10^{-3} m^2/day at the bottom of the clay layer. The larger c_v values at the bottom of the clay layer are consistent with empirical correlations based upon liquid limits (U.S. Navy, 1985) which indicate higher values of c_v with values of liquid limit. The coefficients of consolidation increase with increasing effective stress.

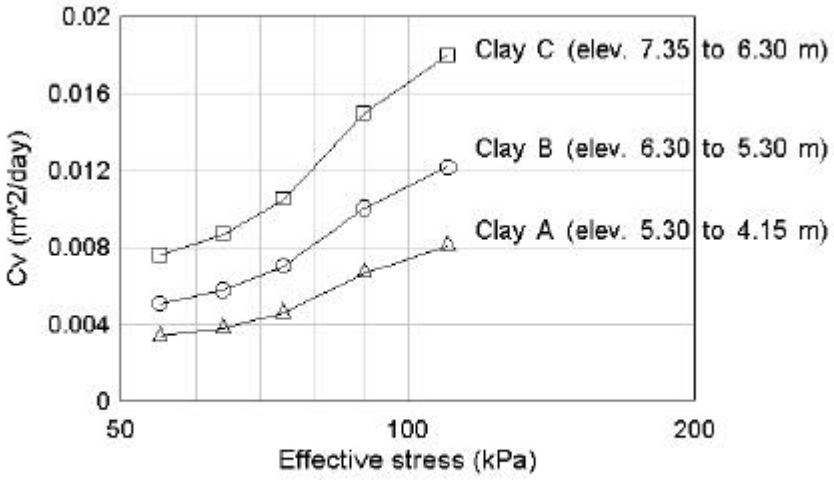

Figure 5.44: Coefficients of consolidation calculated from laboratory falling head permeability tests (after Leroueil et al., 1988).

5.3.4 CONSOL97 Input and Results

The subsurface profile, soil properties and in-situ stresses used as data input for the CONSOL97 analysis are shown in Figure 5.45. The clay layer was divided into sixteen sublayers, each 0.2 meter thick, characterized as soil type A (elevation 7.35 to 6.30 m), type B (elevation 6.30 to 5.30 m) and type C (5.30 to 4.15 m). The interpreted preconsolidation stress profile was estimated from 24 hour incremental oedometer tests. The initial effective overburden stresses were computed using a unit weight of 19.7 kN/m^3 for the upper sand, a unit weight (including seepage forces) of 18.4 kN/m^3 for the clay layer, and an assumed average steady state seasonal groundwater level at elevation 9.0 m in the upper sand.

The loading history at the Berthierville test site has been complicated by seasonal fluctuations in groundwater levels, submergence of the upper sand layer and newly placed fill, and changes in moisture content of the embankment sand fill above the groundwater table. The net affect of all these factors is represented by the total stress changes measured in the middle of the clay layer, which are shown in Figure 5.46. After placement of the embankment in 4.5 days, the applied stress of 39 kPa gradually increased an additional 5.5 kPa to a total stress of 44.5 kPa on day 22 and then remained constant for the remainder of the year. For the next 2 years, the total stresses fluctuated seasonally around a mean value of about 42.5 kPa. Stress conditions used in the CONSOL97 simulation were approximated by using the mean seasonal groundwater elevation of 9.0 m and the total stress history shown in Figure 5.46.

Plots of measured and computed (EVP and EP models) compression vs. logarithm of time for the entire 3.2 m thick clay layer and for two sublayers within the layer are presented in Figures 5.47 to 5.49. The sublayers are 0.9 m thick and are defined by settlement gauges R4 (elevation 6.5), R5 (elevation 5.6) and R6 (elevation 4.7) shown in Figure 5.39. In general, the EVP computations agree reasonably well with the field measurements, although during the first month of loading, the measured settlement rates and magnitudes are slightly greater than those calculated

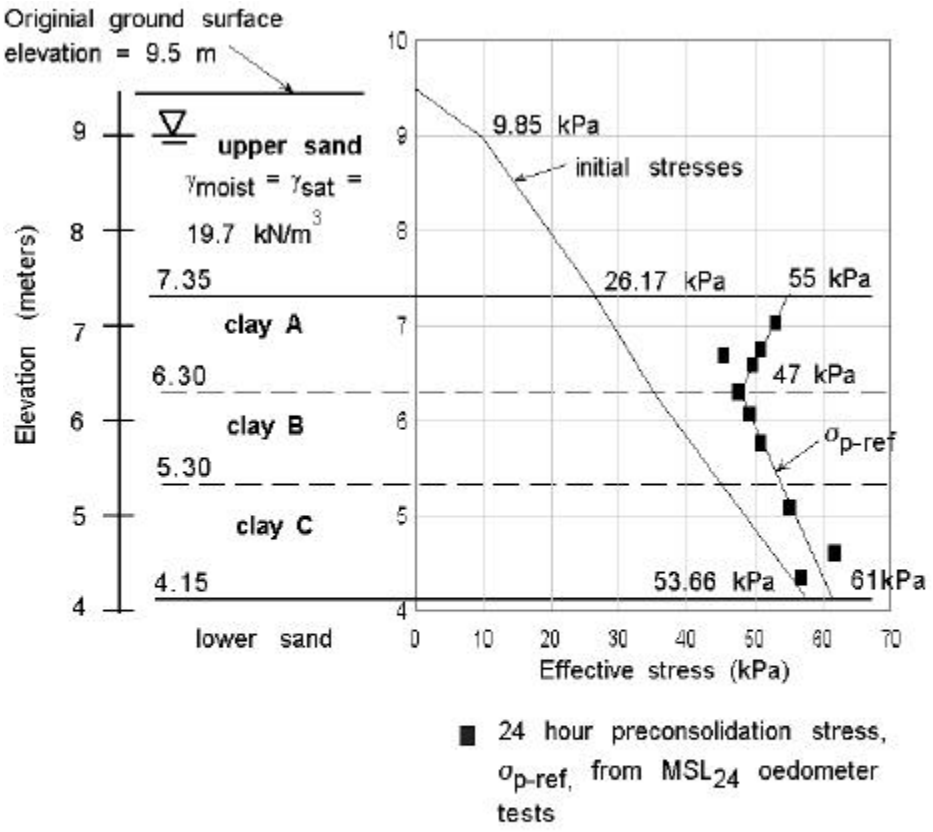

Soil Properties

	σ_{min} (kPa)	C_{zc}	C_{ur}	c_v (m^2/day)
Clay A				
	< 70	0.61	0.017	0.0034
	70	0.56	0.015	0.0044
	75	0.39	0.011	0.0051
	86	0.30	0.008	0.0062
	102	0.26	0.007	0.0080
Clay B				
	< 59	0.64	0.018	0.0048
	59	0.54	0.015	0.0055
	68	0.47	0.013	0.0062
	80	0.36	0.010	0.0080
	100	0.33	0.009	0.0110
Clay C				
	< 59	0.64	0.018	0.0072
	59	0.54	0.015	0.0082
	68	0.47	0.013	0.0093
	80	0.36	0.010	0.0120
	100	0.33	0.009	0.0165

Clay γ_{sat} = 18.4 kN/m^3

Figure 5.45: CONSOL97 input parameters for Berthierville test fill simulation

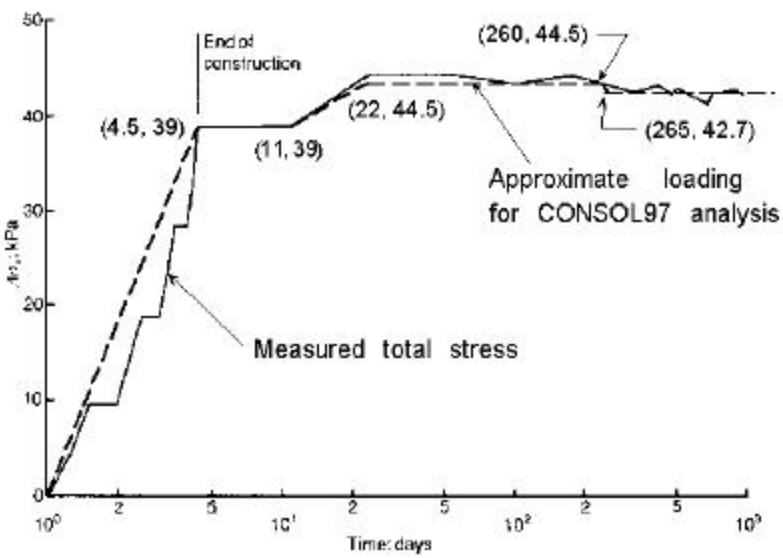

Figure 5.46: Total stress increase at gauge R5 beneath the Berthierville test fill (from Kabbaj et al., 1988).

using the EVP model. After about 3 months, the computed settlement rates and magnitudes are slightly larger than measured values. Table 5.5 summarizes computed and measured strains after 1000 days of consolidation and nearly full dissipation of excess pore pressures. The computed EVP strains for the two clay sublayers are about 10% larger than measured, whereas the computed EVP strain for the entire clay layer is only about 4% larger than measured. In contrast, computed EP strains for the entire clay layer and the two sublayers are consistently less than measured values.

TABLE 5.5
Strains after 1000 days at the Berthierville Test Fill

Sublayer	Strain (%)		
	Measured	CONSOL97	
		EVP Model	EP Model
Gauges R4 and R5 (Elevation 6.5 to 5.6 m) Refer to Figure 5.48	12.8	14.0	11.0
Gauges R5 and R6 (Elevation 5.6 to 4.7) Refer to Figure 5.49	10.8	11.8	9.8
Entire clay layer (Elevation 7.35 to 4.15) Refer to Figure 5.47	11.3	11.7	9.7

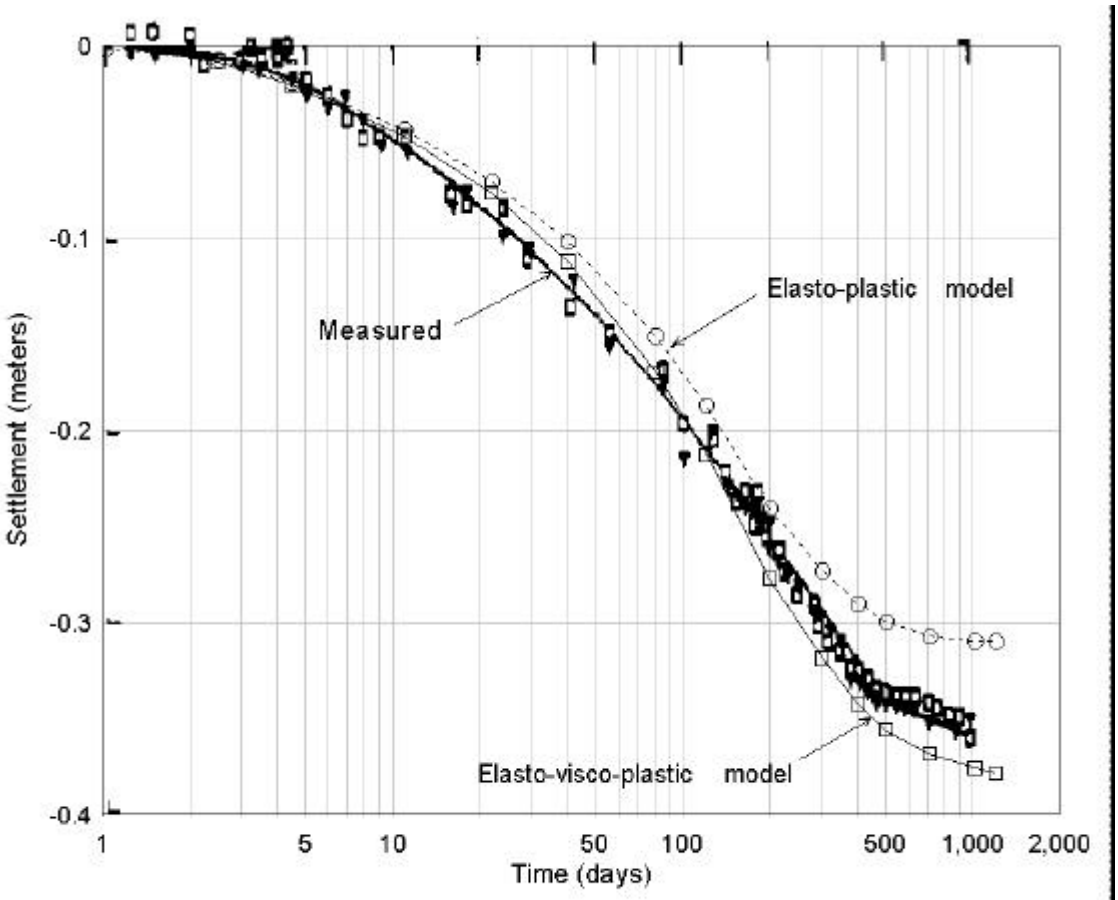

Figure 5.47: Computed and measured settlement of the entire clay layer beneath the Berthierville test fill

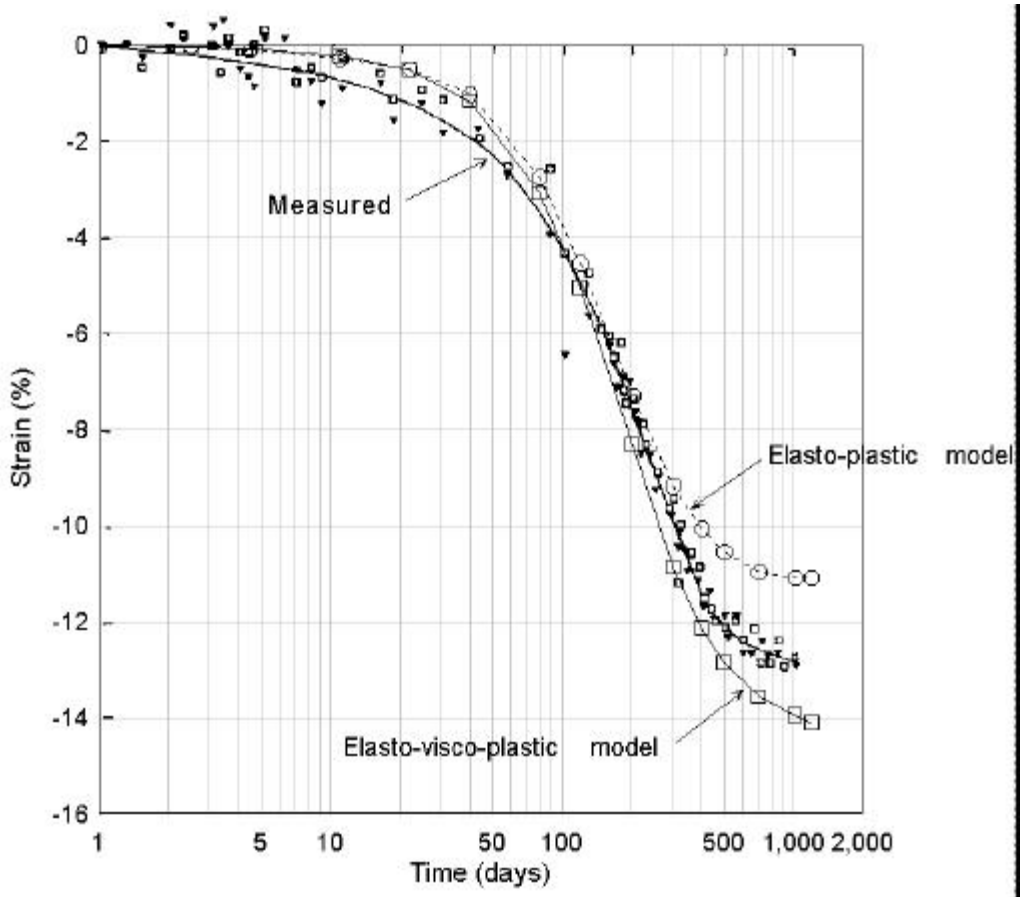

Figure 5.48: Measured and computed strain vs. logarithm of time for the sublayer between elevations 6.5 and 5.6 m beneath the Berthierville test fill

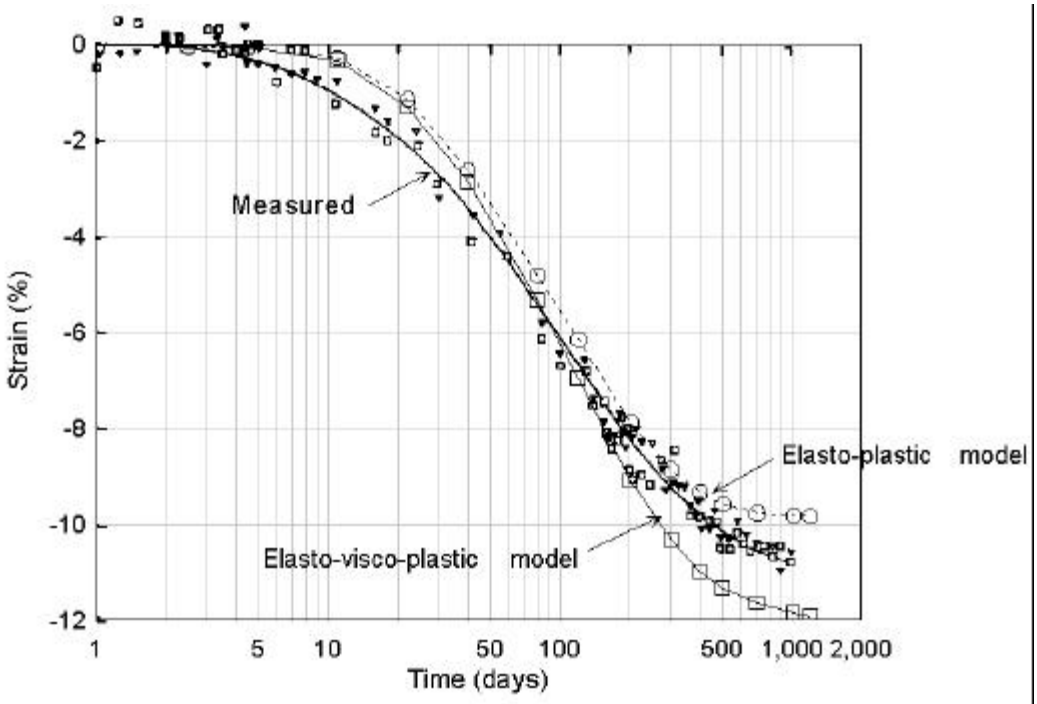

Figure 5.49: Measured and computed strain vs logarithm of time for the sublayer between elevations 5.6 and 4.7 m beneath the Berthierville test fill

The differences between computed and measured rates of settlement are reflected in the pore pressure responses to loading. Figures 5.50 to 5.53 illustrate computed and measured pore pressures at piezometers G1 (elevation 6.85), G2 (elevation 6.10), G3 (elevation 5.25), and G4 (elevation 4.4). The EVP and EP model pore pressures consist of the computed excess pore pressures plus an assumed average seasonal steady state pore pressure corresponding to a piezometric level of 9.0 m in the upper sand and 7.5 m in the lower sand. The computed pore pressures are about 15 kPa larger than measured values at the end of fill placement. However, since the groundwater table was at elevation 8.4 and not elevation 9.0 as assumed in the analyses, the computed pore pressures are actually about 9 kPa $\left(15\text{kPa} - 0.6\text{m} \times 9.81\,\text{kN/m}^3\right)$ larger than measured values. After about 3 months of consolidation, the computed pore pressures are in good agreement with measured average pore pressure trends although the field pore pressures

reflect seasonal groundwater table fluctuations. Conventional EP analyses produce pore pressures that are nearly the same during fill placement and subsequently not more than about 10% (about 5 kPa) less than those from the EVP analyses. Table 5.6 summarizes computed and measured excess pore pressures at the end of fill placement (t = 4.5 days).

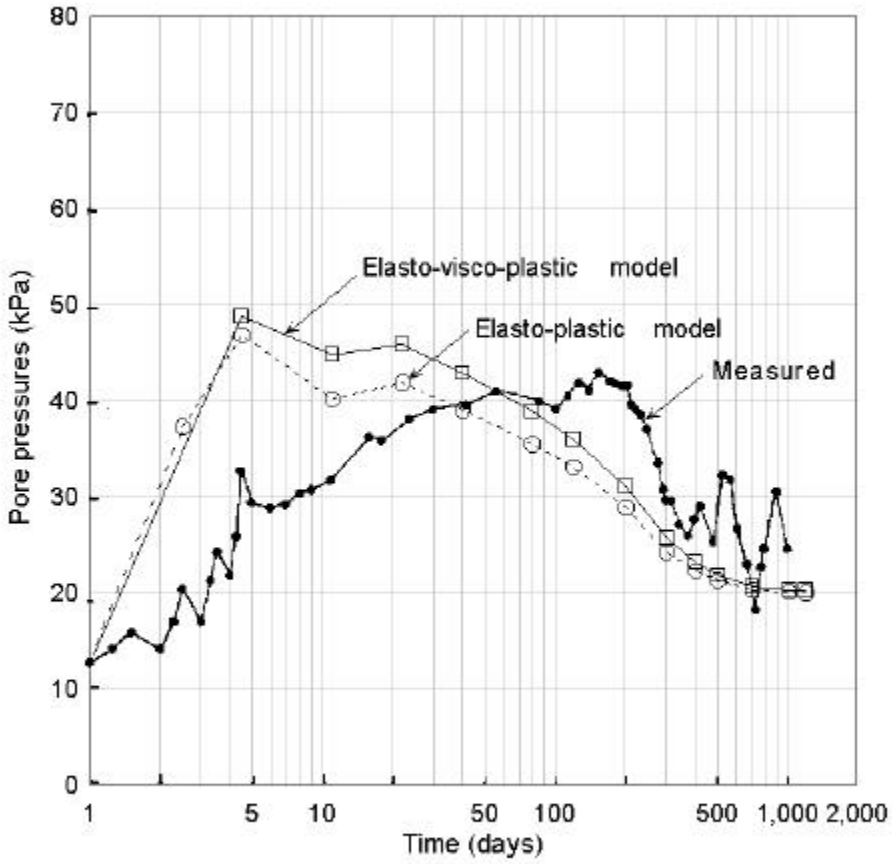

Figure 5.50: Measured and computed development of pore pressures at elevation 6.85 m beneath the Berthierville test fill.

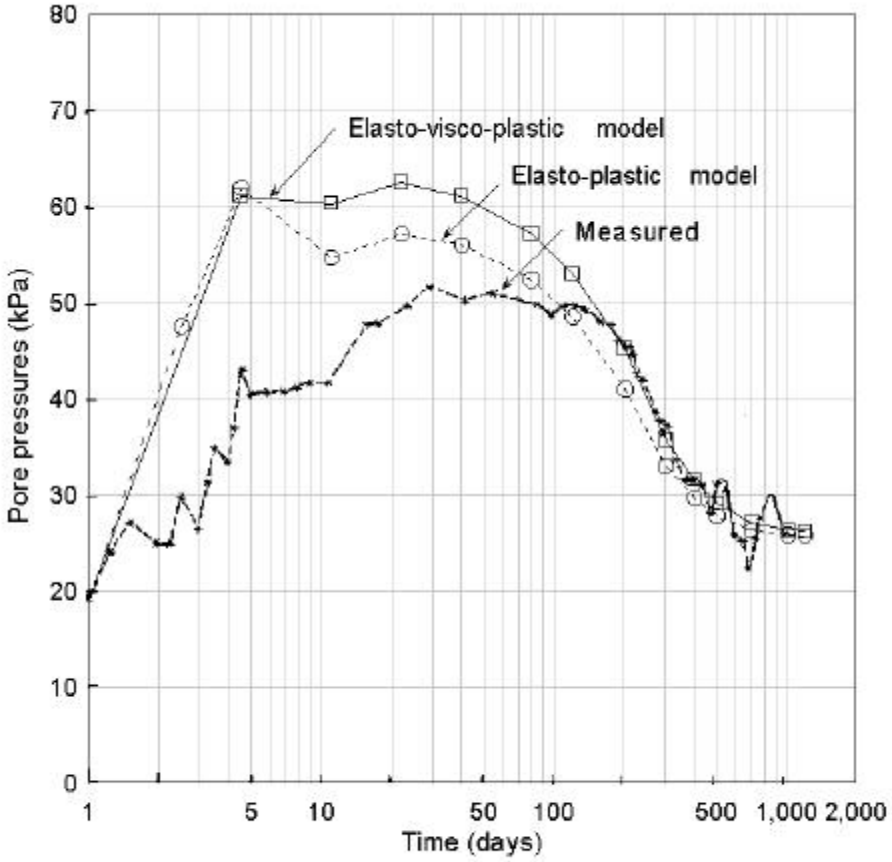

Figure 5.51: Measured and computed development of pore pressures at elevation 6.10 m beneath the Berthierville test fill.

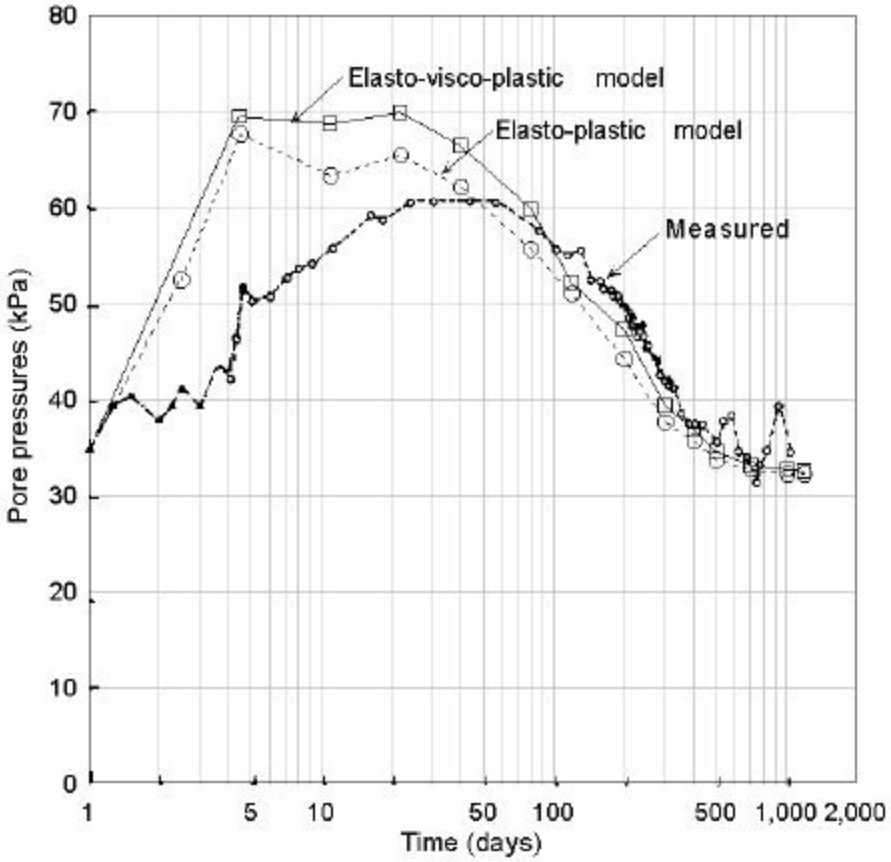

Figure 5.52: Measured and computed development of pore pressures at elevation 5.25 meters beneath the Berthierville test fill.

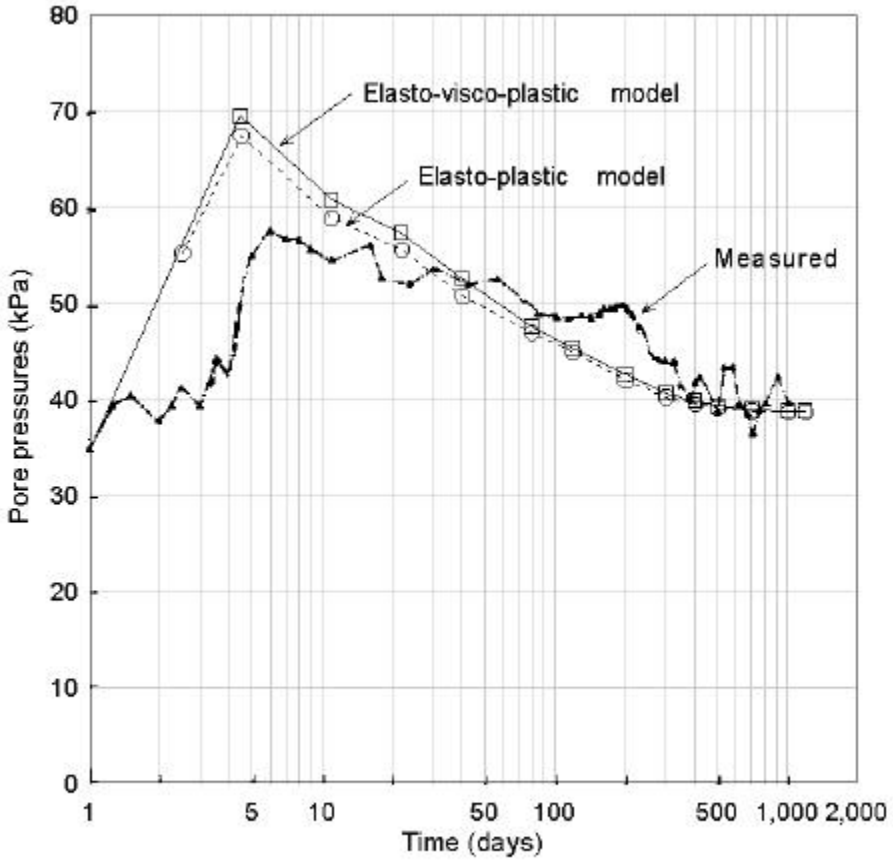

Figure 5.53: Measured and computed development of pore pressures at elevation 4.40 meters beneath the Berthierville test fill.

TABLE 5.6
Excess Pore Pressures at the End of Fill Placement
Berthierville Test Fill

Elevation (meters)	Excess pore pressures (kPa)	
	Measured	CONSOL97 EVP Model
6.85	20	29 to 35
6.10	23	33 to 39
5.25	17	28 to 34
4.40	20	28 to 34

5.3.5 Discussion

The magnitude and timing of groundwater table fluctuations and total stress changes due to seasonal precipitation complicated the analysis and interpretation of this test case. During the first month of the test, the maximum load of 44.5 kPa was applied and the groundwater table in the upper sand increased from elevation 8.2 to 9.5 meters, to produce a significant effect on measured performance. Most notably, measured pore pressures continued to increase, but the incremental changes in pore pressure were not the same as the incremental stress. During the 4-1/2 days of fill placement, the pore pressure increases were about 60% of the applied load. From day 11 to day 22, the total stress increased by 5.5 kPa but the pore pressure increases were about 11.0 kPa.

The smaller-than-expected pore pressure response during fill placement suggests that the in situ clay permeabilities at effective stresses less than the preconsolidation stress are significantly larger than values based on lab permeability tests. Generally good agreement between predicted and measured pore pressures during the later stages of consolidation suggests that the computed permeabilities at effective stresses larger than the preconsolidation stress are reasonable. Since the oedometer c_v values were about one half of the c_v values calculated from lab permeability tests, the analyses also indicate that lab c_v values would significantly underestimate field consolidation rates.

The effect of creep on field behavior is evident from measured pore pressure increases that are double the 5.5 kPa stress increase that occurred from day 11 to day 22. During this time, the groundwater table rose by less than about 0.2 m, which is insufficient to account for the additional 5 to 6 kPa increase in pore pressure. In addition, compression of sublayers R4-R5 and R5-R6 continued after day 22 and for the next month, even though pore pressures remained essentially constant in these sublayers. Therefore the large increase in pore pressures must be the result of creep compression.

Compression of the entire clay layer (Figure 5.47) is better predicted by the CONSOL97 EVP model than by the EP model. The computed EVP strain is 4% larger than the measured value as compared to the EP model strain, which is 14% smaller. Strains within the clay layer are consistently underestimated by the EP model.

5.4 SUMMARY AND CONCLUSIONS

The CONSOL97 computer program was used to simulate test fills at Väsby, Sweden, Skå-Edeby, Sweden, and at Berthierville, Canada. All of the sites are underlain by highly compressible and sensitive clays which have nonlinear strain vs. log effective stress behavior. Except for a desiccated crust layer at the surface, the stress history of the sites varied from nearly normally consolidated clay (Skå-Edeby) to clays with an OCR of 1.4 (Väsby and Berthierville). These test fills represent the best and most comprehensive long term field data on clay consolidation that has been published. A detailed examination of these test cases has demonstrated the difficulties in establishing the absolute predictive capabilities of CONSOL97. Acquisition of comprehensive settlement and pore pressure data from field tests, and determination of in situ soil properties from laboratory tests is not easily achieved. However, the data from these test fills is sufficient to indicate that EVP models with high quality sampling and laboratory test data will produce better predictions of field behavior than conventional EP models. The clearest example of this is the Berthierville case.

Comparisons of CONSOL97 analyses of the Väsby test fill using test results from standard sampling and high quality sampling clearly demonstrated the importance of disturbance effects on soil properties. Standard field sampling of sensitive clays produces sample disturbance that significantly reduces laboratory values of compressibility and permeability, and obscures preconsolidation stresses. In addition, the permeability of desiccated crust layers with macroscopic drainage features such as cracks and root channels is not easily determined, and has

a large effect on pore pressure dissipation and settlement rates. Without high quality compression and permeability test data, there is little need for the complex EVP analysis, because the effects of disturbance are much larger than the difference between the EVP analysis and the conventional EP analysis.

CONSOL97 analyses of normally consolidated site conditions at Skå-Edeby revealed a limitation in the numerical procedures used in the computer program. At the start of consolidation, the model computes very small creep strain rates and effective stress rates that caused numerical instabilities. Limitations imposed on the soil stiffness formulation made it possible to continue the computations but the restrained computations underestimated displacements and pore pressures near the center of the clay layer. These numerical problems affected the Skå-Edeby test fill computations only, and are less significant as OCR increases, as layer thickness decreases, and as compressibility decreases.

Chapter 6

SUMMARY AND CONCLUSIONS

The effects of creep on the compressibility of clays have been observed in laboratory tests and in the field for many years. In recent years, researchers have developed computer programs that include creep effects on one-dimensional consolidation of clays. However, engineers do not include creep effects in their analyses because they do not have access to a general purpose computer program. Some of the programs are based upon incomplete elasto-visco-plastic models. Other programs, which simulate the necessary time-dependent behavior, are not general purpose. Of the thirteen computer programs cited in published literature, only one computer program was available for examination during this study.

This thesis has described the development of a general purpose computer program, CONSOL97, based on Rajot's elasto-visco-plastic creep rate model that can analyze a subsurface profile with multiple soil layers and drainage boundaries. The user may specify any initial pore pressure distribution and any profile of change in vertical stress. The model was specifically formulated to use familiar soil properties (C_c, C_r, σ'_p, C_α, and c_v) based on standard laboratory testing methods. CONSOL97 provides a consistent method for using all of the information obtained from laboratory consolidation tests to estimate rate and magnitude of field settlements.

Practical implementation of Rajot's creep rate model in CONSOL97 has required significant modification to the original computer program as described in Chapter 4. In addition, a user-friendly interface that operates in a Windows environment was developed (Appendix B) for creating the data input file and running the analyses. CONSOL97 can perform both conventional

elasto-plastic, and time-dependent elasto-visco-plastic analyses of a wide range of soil profiles, loading conditions and soil types. Compressible soils can be modeled with linear virgin compression curves characterized by stress independent values of C_c, C_α and c_v, or non-linear virgin compression curves characterized by stress-dependent values of C_c, C_α and c_v.

Although Rajot's basic numerical algorithm is sound, the use of instant elastic, instant plastic and creep strain components has produced a complex computer program that can result in numerical instability, inefficiencies, and inaccuracies in some situations. Other one-dimensional computer programs, that are based on total strain and total strain rate models, are less complex and they conform to Olzsak-Perzyna's general theory for visco-plastic behavior. However, the soil input parameters are unfamiliar quantities derived from CRS tests, which are not routinely performed by practicing engineers.

To simplify and improve computational performance without sacrificing significant accuracy, CONSOL97 was modified to represent sublayers with two-noded linear strain elements, automatically determine the time step size, yield tolerance and convergence criteria, and compute insitu creep rates based upon the estimated age and OCR of the soil.

The results of CONSOL97 simulations of incremental oedometer tests and full scale field tests on one inch thick specimens indicate good agreement with stress-strain and strain-log time lab test results. During unloading, the time-dependent analysis predicts much larger rebound than the lab results because Rajot's model assumes visco-elastic unloading behavior which produces excessive amounts of creep strain. Elasto-plastic (conventional, time-independent) analyses should be used for unloading situations. Computed secondary compression behavior for each load increment above the preconsolidation stress closely matches lab data. At stresses less than the preconsolidation stress, CONSOL97 predicts C_α values that are significantly less than virgin compression values. This behavior is typical of many test results on overconsolidated clays.

Only three well-instrumented and well-documented full scale test fills at Väsby, Sweden, Skå-Edeby, Sweden, and Berthierville, Canada were available for analysis. These test fills represent the best and most comprehensive long term field data on clay consolidation that has been published. Detailed examination of these cases have demonstrated the difficulties in establishing the absolute predictive capabilities of CONSOL97 and other computer programs that use elasto-visco-plastic models. The following conclusions were derived from CONSOL97 analyses of these test fills:

- EVP analyses will produce better predictions of field behavior than conventional EP analyses if the input soil parameters are derived from high quality laboratory test data;
- The permeability of desiccated crusts with macroscopic drainage features such as cracks and root channels has a large effect on pore pressure dissipation and settlement rates;
- Standard undisturbed sampling of sensitive clays produces disturbance that significantly reduces laboratory values of compressibility and permeability, and obscures preconsolidation stresses. Without high quality compression and permeability test data, there is little need for the complex EVP analyses because the effects of disturbance are much larger than the difference between the EVP analysis and the conventional EP analysis;
- CONSOL97 underestimates the displacements and pore pressures near the center of a normally consolidated clay layer. These inaccuracies are caused by limitations imposed on the soil stiffness formulation due to very small creep strain rates and effective stress rates that are computed at the start of consolidation. These numerical problems are less significant as OCR increases, as layer thickness decreases, and as compressibility decreases.

Chapter 7

RECOMMENDATIONS FOR FUTURE RESEARCH

CONSOL97 has the essential characteristics of a useful and practical tool for engineering application to one-dimensional consolidation problems. However, additional research will be needed to improve the elasto-visco-plastic model for some loading situations, to establish the usefulness of the model by comparisons to more field tests and, to develop graphical displays of input and output data.

7.1 ELASTO-VISCO-PLASTIC MODEL

Soil Stiffness Assumption. Rajot's imposition of an upper and lower bound on soil stiffness to avoid numerical instability during the early stages of consolidation, results in settlements and excess pore pressures that are smaller than field values. These errors are more significant for thick compressible deposits of normally to slightly overconsolidated clays and organic soils. The numerical procedures should be modified to avoid numerical difficulties that occur when the stiffness limitations are removed.

Unloading. The unloading portion of Rajot's model produces excessive displacements. During unloading, the model assumes that the dashpot viscosity of the creep portion of the model remains unchanged and equal to the value at the start of unloading. Only the instant portion of the model is changed from plastic to elastic. Some improvements were achieved by recomputing the viscosity during unloading. However, the revised model produced very small creep strains and numerical instability at OCR values greater than about three. Additional modifications are required to avoid these numerical difficulties.

Time Stepping Routine. The same time stepping routine is used during loading for both the EVP and EP analyses and it is based upon the more critical requirements of the EVP analysis. Additional computational efficiencies could be achieved by using larger time steps for the EP analyses.

7.2 FIELD TESTS

Limited availability of comprehensive and reliable field test data and high quality laboratory test data has precluded an absolute determination of the predictive capabilities of CONSOL97. Thick clay layers, such as those found at the Väsby and Skå-Edeby test fills, can require 50 or more years to dissipate excess pore pressures. These extended field test durations have discouraged the implementation of new field tests.

Aboshi (1973) conducted a series of one-dimensional consolidation tests over a period of a few years to study the effects of sample thickness on settlement behavior. The samples were 2, 4.8, 20, 40, and 100 cm in thickness and all had a diameter to height ratio of 3. The 2, 4.8 and 40 cm samples were tested in the lab and the 40 and 100 cm samples were tested in the field. Each sample was constructed by initially consolidating a clay slurry by applying 20 kPa. At the end of primary consolidation, the loads were increased from 20 kPa to 80 kPa. Unfortunately, Aboshi's experiment did not include pore pressure and settlement measurements within the clay layers.

Additional field tests, similar to Aboshi's experiment, should be implemented to acquire useful information about the consolidation behavior of newly sedimented clay layers of varying thickness. The experiment should be designed such that the excess pore pressures dissipate in less than one or two years. Pore pressure and settlement instruments should be installed at regular

depth intervals throughout each sample. Groundwater levels and applied loads should be monitored and maintained at constant levels.

7.3 USER INTERFACE

- Develop a more robust error trapping routine when saving the data input file. The current Visual Basic interface program provides some error traps in each data input screen but it lacks a global review of the final data input file.

- Include graphical profiles of some input data such as a preconsolidation stresses, soil compressibility, etc. so the user can quickly spot any incorrect data input values.

- Include a screen that displays the standard and plotting output text files.

- Provide the CONSOL97 user with options for selecting the types of graphs to be displayed in the Windows environment and which could be printed after completion of the analysis.

References

Aboshi, H. (1973). "An experimental investigation on the similitude in the consolidation of a soft clay, including the secondary creep settlement," *Proceedings of the Eighth International Conference on Soil Mechanics and Foundation Engineering*, Moscow, Vol. 4.3, p.88.

American Society for Testing and Materials (1987). *Annual Book of ASTM Standards, Section 4, Construction, Volume 04.08, Soil and Rock; Building Stones; Geotextiles*, ASTM, 1916 Race Street, Philadelphia, PA, 19103.

Barden, L. (1965). "Consolidation of clay with non-linear viscosity, *Geotechnique*, 15(4), pp. 345-362.

Bjerrum, L. (1967). "Engineering geology of Norwegian normally consolidated marine clays as related to settlements of buildings, 7th Rankine Lecture, *Geotechnique*, 17(2), 81-118.

Buisman (1936). "Results of long duration settlement tests," *Proceedings, First International Conference on Soil Mechanics and Foundation Engineering*, Cambridge, Massachusetts, Vol. 1, pp. 103-107.

Chang, Y.C.E. (1969). "Long Term Consolidation Beneath the Test Fills at Väsby, Sweden," Ph.D. Thesis, University of Illinois.

Chang, Y.C.E. (1981). "Long term consolidation beneath the test fills at Väsby, Sweden," *Swedish Geotechnical Institute Report No. 13*, Linköping, Sweden.

Chang, Y.C.E. (1998). Personal communications

Christie, I.F., Tonks, D.M., (1985). "Developments in the time lines theory of consolidation," *Eleventh Int. Conf. Soil Mech. and Fndn. Engrg.*, 423-426.

Crawford, C.B., (1964). "Interpretation of the consolidation test," *Journal of the Soil Mechanics and Foundations Division*, Proceedings of the ASCE, 90(5), pp. 87-102.

Crawford, C.B., (1988). "On the importance of rate of strain in the consolidation test," *Geotechnical Testing Journal*, 11(1), pp. 60-62.

Crooks, J.H.A., Becker, D.E., Jefferies, M.G., MacKenzie, K. (1984). "Yield behaviour and consolidation, Part I: Pore pressure response," *ASCE, Symposium on Prediction and Case Histories of Consolidation Performance*, San Francisco.

Den Haan, E.J. (1996). "A compression model for non-brittle soft clays and peat," *Geotechnique* 46(1), 1-16.

Duncan, J.M., Rajot, J.P., Perrone, V.J. (1996). "Coupled Analysis of Consolidation and Secondary Compression," *Second International Conference on Soft Soil Engineering*, Nanjing, China, May 27 - 30, 1996.

Duncan, J.M., Smith, R.W., Brandon, T.L., Wong, K.S. (1988). "Consol Version 2.0: A Computer Program for 1-D Consolidation Analysis of Layered Soil Masses," The Charles E. Via, Jr. department of Civil Engineering, 104 Patton Hall, Virginia Polytechnic Institute and State University, Blacksburg, VA, 24061.

Ekström, G. (1927). "Classification of Swedish Agricultural Soil." Sveriges Geologiska undersökning, Series C, No. 345, Stockholm.

Feda, J. (1992). *Creep of Soils and Related Phenomena.* Elsevier Science Publishing Co., New York, N.Y.

Fox, J.P., Edil, T.B., Malkus, D.S., (1994). "Discrete element model for compression of peat," *Computer Methods and Advances in Geomechanics*, Siriwardane and Zaman (eds.), Balkema, Rotterdam.

Garlanger, J.E. (1972). "The consolidation of soils exhibiting creep under constant effective stress," *Geotechnique*, 22(1), 71-78.

Gibson, R.E. and Lo, K.Y. (1961). "A theory of consolidation for soils exhibiting secondary compression, *Norwegian Geotechnical Institute, Proceedings 41*, pp. 3-15.

Hansbo, S. (1960). "Consolidation of Clay, with Special Reference to Influence of Vertical Sand Drains, A study made in connection with full-scale investigations at Skå-Edeby," *Swedish Geotechnical Institute Proceedings, No. 18*, Stockholm.

Hawley, J.G., Borin, D.L.,(1973). "A Unified Theory for the Consolidation of Clays," *Proceedings of the Eighth International Conference on Soil Mechanics and Foundation Engineering*, Vol. 2, pp. 107-119.

Holm, G. and Holtz, R.D. (1977). " A study of large diameter piston samplers," International Symposium on Soft Clay, Bangkok, Thailand, July 5-6, 1977.

Holtz, R.D., Broms, B. (1972). "Long-Term Loading Tests at Skå-Edeby, Sweden," *Proc. of Specialty Conf. on Performance of Earth an Earth Supported Structures*, Purdue, University, 1972, Vol. 1.

Holtz, R.D. and Linskog, G. (1972). "Soil Movements below a Test Embankment." *Proceedings of the Specialty Conference on Performance of Earth and Earth-Supported Structures*. Vol. 1:1. Purdue University.

Jamiolkowski, M., Ladd, C.C., Germaine, J.T. Lancellotta, R., (1985). "New developments in field and laboratory testing of soils: general report." *Proceedings Eleventh Int. Conf. Soil Mech. Fndn. Engng*., San Francisco, 1, pp. 57-153.

Kabbaj, M., Oka., F., Leroueil, S., Tavenas, F., (1986). "Consolidation of Natural Clays and Laboratory Testing," *Consolidation of Soils: Testing and Evaluation, ASTM STP 892*, R.N. Yong and F.C. Townsend, Eds., American Society for Testing and Materials, Philadelphia, pp. 378-404.

Kabbaj, M., Tavenas, F., Leroueil, S., (1988). "In situ and laboratory stress-strain relationships," *Geotechnique*, 38(1), pp. 83-100.

Kuhn, M.R. and Mitchell, J.M. (1993). "New Perspectives on Soil Creep." *Journal of Geotechnical Engineering*, 119(3), pp. 507-524.

Lacasse, S., Berre, T., and Lefebvre, G. (1985). "Block sampling of sensitive clays." *Proceedings 11th ICSMFE*, San Francisco, 2, pp 887-892.

Ladd, C.C. (1973). "Estimating Settlements of Structures Supported on Cohesive Soils," Massachusetts Institute of Technology 1971 Special Summer Program 1.34S, "Soft Ground Construction".

Larsson, R. (1977). "Basic behavior of Scandinavian soft clays," *Swedish Geotechnical Institute, Report No. 4*, Linköping, Sweden.

Larsson, R. (1981). "Drained behaviour of Swedish clays," *Swedish Geotechnical Institute, Report No. 12*, Linköping, Sweden.

Larsson, R. (1986). "Consolidation of Soft Soils," *Swedish Geotechnical Institute, Stockholm, Sweden, Report 29*, Linköping, Sweden.

Larsson, R., Bengtsson, P., Eriksson, L., (1997). "Prediction of settlements of embankments on soft, fine-grained soils," *Swedish Geotechnical Institute, Stockholm, Sweden, Information 13E*, Linköping, Sweden.

Leroueil, S., Diene, M., Tavenas, F., Kabbaj, M., and La Rochelle, P. (1988). "Direct determination of permeability of clay under embankment." *J. Geotech. Engrg. Div.*, ASCE, 114(6), pp. 645-657.

Leroueil, S., Kabbaj, M. (1987). Discussion of "Settlement Analysis of Embankments on Soft Clays," by Mesri, G., and Choi, Y.K., *J. Geotech. Engrg. Div.*, ASCE, 113(9), pp. 1067-1070.

Leroueil, S., (1988). "Tenth Canadian Geotechnical Colloquium: Recent developments in consolidation of natural clays." *Can. Geotech. J.*, 25, pp. 85-107.

Leroueil, S., Kabbaj, M., Tavenas, F., Bouchard, R. (1985). "Stress-strain-strain rate relation for the compressibility of sensitive natural clays, Geotechnique, Vol. 35(2), pp. 159-180.

Leroueil, S., Kabbaj, M., Tavenas, F. (1988). "Study of the validity of a $\sigma'_v - \varepsilon_v - \dot{\varepsilon}_v$ model in insitu conditions," *Soil and Foundations*, 28(3), September 1988, Japanese Society of Soil Mechanics and Foundation Engineering.

Magnan, J.P., Gaghery, S., Brucy, M., Tavenas, F., (1979). "Etude numerique de la consolidation unidimensionnelle en tenant compte des variations de la permeabilite et de la compressibilite du sol, du fluage et de la non-saturation," *Bull. Liaison Laboratoire des Ponts et Chausses*, 103, pp. 83-94.

Matsue, T. and Abe, N. (1985). "Elasto/Viscoplastic constitutive equation of normally consolidated clays based on flow surface theory." *Proceedings Fifth International Conf. Numerical Methods in Geomechanics*, Vol. 1, pp. 407-413, Nagoya.

Meijer, K.L. (1984). "Comparison of finite and infinitesimal strain consolidation by numerical experiments," *International Journal for Numerical and Analytical Methods in Geomechanics*, Vol. 8, no. 6.

Mesri, G., and Godlewski, P.M. (1977). "Time- and Stress- Compressibility Interrelationship," *Journal of the Geotechnical Engineering Division*, ASCE, 103(5), May 1977, pp. 417-430.

Mesri, G., and Choi, Y.K., (1985). "Settlement analysis of embankments on soft clays," *J. Geotech. Engrg. Div.*, ASCE, 111(4), pp. 441-464.

Mesri, G., and Rokhsar, A., (1974). "Theory of Consolidation for Clays," *J. Geotech. Engrg. Div.*, ASCE, 100(8), 889-904.

Mitchell, J.K., Campanella, R.G., and Singh, A. (1968). "Soil creep as a rate process," *J. Geotech. Engrg. Div.*, ASCE, 94(1), pp. 231-253.

Moum, J. (1967). "Determination of inorganic and organic carbon in soil samples." NGI, Internal Report F76.

Niemunis, A., and Krieg, S., (1996). "Viscous behaviour of soil under oedometric conditions," *Can. Geotech. J.*, 33, pp. 159-168.

Oka, F. (1981). Prediction of time-dependent behavior of clay, *Proceedings, Tenth International Conference on Soil Mechanics and Foundation Engineering*, Stockholm, Vol. 1, pp. 215-218.

Olszak, W., Perzyna, P., (1966). "The constitutive equations of the flow theory for a non-stationary yield condition," *Applied Mechanics, Proc. Eleventh International Congress of Applied Mechanics*, pp. 545-553, Springer - Ver lag.

Osterman, J. and Lindskog, G. (1963). "Influence of Lateral Movement in Clay Upon Settlements in Some Test Areas. *Proceedings. Third European Conference on Soil Mechanics and Foundation Engineering*. Wiesbaden, pp. 137-142.

Perzyna, P. (1963). "The constitutive equations for rate-sensitive plastic materials." *Quarterly of Applied Mathematics*, 20: pp. 321-332.

Perzyna, P. (1966). "Fundamental Problems in Viscoplasticity," *Advances in Applied Mechanics*, Vol. 9, pp. 243-377, Academic Press, New York.

Quigley, R.M. (1980). "Geology, mineralogy and geochemistry of Canadian soft soils: a geotechnical perspective," *Canadian Geotechnical Journal*, 17(2), pp. 21-285.

Rajot, J.P. (1992). "A theory for the time dependent yielding and creep of clay," Ph.D. Thesis, Virginia Polytechnic Institute and State University, Blacksburg, Virginia.

Samson, L., and Garneau, R. (1973). "Settlement performance of two embankments on deep compressive soils," *Canadian Geotechnical Journal*, 20(2), pp. 211-266.

Sekiguchi, H. (1984). "Theory of undrained creep rupture of normally consolidated clay based on elasto-viscoplasticity," *Soils and Foundations*, 24(1), pp. 129-147.

Tavenas, F., Leblond, P., Jean, P., and Leroueil, S. (1983). "The permeability of natural soft clays. Part I: Methods of laboratory measurement," *Canadian Geotechnical Journal*, 20, pp. 629-644.

Taylor, D.W., (1942). "Research on Consolidation of Clays," Department of Civil and Sanitary Engineering, Massachusetts Institute of Technology, Cambridge, Massachusetts, Serial 82.

Taylor, D.W., (1948). *Fundamentals of Soil Mechanics*, John Wiley & Sons, New York, 700 pp.

Taylor, D.W., and Merchant, W. (1940). "A theory of clay consolidation accounting for secondary compression," *J. Mathematics and Physics*, 19(3), pp. 167-185.

Terzaghi, K., (1925). *Erdbaumechanik*, Franz Deuticke, Vienna.

Terzaghi, K., (1943). *Theoretical Soil Mechanics*, John Wiley and Sons, New York.

Trask, P.D., Rolston, J.W. (1961). "The Engineering Geology of the San Francisco Bay Area, California," Bulletin of Geological Society of America, September, 1961.

U.S. Navy, (1982). *Navfac DM-7.1, Soil Mechanics, Design Manual 7.1*, Department of the Navy, Naval Facilities Engineering Command, 200 Stovall Street, Alexandria, VA, 22332.

Yin, J.H. and Graham, J., (1996). "Elastic visco-plastic modeling of one-dimensional consolidation," *Geotechnique*, 46(3), pp. 515-527.

Appendix A

VASBY CLAY OEDOMETER CURVES

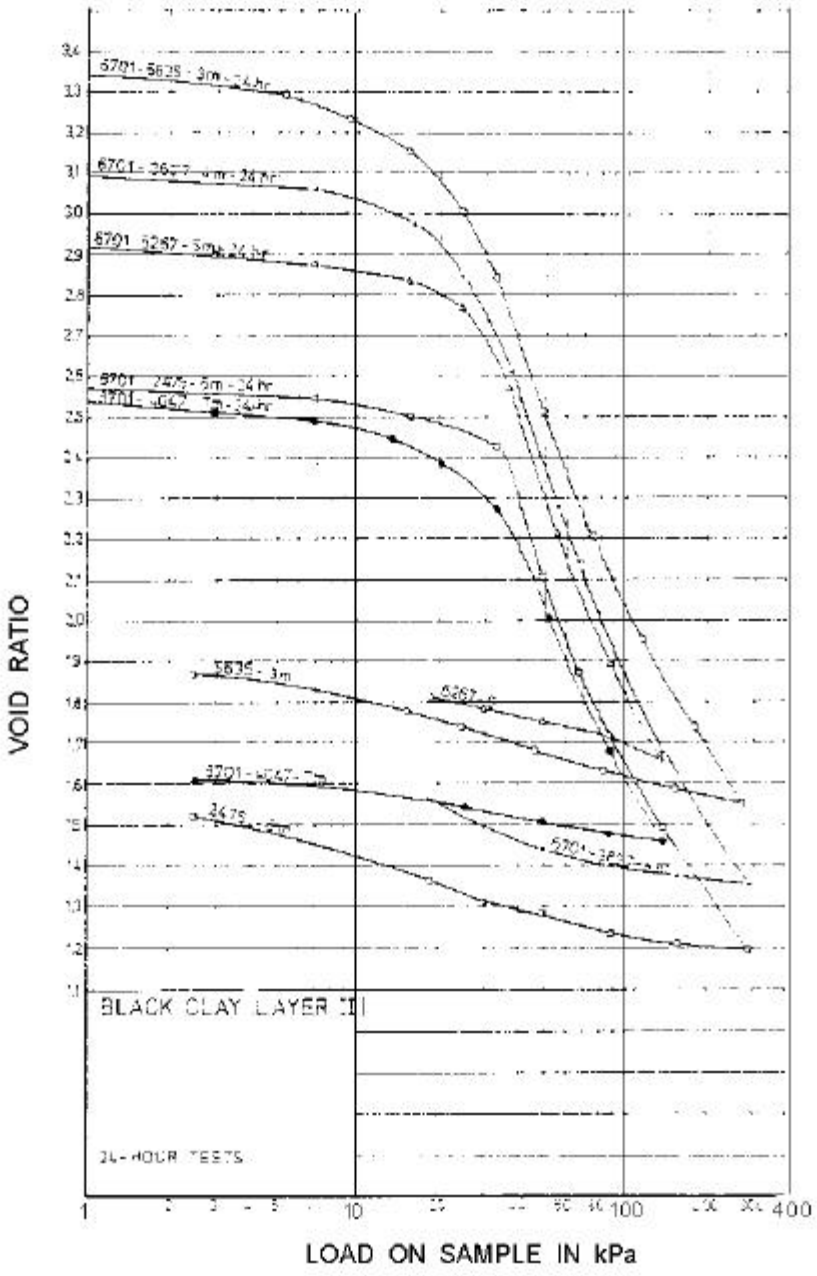

Figure A-1: Oedometer curves with ring friction correction; Vasby clay samples from layer 2, borehole 6701 (from Chang, 1981)

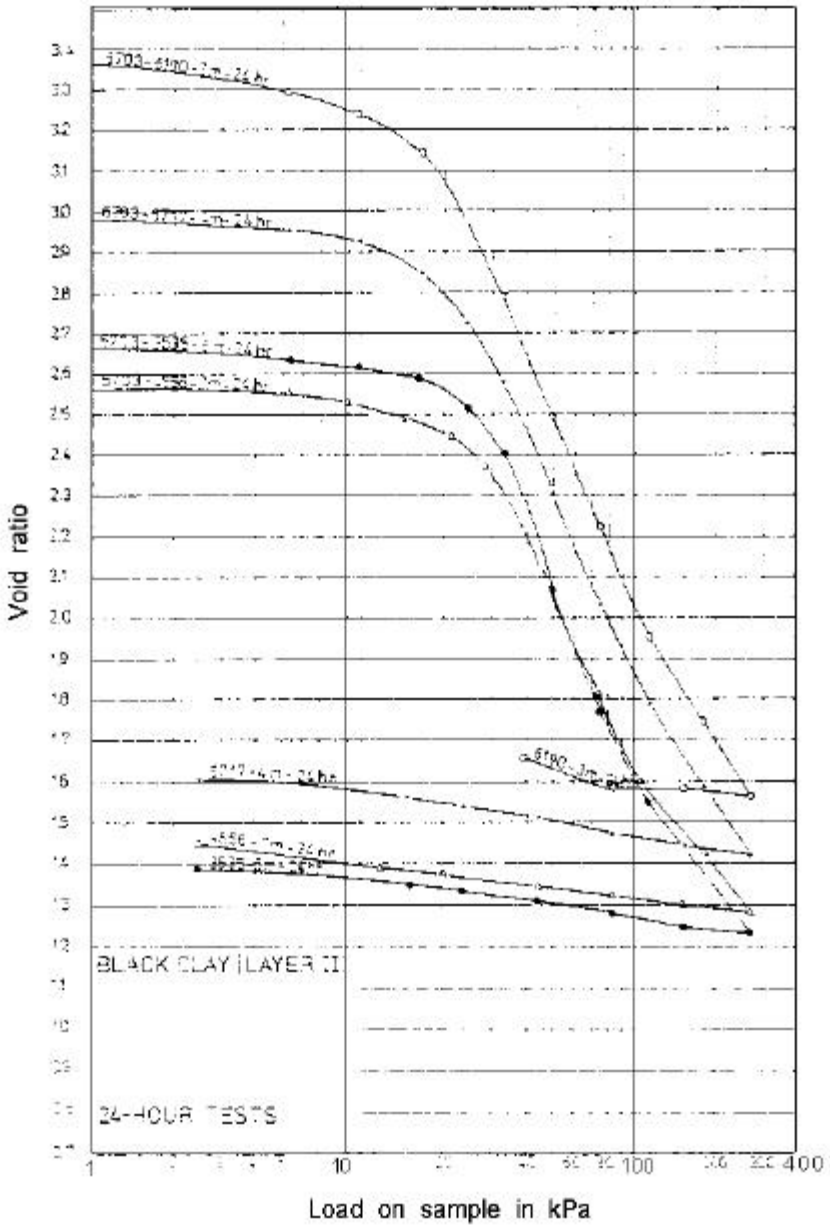

Figure A-2: Oedometer curves with ring friction correction; Vasby clay samples from layer 2, borehole 6703 (from Chang, 1981)

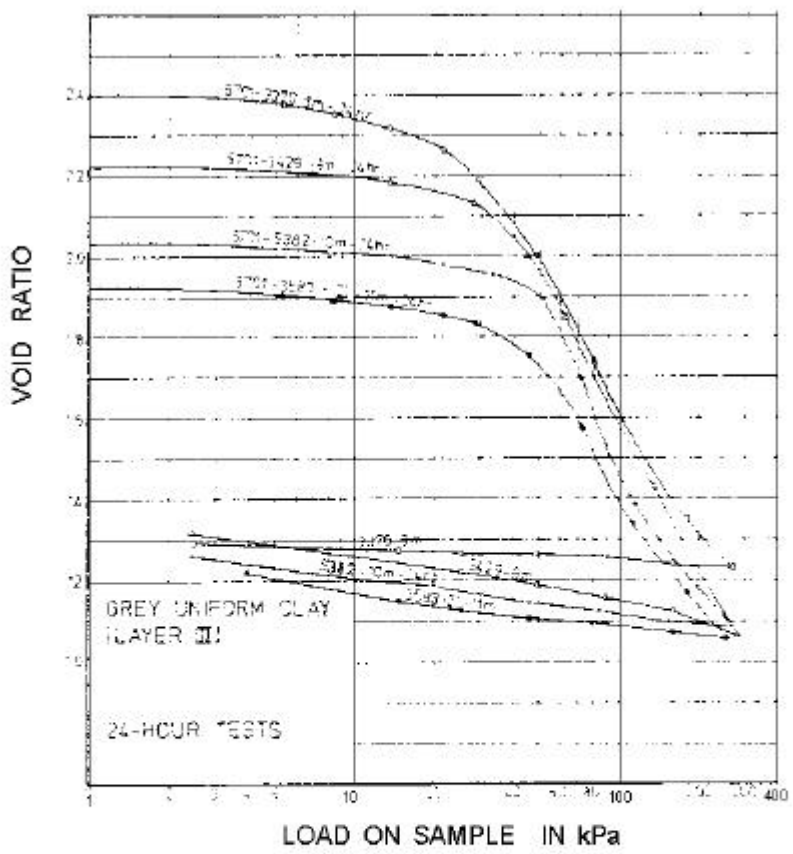

Figure A-3: Oedometer curves with ring friction correction; Vasby clay samples from layer 3, borehole 6701 (from Chang, 1981)

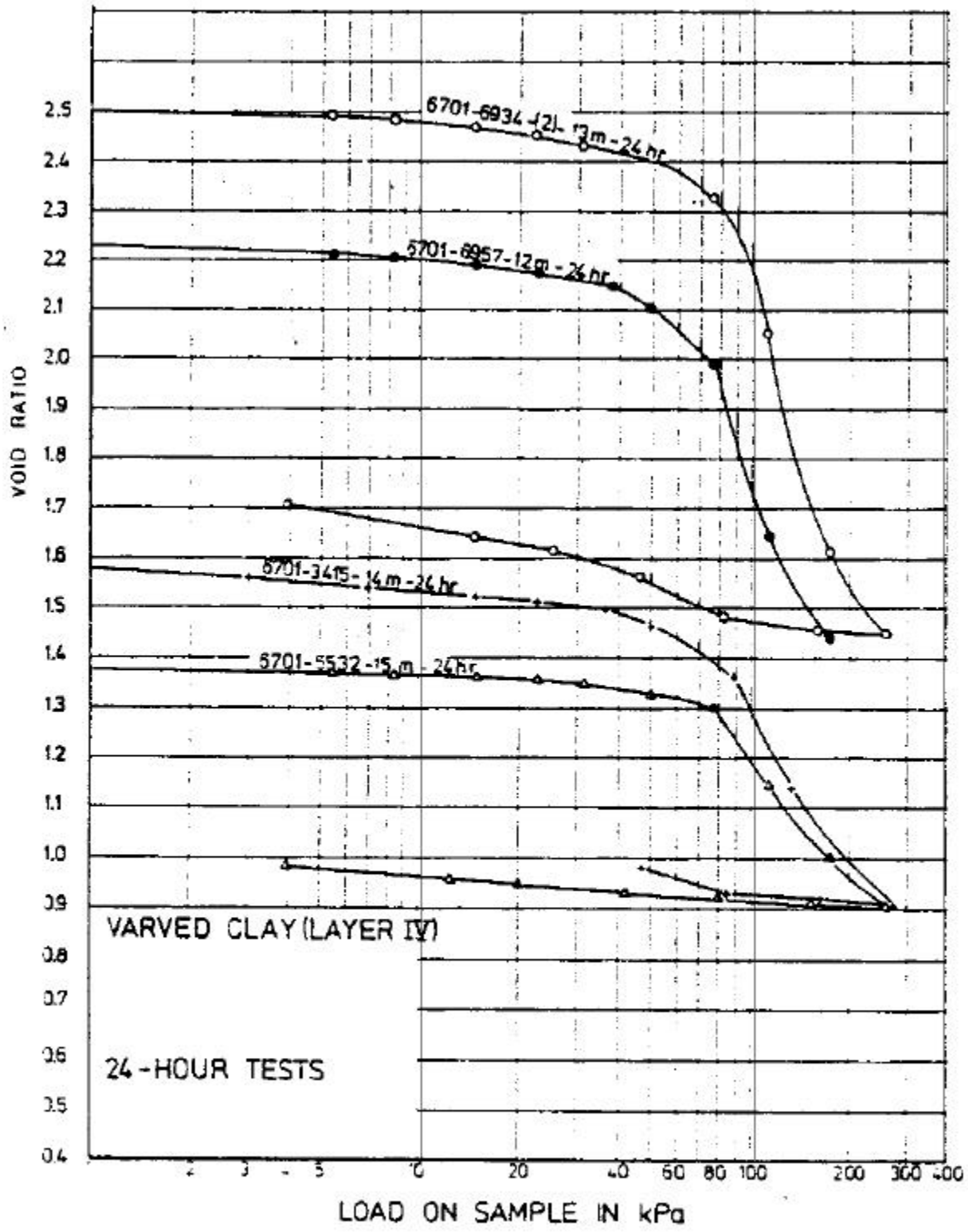

Figure A-4: Oedometer curves with ring friction correction; for Vasby clay samples from layer 4, borehole 6701 (from Chang, 1981)

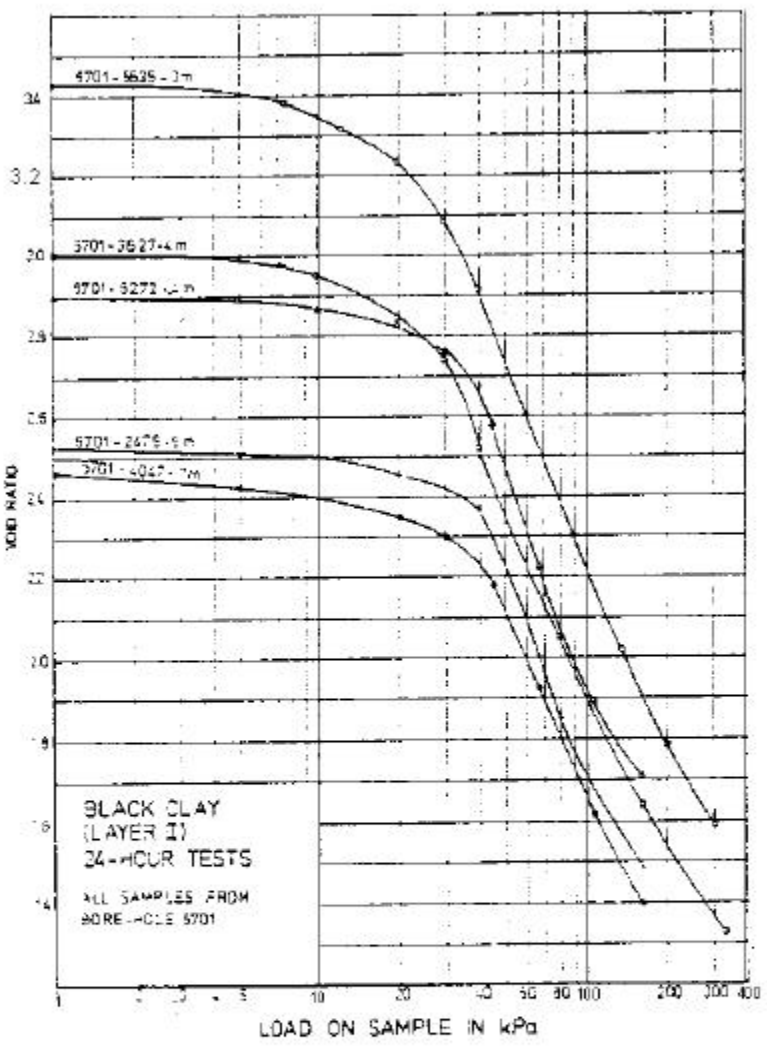

Figure A-5: Oedometer curves without ring friction correction; Vasby clay samples from layer 2, borehole 6701 (from Chang, 1981)

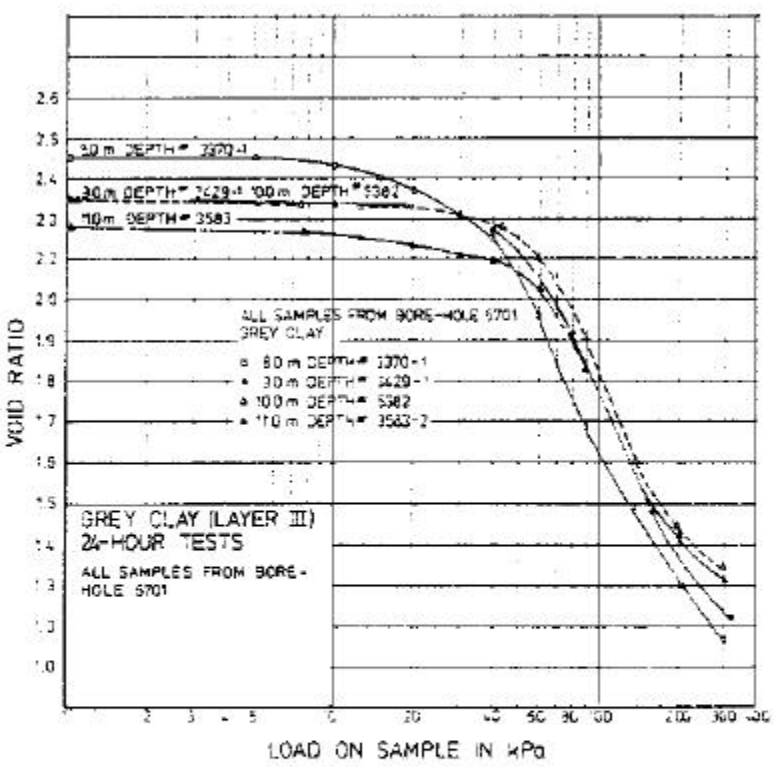

Figure A-6: Oedometer curves without ring friction correction; Vasby clay samples from layer 3, borehole 6701 (from Chang, 1981)

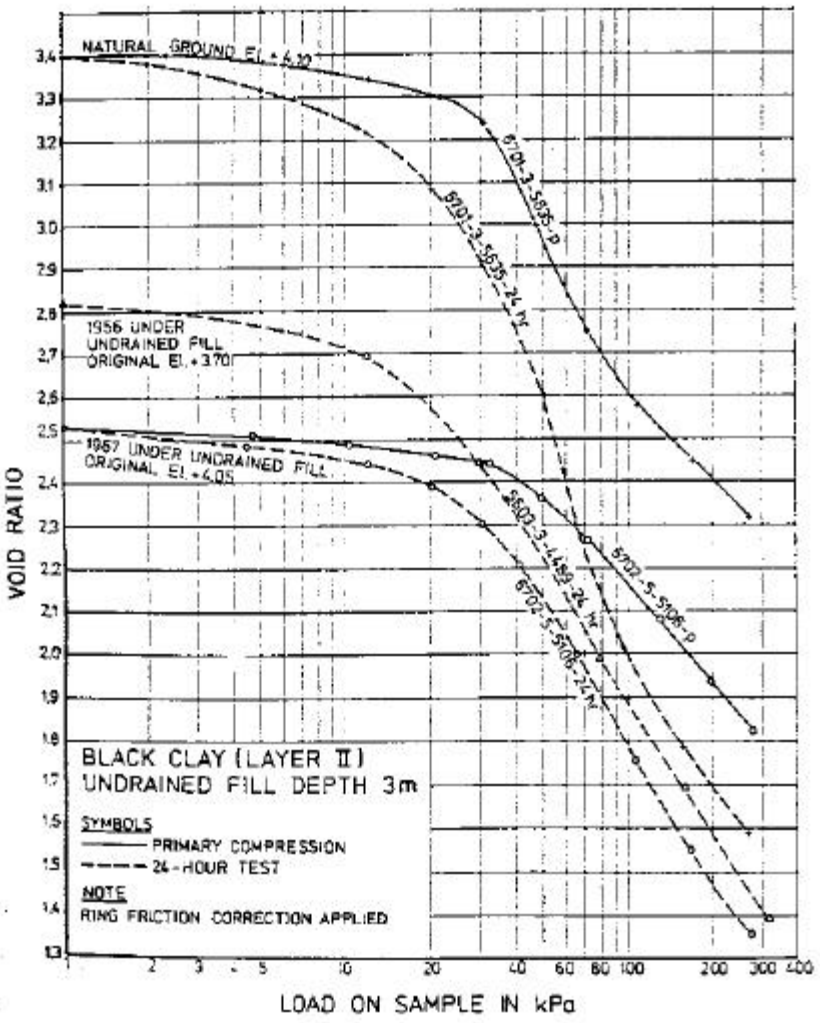

Figure A-7: Oedometer curves with ring friction correction; Vasby clay samples from layer 2, depth 3 meters (from Chang, 1981)

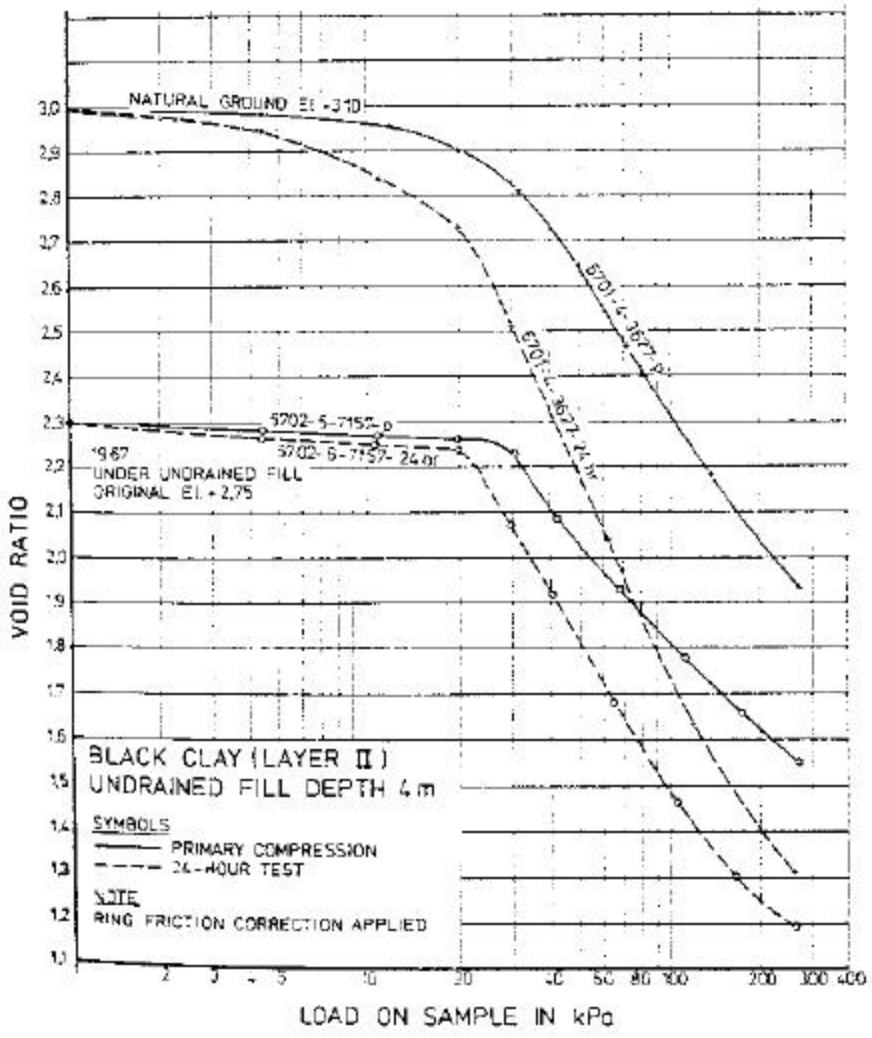

Figure A-8: Oedometer curves with ring friction correction; Vasby clay samples from layer 2, depth 4 meters (from Chang, 1981)

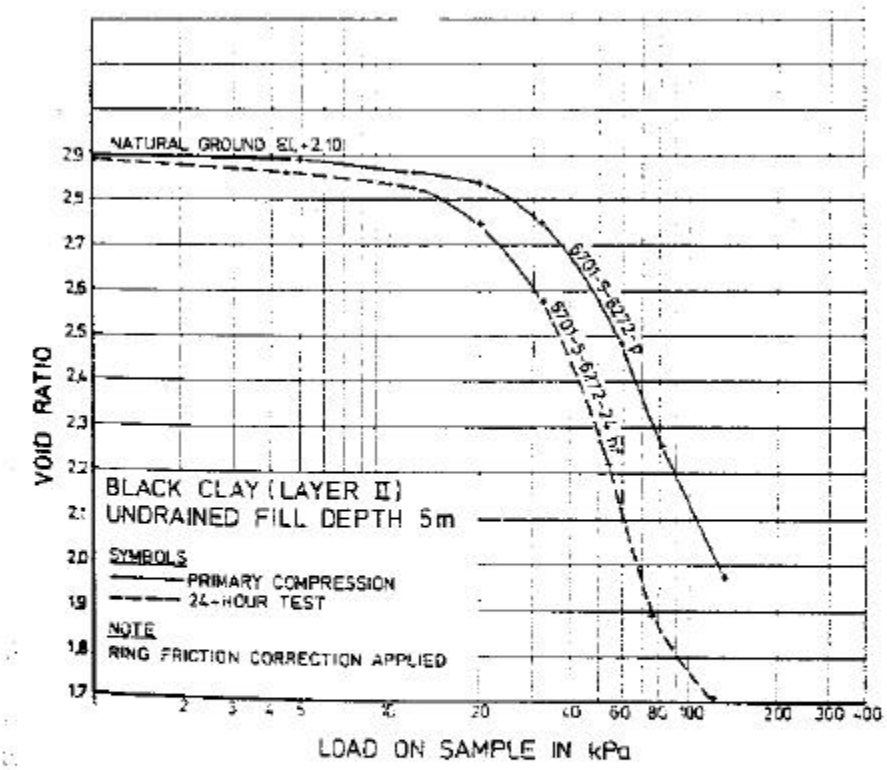

Figure A-9: Oedometer curves with ring friction correction; Vasby clay samples from layer 2, depth 5 meters (from Chang, 1981)

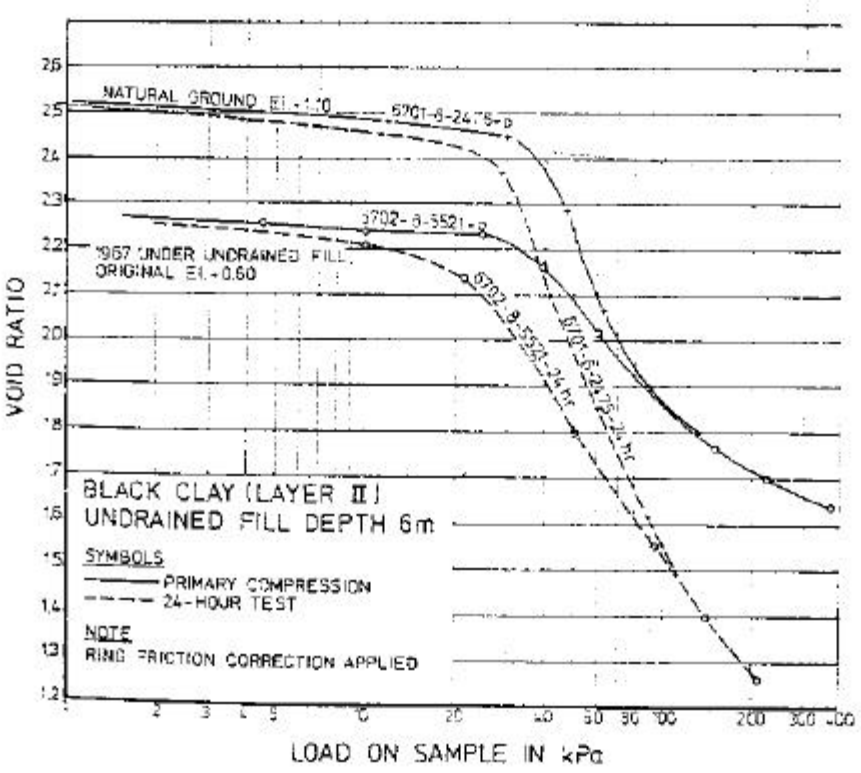

Figure A-10: Oedometer curves with ring friction correction; Vasby clay samples from layer 2, depth 6 meters (from Chang, 1981)

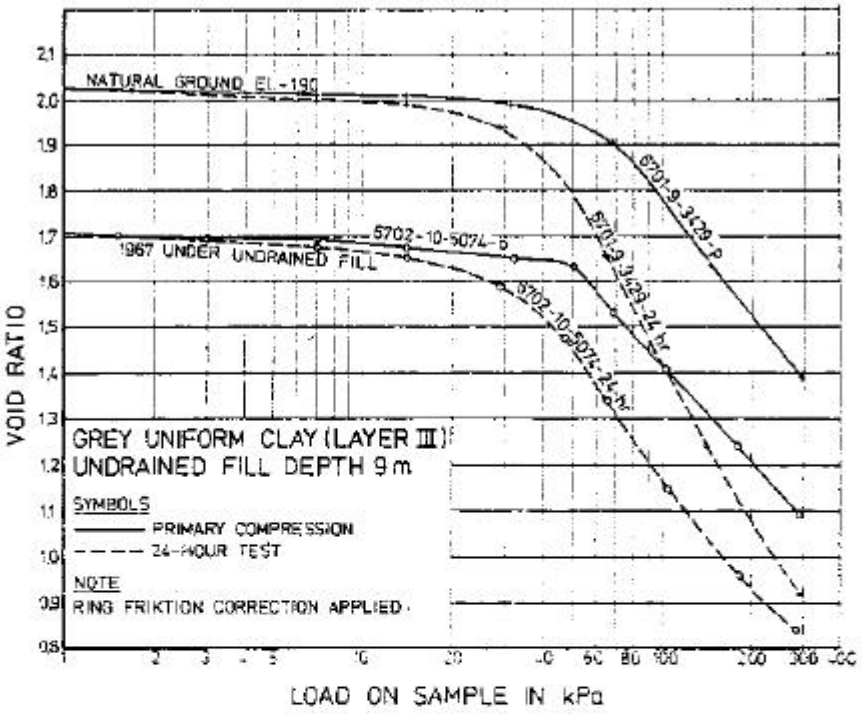

Figure A-11: Oedometer curves with ring friction correction; Vasby clay samples from layer 3, depth 9 meters (from Chang, 1981)

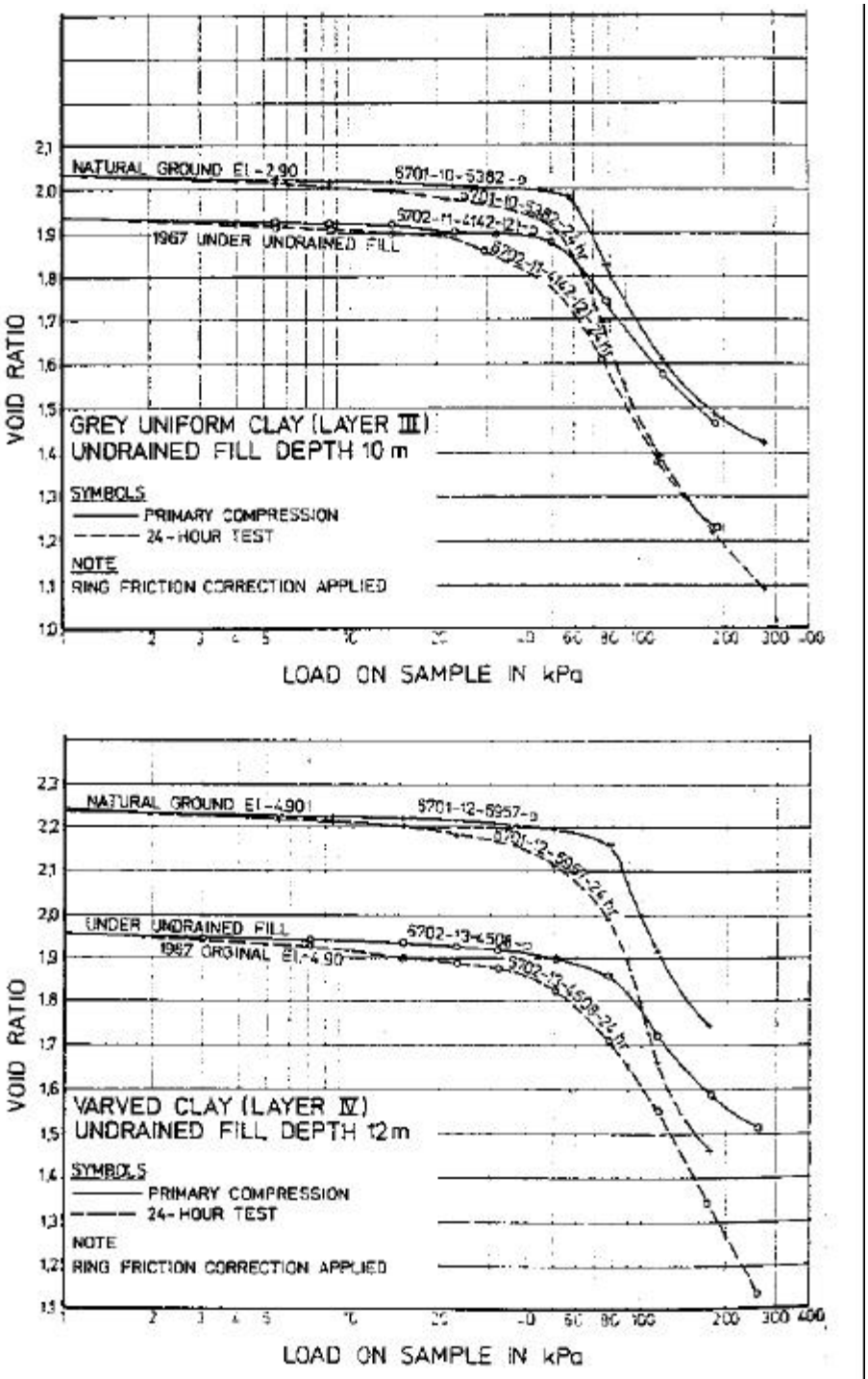

Figure A-12: Oedometer curves with ring friction correction; Vasby clay samples from layer 3, depth 10 m and layer 4, depth 12 m (from Chang, 1981)

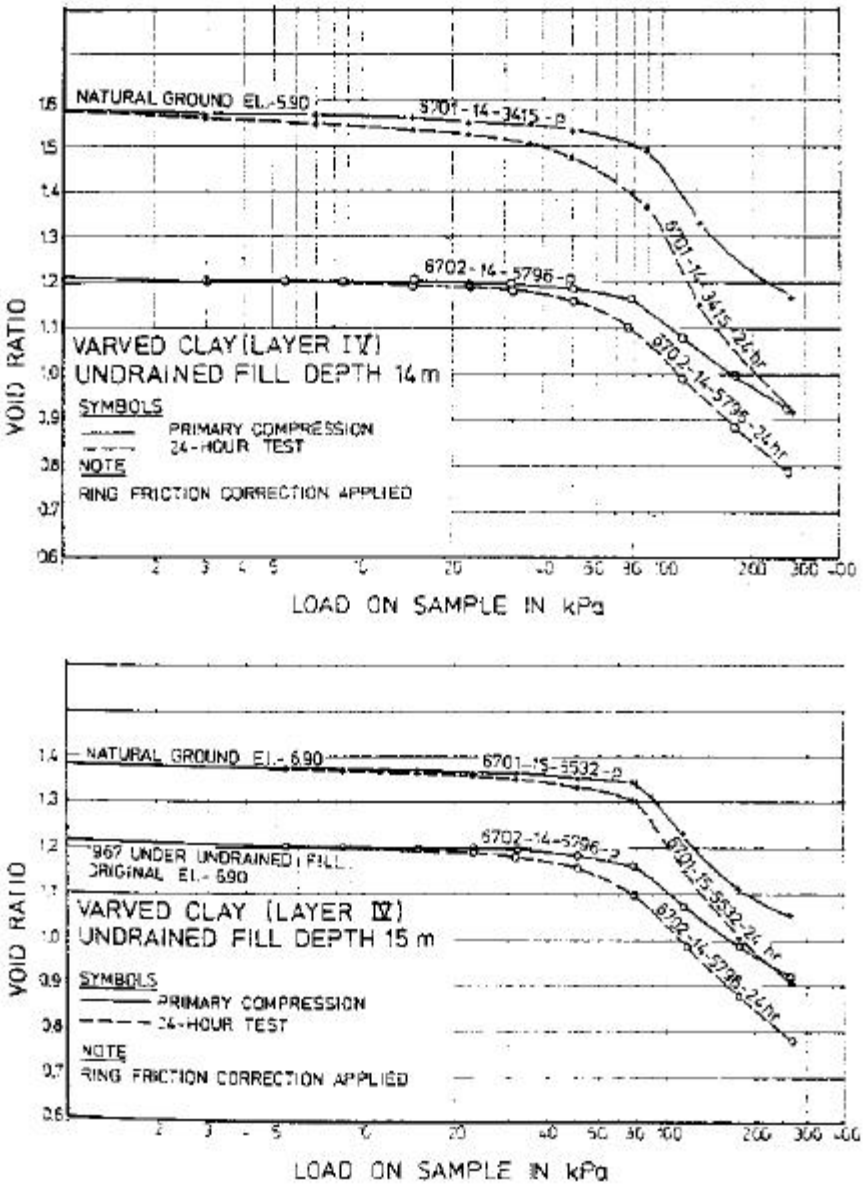

Figure A-13: Oedometer curves with ring friction correction; Vasby clay samples from layer 4, depths 14 m and 15 m (from Chang, 1981)

Appendix B

CONSOL97 USER'S MANUAL

CONSOL97 USER'S MANUAL

by

Vincent J. Perrone
and
J. Michael Duncan

The Charles E. Via Department of Civil Engineering
Virginia Polytechnical Institute and State University
Blacksburg, Virginia

July 1998

Table of Contents

LIST OF TABLES

Section 2

LIST OF FIGURES

Section 2

Section 3

Section 4

1. INTRODUCTION

1.1 PROGRAM DESCRIPTION

Despite recent advances in our understanding of creep effects on one dimensional consolidation behavior, most geotechnical engineers use conventional methods of analysis that do not include the effects of strain rate, duration of loading, or creep on consolidation behavior. These methods, when they involve numerical computer analyses, may account for changes in permeability and non-uniform strain profiles that previously limited the applicability of Terzaghi's consolidation theory. Computer programs such as CONSOL (Duncan et al 1988) are used to predict the magnitude and rate of settlement during primary consolidation. At the end of primary consolidation, secondary compression is added to the calculated settlement. Thus consolidation and secondary compression are separated for ease of computation, ignoring the fact that secondary compression (creep) and consolidation occur simultaneously.

The computer program CONSOL97 calculates settlement for one-dimensional drainage conditions in horizontally layered soil masses. It includes two analysis options: (1) a conventional elasto-plastic (EP) consolidation analysis, and (2) a new time-dependent elasto-visco-plastic (EVP) method of analysis. In the conventional method of analysis, only dissipation of excess pore pressures ("primary consolidation") is considered. The new time-dependent method of analysis uses the same laboratory data, plus the coefficient of secondary compression, and considers the effect of duration and rate of loading on the magnitude and rate of settlements. It models consolidation and creep as simultaneously occurring phenomena. The new theory provides a consistent method for using all of the information obtained from laboratory consolidation tests to estimate the rate and magnitude of field settlements.

The finite element method is used to compute the time rate of consolidation for both the conventional (EP) and new time-dependent (EVP) methods of analysis. The program can analyze problems with the following conditions:

- Stress changes that are uniform or non-uniform with depth. The stress changes in each sublayer can be input by the user, or can be calculated by the computer program for conditions where they are induced by changes in ground water level, or by areal loads of infinite extent, strip loads, or circular loads;

- Variations in soil properties with depth;

- Soil compressibility characterized by linear strain vs. logarithm of effective stress (linear virgin compression curve) or nonlinear strain vs. logarithm of effective stress (piece-wise linear virgin compression curve) relationships;

- Drainage at the top, and/or bottom of the soil profile, and drainage layers within the consolidating soil mass;

- Buoyancy effects due to submergence of the fill material as it settles below the groundwater table.

The program, CONSOL97, is based upon the time-dependent model developed by Jean Pierre Rajot under the direction of Professor J. M. Duncan, at Virginia Polytechnic Institute and State University in Blacksburg, Virginia (Rajot, 1992). Rajot's original computer program (CS1) was modified by Vincent J. Perrone to incorporate a variety of load options, stress-strain behaviors, and output formats, and the addition of an interactive user interface for data input. Virginia Tech civil engineering undergraduate student Derek Wahls assisted in the development of a portion of the user interface and Bob Tipton of Spectrum's Edge Inc., provided helpful advice. The loading options used in CONSOL97 were originally developed in the CONSOL computer program (Duncan et al, 1988) and modified for this program.

1.2 SYSTEM REQUIREMENTS

Operation of CONSOL97 Version 1.0 requires the following hardware and software:

Hardware

- A computer with a 486 coprocessor or a computer with a 386 coprocessor and an 8087 or 80287 math coprocessor or higher.
- At least 4 megabytes of RAM.
- At least one megabyte of hard disk space.
- Any display supported by Windows 3.1 or later.
- A Mouse.

Software

- Windows 3.1 or later, or Windows NT 3.51 or later.

1.3 CONSOL97 SET-UP

The CONSOL97 program is provided on two 3.5-inch high density diskettes. The user should make a back-up copy before proceeding with the set-up instructions. To install CONSOL97, perform the following steps from the Windows environment:

1. Check your main directory for the following DOS extender files: DOSXMSF.exe, DOSXNT.386, DOSXNT.exe. If they are not present, copy them from the 3.5 inch diskette to your DOS directory.

2. Insert the first diskette in Drive A. *Click* **FILE** from the tool bar, *select* **RUN**, and *type* **SETUP** in the command line text box. *Click* **OK** and follow the instructions that appear on the screen.

2. USING CONSOL97

2.1 INTRODUCTION

The data file required to operate CONSOL97 is created from information provided by the user in a series of input screens that operates in a Windows environment. This section describes the data required to operate CONSOL97, discusses how to assemble the data before using the program, and provides an explanation of the procedures for entering data in each screen.

The user specifies the magnitude and location of the applied loads and boundary conditions, and the times at which output results are desired. The computer program selects appropriate intermediate time step increments to solve for displacements and pore water pressures which are accumulated with each time step increment and stored for each output time. The user may specify up to 20 loading cases for a single problem.

The total porewater head at a drainage boundary may not be changed during the analysis. However, if the user selects the load option that simulates a ground water change, the total pore water head at drainage boundaries are adjusted based on the new groundwater elevation. If the groundwater table at the start of the analysis is located below the top of the soil profile, CONSOL97 assumes hydrostatic conditions (total head is constant) throughout the soil profile prior to application of any loads except for the under-consolidated case. Therefore, the pressure head is negative above the groundwater table and positive below the groundwater table, as illustrated in Figure 2-1.

The user should verify that the solution has converged to an acceptable range of accuracy. This can be accomplished by increasing the number of elements and/or increasing the number of time step increments: if the solution has converged, the new solution should be close to the previous solution. For some elasto-visco-plastic analyses, some combinations of subsurface profile,

loading, and soil properties can produce computational failure. In such cases, the user should to perform a conventional elasto-plastic analysis.

2.2 SETTING UP THE PROBLEM

Before creating a data input file, the user first defines the essential features of the problem. The procedure for completing a successful consolidation analysis involves these steps:

1. Evaluate the soil borings and laboratory tests to establish a representative soil profile for analysis.
2. Considering all the available data, select values of C_c, C_r, c_v, C_α, T_{age}, and profiles of P_p' and e for the analysis.
3. Divide the profile into zones that have the same soil properties (C_c, C_r, c_v, C_α, T_{age}) and stress history (overconsolidated, normally consolidated, or under- consolidated).
4. Subdivide each zone into layers (design the finite element mesh).
5. Determine which layers have free draining boundaries.
6. Determine the magnitude of the loads and the times at which they are applied.
7. Decide whether a conventional consolidation analysis or a time-dependent consolidation analysis will be performed.
8. Enter the data in the interactive screens.
9. Analyze the amounts and rates of settlements using the program. If a time-dependent analysis has been performed, compare the results (settlements and pore pressures) with conventional analyses to be sure they are reasonable.
10. Increase the number of layers and the number of time steps to confirm that the solution has converged with sufficient accuracy.

Input data required to achieve an accurate conventional consolidation analysis may not be adequate for the time-dependent analysis which generally requires more layers and longer computing times to achieve accurate results.

2.3 REPRESENTATIVE SOIL PROFILE

A subsurface soil profile that represents the site should be determined from soil borings, laboratory test results and geologic information. It may be necessary to select more than one profile for analysis if conditions vary across the site. In this case, the steps outlined in section 2.2.2 should be repeated for each soil profile.

2.4 SELECTION OF SOIL PROPERTIES AND PRECONSOLIDATION STRESS PROFILE

The values of void ratio (e), virgin compression index (C_c), recompression index (C_r), coefficient of consolidation (c_v), secondary compression coefficient (C_α), and preconsolidation pressure ($P_p^{/}$) are usually based on the results of laboratory tests. Insensitive clays are generally characterized by a linear strain vs. log effective stress relationship (linear virgin compression curve) which can be represented by a single set of C_c, C_α, and c_v values. However, organic and sensitive clays often have non-linear strain vs. log effective stress relationships (curved virgin compression curves). CONSOL97 can accommodate as many five values of C_c, C_α, and c_v for each soil. If the soil profile has more than one soil type, different values of C_c, C_r, c_v, C_α, T_{age} are used for each soil type. A maximum of 20 soil types may be specified in CONSOL97. The geologic age (T_{age}) of the deposit is required for the time-dependent analysis, and it is usually estimated from published information about the age of the geologic unit identified on the site.

A standard 24 hour oedometer test (ASTM 2435) is used to determine consolidation parameters C_c, C_r, c_v, and C_α for each soil type. The values of C_c and C_r for both end of primary and 24 hour strain values are generally the same. However, the 24 hour test results, which include more secondary compression than the end of primary test results, will typically have preconsolidation stresses, $P_p^{/}$, that are about 10 to 20% smaller than end of primary test. Figure 2-2 illustrates the relationship between stress - strain curves for different loading duration. For time-dependent analyses, the user must specify both $P_p^{/}$ and the reference time at which the measured strains occurred. For a 24 hour test, the reference time is 24 hours.

The preconsolidation stress profile is determined from consolidation tests on samples obtained from various depths in the soil profile. For each consolidation test, a range of values of P_p' should be found and plotted on a graph similar to those shown in Figure 2-3, where the bars indicate the possible range of values of P_p' consistent with the test data. The stress history profile line is a "best fit" curve through the ranges of P_p' values. If necessary, the stress history profile may be represented by a discontinuous line. The stress state at any depth in the subsurface profile will either be under consolidated (UC), normally consolidated (NC), or over consolidated (OC). Each of these stress states is illustrated in Figure 2-3.

2.5 DIVISION OF THE SOIL PROFILE INTO SOIL ZONES

A soil zone is a portion of the soil profile that contains one soil type, one type of stress state or preconsolidation profile (UC, NC, OC), and in which the P_p' profile is constant or linearly varying with depth. Drainage boundaries must coincide with the top or bottom of a soil zone. Figure 2-4 illustrates two soil profiles divided into appropriate soil zones based on soil types, P_p' profile, and drainage conditions. Soil zones must be numbered consecutively, starting with number one at the top of the soil profile.

In some situations, the top layer of soil is desiccated, heavily overconsolidated, and much more permeable than the underlying clay. The desiccated crust may be modeled as overburden or as part of the compressible soil profile. If the groundwater table is located at depth, d_w, below the ground surface and the soil above the groundwater table is treated as a compressible soil type, the initial effective stress at the ground surface will be $\sigma_o' = d_w \cdot \gamma_{water}$. The user may wish to model the crust as overburden and ignore the small amount of elastic compression in this layer.

2.6 DIVISION OF SOIL ZONES INTO LAYERS

The selection of an appropriate number of layers for each soil zone depends on the drainage boundary conditions, soil properties, and the type of analysis. A conventional consolidation analysis requires fewer layers than an elasto-visco-plastic analysis to achieve accurate results.

Thinner layers near drainage boundaries (where hydraulic gradients are largest), and thicker layers near the center of a soil layer and near impermeable drainage boundaries, will provide more accurate results and efficient analyses.

The user should model the least permeable soil zone such that the layers near the drainage boundaries are thinner than $0.2H_k$ where, H_k is the longest drainage distance for zone, k. Other zones should be modeled such that the layer thickness at the drainage boundaries are proportional to $\sqrt{c_v}$ for each zone. However, if the layers are made too thin for an elasto-visco-plastic analysis, computational difficulties may occur due to machine precision limitations.

CONSOL97 includes a mesh generation subroutine that can sub-divide each soil zone to produce the following mesh geometries: 1. uniformly thick sub-layers; 2. increasing sub-layer thickness with increasing depth; 3. decreasing sub-layer thickness with increasing depth; 4. increasing sub-layer thickness followed by decreasing layer thickness with depth. The user specifies the desired number of sub-layers and the type of mesh geometry for each zone. If a non-uniform mesh geometry is selected, CONSOL97 sizes the adjacent layers so that each larger layer is twice as thick as the adjacent smaller layer.

2.7 LOADING OPTIONS

As many as 20 load applications may be specified for one CONSOL97 analysis. For each loading the user indicates the time at the beginning of load application and the length of time over which the load is applied (called the "ramp time"). Each load must have a ramp time greater than zero. CONSOL97 determines the minimum allowable loading duration based on the layer thicknesses and c_v. If the ramp time is too small, CONSOL97 increases the value. If shorter ramp times are required, the user should decrease layer thicknesses near drainage boundaries.

The applied loads determine the initial excess pore pressure conditions for the finite element analysis. The initial excess pore pressures are set equal to the changes in vertical stress throughout the depth of the stratum, thus assuming that the change in pore pressure is equal to

the change in vertical stress. This is an accurate assumption for saturated clay and surface loading of infinite horizontal extent. For loads of finite horizontal extent on saturated clay, it is a reasonable approximation to assume that $\Delta u = \Delta\sigma_v$ and this assumption is the one normally used in consolidation analyses. For unsaturated materials, a portion of the compression occurs instantaneously upon application of the load, and Δu may be appreciably smaller than $\Delta\sigma_v$. For these conditions, the assumptions used in CONSOL97 will lead to higher-than-actual pore pressures and slower-than-actual settlement rates.

The changes in vertical stress can be defined by the user at each layer boundary (finite element node) or they can be calculated by CONSOL97. For loads of infinite lateral extent, such as placement or removal of large areal fills, the change in vertical stress is constant over the depth of the stratum:

$$\Delta\sigma_v = \Delta h \cdot \gamma_f \qquad (2.1)$$

where: $\Delta\sigma_v$ is the change in vertical stress, Δh is the thickness of fill added or removed, γ_f is the unit weight of the fill.

The change in vertical stress due to a change in water level is:

$$\Delta\sigma_v = \Delta h_w \cdot \gamma_w \qquad (2.2)$$

where: Δh_w is the change in water level, γ_w is the unit weight of water.

For loads acting over areas of finite lateral extent, such as strip loads, or circular loads, the change in stress are not constant over the depth of the layer. CONSOL97 calculates stress influence factors (I_z) at each node based on equations from Boussinesq's elastic theory. The changes in vertical stress due to a surface load, q, are given by:

$$\Delta\sigma_v = q \cdot I_z \qquad (2.3)$$

Stress influence factors and equations for a uniform strip load of infinite length are shown in Figure 2-5. The equations can be used to calculate the change in vertical stress at any position for a strip of any width. The graph in the lower part of Figure 2-5 shows how the value of I_z changes with depth (z), strip width (b), and distance (x) from the center of the strip.

Stress influence factors beneath the center and the edge of circular loaded areas are shown in Figures 2-6 and 2-7. Boussinesq's solution for I_z beneath the center of the load is shown in Figure 2-6. There is no closed form expression for I_z at other locations beneath circular loaded area. However, approximate values of I_z for stresses beneath the edge of the loaded area are shown by the plotted points and the numerical approximation in Figure 2-7. These were obtained from a chart published in NAVFAC DM 7.1 (1982).

For an under-consolidated soil profile, the reference preconsolidation stresses are less than the computed initial effective stresses, σ'_{vo}, based on hydrostatic pore pressure conditions. CONSOL97 first computes the magnitude of excess pore pressures at each node:

$$\Delta u = \sigma'_{vo} - \sigma'_{p-ref} \qquad (2.4)$$

and then redefines the values of initial effective stress in the under-consolidated layers so that they are equal to the preconsolidation stresses.

Settlement of the ground surface during consolidation can cause submergence of existing or newly placed fill soils. A buoyancy correction is required to account for the resulting changes in excess pore pressure. Figure 2-8 illustrates the correction used in CONSOL97. If the loads are of finite lateral extent, the settlement will not be uniform, and the change in vertical stress due to buoyancy effects will not be uniform across the loaded area. CONSOL97 has two options to account for these effects. The first option approximates these buoyancy effects by adjusting the excess pore pressures at each layer as if the fill were of infinite lateral extent. The second option adjusts the excess pore pressures by an amount that is equal to the correction shown in Figure 2-8, multiplied by the stress influence factors computed for each layer.

CONSOL97 provides the following load options:

Load Option 1: Specified Change in Stress

This load option is used when the other load options cannot adequately describe the loading. The user specifies the change in vertical stress for each layer.

Load Option 2: Change in Water Level

CONSOL97 calculates the change in vertical stress due to a specified change in the water level. If the water level drops below the top of the compressible layer, the pore water pressure above the new water level becomes negative and the change in stress is uniform throughout the compressible layer.

Load Option 3: Large Areal Load

Simulates the placement or removal of a uniform thickness of fill over a large area. The program calculates a uniform change in stress for each layer.

Load Option 4: Infinitely Long Strip

CONSOL97 calculates the change in vertical stress for each layer when a strip load of infinite length is applied on the surface. A strip footing load can be simulated by specifying appropriate values of strip width, fill thickness and unit weight.

Load Option 5: Circular Areal Load

CONSOL97 calculates the change in stress for each layer due to the placement or removal of a circular load on the surface. The load due to a circular or square spread footing can be simulated by specifying appropriate values of diameter, fill thickness and unit weight.

Load Option 6: Specified Stresses

The user specifies the initial pressure, final pressure, and preconsolidation pressure to calculate settlements. This load option is different from load option 1 through 5 because it over-rides the values of P_o', P_f' and $P_p^{/}$ initially calculated by CONSOL97 and any load adjustments due to submergence of newly placed fills. This load option may only be specified at time t=0.

Load Option 7: No External Applied Load (Under-Consolidated Profile)

This load option is used to compute settlements that occur with no additional loads as a result of incomplete consolidation under a previous loading. At the start of the analysis the soil profile will have excess pore pressures which are dissipating and causing additional settlements. CONSOL97 analyzes the dissipation of excess pore pressures and the time rate of settlement. The excess pore pressures are equal to the final effective overburden pressure (at hydrostatic water pressures) minus the preconsolidation pressures specified for each layer. This load option may only be used at time t=0.

2.8 ANALYSIS AND EXAMINATION OF RESULTS

Once the data has been entered and saved in the data file, *name.ext*, the settlements and pore pressures can be computed. The output files will be automatically assigned the data input file name plus an extension: the standard output file will be named *name.out* and the plotting output file will be named *name.plt*.

After the computations are completed, the user should examine the results for data input errors. The results of time-dependent analyses should be compared to the results of conventional analyses.

Editing of data input to correct errors or to study the effects of changes in soil parameters, problem geometry, or loading conditions may be accomplished by opening the existing file. The appropriate data input screen can be selected from the **Input** menu or each screen can be sequentially accessed by clicking **Continue** on each data screen.

2.9 INTERACTIVE DATA INPUT SCREENS

Double click the CONSOL97 icon to run the program. The first screen that appears is the program cover page. *Click* **Continue** to display the data input environment and menu bar. Table 2-1 summarizes the menu options which are described in this section.

2.9.1 Creating a New Data File

Select **New** from the **File** menu. The "Method" screen will appear as shown in Figure 2-9. After entering the required data *click* **Continue** to show the next data input screen. If you *click* **Continue** before providing all of the requested input data, an error message will appear. You must enter the missing data before proceeding to the next screen.

A description of the data input screens is provided below in the sequence in which they appear when creating a new data file:

Methods

Enter a project description and *select* either "conventional consolidation analysis" or "consolidation analysis with creep behavior."

Units Selection

Use the drop-down lists shown in Figure 2-9 to select dimensional units for stress and coefficient of consolidation, and to select either fresh or salt water.

Subsurface Profile

Enter data that defines the general subsurface profile and the unit weight of any overburden soil.

Soil Properties

When this screen appears, conventional soil properties such as the total unit weight, C_c, C_r, c_v, void ratio must be provided (Figure 2-10). If you wish to model the creep behavior of this material (elasto-visco-plastic model), *select* "This soil is a visco-plastic material" and additional text boxes will appear on the bottom half of the screen for C_α, oedometer test reference time, and the estimated geologic age of the soil deposit. If more than one value of C_c, C_α or c_v, is required to define the soil behavior, enter the number of stress-strain segments. *Click* **Continue** to show

the next soil property screen or, if all the soil properties have been provided, the "layer" screen will appear.

Soil Zone Information

This screen appears for each soil zone (Figure 2-11). The preconsolidation stress, elevation, and drainage condition must be provided at the top and bottom of the zone. *Click* "Drained" if drainage occurs at the zone boundary. The selected drainage condition at the bottom of the current layer will automatically appear at the top of the next soil zone.

The soil zone displayed on the screen must be divided into layers, and defined by a soil type, and a stress state. To define the layering you can enter the number of layers in the text box or use the vertical scroll bar and then *select* a mesh geometry from the "Mesh geometry" list shown in figure 2-11.

Enter a "soil type number" and *click* on "consolidation state" to define the current stress state. Double clicking on a consolidation state option will produce a message box that defines each option: under-consolidated is an effective overburden stress that exceeds the preconsolidation stress; normally consolidated is an effective overburden stress that equals the preconsolidation stress; over-consolidated is an effective stress that is less than the preconsolidation stress. If you select normally consolidated, CONSOL97 will compute the correct preconsolidation stresses and over-ride the values provided at the top and bottom of the zone.

Layers for Plot File

A plot file consists of strain, effective stress, yield stress, reference preconsolidation stress, and delayed strain rate vs. time for specified sublayers. *Click* on the text box and enter a value or use the scroll bar to select the total number of sub-layers to include in the plot file. Individual text boxes will appear so the user can enter the sub-layer numbers.

Time and Load Options

Data is entered in the table to specify output times and a loading schedule (Figure 2-12). *Click* on the appropriate text box in the table to enter an output time, t_n. To specify a load option at time, tn, select a load option in the "load option list" and *click* on the load option text box at time, t_n. The user must also specify a ramp time for each load option entered in the table. Load option 7, "under-consolidated soil profile" may only be specified at time, tn = 0. The data in the table may be edited by highlighting values and entering new data.

Load Options

Load option screens will appear in the order that they were specified in the "Time and Load Options" table. All stresses are positive in compression. No data input screen is required for the "Under-Consolidated" load option.

Specified Change in Stress: *Select* "Uniform Stress Change" or "Non Uniform Stress Change." If "Non Uniform Stress Change" is chosen, then additional data entry boxes will appear. Enter the stress change values in the text boxes and *click* **Next** to enter values for all the layers. (Figure 2-13).

Change in Water Level: Enter the new groundwater elevation.

Large Areal Surcharge: You may specify either the new fill elevation or the new height of fill. If you enter a fill height, the fill elevation will be assigned a dummy value of -9999. If you enter a fill elevation, the fill height will be assigned a dummy value of -999. The dummy values are not used in the computations but they are used to determine if the input value refers to fill height or fill elevation.

Infinitely Long Strip: Similar to the large areal surcharge load option, you may specify either the new fill elevation or the new height of fill (Figure 2-14). The stress increase will be computed at the "settlement point distance from the center" that you specify in the text

box. Enter a positive integer value in "buoyancy code" to adjust the load based on the amount of fill that settled below the water level in the previous time step, multiplied by the stress influence factor computed for each layer. Otherwise, the load will be adjusted based on the amount of fill that settled below the water level in the previous time step, multiplied by 1.0.

Circular Areal Load: Similar to the large areal surcharge load option, you may specify either the new fill elevation or the new height of fill. The stress increase will be computed at the "settlement point distance from center" that you specify in the text box. Enter a positive integer value in "buoyancy code" to adjust the load based on the amount of fill that settled below the water level in the previous time step, multiplied by the stress influence factor computed for each layer. Otherwise, the load will be adjusted based on the amount of fill that settled below the water level in the previous time step.

Specified Stresses: Enter values for overburden pressure, preconsolidation pressure and total final stress and *click* **Next** to enter values for the next soil layer. After specifying the stresses for the final layer, *click* **Continue**.

2.9.2 Saving A Data File

To save a data file, *click* **SaveAs** from the **FILE** menu. A directory list will appear so you can select an existing file name or enter a new file name. Saving a file will activate the **Input Data** item on the menu bar.

2.9.3 Opening An Existing Data File

Click **Open** from the **File** menu and *select* a filename from the directory list that appears in the windows screen.

2.9.4 Closing A Data File

Click **Close** from the **File** menu to close the current data file. A message box will ask if you wish to save the data. *Click* "Yes" or "No" to continue.

2.9.5 Editing Input Data.

The **Input Data** item on the menu bar can be used to select data input screens for editing. *Click* **Input Data** to view a list of screen options. *Click* on the desired option and the screen will appear in the window environment. If you selected a screen option such as soil zones, soil properties, or time and load options that contain multiple data forms, the first soil zone, soil property or time/load option will appear. *Click* **Continue** to access subsequent data forms.

2.9.6 Running A CONSOL97 Analysis.

Click **Run Analysis**. If you are using Microsoft Windows 3.1, the current screen will minimize to an icon and a black screen will appear and prompt the user for input and output file names. For Microsoft Windows 95 or later, a "CONSOL.exe" icon will appear at the bottom of the screen. Click the icon to view the black screen. Messages will be printed to the screen to keep you informed of progress during the computations (Figure 2-15). Upon completion of the finite element analysis, the data input windows environment will reappear and with the message: "CONSOL97 Analysis is Finished."

2.10 RUN TIME ERROR AND WARNING MESSAGES

Warning messages that appear on the screen during execution of the finite element code will not terminate execution. However, they will provide you with information about the performance of the computation. For example, a warning "MORE THAN 30 ITERATIONS IN CURRENT TIME STEP" indicates that the numerical convergence could not be attained for the current time step, problem geometry and loading conditions. CONSOL97 will automatically reduce the

incremental time step. However, if this warning continues to appear during subsequent time steps, the computational time may become excessive or the computation may eventually encounter a fatal error message such as "TOO FAR FROM YIELD SURFACE EVEN WITH MINIMUM TIME STEP." In either case you may want to redesign the mesh geometry and output time sequence to improve computational efficiency or to avoid a fatal error. Run time errors and warning messages are listed in Section 5.

2.11 DATA INPUT FILE

Each data input file created by entering data in the input screens consists of five major components that are required to define each consolidation problem:

1. Control - descriptive title, computational and output control information;
2. Profile - subsurface profile and finite element mesh;
3. Properties - soil properties and stress state;
4. Boundary - boundary conditions for drainage and deformation;
5. Loading - loading conditions;

Tables 2-2 and 2-3 summarize the input variables required for execution of CONSOL97. The fortran source code uses free format for data input. Therefore, the only format requirement for the data input file is that individual values must be separated by a comma or a blank space. A detailed description of each variable name, listed in alphabetical order, can be found in Sections 2.11.1 to 2.11.5 according to the type of "data file component" indicated in the last column of Table 2-2. Alternatively a description of each variable may be found in the "Index of Data Input Variables" in Section 6. The structure charts in Figures 2-16(a), 2-16(b) and 2-16(c) illustrate the sequence in which CONSOL97 reads the input data. An example data file is presented in Table 2-4.

2.11.1 Problem Description and Control

Control variables provided by the user:

Variable	Description
ACONSOL	Dimensional units for coefficient of consolidation.
ASTRESS	Dimensional units for stress.
AWATER	Fresh or salt water.
IFILE	If a time-dependent analysis, select the type of output. Ifile=0 for standard output. Ifile=1 for detailed output. For conventional elasto-plastic analyses, leave blank.
LAYDAT(J)	Layer numbers to be included in the plot file output.
LAYOUT	Number of layers to include in the plot file output.
LUNIT	Index that designates desired dimensional units options. Select a value from 1 to 15.

DIMENSIONAL UNIT OPTIONS

	psf	ksf	tsf	kPa	tsm
minute	1	2	3	4	5
day	6	7	8	9	10
year	11	12	13	14	15

METHOD	Method of analysis: time-dependent method =0; conventional method =1
NTO	Number of designated output times.
NX1	Number of time steps between any two output times
TITL	Problem description
VTO(K)	Output time. K=1 to NTO

Internal control variables programmed in CONSOL97:

Variable	Description
NPE	Number of nodal points on an element. NPE=2
P1KPA	Number of stress units in one kPa (determined from LUNIT).
ERROR	The allowable convergence error on computed displacements and pore pressures. ERROR= 10^{-2} after load has been applied.
T1(J,K)	Yield surface tolerance for the top (K=1) and bottom (K=2) of layer J. For EVP model, T1=0.1; for EP model, T1=0.01. Values apply after the load is applied.
T1DAY	Number of time units in one day (determined from LUNIT).
THETA	Coefficient for time integration. Theta= 2/3
VTSMIN	Minimum time step size.

Variable	Description
TMAX	Maximum output time computed from specified output times, VTO(K) and the number of time steps, NX1.

2.11.2 Subsurface Profile and Finite Element Mesh

The code will generate the finite element mesh after specifying the following information:

Variable	Description
ELEV(J)	Elevation of each soil zone boundary, J = 1 to NP
ELSURF0	Ground surface elevation
ELW	Groundwater elevation
MATL0(J)	Soil number for zone J.
NE(J)	Number of layers in each soil zone J.
NMAT	Number of soil types.
NMESH(J)	Type of layer generator for soil zone J: increasing layer thickness with depth = 1; decreasing layer thickness with depth = 2; increasing layer thickness to mid-layer and decreasing thickness below mid-layer = 3; uniform layer thickness = 4.
NP	Number of points to describe soil zone boundaries. The points are labeled from top to bottom.
NPE	Number of nodal points on and element. NPE=2
ST(J)	Stress history of soil zone J: NC = normally consolidated; OC = over consolidated; UC = under consolidated.

2.11.3 Soil Properties

A set of material properties is required for each soil zone, pore fluid, and existing fill soils.

Variable	Description
AGE(J):	Estimated geologic age of soil J.
BMW:	Bulk modulus of water
CEC2(J,K):	Secondary compression ratio for segment K in the normally consolidated range of soil J.
CC(J,K):	Virgin compression index, C_c, for segment K of soil J.
CR(J):	Recompression index, C_r, for each soil J.
CV(J,K):	Coefficient of consolidation, c_v, for segment K of soil J.
ER(J)	Initial void ratio, e_o, of soil J.
GAMF	Moist unit weight, γ_m of fill.

Variable	Description
GAMS(J)	Saturated unit weight, γ_{sat} of soil J.
GAMSAT	Saturated unit weight, γ_{sat} of fill.
GW:	Unit weight of pore fluid, γ_w.
MODE(J)	Type of model to use with soil material (J): time-dependent model = 0; conventional model = 1.
NMAT:	Number of different soil materials.
NEP(J):	Number of points to define e-log p curve for soil type J.
PP(J):	Initial reference preconsolidation pressure at soil zone boundary J.
SIG(J,K)	Effective stress number K that separates non-linear segments of the e-log p curve for soil type J.
T0(J):	Reference time for lab test on soil J. Usually 24 hours.

2.11.4 Boundary Conditions

Boundary condition variables provided by the user:

Variable	Description
NBDFP	Number of drainage boundaries.
NNP(J)	Node numbers where drainage occurs. Node 1 is at the bottom of the soil profile.
ELW	Groundwater elevation

Internal boundary variables programmed in CONSOL97:

Variable	Description
NBDFV	Number of nodes with specified displacement. Only the bottom of the soil profile has a specified displacement and NBDFV=1.
NNV(J)	Node numbers with specified displacements. NNV(J) at the bottom of the soil profile.
VBDFT(J)	Displacement at node J. No displacement condition is set at the bottom of the soil profile. VBDFT(J)= 0
VBDFT(K)	Hydrostatic pore water pressures at each specified drainage boundary. Values are computed from the specified groundwater elevation, ELW.

2.11.5 Loading Conditions

Load variables provided by the user:

Variable	Description
NTL	Number of loads.
LOADCASE(K)	Load option number for load application K: 1= specified change in stress; 2= groundwater change; 3= large areal load; 4= strip load; 5= circular load; 6= specified stresses.
1. Specified change in stress	
DELTA1(K)	Stress change in layer K.
2. Groundwater lowering	
ELNW	New groundwater elevation.
3. Large areal fill	
ELFL	Areal fill elevation.
HFILL	Areal fill thickness.
GAMFL	Moist unit weight of fill.
GAMSATL	Saturated unit weight of fill.
4. Strip fill	
ELFS	Strip fill elevation.
HFILLS	Strip fill thickness.
GAMFS	Moist unit weight of strip fill.
GAMSATS	Saturated unit weight of strip fill.
DIAMS	Width of strip fill.
ARS	Location on strip fill: 0 = center of strip; 1= edge of strip.
IBUOYS	Buoyancy correction number: = 0 full correction for fill submergence; =1 for change in stress multiplied by strip load influence factors
5. Circular fill	
ELFC	Circular fill elevation.
HFILLC	Circular fill thickness.
GAMFC	Moist unit weight of circular fill.
GAMSATC	Saturated unit weight of circular fill.
DIAMC	Diameter of circular fill.
ARC	Location on circular fill: 0 = center of fill; 1= edge of circle
IBOUYC	Buoyancy correction number: = 0 full correction for fill submergence; =1 for change in stress multiplied by strip load influence factors
6. Specified stresses	
OVER(K,N6)	Initial effective overburden pressure for layer K.
PO(J)	Initial effective stress in sublayer J
PRECONS(K)	Effective preconsolidation stress for sublayer K.
PFINAL(K)	Final effective stress for sublayer K

Variable	**Description**

7. No externally applied load (underconsolidated)
No data input required. This option may only be used at time, t=0.

VTIME(K)	Starting time at which the new load K is applied.
RAMP(K)	Duration of loading period for load K.

Internal loading variables programmed in CONSOL97:

ITIMAR(K)	Load time attendance roster. Value indicates the sequence of load applications at each output time K.

Table 2-1
Menu Options

Menubar Command	Command options	Description
FILE	New	Creates a new data input file.
	Open	Opens an existing data file.
	Save As	Saves the current file. A dialogue box will appear so you can select or enter a file name.
	Exit	Quit CONSOL97 application. A message box will appear and ask if you want to save the file. *Click* Yes or No.
	Close	Closes the existing file. A message box will appear and ask if you want to save the file. *Select* Yes or No
EDIT	Undo	Undo the last edit
	Cut	Cut the selected text from the data input form
	Copy	Copy the selected text.
	Paste	Paste the "cut" or "copy" text at the current cursor location.
INPUT FORMS	Units Selection	Dimensional units of stress, coefficient of consolidation, and the type of water.
	Method and Title	*Select* a method of analysis and enter text that describes the problem.
	Subsurface Profile	Defines the subsurface profile and groundwater table.
	Plot Files	Specify the layers for plotting data output
	Soil Properties	C_c, C_r, C_α, c_v, unit weights, void ratio, geologic age, and reference time.
	Loads	*Select* load options, specify loading time and duration, output times, and the number of time steps between each output time. Enter appropriate data for each specified load option.
	Layer Conditions	At the zone boundaries specify the elevations, preconsolidation stresses, and drainage conditions. Within the zone, specify the material number, consolidation state, number of layers, and the mesh geometry.
UNITS CONVERSION	Length	Converts length units.
	Stress	Converts stress units.
	Cv	Converts coefficient of consolidation units.
RUN ANALYSIS		Runs CONSOL97 using the current data input file

TABLE 2-2
INPUT DATA FILE FORMAT

The data input uses free format. Each value must be separated by either a comma or a blank space.

Input Variable	Description	Data File Component
ASTRESS	Stress units	control
ACONSOL	Coefficient of consolidation units	
AWATER	fresh or salt water	
METHOD	Method of Analysis	
IFILE	Type of time-dependent output	
TITL	Problem description	
LUNIT	Index designating output units.	
P1KPA, T1DAY	Units conversion	
NMAT, NP	Number of materials and soil zone boundaries.	profile
GW, BMW	Unit weight and bulk modulus of water.	properties
GAMSAT, GAMF	Saturated and moist fill unit weight.	
For J= 1, NMAT: MODE(J)	Type of soil model for each soil zone.	
For J=1, NMAT Mode=0 (EVP) *ER(J),CC(J,1),CR(J),GAM(J),CV(J,1), NEP(J)* *TAGE(J),T0(J),CEC2(J,1)* *If NEP(J)>1 Then* *For K=2,NEP(J)* *CC(J,K),CEC2(J,K),CV(J,K),SIG(J,K-1)* Mode=1 (EP) ER(J),CC(J,1)CR(J),GAM(J),CV(J,1), NEP(J) If NEP(J)>1 Then For K=2,NEP(J) CC(J,K),CV(J,K),SIG(J,K-1)	Soil properties and the number of points NEP(J) that define the e-log p curve for soil type J.	
Elev(1)	Elevation at top of compressible layer	profile
For J=1,NZ ELEV(J+1),NE(J),NMESH(J), MATL0(J),ST0(J),PP(J,1),PP(J,2), T1(J,1),T1(J,2)	Defines each soil zone: bottom elevation, number of layers, mesh geometry, material type, stress state, preconsolidation pressure at top and bottom, tolerance at top and bottom.	profile, properties, control
LAYOUT	Number of layers to include in the plot file.	control
For J = 1, LAYOUT: LAYDAT(J)	Layer number for plot file.	
ELSURF0, ELW	Surface and groundwater elevations.	profile
NTO, TMAX, NX1	Output time information, and number steps	control
For J = 1, NTO: VTO(J)	Output times	
For J= 1, NTO: ITIMAR(J)	Load time attendance roster.	loading
NBDFP	Number of drainage boundaries	boundary
For J= 1, NBDFP: NNP(J)	Node numbers that are drainage boundaries. Node 1 is at the bottom of the profile.	

Input Variable	Description	Data File Component
NTL	Number of loads.	loading
For J = 1, NTL: LOADCASE(J)	Load option number	
VTIME(1), RAMP(1)	First load time	
For J = 2, NTL: VTIME(J), RAMP(J)	Load time information	
For J = 1, NTL Read required data for loadcase (J)	Loading parameters See Table 2-3.	

TABLE 2-3
LOADCASE INPUT DATA FILE FORMAT

The data input uses free format. Each value must be separated by either a comma or a blank space.

Loadcase	Input Variable	Description
1 - Specified change in stress	For each layer J = 1, NEM DELTA(J)	Stress increment in each layer
2 - Groundwater lowering	ELNW	New groundwater elevation.
3 - Large areal fill	ELFL, HFILL, GAMFL, GAMSATL	Areal fill dimensions and properties.
4 - Strip fill	ELFS, HFILLS, GAMFS, GAMSATS, DIAMS, ARS, IBUOYS	Strip fill dimensions and properties.
5 - Circular fill	ELFC, HFILLC, GAMFC, GAMSATC, DIAMC,ARC, IBUOYC	Circular fill dimensions and properties.
6 - Specified stresses	For each layer J = 1, NEM PO(J), PP(J), PFINAL(J)	Stresses in each layer
7 - No external applied load (under consolidated)	No data input required. This option may only be used at time, t = 0.	

Table 2-4
EXAMPLE DATA INPUT FILE

Input data	Data description
kPa	Dimensional units for stress.
m^2/day	Units for coefficient of consolidation
fresh	Type of water
0, ...	Method of analysis
0, ...	Type of output (regular or detailed)
CS45A; LOAD2; EP; Double drain; 3.0 m	Title
9, ...	Dimensional Units Option
1.0,1.0, ...	Units conversion factors P1KPA and T1DAY
1,2, ...	Number of soil zones and number of points to describe profile.
10.,2.0E+06, ...	Unit wgt. of water, bulk modulus of water
22.0,20.0, ...	Overburden saturated and moist unit weights
0, ...	Type of soil model for each soil zone
2.0,1.05,0.0498,20.0,2.22E-02,1, 10000.,1.0,0.008, ...	Soil properties
99.0, ...	Elevation of top of compressible layer
96.00,15,4,1,'OC',25.0,45.0,0.10,0.10, ...	Elevation bottom of layer, number of elements, mesh generator, material number, stress state, Pp' top, Pp' bottom, tolerance at top of layer, tolerance at bottom of layer.
3	Number of layers for plot file
2,8,14, ...	Layer numbers
100.0,100.0, ...	Surface elevation, groundwater elevation
11,1000., ...	Number of output times, maximum time
10.,30.,80.,130.,200.,300.,500., 800.,900.,990.,1000., ...	Output times
0,0,0,0,0,0,0, 0,0,0,0, ...	Load time attendance roster
2, ...	Number of drainage boundaries
1,16, ...	Node numbers at drainage boundaries
1, ...	Number of load applications
2, ...	Loadcase numbers
0.,0.1, ...	Time at start of load, duration to apply full load
99.0	Loadcase input parameters
(end of data file)	

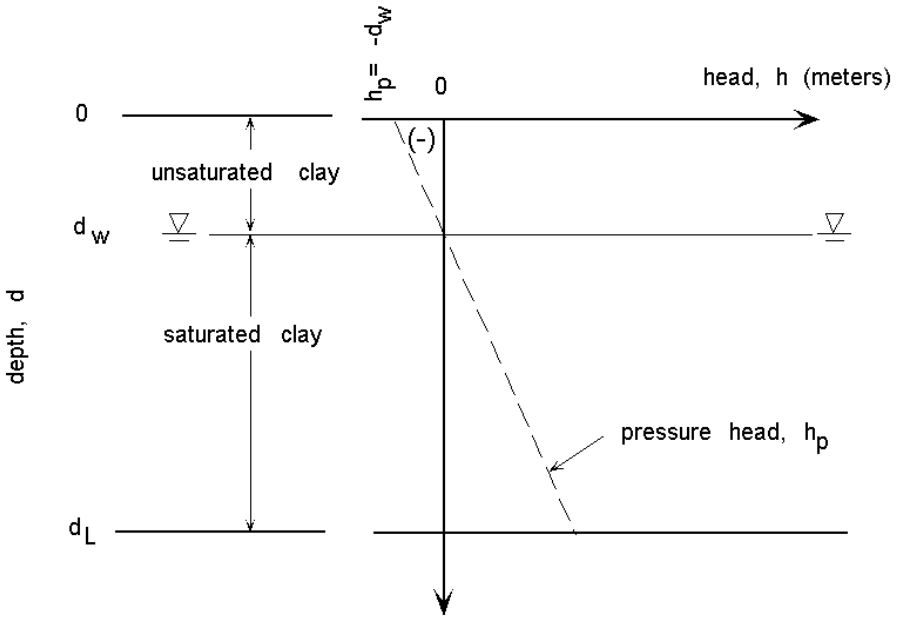

Figure 2-1: Long-term steady state head profile used by CONSOL97

manual/chapter2/fig2_1.cvs

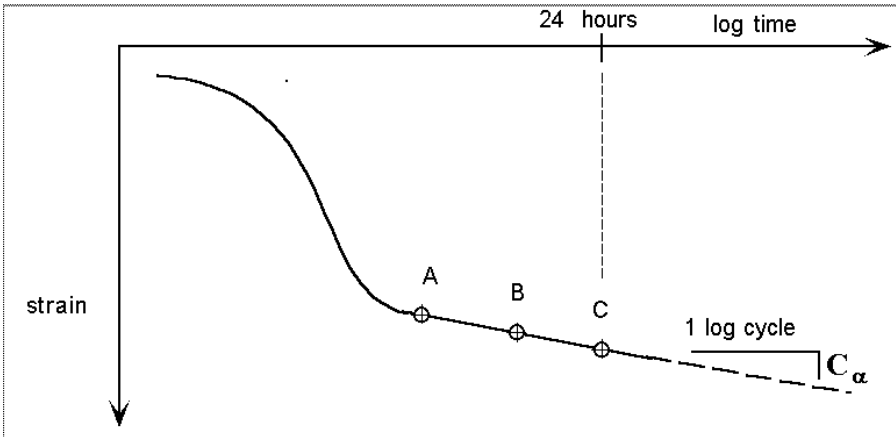

(a) Strain versus time curve for load increment from σ'_o to σ'_f

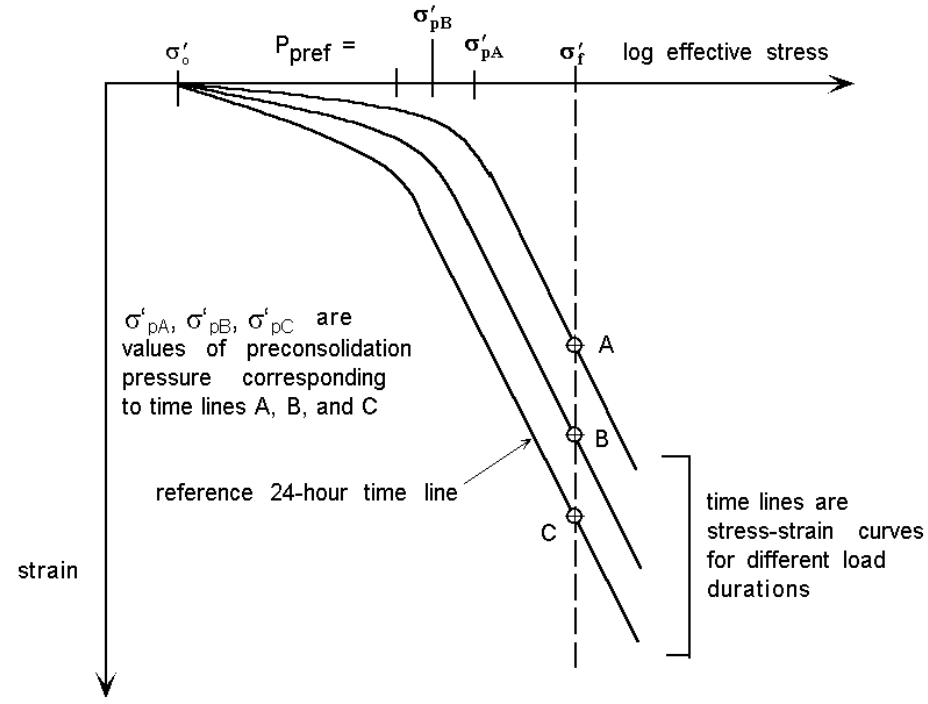

(b) Stress-strain curves

Figure 2-2: Laboratory strain-time and stress-strain curves for time-dependent model

manual/chapter2/fig2_2.cvs

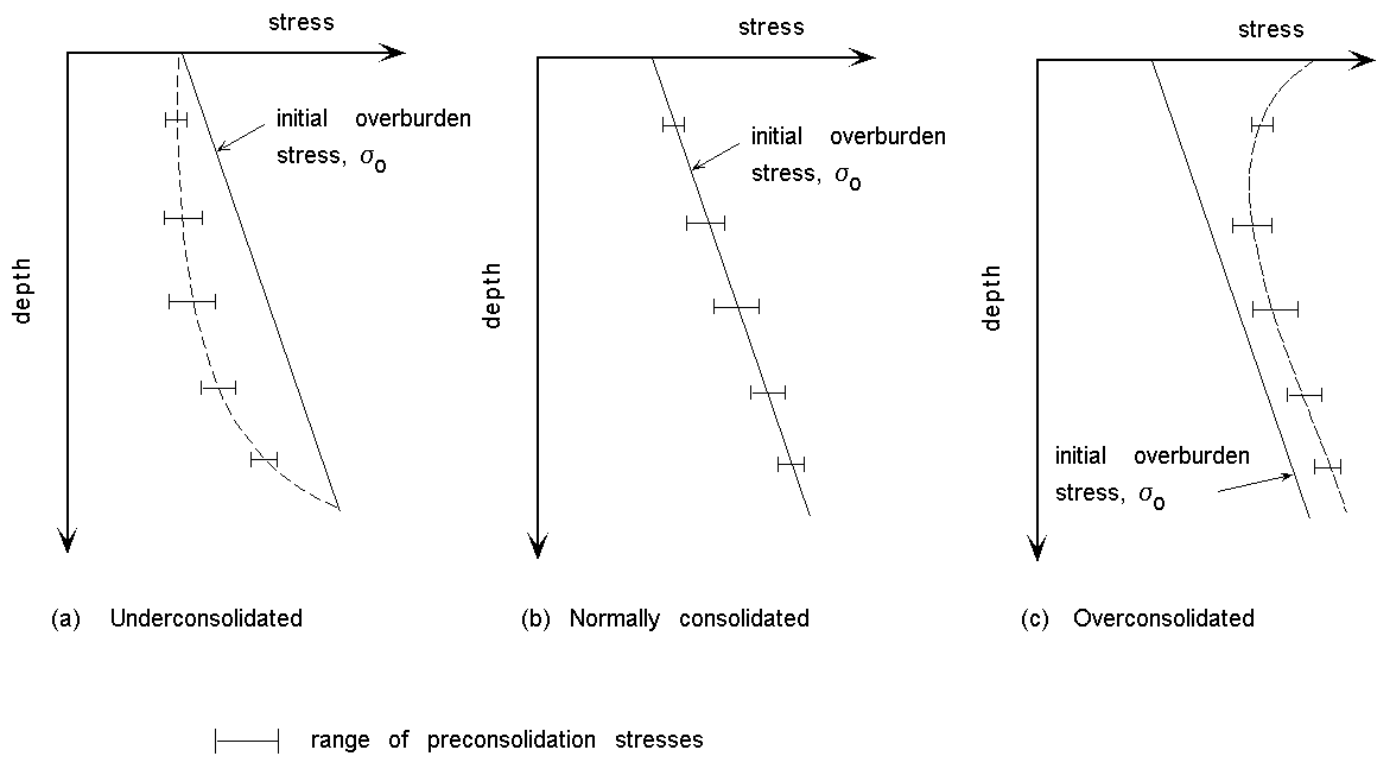

Figure 2-3: Preconsolidation stress profiles

manual/chapter2/fig2_3.cvs

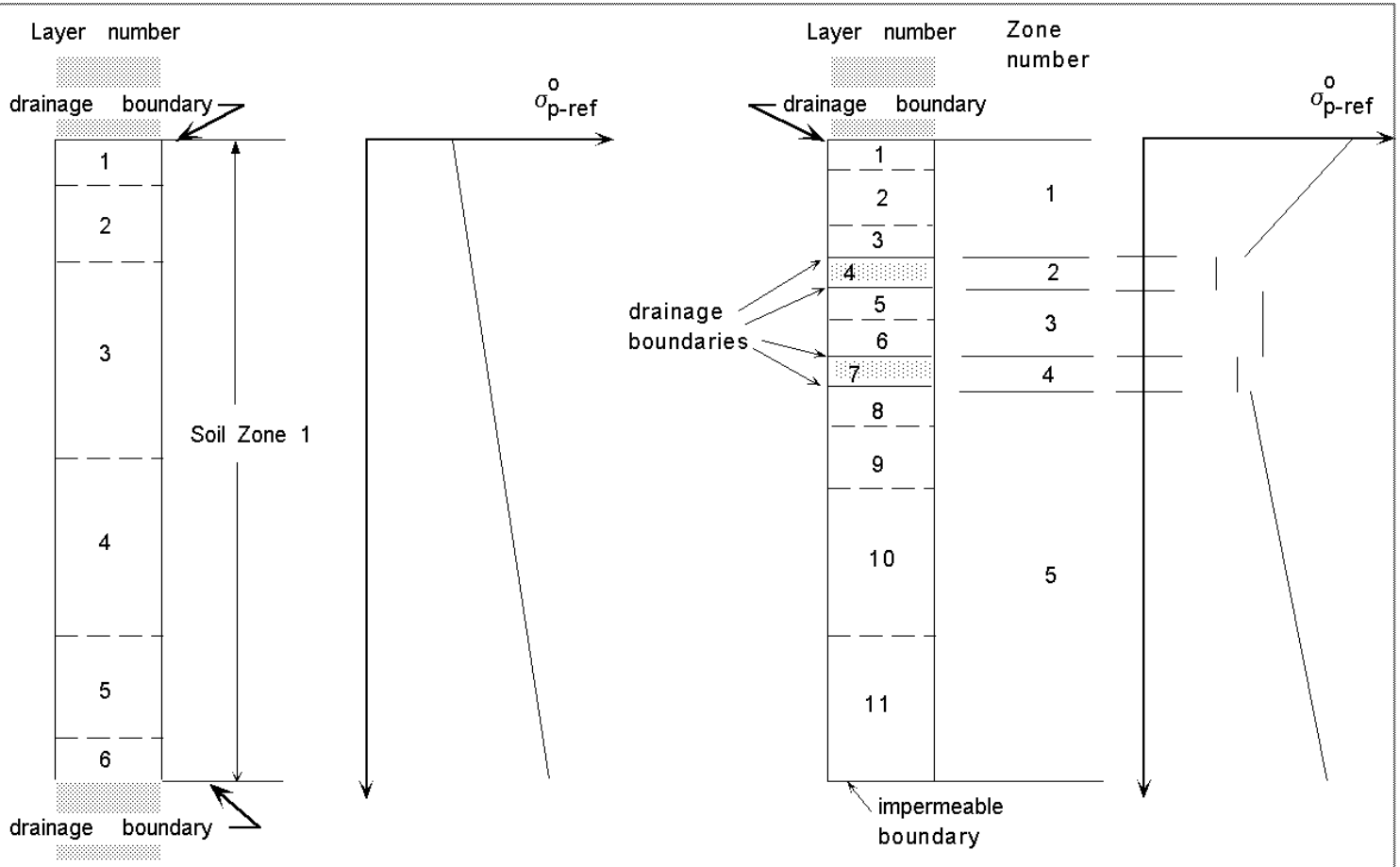

Figure 2-4: Divison of a subsurface profile into zones and layers

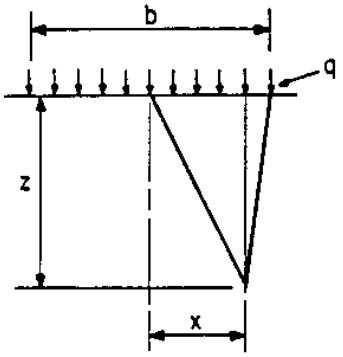

b = width of strip

x = distance from of strip

The equations for the Boussinewq Stress Influence Factor, I:

$$\alpha = \tan^{-1}\left[(x - b/2)/z\right] \qquad \ldots(1)$$

$$\beta = \tan^{-1}\left[(x + b2)/z\right] - \alpha \qquad \ldots(2)$$

$$I = 1/\pi\left[\beta + \sin(\beta)\cos(\beta + 2\alpha)\right] \qquad \ldots(3)$$

The change in vertical stress is then given by:

$$\Delta\sigma = I \cdot q \qquad \ldots(4)$$

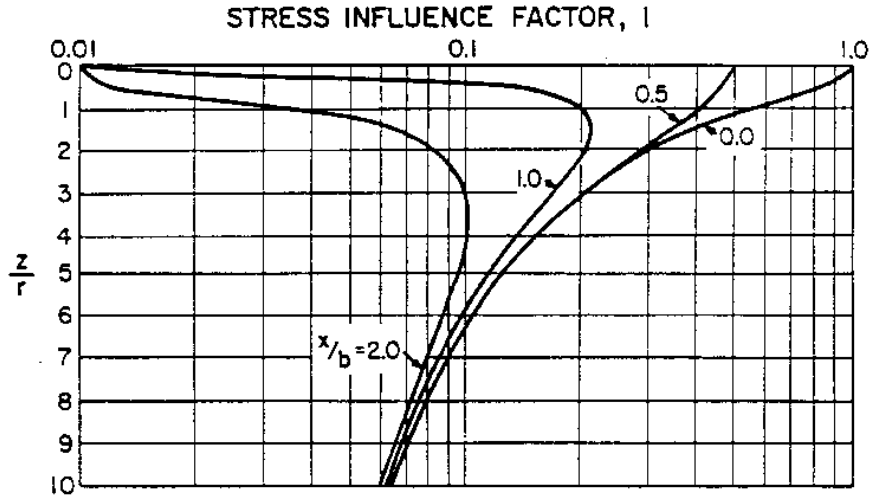

Figure 2-5: Boussinesq stress influence factors for an infinitely long strip load (from Duncan et al. 1988)

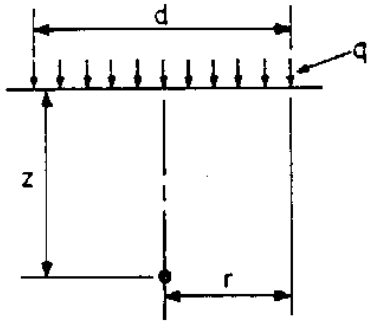

z = depth

r = radius = d/2

The equation for the Boussinesq Stress Influence Factor, I:

$$I = 1.0 - \frac{1}{(r/z)^2 + 1}^{1.5} \qquad \ldots(1)$$

The change in vertical stress is then given by:

$$\Delta\sigma = I.q \qquad \ldots(2)$$

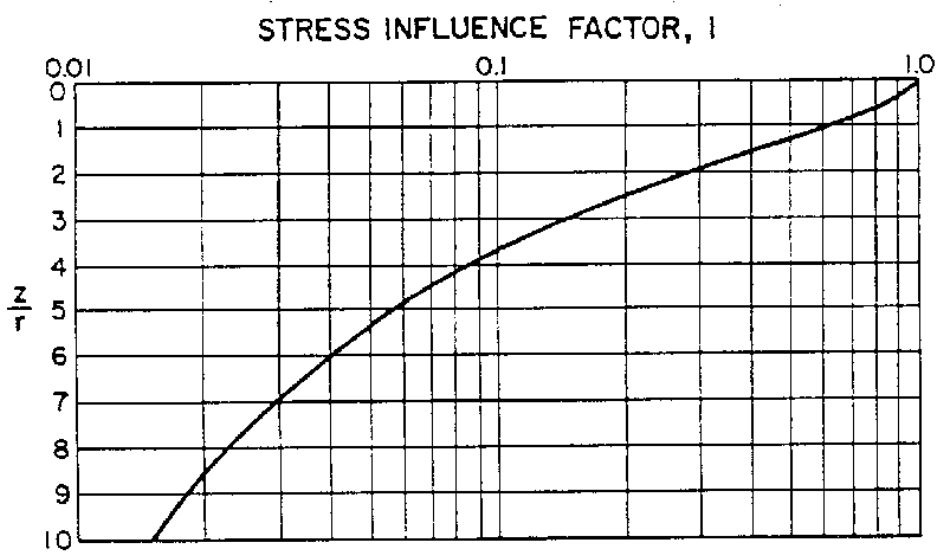

Figure 2-6: Boussinesq stress influence factors for stresses beneath the center of a circular loaded area (from Duncan et al. 1988)

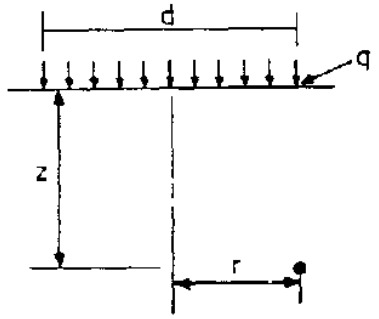

z = depth

r = radius = d/2

The equation for the Boussinesq Stress Influence Factor, I:

for $z/r \leq 0.5$:	$\alpha = -0.3010 - 0.1412*z/r$	...(1)
for $0.5 \leq z/r < 1.0$:	$\alpha = -0.2617 - 0.2197*z/r$	...(2)
for $1.0 \leq z/r < 1.5$:	$\alpha = -0.2403 - 0.2411*z/r$	...(3)
for $1.5 \leq z/r < 4.0$:	$\alpha = -0.2883 - 0.2092*z/r$	...(4)
for $4.0 \leq z/r < 7.0$:	$\alpha = -0.4888 - 0.1590*z/r$	...(5)
for $7.0 \leq z/r$:	$\alpha = -1.0844 - 0.0739*z/r$	...(6)

The stress influence factor is given by:

$$I = 10^{\alpha} \quad \text{...(7)}$$

The change in vertical stress is then given by:

$$\Delta\sigma = I \cdot q \quad \text{...(8)}$$

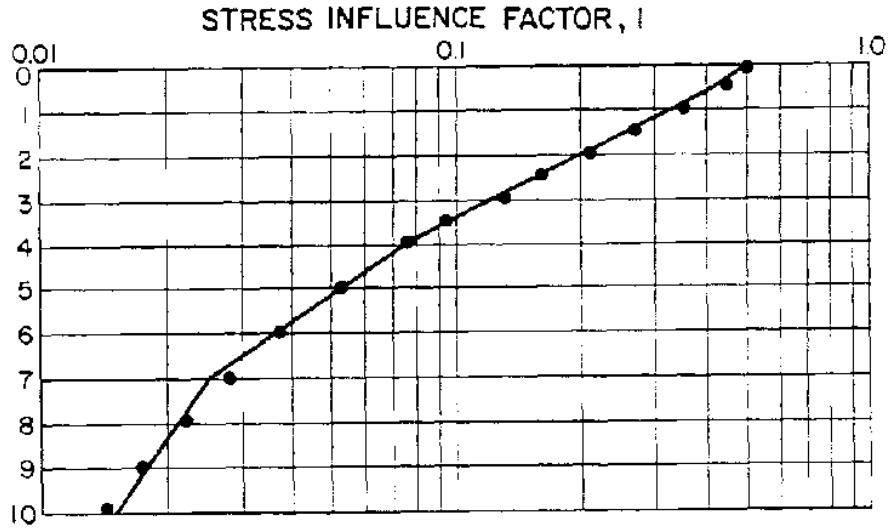

Figure 2-7: Boussinesq stress influence factors for stresses beneath the edge of a circular loaded area (from Duncan et al 1988)

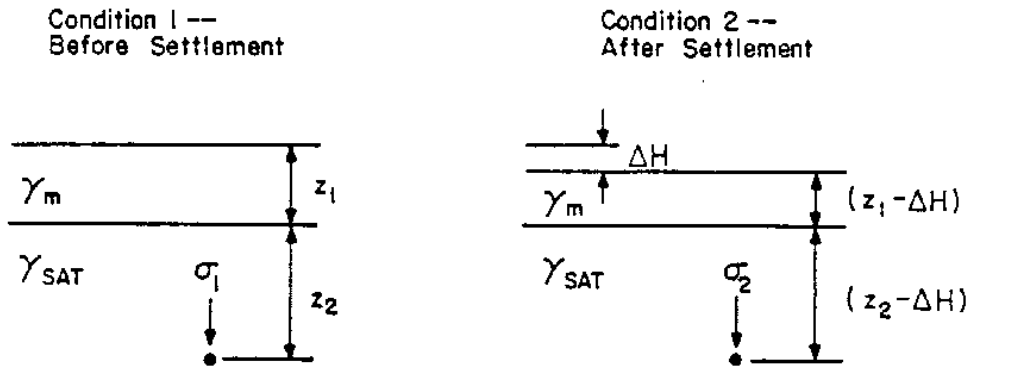

$\sigma_1' = z_1\ \gamma_m + z_2\ (\gamma_{sat} - \gamma_w)$ $\sigma_2' = (z_1 - \Delta H)\ \gamma_m + (z_2 + \Delta H)(\gamma_{sat} - \gamma_w)$

The change in equilibrium effective stress (after all excess pore pressure has dissipated) due to submergence of a layer of fill thickness, ΔH, can be expressed as:

$$\Delta\sigma' = \sigma_2' - \sigma_1' \qquad \ldots(1)$$

$$\Delta\sigma' = (z_1 - \Delta H)\ \gamma_m + (z_2 + \Delta H)(\gamma_{sat} - \gamma_w)$$

$$- z_1\ \gamma_m + z_2(\gamma_{sat} - \gamma_w) \qquad \ldots(2)$$

$$\Delta\sigma' = -\Delta H\gamma_m + \Delta H(\gamma_{sat} - \gamma_w) \qquad \ldots(3)$$

$$\Delta\sigma' = -\Delta H(\gamma_m + \gamma_w - \gamma_{sat}) \qquad \ldots(4)$$

The change in excess spore pressure (before any drainage or dissipation) is equal to the long term change in effective stress:

$$\Delta_u = \Delta\sigma' \qquad \ldots(5)$$

$$\Delta_u = -\Delta H(\gamma_m + \gamma_w - \gamma_{sat}) \qquad \ldots(6)$$

Figure 2-8: Derivation of correction for buoyancy effect (from Duncan et al 1988)

consol97/manual/chapter2/fig2_8.cvs
fig411.tif

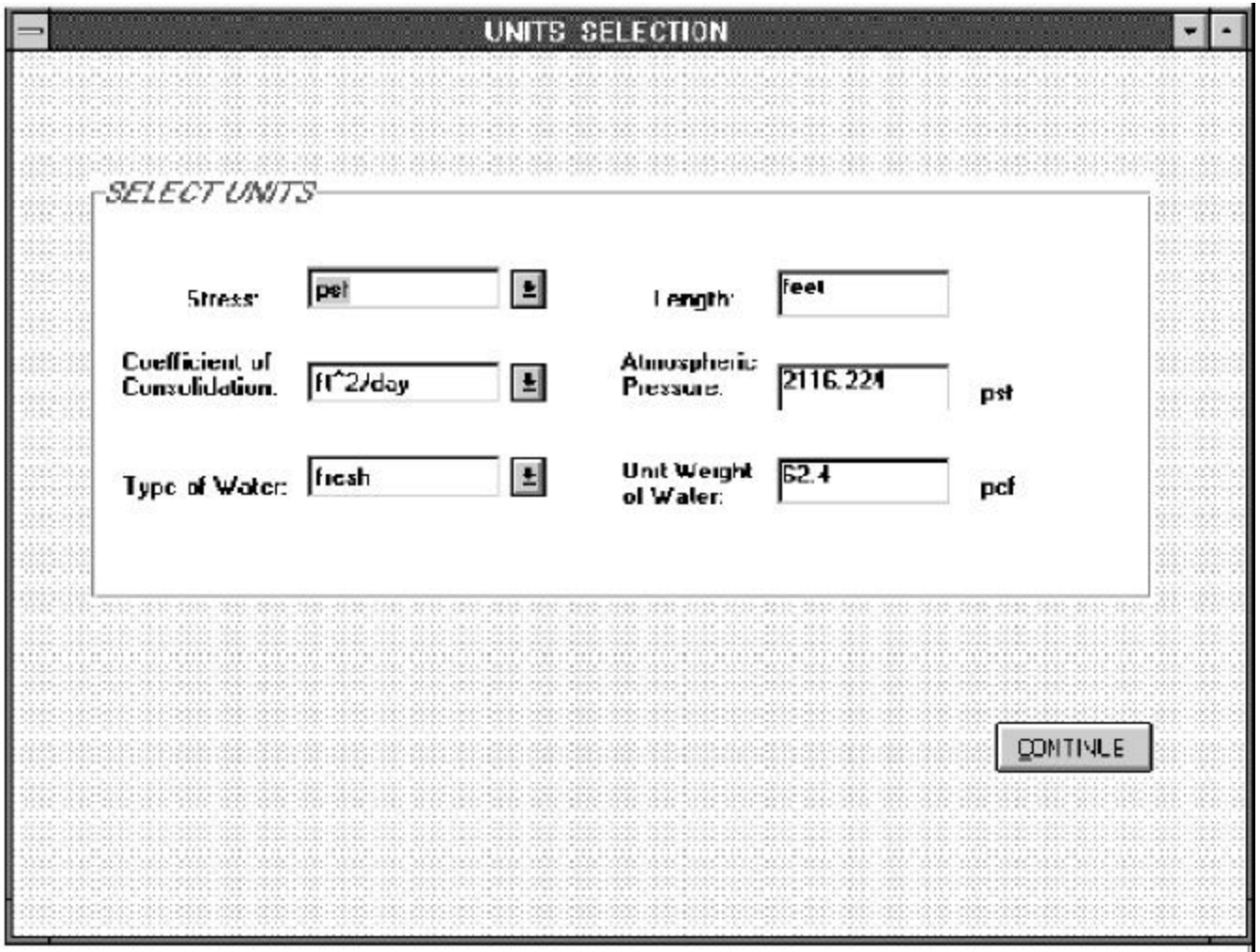

Figure 2-9: Units selection screen

manual/chapter2/fig2_9.cvs

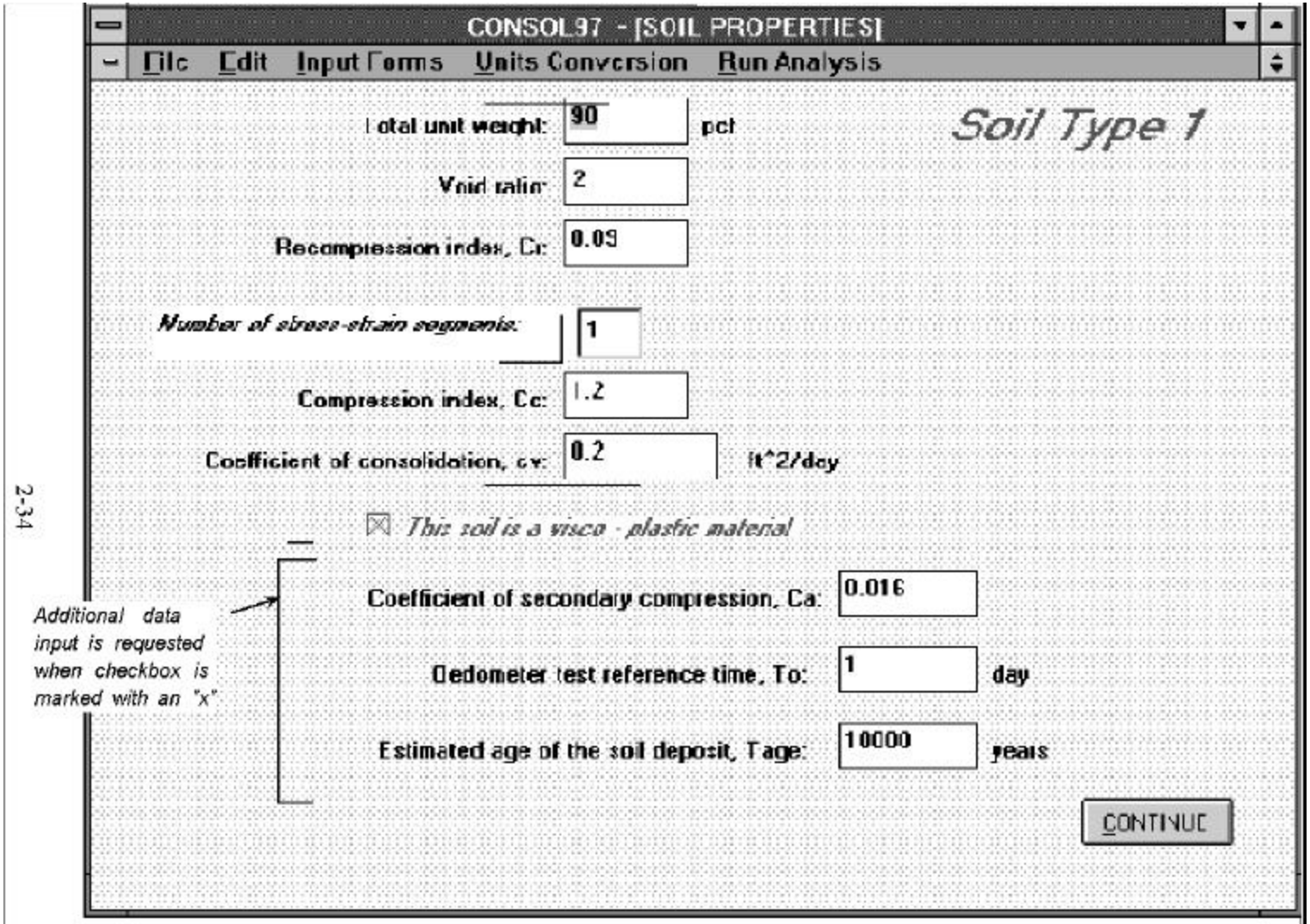

Figure 2.10: Soil properties screen

manual/chapter2/fig2_10.cvs

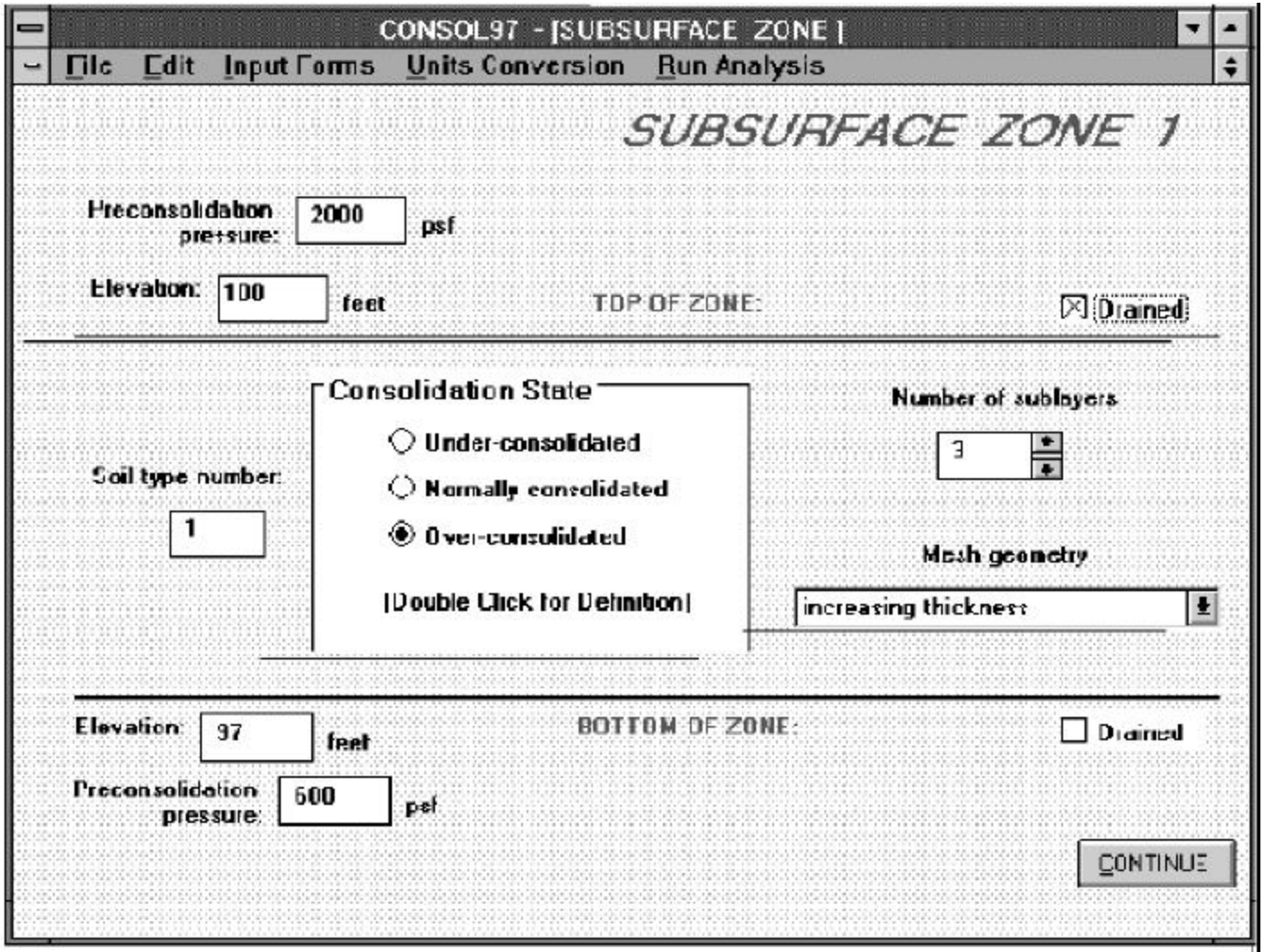

Figure 2-11: Soil zone screen

manual/chapter2/fig2_11.cvs

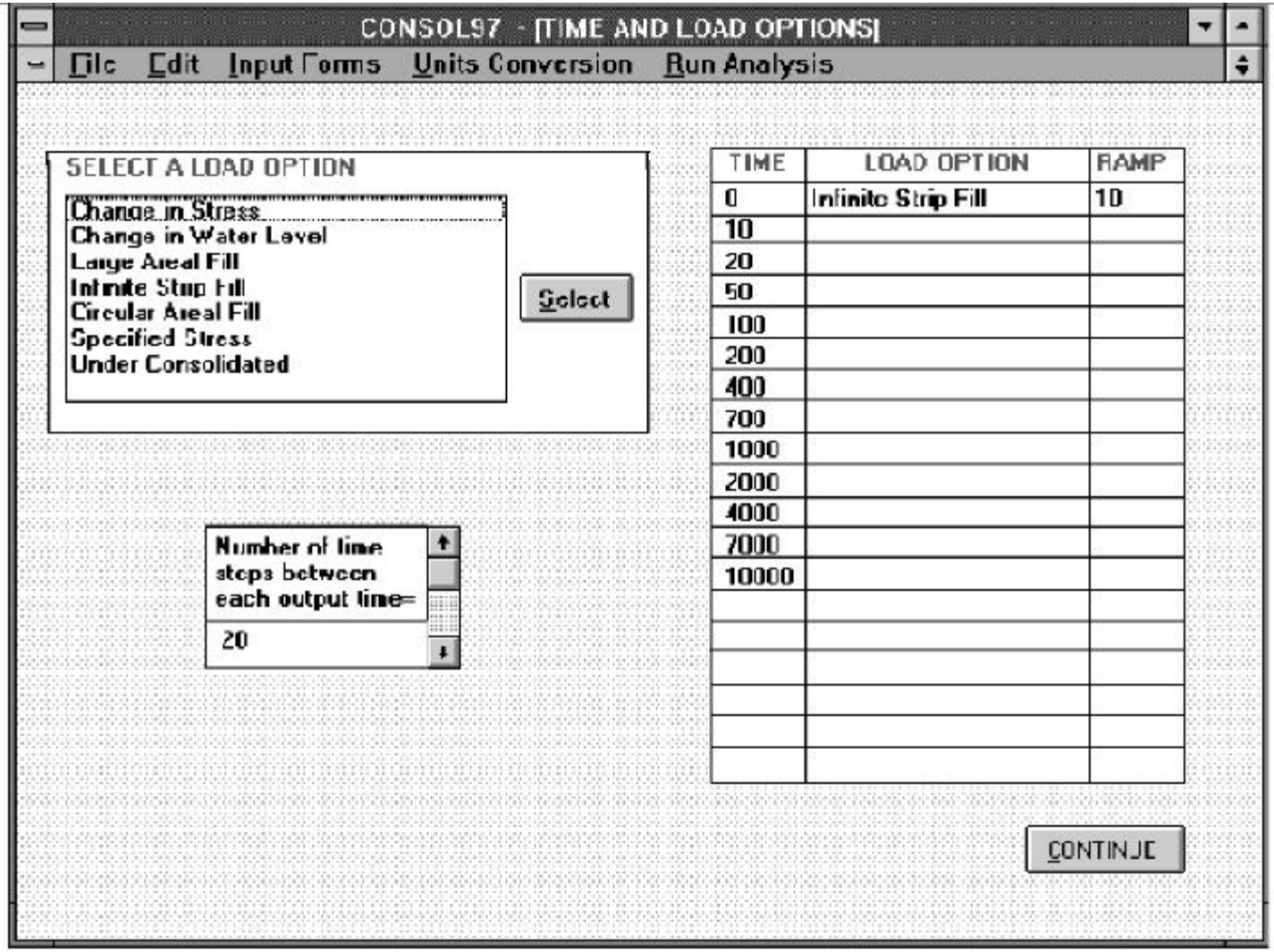

Figure 2-12: Time and load options screen

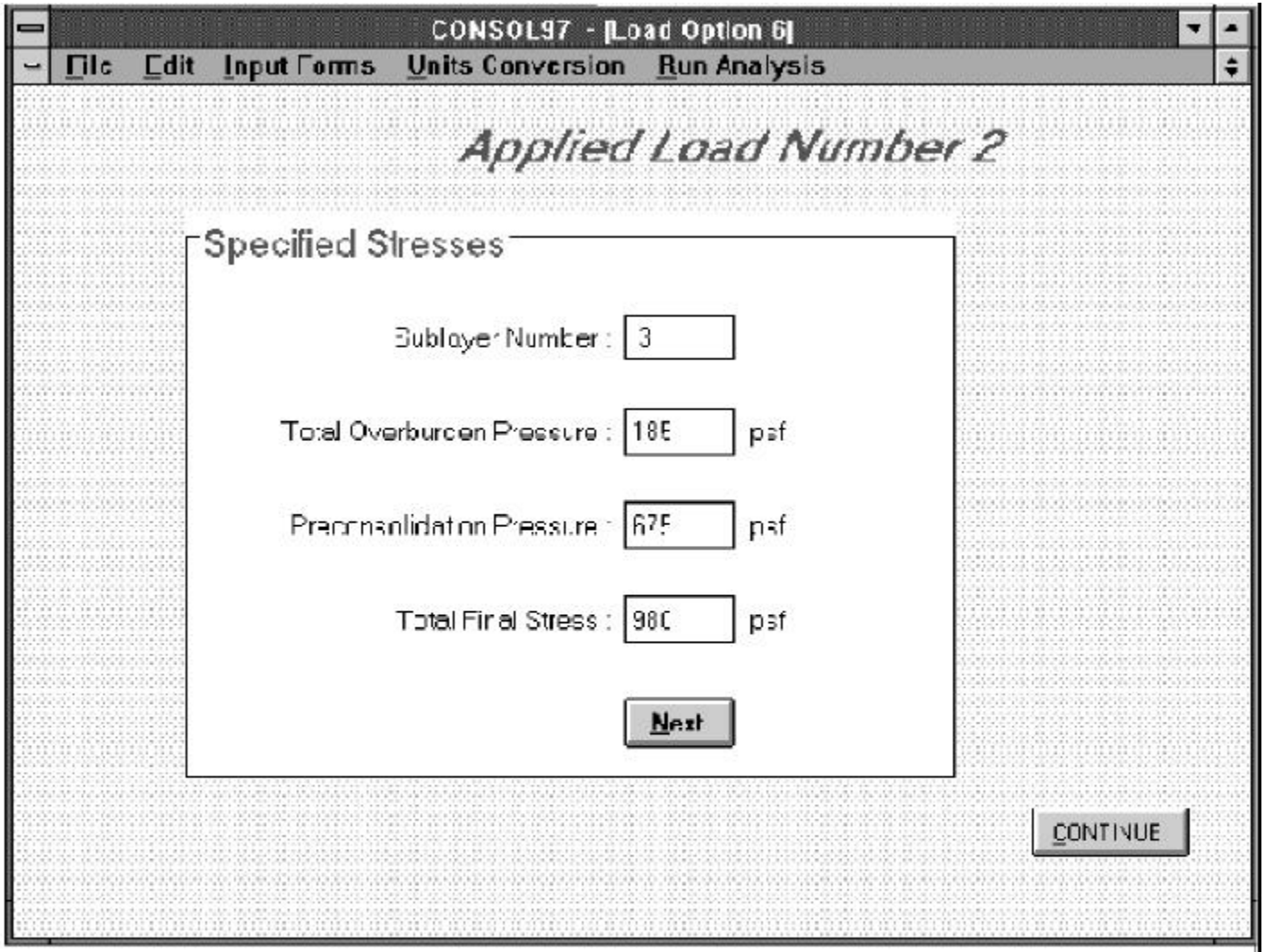

Figure 2-13: Specified stress change screen

manual/chapter3/fig3_13.cvs

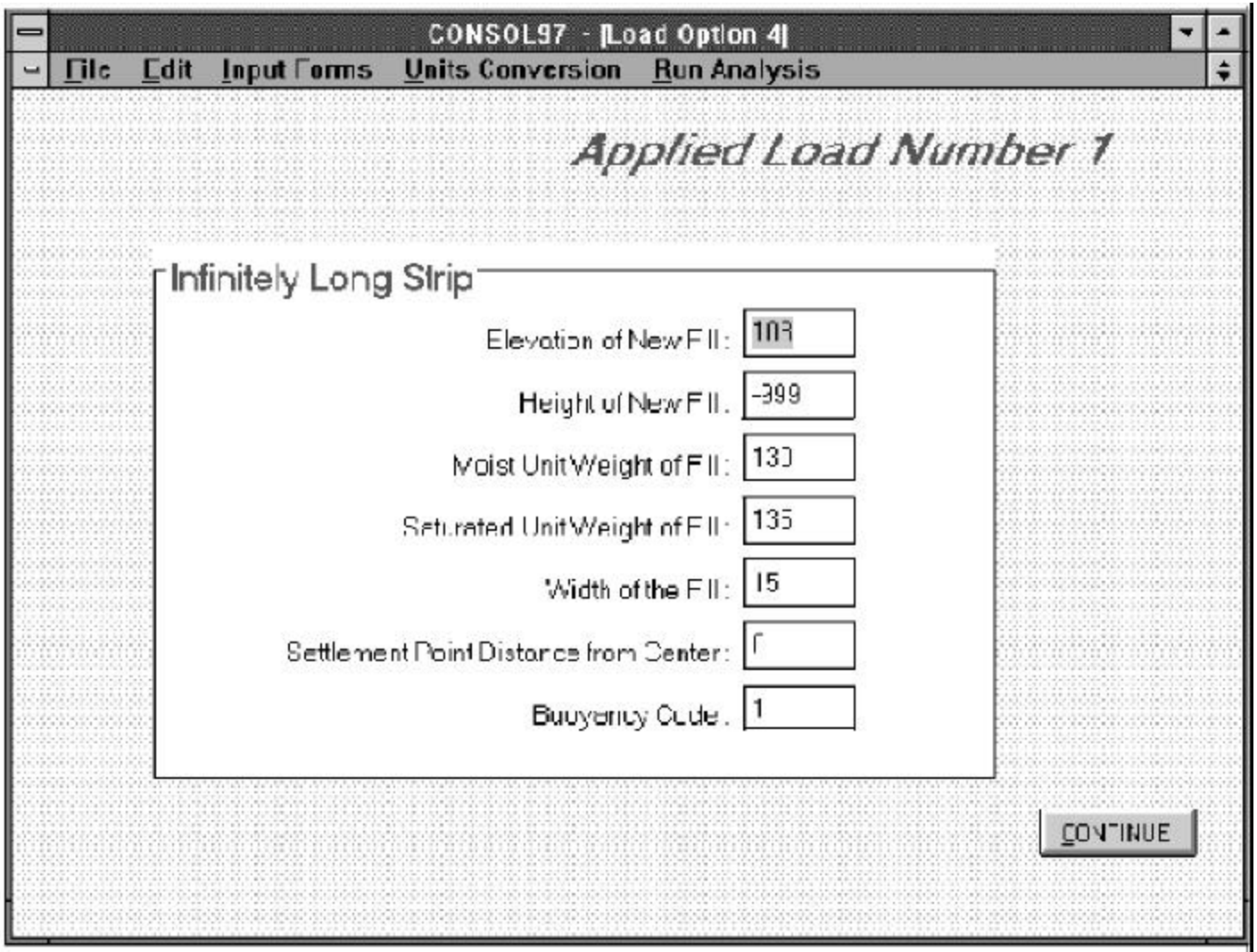

Figure 2-14: Infinitely long strip load screen

manual/chapter2/fig2_14.cvs

```
      CONSOL97 IS COMPUTING .............
            Computation for output time       5.00 is: 20% complete
            Computation for output time       5.00 is: 40% complete
            Computation for output time       5.00 is: 60% complete
            Computation for output time       5.00 is: 80% complete
            Computation for output time       5.00 is: 100% complete


CURRENT TIME IS:  5.00              ITERATION(S):  4

      TOTAL SETTLEMENT:   0.0221

      EXCESS PORE PRESSURES:
            Min. at Sublayer        Max. at Sublayer
            .0000D+00    1         .7523D+03    4


CONSOL97 IS COMPUTING .............
      Computation for output time       10.00 is: 20% complete
```

Figure 2-15: Run time messages

DATA INPUT

Read units for stress, ASTRESS, and coefficient of consolidation, ACONSOL and type of water, AWATER. Read method of analysis: METHOD= 0 for time-dependent; =1 or greater for conventional analysis.

Is this a time-dependent analysis?	
YES	NO
Read IFILE: 0 = regular output; 1= detailed output	

Read project description, TITL. Read code for output labels, LUNIT.

Read no. of units in 1 kPa and 1 day, P1KPA, T1DAY

Read number of material types, NMAT, and number of points to describe profile, NP

Read unit weight, GW, and bulk modulus, BW, of water.

Read the saturated and moist unit weights of overburden, GAMSAT, GAMF

Do for each soil type J = 1, NMAT

Read the model type, MODE(J): 0 = EVP; 1 or greater= EP (conventional)

Read soil properties for each material type J = 1 to NMAT

K=1 (first linear segment of virgin compression curve)

Is this a visco - plastic material ?	
YES	NO
Read ER(J), CC(J,1), CR(J), CEC2(J,1), GAMS(J), CV(J,1), NEP(J). Read TAGE(J), T0(J)	Read ER(J), CC(J,1), CR(J), GAMS(J), CV(J,1), NEP(J).

Is there more than one linear stress-strain segment?

YES

NO

Do for each segment K = 2 to NEP(J)

Is this a visco - plastic material ?	
YES	NO
Read ER(J), CC(J,K), CR(J), CEC2(J,K), GAMS(J), CV(J,K).	Read ER(J), CC(J,K), CR(J), GAMS(J), CV(J,K).

Figure 2-16(a): Data input structure chart

DATA INPUT (Continued)

Read top elevation of compressible soil zone, ELEV(1)

Do for each soil zone J = 1 to NZ

Read bottom elev. ELEV(J+1), number layers NE(J), mesh geometry NMESH(J), material type MATL0(J), stress state ST0(J), top preconsolidation stress PP(J,1), bottom preconsolidation stress PP(J,2), top yield tolerance T1(J,1), bottom yield tolerance T1(J,2).

Read number of sublayers, LAYOUT, to include in plot file output.

Are layers specified for the plot file ?

YES

Do for each specified layer, J = 1, LAYOUT

Read the layer number, LAYDAT(J)

NO

Read ground surface elevation, ELSURF0, and groundwater elevation, ELW

Read the number of specified output times, NTO, and the maximum output time, TMAX, and number of incrmenets between successive outputs, NX1.

Do for each output time, J = 1, NTO

Read the output time, VTO(J)

Do for each output time, J = 1, NTO

Read values of load time attendance roster, ITIMAR(J)

Read the number of drainage boundaries, NBDFP

Do for each drainage boundary J = 1 to NBDFP

Read the node number of each drainage boundary NNP(J).

Read the number of times the load is specified, NTL

Figure 2-16(b): Data input structure chart

DATA INPUT (Continued)

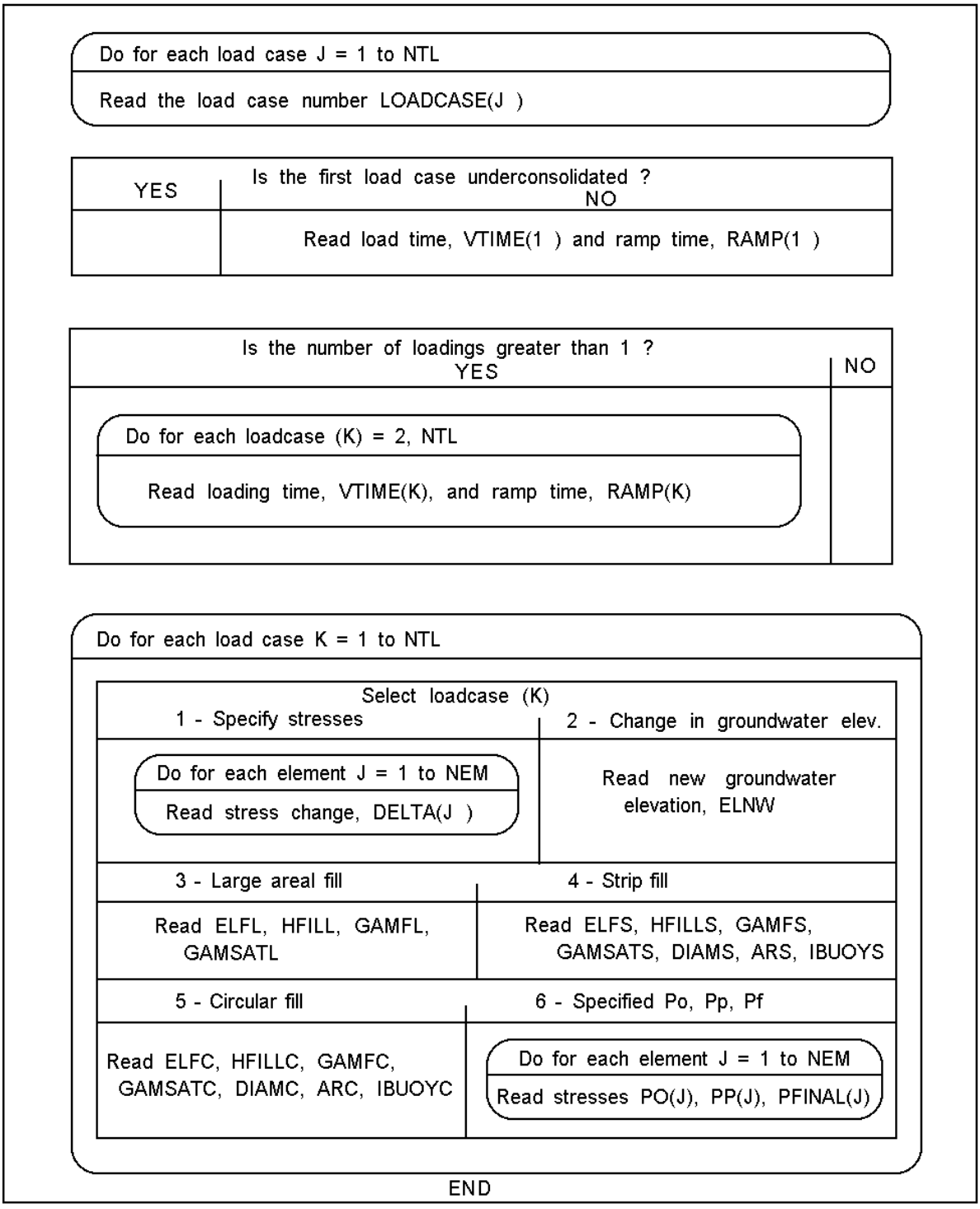

Figure 2-16(c): Data input structure chart

3. EXAMPLE PROBLEMS

Two example problems are presented to demonstrate the use of CONSOL97. The data files, *ex_1.dat* and *ex_2.dat* and the output files *ex_1.out, ex_1.plt*, *ex_2.out*, and *ex_2*.plt are included on the distribution disk.

3.1 EXAMPLE 1

This example illustrates an elasto-visco-plastic consolidation analysis of a 3.2 meter layer of overconsolidated clay due to placement of a large areal load. A 2.15 meter thick layer of sand overlies the compressible clay layer. The subsurface profile and soil properties are shown on Figure 3-1.

The compressible soil layer is doubly drained and it has been divided into two zones labeled clay A and clay B. Each zone was subdivided into uniformly thick layers. The upper sand layer was modeled as overburden soil (incompressible and free-draining). Two soil types with nonlinear virgin compression curves were used to represent zones A and B in the compressible clay layer. Preconsolidation stresses, σ_{p-ref}, from standard 24 hour oedometer tests were used to determine the preconsolidation stress profile.

A fill height of 2.4 meters was placed in 4.5 days. The stress at the ground surface and throughout the clay layer was 39.0 kPa. Reductions in applied stress due to submergence of the overburden and/or fill soils are automatically included in the computations.

The standard output file is shown in Figure 3-2 and the plotting output file is shown in Figure 3-3. The data input file is presented in Figure 3-4.

3.2 EXAMPLE 2

Example 2 illustrates the strip loading option for simulating elasto-visco-plastic consolidation of a strip fill placed on 30 feet of compressible clay. Figure 3-5 illustrates the subsurface profile and soil properties. The subsoil has been divided into four zones based on the preconsolidation stress profile and the soil properties. Zone one consists of a 3 foot thick clay crust above the groundwater table. Zones 2 and 4 are overconsolidated saturated clay. Zone 3 is a sand layer. Drainage boundaries are located at the top and bottom of the profile and at the top and bottom of the internal sand layer. Each soil zone was divided into layers that are thinner at drainage boundaries than at the center of the clay layer.

The clay soils were represented by two soil types, clay A and B. The crust at the top of the profile is desiccated and has a coefficient of consolidation that is an order of magnitude larger than the saturated clay B soils. The virgin compression curve for clay B is nonlinear.

The groundwater table is located at a depth of 3 feet and the groundwater conditions are hydrostatic. Therefore, the pore pressures in the unsaturated soils above the water table are negative.

The eight foot high embankment fill was modeled as a strip load with an average width of 15 feet. The embankment was constructed in 10 days. The applied stress at the ground surface is 1040 psf decreasing to 320 psf at a depth of 30 feet. Reductions in applied stress due to submergence of the overburden and/or fill soils are automatically included in the computations and are based on the strip load influence factors (Bouyancy correction code = 1).

The standard output file is shown in Figure 3-6 and the plotting output file is shown in Figure 3-7. The data input file is presented in Figure 3-8.

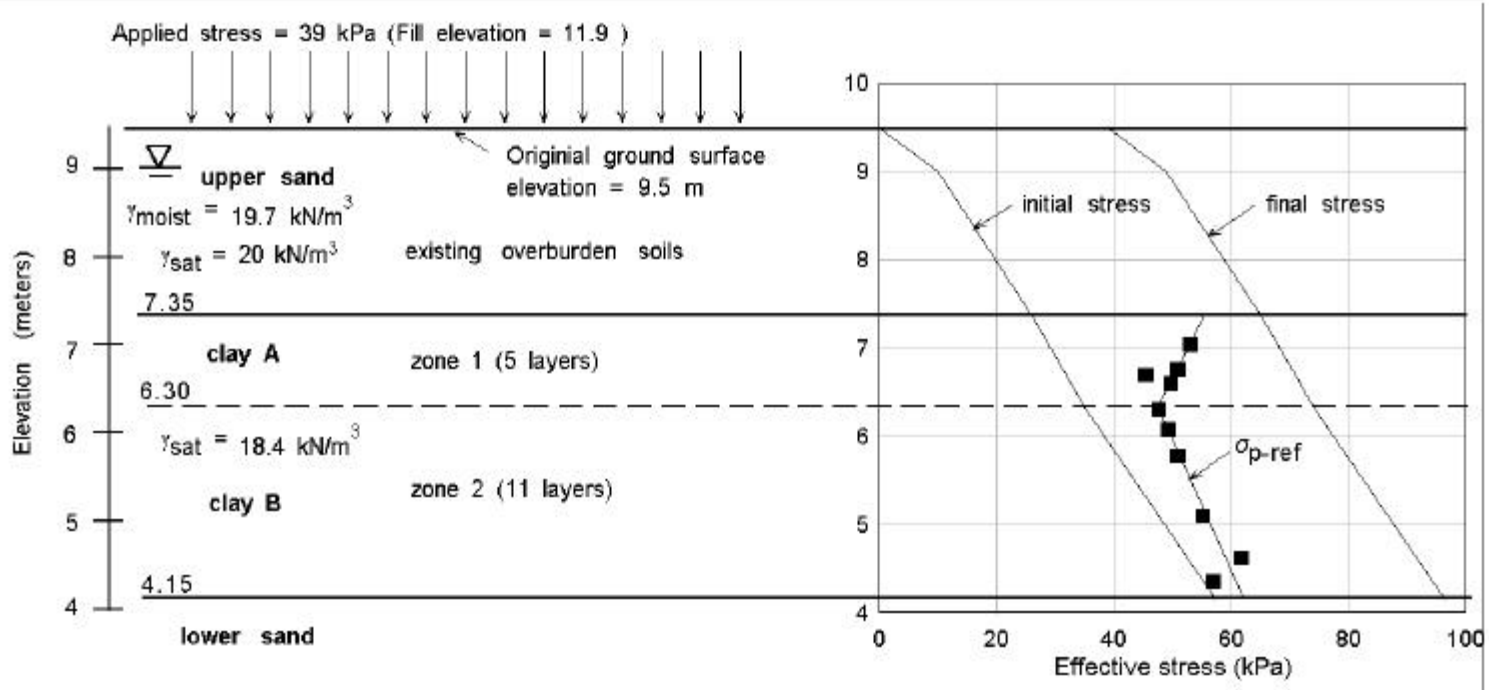

SOIL PROPERTIES

	σ_{min} (kPa)	Cεc	Cα	c_v (m^2/day)	Age (years)
Clay A	<70	0.60	0.0170	0.004	10,000
	70	0.56	0.0150	0.004	
Clay B	<59	0.64	0.0180	0.006	10,000
	59	0.54	0.0150	0.006	

■ 24 hour preconsolidation stress, $\sigma_{p\text{-}ref}$, from oedometer tests

Figure 3-1: Example 1 subsurface profile and soil properties

consol97/manual/chapter3\fig3-1.cvs

```
*************************************************
*                                               *
*       CONSOL97:FINITE ELEMENT PROGRAM         *
*      FOR ANALYSIS OF 1-D CONSOLIDATION        *
*         OF AN ELASTO-VISCO-PLASTIC            *
*       AND/OR AN ELASTO-PLASTIC MEDIUM         *
*                                               *
*   Theory developed by J.P. Rajot, April 1992  *
*  Program developed by V.J. Perrone, April 1998*
*                                               *
*                 Version: 1.0                  *
*                                               *
*************************************************


DATE:  5/20/1998     TIME:  5:56:56 pm

INPUT FILE:  C:\CONSOL97\MANUAL\EX_1.DAT
OUTPUT FILE: C:\CONSOL97\MANUAL\EX_1.OUT
PLOT FILE:   C:\CONSOL97\MANUAL\EX_1.PLT


TITLE: "Example Problem 1: large areal fill"


**** C O N T R O L   D A T A ****

NUMBER OF SOIL SUBLAYERS ..........................   16
NUMBER OF DIFFERENT SOILS .........................    2
ELEVATION OF THE GROUND SURFACE ...................    9.50(meters)
TOP ELEVATION OF THE COMPRESSIBLE SOIL MASS.........   7.35(meters)
GROUNDWATER ELEVATION .............................    9.00(meters)
UNIT WEIGHT OF WATER ..............................    9.81(kN/m^3)
MST. UT. WGT. OF SOIL ABOVE COMPRESSIBLE MASS ......   19.70(kN/m^3)
SAT. UT. WGT. OF SOIL ABOVE COMPRESSIBLE MASS ......   20.00(kN/m^3)


**** D R A I N A G E   B O U N D A R I E S ****

SUBLAYER BOUNDARY NUMBERS:     1   17


**** S O I L   P R O P E R T I E S ****
                                  SECOND.  UNIT     CONSOL.  GEOL.   REF.
            VOID   COMP.   RECOMP. COMP.    WEIGHT   COEFF.   AGE     TIME
SOIL  MODEL RATIO  INDEX   INDEX    COEFF.  (kN/m^3) (m^2/day)(years)  (days)

  1    EVP    2.00   1.800  .0600   .01700    18.40   .400E-02  .1E+04   1.0
  2    EVP    2.00   1.920  .0600   .01800    18.40   .600E-02  .1E+04   1.0
```

Figure 3-2: Example 1 standard output file

```
                SOIL  1 NON-LINEAR E VS. LOG P

                  COMP. INDEX   CALPHA     CV          MAX. STRESS

                      1.800     .01700     .400E-02        70.00
                      1.680     .01500     .400E-02  GREATER THAN   70.00


                SOIL  2 NON-LINEAR E VS. LOG P

                  COMP. INDEX   CALPHA     CV          MAX. STRESS

                      1.920     .01800     .600E-02        59.00
                      1.620     .01500     .600E-02  GREATER THAN   59.00


**** S U B L A Y E R   D A T A ****

                                                                 OVERBN     PRECONS
       SOIL     ---- ELEVATION (meters)----   THICK  PRESSURE   PRESSURE
LAYER  TYPE      TOP     CENTER    BOTTOM   (meters)   (kPa)      (kPa)

  1       1      7.35     7.25      7.15      .200      27.52      54.20
  2       1      7.15     7.05      6.95      .200      29.24      52.60
  3       1      6.95     6.85      6.75      .200      30.96      51.00
  4       1      6.75     6.65      6.55      .200      32.68      49.40
  5       1      6.55     6.45      6.35      .200      34.39      47.80
  6       2      6.35     6.25      6.15      .200      36.11      47.64
  7       2      6.15     6.05      5.95      .200      37.83      48.91
  8       2      5.95     5.85      5.75      .200      39.55      50.18
  9       2      5.75     5.65      5.55      .200      41.27      51.45
 10       2      5.55     5.45      5.35      .200      42.98      52.73
 11       2      5.35     5.25      5.15      .200      44.70      54.00
 12       2      5.15     5.05      4.95      .200      46.42      55.27
 13       2      4.95     4.85      4.75      .200      48.14      56.55
 14       2      4.75     4.65      4.55      .200      49.86      57.82
 15       2      4.55     4.45      4.35      .200      51.57      59.09
 16       2      4.35     4.25      4.15      .200      53.29      60.36


**** L O A D I N G   I N F O R M A T I O N ****

      NUMBER OF LOAD APPLICATIONS:    1

      LOAD NUMBER    START LOADING    FINISH LOADING
                         (days)           (days)

           1              .00             4.50


**** T I M E   I N F O R M A T I O N ****

      NUMBER OF OUTPUT TIMES :  15
      OUTPUT TIMES  (days) :
            1.00      2.50      4.50     11.00     22.00
           40.00     80.00    120.00    200.00    300.00
          400.00    500.00    700.00   1000.00   1200.00

                     (end of input data)
```

Figure 3-2 (continued): Example 1 standard output file

F I N I T E E L E M E N T S O L U T I O N

```
                    LOAD STEP NUMBER:   1
                    TIME  (days) :     .00

                    LOAD TYPE: LARGE AREAL SURCHARGE

              NEW FILL ELEVATION:     11.90
              NEW HEIGHT OF FILL:      2.40
          MOIST SOIL UNIT WEIGHT:     16.25
      SATURATED SOIL UNIT WEIGHT:     20.00


      LAYER    STRESS        FINAL
              INCREMENT   EFFECTIVE STRESS
                (kPa)         (kPa)

         1       39.00        66.52
         2       39.00        68.24
         3       39.00        69.96
         4       39.00        71.68
         5       39.00        73.39
         6       39.00        75.11
         7       39.00        76.83
         8       39.00        78.55
         9       39.00        80.27
        10       39.00        81.98
        11       39.00        83.70
        12       39.00        85.42
        13       39.00        87.14
        14       39.00        88.86
        15       39.00        90.57
        16       39.00        92.29


---------- CONVERGED SOLUTION FOR TIME:    1.07  (days)  ------------

NUMBER OF LOADS APPLIED:   1         TOTAL SETTLEMENT:  .002(meters)

              INITIAL                CHANGE   REFERENCE             EXCESS
              CENTER      INITIAL    IN       PRECONS    EFFECT     PORE
        SOIL  ELEVATION   THICK      THICK    PRESSURE   STRESS     PRESSURE
LAYER   TYPE   (meters)   (meters)   (meters)  (kPa)      (kPa)      (kPa)

   1      1      7.25      .20      .0005       54.38      33.84        2.92
   2      1      7.05      .20      .0001       52.53      31.41        7.06
   3      1      6.85      .20      .0001       51.04      31.53        8.66
   4      1      6.65      .20      .0000       49.37      32.74        9.17
   5      1      6.45      .20      .0000       47.83      34.38        9.25
   6      2      6.25      .20      .0000       47.61      36.08        9.26
   7      2      6.05      .20      .0000       50.04      37.82        9.24
```

Figure 3-2 (continued): Example 1 standard output file

8	2	5.85	.20	.0000	52.19	39.54	9.24
9	2	5.65	.20	.0000	54.23	41.27	9.23
10	2	5.45	.20	.0000	54.57	43.03	9.19
11	2	5.25	.20	.0000	53.99	44.75	9.18
12	2	5.05	.20	.0000	55.29	46.58	9.07
13	2	4.85	.20	.0000	56.52	48.49	8.88
14	2	4.65	.20	.0001	57.86	50.58	8.50
15	2	4.45	.20	.0000	59.03	52.75	8.06
16	2	4.25	.20	.0008	60.81	58.60	3.92

---------- CONVERGED SOLUTION FOR TIME: 2.53 (days) ----------

NUMBER OF LOADS APPLIED: 1 TOTAL SETTLEMENT: .007(meters)

LAYER	SOIL TYPE	INITIAL CENTER ELEVATION (meters)	INITIAL THICK (meters)	CHANGE IN THICK (meters)	REFERENCE PRECONS PRESSURE (kPa)	EFFECT STRESS (kPa)	EXCESS PORE PRESSURE (kPa)
1	1	7.25	.20	.0012	54.57	44.44	4.97
2	1	7.05	.20	.0005	52.59	38.29	12.84
3	1	6.85	.20	.0003	51.05	35.53	17.31
4	1	6.65	.20	.0001	49.37	34.84	19.72
5	1	6.45	.20	.0001	47.84	35.34	20.94
6	2	6.25	.20	.0000	47.61	36.53	21.47
7	2	6.05	.20	.0000	48.93	38.07	21.65
8	2	5.85	.20	.0000	50.17	39.72	21.72
9	2	5.65	.20	.0000	51.46	41.44	21.71
10	2	5.45	.20	.0000	52.73	43.21	21.66
11	2	5.25	.20	.0000	53.99	45.01	21.58
12	2	5.05	.20	.0000	55.29	46.87	21.44
13	2	4.85	.20	.0000	56.52	48.82	21.21
14	2	4.65	.20	.0001	57.87	50.97	20.78
15	2	4.45	.20	.0000	59.03	53.53	19.93
16	2	4.25	.20	.0052	67.60	65.51	9.67

---------- CONVERGED SOLUTION FOR TIME: 4.53 (days) ----------

NUMBER OF LOADS APPLIED: 1 TOTAL SETTLEMENT: .020(meters)

LAYER	SOIL TYPE	INITIAL CENTER ELEVATION (meters)	INITIAL THICK (meters)	CHANGE IN THICK (meters)	REFERENCE PRECONS PRESSURE (kPa)	EFFECT STRESS (kPa)	EXCESS PORE PRESSURE (kPa)
1	1	7.25	.20	.0035	57.74	55.81	10.53
2	1	7.05	.20	.0009	52.73	44.59	23.46
3	1	6.85	.20	.0007	51.13	41.87	27.90
4	1	6.65	.20	.0003	49.40	39.83	31.66
5	1	6.45	.20	.0003	47.85	38.73	34.48
6	2	6.25	.20	.0001	47.62	38.80	36.12
7	2	6.05	.20	.0001	48.93	39.74	36.91
8	2	5.85	.20	.0001	50.17	40.96	37.41
9	2	5.65	.20	.0001	51.46	42.43	37.65

Figure 3-2 (continued): Example 1 standard output file

```
  10      2      5.45     .20     .0000       52.73     44.10       37.70
  11      2      5.25     .20     .0000       53.99     45.89       37.63
  12      2      5.05     .20     .0001       55.29     47.72       37.52

  13      2      4.85     .20     .0001       56.66     49.77       37.19
  14      2      4.65     .20     .0002       58.09     52.13       36.55
  15      2      4.45     .20     .0010       59.58     57.12       33.27
  16      2      4.25     .20     .0124       79.35     76.97       15.14



***** C O M P L E T E   S E T T L E M E N T   R E C O R D *****

                                          AVERAGE      SURFACE
           TIME     LOAD      SETTLEMENT  STRAIN       ELEVATION
          (days)   NUMBER     (meters)      (%)        (meters)

            .00         1       .0000        .00          9.50
           1.07                 .0015        .05          9.50
           2.53                 .0075        .23          9.49
           4.53                 .0197        .62          9.48
          11.07                 .0447       1.40          9.46
          22.02                 .0692       2.16          9.43
          40.07                 .0994       3.11          9.40
          80.63                 .1498       4.68          9.35
         120.54                 .1881       5.88          9.31
         202.71                 .2462       7.69          9.25
         302.66                 .2917       9.12          9.21
         402.54                 .3197       9.99          9.18
         502.53                 .3372      10.54          9.16
         707.97                 .3569      11.15          9.14
        1013.06                 .3698      11.56          9.13
        1200.00                 .3745      11.70          9.13
    LOAD NUMBER 1 : LARGE AREAL SURCHARGE


NUMBER OF TIME STEPS =       403
TOTAL NUMBER OF COMPUTATION ITERATIONS =       505


   Current date and finish time...
      5/20/1998
      5:57:25 pm
```

Figure 3-2 (continued): Example 1 standard output file

PLOT FILE: C:\CONSOL97\MANUAL\EX_1.PLT

TITLE: "Example Problem 1: Embankment fill "

***** C O M P L E T E S E T T L E M E N T R E C O R D *****

TIME (days)	SETTLEMENT (meters)	SURFACE ELEVATION (meters)
.00	.0000	9.50
1.07	.0015	9.50
2.53	.0075	9.49
4.53	.0197	9.48
11.07	.0447	9.46
22.02	.0692	9.43
40.07	.0994	9.40
80.63	.1498	9.35
120.54	.1881	9.31
202.71	.2462	9.25
302.66	.2917	9.21
402.54	.3197	9.18
502.53	.3372	9.16
707.97	.3569	9.14
1013.06	.3698	9.13
1200.00	.3745	9.13
.00	.0000	.00

SUBLAYER OUTPUT

OUTPUT FOR SUBLAYER NUMBER: 1

TIME (days)	INITIAL STRAIN (%)	DELAYED STRAIN (%)	TOTAL STRAIN (%)	EFFECT. STRESS (kPa)	YIELD . PRESSURE (kPa)	REFERENCE PRECONS. PRESSURE (kPa)	DELAYED STRAIN RATE (days-1)
.00	.0000	.0000	.0000	27.52	54.20	54.20	.20D-07
1.07	.2525	.0124	.2649	33.84	49.72	54.38	.35D-03
2.53	.4896	.0990	.5886	44.44	51.01	54.57	.74D-03
4.53	1.3579	.4086	1.7665	55.81	55.81	57.74	.23D-02
11.07	2.9772	1.1757	4.1530	59.88	59.88	67.43	.13D-03
22.02	3.3084	1.2768	4.5852	60.84	60.84	69.35	.85D-04
40.07	3.5008	1.3538	4.8546	61.41	61.41	72.10	.31D-04
80.63	3.6453	1.4343	5.0795	61.84	61.84	73.78	.18D-04
120.54	3.7061	1.5026	5.2087	62.03	62.03	74.18	.17D-04
202.71	3.8117	1.5576	5.3693	62.36	62.36	77.69	.41D-05
302.66	3.8895	1.5785	5.4680	62.63	62.63	81.04	.11D-05
402.54	3.9480	1.5913	5.5393	62.81	62.81	81.24	.11D-05
502.53	3.9705	1.6029	5.5734	62.89	62.89	81.30	.12D-05

Figure 3-3: Example 1 plotting output file

707.97	3.9897	1.6243	5.6141	62.95	62.95	82.96	.60D-06
1013.06	3.9845	1.6390	5.6235	62.93	62.93	83.48	.48D-06
1200.00	3.9792	1.6425	5.6217	62.91	62.91	89.66	.42D-07

OUTPUT FOR SUBLAYER NUMBER: 3

TIME (days)	INITIAL STRAIN (%)	DELAYED STRAIN (%)	TOTAL STRAIN (%)	EFFECT. STRESS (kPa)	YIELD . PRESSURE (kPa)	REFERENCE PRECONS. PRESSURE (kPa)	DELAYED STRAIN RATE (days-1)
.00	.0000	.0000	.0000	30.96	51.00	51.00	.20D-07
1.07	.0354	.0001	.0354	31.53	38.77	51.04	.63D-06
2.53	.1392	.0077	.1470	35.53	45.16	51.05	.11D-03
4.53	.2820	.0437	.3258	41.87	45.25	51.13	.11D-03
11.07	.5901	.1388	.7289	46.64	46.64	52.04	.18D-03
22.02	1.2444	.3921	1.6365	48.60	48.60	53.81	.23D-03
40.07	2.1060	.6611	2.7670	50.50	50.50	56.84	.13D-03
80.63	3.2539	1.0842	4.3381	53.27	53.27	60.67	.87D-04
120.54	3.9862	1.3839	5.3701	55.23	55.23	63.39	.67D-04
202.71	5.1502	1.7664	6.9166	58.62	58.62	68.70	.33D-04
302.66	6.1108	2.0049	8.1157	61.54	61.54	73.16	.20D-04
402.54	6.7231	2.1636	8.8867	63.46	63.46	76.29	.14D-04
502.53	7.0507	2.2933	9.3440	64.52	64.52	77.81	.12D-04
707.97	7.3534	2.4800	9.8335	65.55	65.55	81.08	.52D-05
1013.06	7.4794	2.6139	10.0933	66.00	66.00	82.22	.41D-05
1200.00	7.5065	2.6752	10.1817	66.11	66.11	86.24	.85D-06

OUTPUT FOR SUBLAYER NUMBER: 7

TIME (days)	INITIAL STRAIN (%)	DELAYED STRAIN (%)	TOTAL STRAIN (%)	EFFECT. STRESS (kPa)	YIELD . PRESSURE (kPa)	REFERENCE PRECONS. PRESSURE (kPa)	DELAYED STRAIN RATE (days-1)
.00	.0000	.0000	.0000	37.83	48.91	48.91	.15D-07
1.07	.0092	.0000	.0092	37.82	37.84	50.04	-.11D-08
2.53	.0148	.0000	.0148	38.07	40.18	48.93	.45D-06
4.53	.0521	.0010	.0531	39.74	42.68	48.93	.12D-04
11.07	.1949	.0147	.2096	43.17	43.17	50.93	.59D-05
22.02	.5489	.0274	.5762	43.85	43.85	51.06	.12D-04
40.07	1.1474	.0706	1.2180	44.99	44.99	50.92	.47D-04
80.63	2.5860	.3065	2.8925	48.15	48.15	54.82	.64D-04
120.54	4.0650	.5681	4.6331	51.38	51.38	59.11	.63D-04
202.71	6.5459	1.0249	7.5708	57.29	57.29	66.33	.50D-04
302.66	8.5067	1.4422	9.9489	63.09	63.09	73.30	.36D-04
402.54	9.5675	1.7508	11.3183	66.76	66.76	78.17	.27D-04
502.53	10.1782	1.9914	12.1695	69.04	69.04	81.40	.22D-04
707.97	10.7393	2.3515	13.0909	71.35	71.35	85.07	.15D-04
1013.06	10.9565	2.7016	13.6582	72.40	72.40	87.44	.94D-05
1200.00	10.9934	2.8613	13.8547	72.63	72.63	88.29	.75D-05

Figure 3-3 (continued): Example 1 plotting output file

OUTPUT FOR SUBLAYER NUMBER: 11

TIME (days)	INITIAL STRAIN (%)	DELAYED STRAIN (%)	TOTAL STRAIN (%)	EFFECT. STRESS (kPa)	YIELD . PRESSURE (kPa)	REFERENCE PRECONS. PRESSURE (kPa)	DELAYED STRAIN RATE (days-1)
.00	.0000	.0000	.0000	44.70	54.00	54.00	.11D-07
1.07	-.0042	.0000	-.0042	44.75	45.64	53.99	.92D-07
2.53	.0009	.0000	.0009	45.01	45.79	53.99	.14D-06
4.53	.0177	.0003	.0180	45.89	47.92	53.99	.43D-05
11.07	.1181	.0054	.1234	48.22	48.22	54.24	.12D-04
22.02	.4507	.0312	.4818	49.47	49.47	54.97	.36D-04
40.07	1.3492	.1214	1.4705	51.74	51.74	57.89	.53D-04
80.63	3.2861	.3935	3.6796	56.46	56.46	64.76	.69D-04
120.54	4.6885	.6602	5.3488	60.29	60.29	68.95	.62D-04
202.71	6.4432	1.0899	7.5331	66.19	66.19	76.39	.45D-04
302.66	7.7911	1.4712	9.2623	71.20	71.20	82.91	.33D-04
402.54	8.5927	1.7603	10.3530	74.46	74.46	87.34	.26D-04
502.53	9.0486	1.9882	11.0368	76.45	76.45	90.27	.21D-04
707.97	9.4625	2.3326	11.7950	78.45	78.45	93.65	.14D-04
1013.06	9.6168	2.6707	12.2874	79.36	79.36	95.92	.91D-05
1200.00	9.6390	2.8259	12.4649	79.54	79.54	96.76	.73D-05

OUTPUT FOR SUBLAYER NUMBER: 15

TIME (days)	INITIAL STRAIN (%)	DELAYED STRAIN (%)	TOTAL STRAIN (%)	EFFECT. STRESS (kPa)	YIELD . PRESSURE (kPa)	REFERENCE PRECONS. PRESSURE (kPa)	DELAYED STRAIN RATE (days-1)
.00	.0000	.0000	.0000	51.57	59.09	59.09	.66D-08
1.07	-.0044	.0007	-.0037	52.75	55.26	59.03	.17D-04
2.53	.0085	.0012	.0097	53.53	54.53	59.03	.11D-04
4.53	.4748	.0275	.5023	57.12	57.12	59.58	.37D-03
11.07	3.4524	.4923	3.9447	66.78	66.78	72.02	.47D-03
22.02	4.9147	.9259	5.8406	72.25	72.25	78.73	.33D-03
40.07	5.7706	1.3734	7.1440	75.93	75.93	85.06	.13D-03
80.63	6.4906	1.7358	8.2263	79.38	79.38	90.24	.76D-04
120.54	6.7940	1.9978	8.7919	81.00	81.00	92.81	.58D-04
202.71	7.1191	2.3825	9.5017	83.02	83.02	96.21	.39D-04
302.66	7.3167	2.7083	10.0250	84.52	84.52	98.89	.28D-04
402.54	7.4149	2.9526	10.3675	85.46	85.46	100.72	.22D-04
502.53	7.4582	3.1464	10.6047	86.01	86.01	102.01	.18D-04
707.97	7.4789	3.4438	10.9227	86.55	86.55	103.72	.12D-04
1013.06	7.4810	3.7426	11.2236	86.76	86.76	105.22	.81D-05
1200.00	7.4813	3.8822	11.3635	86.79	86.79	105.89	.66D-05

Figure 3-3 (continued): Example 1 plotting output file

```
"kPa"
"m^2/day"
"fresh"
0
0
"Example problem 1: Large areal surcharge"
9
1,1
2,3
9.81,2000000
20,19.7
0
0
2,1.8,.06,18.4,.004,2
1000,1,.017
1.68,.015,.004,70
2,1.92,.06,18.4,.006,2
1000,1,.018
1.62,.015,.006,59
7.35
6.35,5,4,1,"OC",55,47,.1,.1
4.15,11,4,2,"OC",47,61,.1,.1
5
1
3
7
11
15
9.5,9
15,1200,20
1
2.5
4.5
11
22
40
80
120
200
300
400
500
700
1000
1200
0
0
0
0
0
0
0
0
0
0
0
0
0
0
0
```

Figure 3-4: Example 1 data input file

```
2
1
17
1
3
0,4.5
11.9,-999,16.25,20
```

Figure 3-4 (continued): Example 1 data input file

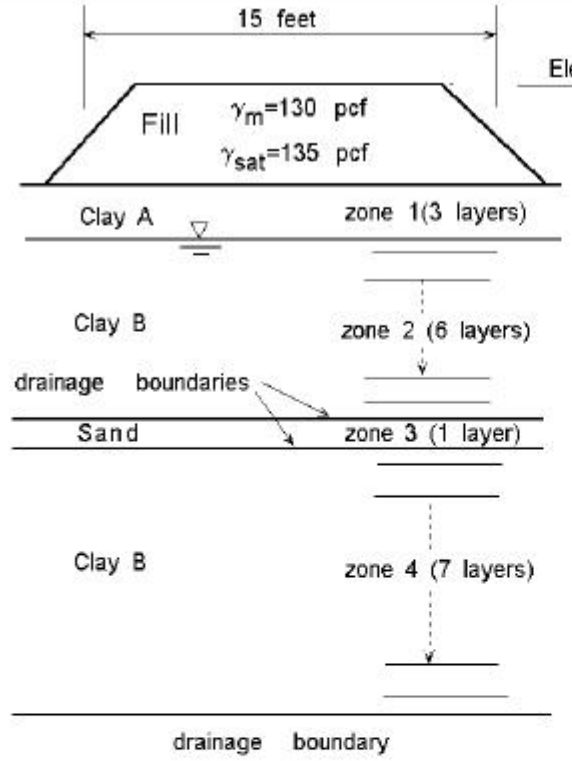

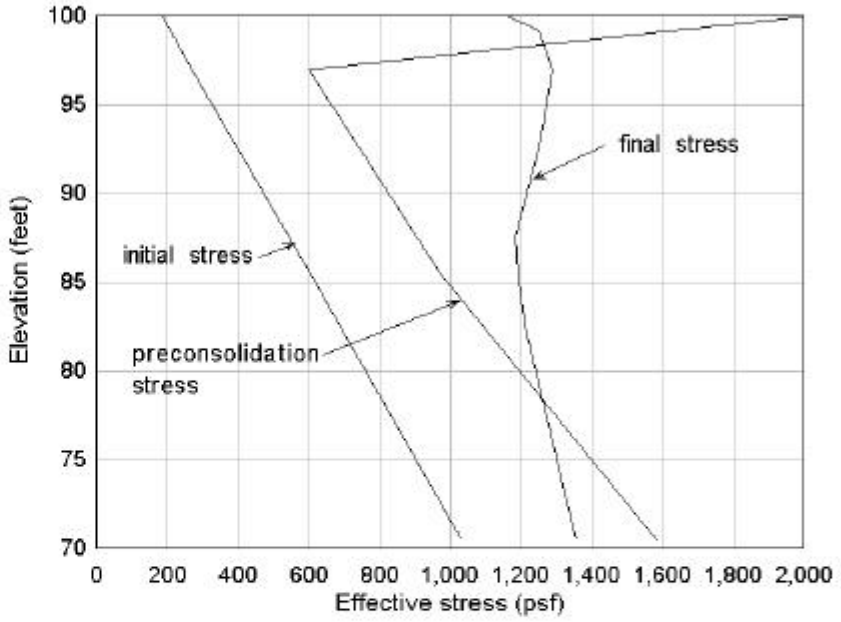

SOIL PROPERTIES

	γ (pcf)	e_0	C_c	C_r	$c_{v(ft^2/day)}$	C_α	Age (yrs)
Clay A	90	2.0	1.2	0.09	0.2	0.016 0	1000
Clay B(σ'<1000 psf)	90	2.0	1.4	0.09	0.02	0.0187	1000
Clay B(σ'>1000 psf)			1.0	0.09	0.028	0.0147	1000
Sand	120	0.5	0.070	0.007	2.0	----	----

Figure 3-5: Example 2 subsurface profile and soil properties

consol97\manual\chapter3\fig3-4.cvs
stress2.grf

```
*************************************************
*                                               *
*        CONSOL97:FINITE ELEMENT PROGRAM        *
*       FOR ANALYSIS OF 1-D CONSOLIDATION       *
*          OF AN ELASTO-VISCO-PLASTIC           *
*        AND/OR AN ELASTO-PLASTIC MEDIUM        *
*                                               *
*   Theory developed by J.P. Rajot, April 1992  *
*  Program developed by V.J. Perrone, April 1998*
*                                               *
*                  Version: 1.0                 *
*                                               *
*************************************************


DATE:  5/21/1998     TIME:  9:16:29 pm

INPUT FILE:  c:\consol97\manual\chapter4\ex_2.dat
OUTPUT FILE: c:\consol97\manual\chapter4\ex_2.out
PLOT FILE:   c:\consol97\manual\chapter4\ex_2.plt


TITLE: "Example 2: Infinitely long strip load on a clay crust."


**** C O N T R O L   D A T A ****

NUMBER OF SOIL SUBLAYERS ..........................   17
NUMBER OF DIFFERENT SOILS .........................    3
ELEVATION OF THE GROUND SURFACE ...................  100.00( feet )
TOP ELEVATION OF THE COMPRESSIBLE SOIL MASS.........  100.00( feet )
GROUNDWATER ELEVATION .............................   97.00( feet )
UNIT WEIGHT OF WATER ..............................   62.40(pcf)
MST. UT. WGT. OF SOIL ABOVE COMPRESSIBLE MASS ......   90.00(pcf)
SAT. UT. WGT. OF SOIL ABOVE COMPRESSIBLE MASS ......   92.00(pcf)


**** D R A I N A G E   B O U N D A R I E S ****

SUBLAYER BOUNDARY NUMBERS:     1   10   11   18


**** S O I L   P R O P E R T I E S ****

                                    SECOND.  UNIT     CONSOL.  GEOL.   REF.
            VOID   COMP.   RECOMP.  COMP.    WEIGHT   COEFF.   AGE     TIME
SOIL  MODEL RATIO  INDEX   INDEX    COEFF.  (pcf)    (ft^2/day(years)  (days)

  1    EVP    2.00   1.200  .0900   .01600    90.00   .200E+00  .1E+05   1.0
  2    EVP    2.00   1.400  .0900   .01870    90.00   .200E-01  .1E+05   1.0
  3    EP      .50    .070   .0070            120.00   .200E+01
```

Figure 3-6: Example 2 standard output file

```
SOIL  2 NON-LINEAR E VS. LOG P

  COMP. INDEX   CALPHA     CV          MAX. STRESS


      1.400     .01870     .200E-01      1000.00
      1.100     .01470     .280E-01  GREATER THAN 1000.00
```

**** S U B L A Y E R D A T A ****

LAYER	SOIL TYPE	ELEVATION (feet) TOP	CENTER	BOTTOM	THICK (feet)	OVERBN PRESSURE (psf)	PRECONS PRESSURE (psf)
1	1	100.00	99.79	99.57	.429	193.11	1900.00
2	1	99.57	99.14	98.71	.857	210.86	1600.00
3	1	98.71	97.86	97.00	1.714	246.34	1000.00
4	2	97.00	96.61	96.21	.786	280.84	612.14
5	2	96.21	95.43	94.64	1.571	313.37	648.57
6	2	94.64	93.07	91.50	3.143	378.43	721.43
7	2	91.50	89.93	88.36	3.143	465.17	818.57
8	2	88.36	87.57	86.79	1.571	530.23	891.43
9	2	86.79	86.39	86.00	.786	562.76	927.86
10	3	86.00	85.50	85.00	1.000	602.40	970.00
11	2	85.00	84.75	84.50	.500	638.10	1010.00
12	2	84.50	84.00	83.50	1.000	658.80	1040.00
13	2	83.50	82.50	81.50	2.000	700.20	1100.00
14	2	81.50	79.50	77.50	4.000	783.00	1220.00
15	2	77.50	75.36	73.21	4.286	897.34	1385.71
16	2	73.21	72.14	71.07	2.143	986.06	1514.29
17	2	71.07	70.54	70.00	1.071	1030.41	1578.57

**** L O A D I N G I N F O R M A T I O N ****

NUMBER OF LOAD APPLICATIONS: 1

LOAD NUMBER	START LOADING (days)	FINISH LOADING (days)
1	.00	10.00

**** T I M E I N F O R M A T I O N ****

NUMBER OF OUTPUT TIMES : 12
OUTPUT TIMES (days) :

10.00	20.00	50.00	100.00	200.00
400.00	700.00	1000.00	2000.00	4000.00
7000.00	10000.00			

(end of input data)

Figure 3-6 (continued): Example 2 standard output file

F I N I T E E L E M E N T S O L U T I O N

LOAD STEP NUMBER: 1
TIME (days) : .00

LOAD TYPE: INFINITELY LONG STRIP LOAD

```
     NEW STRIP FILL ELEVATION:    108.00
        NEW STRIP FILL HEIGHT:      8.00
       MOIST SOIL UNIT WEIGHT:    130.00
   SATURATED SOIL UNIT WEIGHT:    135.00
              STRIP FILL WIDTH:     15.00
DISTANCE FROM CENTER OF STRIP:       .00
     BUOYANCY CORRECTION CODE:       1

LAYER    STRESS        FINAL
        INCREMENT   EFFECTIVE STRESS
          (psf)         (psf)

   1     1039.96      1233.07
   2     1038.88      1249.74
   3     1027.11      1273.46
   4     1006.61      1287.45
   5      969.67      1283.04
   6      874.81      1253.24
   7      743.72      1208.89
   8      653.16      1183.39
   9      613.61      1176.37
  10      586.51      1188.91
  11      564.88      1202.98
  12      544.92      1203.72
  13      508.70      1208.90
  14      448.59      1231.59
  15      382.16      1279.50
  16      340.73      1326.78
  17      323.39      1353.80
```

Figure 3-6 (continued): Example 2 standard output file

---------- CONVERGED SOLUTION FOR TIME: 10.00 (days) ------------

NUMBER OF LOADS APPLIED: 1 TOTAL SETTLEMENT: .123(feet)

LAYER	SOIL TYPE	INITIAL CENTER ELEVATION (feet)	INITIAL THICK (feet)	CHANGE IN THICK (feet)	REFERENCE PRECONS PRESSURE (psf)	EFFECT STRESS (psf)	EXCESS PORE PRESSURE (psf)
1	1	99.79	.43	.0149	2044.90	1115.65	109.74
2	1	99.14	.86	.0235	1691.43	870.47	371.60
3	1	97.86	1.71	.0296	1031.22	633.80	632.08
4	2	96.61	.79	.0062	617.05	457.96	822.06
5	2	95.43	1.57	.0027	648.97	354.24	921.63
6	2	93.07	3.14	-.0011	815.55	369.08	877.71
7	2	89.93	3.14	.0012	818.56	478.68	724.72
8	2	87.57	1.57	.0032	892.09	611.82	566.74
9	2	86.39	.79	.0154	995.78	921.90	249.94
10	3	85.50	1.00	.0050	1184.58	1184.58	.00
11	2	84.75	.50	.0119	1135.87	1058.21	140.60
12	2	84.00	1.00	.0039	1043.27	856.41	343.29
13	2	82.50	2.00	.0024	1100.40	763.82	441.33
14	2	79.50	4.00	-.0001	1219.98	781.02	447.26
15	2	75.36	4.29	-.0002	1033.25	893.71	382.97
16	2	72.14	2.14	.0018	1514.50	1049.05	275.22
17	2	70.54	1.07	.0030	1581.44	1250.54	100.87

---------- CONVERGED SOLUTION FOR TIME: 20.06 (days) ------------

NUMBER OF LOADS APPLIED: 1 TOTAL SETTLEMENT: .224(feet)

LAYER	SOIL TYPE	INITIAL CENTER ELEVATION (feet)	INITIAL THICK (feet)	CHANGE IN THICK (feet)	REFERENCE PRECONS PRESSURE (psf)	EFFECT STRESS (psf)	EXCESS PORE PRESSURE (psf)
1	1	99.79	.43	.0154	2051.51	1170.89	48.41
2	1	99.14	.86	.0273	1711.12	1058.10	177.88
3	1	97.86	1.71	.0445	1070.24	906.23	353.63
4	2	96.61	.79	.0314	756.00	684.73	589.40
5	2	95.43	1.57	.0107	652.92	479.00	791.20
6	2	93.07	3.14	.0020	721.42	397.39	844.27
7	2	89.93	3.14	.0028	818.70	497.47	701.58
8	2	87.57	1.57	.0089	904.14	751.01	423.73
9	2	86.39	.79	.0320	1147.83	1027.78	140.46
10	3	85.50	1.00	.0050	1184.58	1181.14	.00
11	2	84.75	.50	.0180	1370.72	1115.31	80.20
12	2	84.00	1.00	.0120	1013.26	953.12	243.38
13	2	82.50	2.00	.0049	1101.56	832.63	369.54
14	2	79.50	4.00	.0009	1219.97	796.65	429.00
15	2	75.36	4.29	.0006	1385.66	907.96	366.48
16	2	72.14	2.14	.0038	1515.35	1119.11	203.16
17	2	70.54	1.07	.0040	1592.97	1290.20	59.32

Figure 3-6 (continued): Example 2 standard output file

---------- CONVERGED SOLUTION FOR TIME: 51.10 (days) ------------

NUMBER OF LOADS APPLIED: 1 TOTAL SETTLEMENT: .402(feet)

LAYER	SOIL TYPE	INITIAL CENTER ELEVATION (feet)	INITIAL THICK (feet)	CHANGE IN THICK (feet)	REFERENCE PRECONS PRESSURE (psf)	EFFECT STRESS (psf)	EXCESS PORE PRESSURE (psf)
1	1	99.79	.43	.0154	2052.80	1176.94	31.50
2	1	99.14	.86	.0282	1716.15	1109.52	115.61
3	1	97.86	1.71	.0743	1195.97	1018.36	230.77
4	2	96.61	.79	.0665	967.83	837.49	426.12
5	2	95.43	1.57	.0397	711.73	609.49	650.58
6	2	93.07	3.14	.0145	723.82	513.17	719.36
7	2	89.93	3.14	.0112	820.32	592.85	598.43
8	2	87.57	1.57	.0269	955.83	799.93	367.99
9	2	86.39	.79	.0393	1226.50	1044.04	117.79
10	3	85.50	1.00	.0050	1184.58	1175.02	.00
11	2	84.75	.50	.0203	1431.35	1144.77	44.83
12	2	84.00	1.00	.0276	1253.58	1038.89	151.93
13	2	82.50	2.00	.0112	1015.22	927.13	269.72
14	2	79.50	4.00	.0061	1220.63	874.35	346.62
15	2	75.36	4.29	.0049	1385.82	978.17	292.27
16	2	72.14	2.14	.0053	1516.81	1167.93	150.79
17	2	70.54	1.07	.0054	1607.77	1303.64	42.50

---------- CONVERGED SOLUTION FOR TIME: 101.13 (days) ------------

NUMBER OF LOADS APPLIED: 1 TOTAL SETTLEMENT: .590(feet)

LAYER	SOIL TYPE	INITIAL CENTER ELEVATION (feet)	INITIAL THICK (feet)	CHANGE IN THICK (feet)	REFERENCE PRECONS PRESSURE (psf)	EFFECT STRESS (psf)	EXCESS PORE PRESSURE (psf)
1	1	99.79	.43	.0154	2052.98	1176.60	20.14
2	1	99.14	.86	.0287	1718.82	1139.18	74.27
3	1	97.86	1.71	.0982	1308.69	1083.79	153.79
4	2	96.61	.79	.0852	1115.42	939.99	312.30
5	2	95.43	1.57	.0948	858.90	718.26	530.90
6	2	93.07	3.14	.0297	747.10	586.46	636.22
7	2	89.93	3.14	.0211	834.53	657.49	525.42
8	2	87.57	1.57	.0520	1052.47	861.59	298.99
9	2	86.39	.79	.0429	1390.68	1063.42	91.52
10	3	85.50	1.00	.0050	1184.58	1168.42	.00
11	2	84.75	.50	.0209	1551.31	1151.10	32.15
12	2	84.00	1.00	.0335	1314.66	1065.07	119.62
13	2	82.50	2.00	.0279	1020.31	964.33	226.80
14	2	79.50	4.00	.0109	1004.92	940.81	275.11
15	2	75.36	4.29	.0094	1386.96	1051.15	215.00
16	2	72.14	2.14	.0076	1531.63	1203.67	111.21
17	2	70.54	1.07	.0066	1650.05	1310.51	31.99

Figure 3-6 (continued): Example 2 standard output file

---------- CONVERGED SOLUTION FOR TIME: 203.74 (days) ------------

NUMBER OF LOADS APPLIED: 1   TOTAL SETTLEMENT: .832(feet)

LAYER	SOIL TYPE	INITIAL CENTER ELEVATION (feet)	INITIAL THICK (feet)	CHANGE IN THICK (feet)	REFERENCE PRECONS PRESSURE (psf)	EFFECT STRESS (psf)	EXCESS PORE PRESSURE (psf)
1	1	99.79	.43	.0154	2053.26	1170.93	10.85
2	1	99.14	.86	.0291	1721.41	1158.45	40.05
3	1	97.86	1.71	.1146	1434.11	1136.62	86.17
4	2	96.61	.79	.0993	1286.44	1036.90	200.90
5	2	95.43	1.57	.1442	1027.46	834.21	401.00
6	2	93.07	3.14	.0922	817.26	655.16	554.93
7	2	89.93	3.14	.0498	877.24	693.73	478.48
8	2	87.57	1.57	.0706	1137.32	902.65	248.52
9	2	86.39	.79	.0434	1552.92	1078.20	67.90
10	3	85.50	1.00	.0050	1184.58	1159.98	.00
11	2	84.75	.50	.0212	1658.20	1155.92	19.20
12	2	84.00	1.00	.0387	1460.73	1101.71	75.14
13	2	82.50	2.00	.0490	1265.37	1020.65	163.16
14	2	79.50	4.00	.0278	1011.57	980.29	229.18
15	2	75.36	4.29	.0122	1409.96	1073.51	187.14
16	2	72.14	2.14	.0117	1571.01	1220.85	89.13
17	2	70.54	1.07	.0074	1731.21	1313.91	23.94

---------- CONVERGED SOLUTION FOR TIME: 408.96 (days) ------------

NUMBER OF LOADS APPLIED: 1   TOTAL SETTLEMENT: 1.150(feet)

LAYER	SOIL TYPE	INITIAL CENTER ELEVATION (feet)	INITIAL THICK (feet)	CHANGE IN THICK (feet)	REFERENCE PRECONS PRESSURE (psf)	EFFECT STRESS (psf)	EXCESS PORE PRESSURE (psf)
1	1	99.79	.43	.0154	2053.90	1155.71	6.42
2	1	99.14	.86	.0289	1750.31	1155.08	23.79
3	1	97.86	1.71	.1246	1490.68	1151.23	52.16
4	2	96.61	.79	.1074	1393.85	1090.86	127.93
5	2	95.43	1.57	.1836	1187.15	938.42	278.47
6	2	93.07	3.14	.1985	983.34	772.47	421.10
7	2	89.93	3.14	.1231	993.82	776.46	381.70
8	2	87.57	1.57	.0846	1261.31	940.33	198.50
9	2	86.39	.79	.0436	1736.62	1081.95	52.56
10	3	85.50	1.00	.0050	1184.58	1148.90	.00
11	2	84.75	.50	.0213	1709.88	1153.25	11.20
12	2	84.00	1.00	.0422	1528.19	1121.67	44.88
13	2	82.50	2.00	.0668	1391.83	1071.71	102.49
14	2	79.50	4.00	.0582	1341.04	1042.79	158.20
15	2	75.36	4.29	.0238	1444.70	1110.49	142.93
16	2	72.14	2.14	.0152	1593.96	1230.53	73.01
17	2	70.54	1.07	.0076	1732.67	1312.29	19.45

Figure 3-6 (continued): Example 2 standard output file

---------- CONVERGED SOLUTION FOR TIME: 714.05 (days) ------------

NUMBER OF LOADS APPLIED: 1   TOTAL SETTLEMENT: 1.454(feet)

INITIAL CENTER	INITIAL	CHANGE IN	REFERENCE PRECONS	EFFECT	EXCESS PORE

LAYER	SOIL TYPE	ELEVATION (feet)	THICK (feet)	THICK (feet)	PRESSURE (psf)	STRESS (psf)	PRESSURE (psf)
1	1	99.79	.43	.0153	2054.58	1139.43	3.63
2	1	99.14	.86	.0285	1714.67	1146.38	13.45
3	1	97.86	1.71	.1316	1530.61	1154.77	29.80
4	2	96.61	.79	.1125	1472.24	1125.69	74.65
5	2	95.43	1.57	.2110	1338.59	1028.39	170.72
6	2	93.07	3.14	.2978	1171.69	904.52	273.01
7	2	89.93	3.14	.2092	1164.92	891.01	253.52
8	2	87.57	1.57	.1004	1360.39	996.61	130.25
9	2	86.39	.79	.0438	1770.89	1089.58	33.68
10	3	85.50	1.00	.0049	1184.58	1138.15	.00
11	2	84.75	.50	.0211	1710.33	1147.33	6.77
12	2	84.00	1.00	.0443	1555.49	1129.24	27.32
13	2	82.50	2.00	.0776	1476.58	1100.19	64.69
14	2	79.50	4.00	.0855	1417.12	1086.06	106.70
15	2	75.36	4.29	.0434	1499.74	1143.96	102.47
16	2	72.14	2.14	.0192	1646.68	1242.89	54.40
17	2	70.54	1.07	.0081	1737.56	1311.31	14.50

---------- CONVERGED SOLUTION FOR TIME: 1013.54 (days) ------------

NUMBER OF LOADS APPLIED: 1 TOTAL SETTLEMENT: 1.640(feet)

LAYER	SOIL TYPE	INITIAL CENTER ELEVATION (feet)	INITIAL THICK (feet)	CHANGE IN THICK (feet)	REFERENCE PRECONS PRESSURE (psf)	EFFECT STRESS (psf)	EXCESS PORE PRESSURE (psf)
1	1	99.79	.43	.0153	2055.01	1129.15	2.03
2	1	99.14	.86	.0281	1710.91	1140.47	7.49
3	1	97.86	1.71	.1357	1790.74	1156.01	16.82
4	2	96.61	.79	.1154	1519.47	1145.61	43.23
5	2	95.43	1.57	.2248	1434.89	1086.22	101.81
6	2	93.07	3.14	.3534	1309.55	998.07	169.46
7	2	89.93	3.14	.2662	1292.08	974.93	161.10
8	2	87.57	1.57	.1102	1415.96	1036.67	82.73
9	2	86.39	.79	.0440	1776.89	1095.12	21.13
10	3	85.50	1.00	.0049	1184.58	1131.45	.00
11	2	84.75	.50	.0211	1707.82	1142.94	4.70
12	2	84.00	1.00	.0456	1569.92	1131.34	19.00
13	2	82.50	2.00	.0838	1511.04	1113.82	45.24
14	2	79.50	4.00	.1026	1468.05	1112.22	75.42
15	2	75.36	4.29	.0583	1543.58	1169.06	73.00
16	2	72.14	2.14	.0225	1686.97	1254.60	38.81
17	2	70.54	1.07	.0084	1858.85	1311.83	10.29

Figure 3-6 (continued): Example 2 standard output file

---------- CONVERGED SOLUTION FOR TIME: 2041.08 (days) ------------

NUMBER OF LOADS APPLIED: 1 TOTAL SETTLEMENT: 1.880(feet)

LAYER	SOIL TYPE	INITIAL CENTER ELEVATION (feet)	INITIAL THICK (feet)	CHANGE IN THICK (feet)	REFERENCE PRECONS PRESSURE (psf)	EFFECT STRESS (psf)	EXCESS PORE PRESSURE (psf)
1	1	99.79	.43	.0152	2055.60	1115.76	.35
2	1	99.14	.86	.0275	1781.35	1131.60	1.30
3	1	97.86	1.71	.1369	1892.52	1155.04	2.90
4	2	96.61	.79	.1185	1677.71	1166.45	7.80

```
   5      2     95.43    1.57     .2404     1611.75   1155.17       18.82
   6      2     93.07    3.14     .4192     1535.55   1123.28       31.58
   7      2     89.93    3.14     .3271     1495.60   1095.52       29.74
   8      2     87.57    1.57     .1263     1525.21   1095.07       14.86
   9      2     86.39     .79     .0445     1826.45   1103.63        3.74
  10      3     85.50    1.00     .0049     1184.58   1122.95         .00
  11      2     84.75     .50     .0212     1709.29   1137.61        1.85
  12      2     84.00    1.00     .0486     1604.45   1134.98        7.46
  13      2     82.50    2.00     .0951     1577.13   1134.09       17.60
  14      2     79.50    4.00     .1321     1561.73   1152.15       28.99
  15      2     75.36    4.29     .0849     1623.94   1208.73       27.79
  16      2     72.14    2.14     .0287     1728.17   1273.79       14.68
  17      2     70.54    1.07     .0088     1866.26   1313.55        3.88


---------- CONVERGED SOLUTION FOR TIME: 4092.93  (days)  ------------

NUMBER OF LOADS APPLIED:   1         TOTAL SETTLEMENT: 1.999( feet )

                INITIAL              CHANGE   REFERENCE             EXCESS
                CENTER      INITIAL  IN       PRECONS    EFFECT     PORE
      SOIL      ELEVATION   THICK    THICK    PRESSURE   STRESS     PRESSURE
LAYER TYPE       ( feet )   ( feet ) ( feet )  (psf)      (psf)      (psf)

   1      1     99.79     .43     .0152     2055.92   1108.43         .10
   2      1     99.14     .86     .0270     1815.56   1124.95         .38
   3      1     97.86    1.71     .1365     2216.23   1149.58         .87
   4      2     96.61     .79     .1205     1706.78   1164.62        2.29
   5      2     95.43    1.57     .2479     1668.63   1161.53        5.39
   6      2     93.07    3.14     .4422     1620.24   1139.64        8.85
   7      2     89.93    3.14     .3504     1579.43   1111.56        8.27
   8      2     87.57    1.57     .1342     1580.50   1101.02        4.15
   9      2     86.39     .79     .0445     1826.09   1101.85        1.04
  10      3     85.50    1.00     .0049     1184.58   1118.67         .00
  11      2     84.75     .50     .0217     1718.66   1134.60         .74
  12      2     84.00    1.00     .0521     1644.16   1135.50        2.97
  13      2     82.50    2.00     .1048     1634.66   1141.13        6.86
  14      2     79.50    4.00     .1523     1626.73   1166.92       10.96
  15      2     75.36    4.29     .1025     1676.83   1223.42       10.32
  16      2     72.14    2.14     .0335     1757.98   1280.55        5.43
  17      2     70.54    1.07     .0093     1871.83   1313.63        1.44
```

Figure 3-6 (continued): Example 2 standard output file

---------- CONVERGED SOLUTION FOR TIME: 7143.81 (days) ------------

NUMBER OF LOADS APPLIED: 1 TOTAL SETTLEMENT: 2.079(feet)

LAYER	SOIL TYPE	INITIAL CENTER ELEVATION (feet)	INITIAL THICK (feet)	CHANGE IN THICK (feet)	REFERENCE PRECONS PRESSURE (psf)	EFFECT STRESS (psf)	EXCESS PORE PRESSURE (psf)
1	1	99.79	.43	.0152	2056.13	1103.48	.06
2	1	99.14	.86	.0266	1885.01	1120.13	.20
3	1	97.86	1.71	.1364	2380.30	1145.05	.47
4	2	96.61	.79	.1223	1736.31	1160.85	1.22
5	2	95.43	1.57	.2534	1709.07	1159.41	2.84
6	2	93.07	3.14	.4554	1668.98	1139.63	4.65
7	2	89.93	3.14	.3637	1627.62	1111.92	4.34
8	2	87.57	1.57	.1397	1619.66	1099.85	2.18
9	2	86.39	.79	.0445	1825.65	1099.39	.54
10	3	85.50	1.00	.0049	1184.58	1115.85	.00
11	2	84.75	.50	.0223	1731.72	1132.21	.42
12	2	84.00	1.00	.0552	1679.42	1134.17	1.67
13	2	82.50	2.00	.1123	1677.96	1141.69	3.85
14	2	79.50	4.00	.1657	1667.55	1169.55	6.16
15	2	75.36	4.29	.1142	1710.38	1226.07	5.83
16	2	72.14	2.14	.0374	1780.51	1281.24	3.10
17	2	70.54	1.07	.0098	1877.67	1312.69	.83

---------- CONVERGED SOLUTION FOR TIME:10000.00 (days) ------------

NUMBER OF LOADS APPLIED: 1 TOTAL SETTLEMENT: 2.128(feet)

LAYER	SOIL TYPE	INITIAL CENTER ELEVATION (feet)	INITIAL THICK (feet)	CHANGE IN THICK (feet)	REFERENCE PRECONS PRESSURE (psf)	EFFECT STRESS (psf)	EXCESS PORE PRESSURE (psf)
1	1	99.79	.43	.0151	2063.24	1100.40	.04
2	1	99.14	.86	.0263	1899.21	1117.11	.13
3	1	97.86	1.71	.1363	2453.05	1142.15	.31
4	2	96.61	.79	.1235	1759.15	1158.26	.82
5	2	95.43	1.57	.2567	1735.34	1157.45	1.92
6	2	93.07	3.14	.4630	1698.19	1138.54	3.13
7	2	89.93	3.14	.3714	1656.32	1111.12	2.92
8	2	87.57	1.57	.1431	1644.61	1098.62	1.47
9	2	86.39	.79	.0446	1826.03	1097.75	.36
10	3	85.50	1.00	.0049	1184.58	1114.11	.00
11	2	84.75	.50	.0228	1742.96	1130.65	.29
12	2	84.00	1.00	.0571	1703.51	1133.04	1.19
13	2	82.50	2.00	.1169	1705.47	1141.28	2.74
14	2	79.50	4.00	.1740	1692.08	1169.97	4.41
15	2	75.36	4.29	.1216	1731.30	1226.56	4.20
16	2	72.14	2.14	.0402	1796.23	1281.08	2.25
17	2	70.54	1.07	.0103	1883.03	1311.95	.60

Figure 3-6 (continued): Example 2 standard output file

***** C O M P L E T E S E T T L E M E N T R E C O R D *****

TIME (days)	LOAD NUMBER	SETTLEMENT (feet)	AVERAGE STRAIN (%)	SURFACE ELEVATION (feet)

```
           .00         1      .0000        .00       100.00
         10.00                .1231        .41        99.88
         20.06                .2243        .75        99.78
         51.10                .4017       1.34        99.60
        101.13                .5900       1.97        99.41
        203.74                .8316       2.77        99.17
        408.96               1.1496       3.83        98.85
        714.05               1.4541       4.85        98.55
       1013.54               1.6402       5.47        98.36
       2041.08               1.8799       6.27        98.12
       4092.93               1.9995       6.66        98.00
       7143.81               2.0790       6.93        97.92
      10000.00               2.1277       7.09        97.87
    LOAD NUMBER 1 : INFINITELY LONG STRIP


NUMBER OF TIME STEPS =      2347
TOTAL NUMBER OF COMPUTATION ITERATIONS =      2483


   Current date and finish time...
      5/21/1998
      9:18:29 pm
```

Figure 3-6 (continued): Example 2 standard output file

PLOT FILE: c:\consol97\manual\chapter4\ex_2.plt

TITLE: "Example 2: Infinitely long strip load on a clay crust."

***** C O M P L E T E S E T T L E M E N T R E C O R D *****

TIME (days)	SETTLEMENT (feet)	SURFACE ELEVATION (feet)
.00	.0000	100.00
10.00	.1231	99.88
20.06	.2243	99.78
51.10	.4017	99.60
101.13	.5900	99.41
203.74	.8316	99.17
408.96	1.1496	98.85
714.05	1.4541	98.55
1013.54	1.6402	98.36
2041.08	1.8799	98.12
4092.93	1.9995	98.00
7143.81	2.0790	97.92
10000.00	2.1277	97.87

SUBLAYER OUTPUT

OUTPUT FOR SUBLAYER NUMBER: 3

TIME (days)	INITIAL STRAIN (%)	DELAYED STRAIN (%)	TOTAL STRAIN (%)	EFFECT. STRESS (psf)	YIELD . PRESSURE (psf)	REFERENCE PRECONS. PRESSURE (psf)	DELAYED STRAIN RATE (days-1)
.00	.0000	.0000	.0000	246.34	1000.00	1000.00	.19D-08
10.00	1.2341	.4930	1.7271	633.80	949.80	1031.22	.10D-02
20.06	1.7486	.8456	2.5942	906.23	906.23	1070.24	.15D-03
51.10	2.8625	1.4735	4.3360	1018.36	1018.36	1195.97	.17D-03
101.13	3.6714	2.0583	5.7297	1083.79	1083.79	1308.69	.89D-04
203.74	4.2187	2.4638	6.6825	1136.62	1136.62	1434.11	.32D-04
408.96	4.3299	2.9373	7.2672	1151.23	1151.23	1490.68	.18D-04
714.05	4.3387	3.3350	7.6738	1154.77	1154.77	1530.61	.10D-04
1013.54	4.3526	3.5643	7.9169	1156.01	1156.01	1790.74	.28D-06
2041.08	4.3557	3.6282	7.9839	1155.04	1155.04	1892.52	.76D-07
4092.93	4.3310	3.6300	7.9610	1149.58	1149.58	2216.23	.18D-08
7143.81	4.3247	3.6302	7.9549	1145.05	1145.05	2380.30	.31D-09
10000.00	4.3214	3.6302	7.9516	1142.15	1142.15	2453.05	.15D-09

Figure 3-7: Example 2 plotting output file

OUTPUT FOR SUBLAYER NUMBER: 5

TIME (days)	INITIAL STRAIN (%)	DELAYED STRAIN (%)	TOTAL STRAIN (%)	EFFECT. STRESS (psf)	YIELD . PRESSURE (psf)	REFERENCE PRECONS. PRESSURE (psf)	DELAYED STRAIN RATE (days-1)
.00	.0000	.0000	.0000	313.37	648.57	648.57	.22D-08
10.00	.1616	.0099	.1715	354.24	527.51	648.97	.64D-04
20.06	.5551	.1252	.6803	479.00	540.64	652.92	.99D-04
51.10	1.8978	.6293	2.5270	609.49	609.49	711.73	.22D-03
101.13	4.6101	1.4257	6.0358	718.26	718.26	858.90	.12D-03
203.74	6.9113	2.2673	9.1786	834.21	834.21	1027.46	.63D-04
408.96	8.5153	3.1680	11.6833	938.42	938.42	1187.15	.34D-04
714.05	9.5573	3.8704	13.4277	1028.39	1028.39	1338.59	.15D-04
1013.54	10.0642	4.2392	14.3034	1086.22	1086.22	1434.89	.11D-04
2041.08	10.6157	4.6795	15.2952	1155.17	1155.17	1611.75	.31D-05
4092.93	10.6574	5.1211	15.7785	1161.53	1161.53	1668.63	.16D-05
7143.81	10.6550	5.4701	16.1251	1159.41	1159.41	1709.07	.88D-06
10000.00	10.6528	5.6829	16.3357	1157.45	1157.45	1735.34	.60D-06

OUTPUT FOR SUBLAYER NUMBER: 9

TIME (days)	INITIAL STRAIN (%)	DELAYED STRAIN (%)	TOTAL STRAIN (%)	EFFECT. STRESS (psf)	YIELD . PRESSURE (psf)	REFERENCE PRECONS. PRESSURE (psf)	DELAYED STRAIN RATE (days-1)
.00	.0000	.0000	.0000	562.76	927.86	927.86	.17D-08
10.00	1.5173	.4480	1.9654	921.90	921.90	995.78	.13D-02
20.06	2.8466	1.2294	4.0759	1027.78	1027.78	1147.83	.51D-03
51.10	2.9730	2.0318	5.0048	1044.04	1044.04	1226.50	.16D-03
101.13	3.0022	2.4563	5.4585	1063.42	1063.42	1390.68	.14D-04
203.74	3.0240	2.4962	5.5202	1078.20	1078.20	1552.92	.15D-05
408.96	3.0352	2.5097	5.5449	1081.95	1081.95	1736.62	.13D-06
714.05	3.0630	2.5128	5.5758	1089.58	1089.58	1770.89	.94D-07
1013.54	3.0887	2.5157	5.6044	1095.12	1095.12	1776.89	.98D-07
2041.08	3.1367	2.5234	5.6601	1103.63	1103.63	1826.45	.62D-07
4092.93	3.1265	2.5360	5.6625	1101.85	1101.85	1826.09	.60D-07
7143.81	3.1135	2.5540	5.6675	1099.39	1099.39	1825.65	.58D-07
10000.00	3.1056	2.5709	5.6765	1097.75	1097.75	1826.03	.55D-07

OUTPUT FOR SUBLAYER NUMBER: 11

TIME (days)	INITIAL STRAIN (%)	DELAYED STRAIN (%)	TOTAL STRAIN (%)	EFFECT. STRESS (psf)	YIELD . PRESSURE (psf)	REFERENCE PRECONS. PRESSURE (psf)	DELAYED STRAIN RATE (days-1)
.00	.0000	.0000	.0000	638.10	1010.00	1010.00	.12D-08
10.00	1.8633	.5120	2.3753	1058.21	1058.21	1135.87	.13D-02
20.06	2.5180	1.0901	3.6081	1115.31	1115.31	1370.72	.57D-04
51.10	2.7851	1.2760	4.0611	1144.77	1144.77	1431.35	.38D-04
101.13	2.8407	1.3419	4.1825	1151.10	1151.10	1551.31	.69D-05
203.74	2.8820	1.3669	4.2489	1155.92	1155.92	1658.20	.16D-05
408.96	2.8578	1.3940	4.2519	1153.25	1153.25	1709.88	.77D-06
714.05	2.8120	1.4154	4.2275	1147.33	1147.33	1710.33	.68D-06
2041.08	2.7448	1.4972	4.2420	1137.61	1137.61	1709.29	.57D-06
1013.54	2.7800	1.4353	4.2153	1142.94	1142.94	1707.82	.65D-06
4092.93	2.7292	1.6028	4.3319	1134.60	1134.60	1718.66	.47D-06

Figure 3-7 (continued): Example 2 plotting output file

```
 7143.81    2.7221   1.7306   4.4527  1132.21  1132.21  1731.72   .38D-06
10000.00    2.7203   1.8333   4.5536  1130.65  1130.65  1742.96   .32D-06
```

Figure 3-7 (continued): Example 2 plotting output file

```
"psf"
"ft^2/day"
"fresh"
0
0
"Example 2: Infinitely long strip load on a clay crust."
6
20.89,1
3,5
62.4,1.27347E+07
92,90
0
0
1
2,1.2,.09,90,.2,1
10000,1,.016
2,1.4,.09,90,.02,2
10000,1,.0187
1.1,.0147,.028,1000
.5,.07,.007,120,2,1
100
97,3,1,1,"OC",2000,600,.1,.1
86,6,3,2,"OC",600,940,.1,.1
85,1,4,3,"OC",940,1000,.01,.01
70,7,3,2,"OC",1000,1600,.1,.1
4
3
5
9
11
100,97
12,10000,20
10
20
50
100
200
400
700
1000
2000
4000
7000
10000
0
0
0
0
0
0
0
0
0
0
0
0
```

Figure 3-8: Example 2 data input file

```
4
1
8
9
18
1
4
0,10
108,-999,130,135,15,0,1
```

Figure 3-8 (continued): Example 2 data input file

4. METHODS OF ANALYSIS

4.1 CONVENTIONAL METHOD

Conventional one-dimensional consolidation analyses use soil parameters determined from oedometer tests of soil specimens that are typically one inch thick with drainage at the top and bottom. The specimens are loaded incrementally, and each load is maintained until excess pore pressures have dissipated (end-of-primary) or for a standard duration of 24 hours (ASTM D2435). Figure 4-1(a) illustrates a typical plot of strain vs. log time for one load increment. The end of primary consolidation at time, t_p, is determined graphically and represents the full dissipation of excess pore pressures generated by load application. After time, t_p, secondary compression occurs at constant effective stress, and the slope, C_α, of the strain vs. log time plot is constant. The end-of-primary or the 24 hour void ratios are plotted for each effective stress, σ'. The relationship is non-linear and usually plotted as e vs. logarithm σ', as shown in Figure 4-1(b).

In the conventional method of analysis, the preconsolidation pressure, P'_p, (Figure 4-1(b)) is considered to be the greatest stress to which the soil has been previously consolidated, and includes the effects of aging, cementation, desiccation, and other factors. Soil compressibility significantly increases when effective stresses exceed P'_p. The compressibility at effective stresses less than P'_p (overconsolidated range of stresses), is designated by the recompression index, C_r, which is the slope of the void ratio vs. log stress plot. For effective stresses equal to or greater than P'_p (normally consolidated range of stresses) soil compressibility is designated by the compression index, C_c, which is typically about 5 to 10 times as large as C_r.

Conventional consolidation analyses estimate the excess pore water pressures during primary consolidation and the resulting strains caused by the increase in effective stresses throughout the soil mass as these excess pore pressures dissipate. The basic equations that govern one dimensional consolidation are:

1. Stress equilibrium: $\frac{\partial \sigma_z}{\partial z} = f_z$ (4.5)

where: s_z = total vertical stress, f_z = unit body force, z = depth.

2. Flow continuity through porous media: $\frac{k_z}{\gamma_w} \cdot \frac{\partial^2 \bar{u}}{\partial z^2} + \frac{\partial v_z}{\partial t} = 0$ (4.6)

where: k_z = vertical permeability, v_z = volumetric strain, g_w = unit weight of water, $\bar{u}$ = total head, t = time.

3. Effective stress principle: $\sigma_z = \sigma'_z + u_p$ (4.7)

where: s'_z = effective vertical stress, u_p = excess pore pressure = $\bar{\mu} - z_d \cdot \gamma_w$, z_d = distance from reference datum.

4. Effective stress-strain relationship: $d\varepsilon_z = \frac{dv_z}{dz} = m_v \cdot d\sigma'_z$ (4.8)

where: $m_v = \frac{\partial \varepsilon_z}{\partial \sigma'_z} = \frac{C_c}{2.3 \cdot (1 + e_o) \cdot \sigma'_z}$, or $\frac{C_r}{2.3 \cdot (1 + e_o) \cdot \sigma'_z}$, (4.9)

e_z = vertical strain.

Combining these equations, the basic differential equation governing one-dimensional consolidation settlement can be expressed as follows:

$$\frac{k}{m_v \cdot \gamma_w} \cdot \frac{\partial^2 u_p}{\partial z^2} = \frac{\partial u_p}{\partial t} \quad (4.10)$$

Since the coefficient of consolidation, c_v is: $c_v = \frac{k}{m_v \cdot \gamma_w}$ (4.11)

Substitution in equation 4.10 gives Terzaghi's consolidation theory:

$$c_v \cdot \frac{\partial^2 u_p}{\partial z^2} = \frac{\partial u_p}{\partial t} \quad (4.12)$$

Combining the force equilibrium equation 4.5, effective stress equation 4.7, and the effective stress-strain equation 4.8 provides the remaining equation for consolidation analysis:

$$\frac{1}{m_v} \frac{\partial^2 w_z}{\partial z^2} + \frac{\partial u_p}{\partial z} - f_z = 0 \quad (4.13)$$

Simultaneous solution of equations 4.12 and 4.13 produces the excess pore pressures and displacements after each time step, Δt. CONSOL97 recomputes the soil stiffness, m_v, and the permeability, k, of each sublayer at each time step using the following relationship from Terzaghi's consolidation theory:

$$k = c_v \cdot m_v \cdot \gamma_w \tag{4.14}$$

Substituting equation (5) we have:

$$k = \frac{c_v \cdot C_c \cdot \gamma_w}{2.3 \cdot (1 + e_o) \cdot \sigma'_{equiv}} \tag{4.15}$$

where σ_{equiv} is the equivalent effective stress. For effective stresses, σ'_z, greater than or equal to P'_p, $\sigma_{equiv} = \sigma'_z$. If the current stress is less than the preconsolidation stress, permeability is computed based upon the assumptions illustrated in Figure 4-2. The equivalent effective stress is the stress that produces the current void ratio on the virgin compression curve:

$$\sigma'_{equiv} = Pp \cdot \exp\left[\left(\frac{2.3}{C_{\varepsilon c}}\right) \cdot (\varepsilon_t - \varepsilon_e)\right] \tag{4.16}$$

where: P_p = preconsolidation stress, C_{ec} = virgin compression index, e_t = total strain, e_e = elastic recompression strain from the initial overburden stress to the preconsolidation stress, P_p.

4.2 TIME-DEPENDENT METHOD

In conventional settlement analysis, primary and secondary compression (creep at constant effective stress) are treated as separate and distinct phenomena. No attempt is made to model the time-dependent creep and stress dependent soil behavior during primary consolidation. However, the total change in void ratio can be expressed as:

$$\Delta e = \int_0^{t_p} \left[\left(\frac{\partial e}{\partial \sigma'_z} \right) \frac{d\sigma'_z}{dt} + \left(\frac{\partial e}{\partial t} \right)_{\sigma'_z} \right] dt + \int_{t_p}^{t} \left(\frac{\partial e}{\partial t} \right)_{\sigma'_z} dt \tag{4.17}$$

where: Δe = change in void ratio, t_p = time at the end of primary consolidation when $d\sigma'_z / dt = 0$.

The first and second terms of equation 4.17 comprise the volumetric changes that occur during primary consolidation when excess pore pressures are dissipating. It consists of a stress-dependent and a time-dependent component. The third term of equation 4.17 represents volumetric changes due to secondary compression that occur at constant effective stress. The individual stress- and time- dependent strain components that occur during primary consolidation cannot be determined by current testing methods. The new time-dependent method of analysis provides a consistent theory for modeling both creep and pore pressure dissipation as simultaneous phenomena.

When clay is subjected to an increase in load, either in the laboratory or the field, compression continues at a diminishing rate after effective stress has reached a constant value as shown for this secondary compression phase in Figures 4-1 and 4-3(a). In incremental laboratory consolidation tests, where loads are applied at 24 hour intervals, secondary compression strains that occur between the end of primary consolidation and 24 hours influence the position of the measured stress-strain curve, as shown in Figure 4-3(b). If the duration of each load increment was longer, the measured strains would be larger, because more secondary compression would occur in the longer loading period. If the duration of each load was shorter, the measured strains would be smaller, because less secondary compression would occur.

The effects of time on clay compressibility are evident both in the position of the stress-strain curve and the magnitude of the preconsolidation pressure. Taylor (1942, 1948), Crawford (1964, 1988), and Bjerrum (1967) have shown that, as a result of secondary compression, there is not a unique stress-strain curve for one-dimensional compression of clay. Unlike the conventional model, the time-dependent model consists of a set of stress-strain curves for one-dimensional compression of clay. These curves, called “time lines,” each correspond to a different duration of the applied load. The magnitude of the preconsolidation pressure, P_p', is different for each time line. Load duration thus affects both the stress-strain curve and the preconsolidation pressure.

The rheologic physical model developed by Rajot (1992) is shown in Figure 4-4. The instant component of compression is elasto-plastic, with an elastic spring and rigid-plastic slider. Deformations of the spring correspond to recoverable volume changes ($d\varepsilon_i^e$). Deformations of the slider correspond to instant non-recoverable volume changes ($d\varepsilon_i^p$) that occur when the effective stress exceeds the critical effective stress. The non-recoverable creep component of compression ($d\varepsilon_c^p$) is represented by the extended Kelvin element shown on the right side of Figure 4-4. Deformation of this part of the model corresponds to time-dependent non-recoverable volume changes (creep). Since the extended Kelvin element is in series with the instant spring and slider, the model produces simultaneous creep deformations and instant compression. Characteristic of all elasto-visco-plastic models, the soil skeleton is always yielding due to any increase in loading.

Both the non-recoverable instant plastic compression and the creep compression will cause hardening, or an increase in the critical effective stress at which instant plastic strains will occur. The relationship between critical stress and creep is defined by the location of the time lines which also represent critical stress loci corresponding to different rates of creep compression. During any loading increment, the time-dependent model computes the instant elastic deformations, instant plastic deformations and the creep deformations and creep strain rates for each time step. The current creep strain rate is compared to the creep strain rate for the time line (critical stress locus) at the current strain and effective stress to determine if the current effective stress equals the critical stress. Instant plastic compression will occur when the current effective stress equals the critical stress. The instant component of compression is elastic when the current effective stress is less than the critical stress.

Figure 4-5 illustrates the stress-strain path and critical stress determination for an over-consolidated soil sample loaded from an initial effective stress σ'_A to a final effective stress, σ'_c. The effective stress changes from point A to B produce creep rates that are faster than the creep rate on the time lines that are crossed by path AB. Therefore, for loading from point A to B, the critical stress, σ'_{px}, is always larger than the current effective stress, σ'_x. From point B to C, the

current creep rate equals the creep rate of the time line on which BC lies. Because the stress-strain path follows the time line, the critical stress, σ'_p, is always equal to the current effective stress along path AB.

The relationship between yielding and creep compression during pore water pressure dissipation due to a load increment from σ'_o to σ'_d is illustrated in Figure 4-6:

Point O to B: The rate of creep compression is higher than the creep strain rate for the time lines crossed, and thus is too high to allow instant plastic compression under the current effective stress. Compression is due to instant elastic strain and creep strain. Hardening occurs due to the creep strain and the one day reference preconsolidation pressure increases from σ'_{Po} to σ'_{PB}. The effective stress-strain relationship for the model in this condition is:

$$d\varepsilon = \frac{C_{\varepsilon r}}{2.3\sigma'} d\sigma' - \frac{d\dot{\varepsilon}_c^p}{\dot{\varepsilon}_c^p} \qquad (4.18)$$

The negative sign before the last term on the right side of equation 4.18 results in a positive quantity for path OB because the creep strain rate, $\dot{\varepsilon}_c^p$, is positive and the change in creep strain rate, $d\dot{\varepsilon}_c^p$, is negative.

Point B to D: Compression of the soil skeleton involves instant plastic and creep strain. The actual rate of creep compression corresponds to the creep strain rate of the time line at the current effective stress and strain for every point along the path BD. The current effective stress is thus equal to the critical stress at every instant. Hardening occurs due to instant plastic strain and creep strain, and the corresponding one day reference preconsolidation pressure increases to σ'_{PD}. The effective stress-strain relationship for the model in this condition is:

$$d\varepsilon = \frac{C_{\varepsilon c}}{2.3\sigma'} d\sigma' - \frac{C_\alpha}{2.3} \frac{d\dot{\varepsilon}_c^p}{\dot{\varepsilon}_c^p} \qquad (4.19)$$

The relationship among $d\sigma'$, $d\dot{\varepsilon}_c^p$ and $d\varepsilon$ represented by equation 4.19 and illustrated in Figure 4-7 may be characterized by three types of behavior: (1) When $d\dot{\varepsilon}_c^p$ is positive (the rate of creep compression is increasing), the compressibility ($d\varepsilon / d\sigma'$) is less than the compressibility along a time-line; (2) When $d\dot{\varepsilon}_c^p$ is zero (the rate of creep compression is constant), compression occurs along a time-line; and (3) When $d\dot{\varepsilon}_c^p$ is negative (the rate of creep compression is decreasing), the effective stress-strain curve is steeper than a time-line.

When the effective stress becomes constant, the model simulates the transition to secondary compression. A special case of equation 4.19 occurs for $d\sigma' = 0$, in which case all of the compression is time-delayed creep (secondary compression):

$$d\varepsilon = d\varepsilon_c^p = -\frac{C_\alpha}{2.3}\frac{d\dot{\varepsilon}_c^p}{\dot{\varepsilon}_c^p} \tag{4.20}$$

The time-dependent model of CONSOL97 is based upon the basic equations 4.5 to 4.7. The constitutive equation given by equation 4.8 is replaced by equations 4.18 for strains in the elastic domain and by equation 4.19 for strain in the plastic domain.

As with the conventional analysis, these equations are solved for displacements and pore pressures and the permeability is updated at each time step. However, the displacements now consist of instant and creep components and the reference preconsolidation pressure must be recomputed at each time step to reflect the current creep strain rate. The equation for computing new permeabilities during consolidation was given by equation 4.15:

$$k = \frac{c_v \cdot C_c \cdot \gamma_w}{2.3 \cdot (1 + e_o) \cdot \sigma'_{equiv}} \tag{4.15}$$

and requires an equivalent effective stress, σ'_{equiv}, on the reference time line that produces the current void ratio on the reference virgin compression curve. The equivalent effective stress on the non-linear strain vs effective stress line is illustrated in Figure 4-8 and can be expressed as follows:

$$\sigma'_{equiv} = \sigma'^{(o)}_{p-ref} \exp\left[\frac{2.3}{C_{\varepsilon c}}\left\{\varepsilon_A - \frac{C_{\varepsilon r}}{2.3}\ln\left(\frac{\sigma^{(o)}_{p-ref}}{\sigma'_o}\right)\right\}\right] \qquad (4.21)$$

The value of c_v in equation 4.15 corresponds to the effective stress, σ'_{equiv}.

4.3 NUMERICAL SIMULATION

CONSOL97 uses the finite element method to compute displacements and pore water pressures at prescribed locations within the soil mass during the consolidation process. The subsurface profile is represented by discrete elements, and the loads and drainage conditions are specified on the boundaries. The incremental form of the conventional or the time-dependent constitutive models and the flow equations are used to formulate the element stiffness matrices. Rajot used an infinitesimal strain solution based on the results of a comparative study by Meijer (1984) which found little difference between finite strain and infinitesimal strain solutions for clay soils.

The element stiffness matrices used in CONSOL97 were derived by applying Galerkin's method of weighted residuals and Green's theorem to write these governing equations in integral form. Green's theorem was used to transfer differentiation from the independent variables to the weighting functions over the element, and to generate boundary terms. In the Galerkin method, the trial functions (shape functions) and weighting functions are the same. The CONSOL97 program interpolates the displacements and pore pressures using linear trial functions.

Displacements and pore pressures are calculated incrementally for each time step. At the start of the computations, it is assumed that the soil profile has achieved secondary compression and a corresponding creep rate consistent with the geologic age and OCR of the soil. The field value of secondary compression coefficient, $C_{\alpha field}$ is computed based on the following relationship:

$$C_{\alpha field} = \left(C_{\varepsilon c} - C_{\varepsilon r}\right)\left(\frac{\ln(OCR)}{\ln\left(t_{age}/t_{ref}\right)}\right) \qquad (4.22)$$

where t_{age} is the geologic age of the deposit. The value of C_α used in the analyses varies between $C_{\alpha field}$ and $C_{\alpha\,lab}$. The value of C_α is adjusted continuously until the computed effective stress σ'_v becomes equal to σ'^{o}_{p-ref} using the following parabolic equation:

$$C_\alpha = C_{\alpha lab} - \left(C_{\alpha lab} - C_{\alpha field}\right)\left(\frac{\left(\sigma^{o}_{p-ref}/\sigma'_v\right)-1}{\left(\sigma^{o}_{p-ref}/\sigma'^{o}_{v}\right)-1}\right)^{1/2} \qquad (4.23)$$

The rate of creep compression and the yield computations are based upon C_α from equation 4.22. If the soil deposit has been mechanically over-consolidated and the C_α computations indicate that $C_{\alpha\,field}$ exceeds $C_{\alpha\,lab}$, then $C_{\alpha\,field}$ is set equal to $C_{\alpha\,lab}$.

Nonlinear stress-strain behavior and the change from instant elastic to instant plastic behavior at the critical stress level is accommodated through the use of convergence criteria, and by providing an automatic time stepping routine. If one of the convergence criteria is not satisfied for a time step, the time step size is halved and the computation is repeated. After convergence, the value of the next time step is anticipated based on previous values. Figure 4-9 illustrates the general computational procedure involved in CONSOL97, which is summarized here:

1. Compute the initial effective stress and pore pressure conditions for static equilibrium and hydrostatic conditions prior to load application.

2. Set the initial values of the reference preconsolidation pressure and compute the creep rate of the reference time line based on laboratory test results.

3. Set the initial values of critical stress corresponding to the initial creep rate. It is assumed that the current effective overburden pressure is the initial critical stress and the corresponding creep rate is calculated.

4. Initialize the stresses in the creep component of the model.

5. For a time step increment, Δt, apply any load increments and compute displacements and pore pressures

6. Check for convergence of displacements, pore pressures, and stresses. If converged, update stresses and strains. If not converged, return to step 5 and repeat the computation using new stiffness values for the instant and creep components of the model.

7. Compute the critical effective stresses for each element.

8. For each element, compare the current effective stress with the critical effective stress. If the current stress does not exceed the critical stress by the specified tolerable value, then update the critical stress values and continue. Otherwise, reduce the time step size and return to step 5.

Element stresses are computed using full integration in which the number of Gauss points equals the number of nodal points.

After each time step increment, the permeability or each sublayer is updated in accordance with the new effective stress, s'_z and the assumption that the permeability varies linearly with the log of void ratio change. Therefore, it is only necessary to specify c_v in the normally consolidated stress range.

4.3.1 Automatic Time Stepping

If one of the convergence criteria is not satisfied from time step, t_n to t_{n+1}, the time step size is halved and the computation is repeated from time step tn. After convergence is achieved, the value of the next time step is anticipated based on the previous three time step sizes. Time step sizes can range upward from the minimum allowable value computed by CONSOL97 for each sublayer:

$$\Delta t_{min} = 10^{-2} \cdot \frac{\Delta h^2}{c_v} \qquad (4.24)$$

where Δh is the sublayer thickness, to a maximum value specified by the user. CONSOL97 uses the following procedure to select a suitable time step size during the computations:

1. Use equation 4.24 to compute Δt_{min} for each element. Select the smallest value for use in the analysis.
2. Compute Δt_{max} by dividing each time period between two consecutive output times into equal time step intervals. A value for the number of intervals is specified by the user. The following equation can be used to estimate Δt_{max}:

$$\Delta t_{max} = 0.1 \cdot \frac{\left(H_k / nel\right)^2}{c_v} \qquad (4.25)$$

   where H_k is the longest drainage distance for layer k and nel is the number of elements in the layer.
3. During application of the load and for a duration equal to $100 \cdot \Delta t_{min}$ after the full load application, use the time step Δt_{min}, and remove the convergence and yield tolerance criteria.
4. Subsequent time step sizes are automatically selected such that (a) $\Delta t_{min} \le \Delta t \le \Delta t_{max}$, (b) the criteria for convergence equal 10^{-2} is satisfied, and (c) a yield tolerance is satisfied.

4.3.2 Convergence Criteria

At each time step, CONSOL97 checks four convergence criteria:

Criterion 1: Nodal Displacement

The change in displacements from one iteration to the next (between time *t* and *t+Dt*) :

$$\sum_{1}^{n} \left[\left(w_{t+\Delta t)} - w_t\right)^2 \Big/ \left(w_t\right)^2 \right] \le 1.0E-6 \qquad (4.26)$$

where: n = number of nodal points or sublayer boundaries in the problem, w_t = displacement at each node at time *t* or *t+Dt*.

Criterion 2: Nodal Pore Pressure

The global change in pore pressures from one iteration to the next (between time t and $t+Dt$):

$$\sum_{1}^{n}\left[(u_{t+\Delta t)}-u_t)^2 \Big/ (u_t)^2\right] \le 1.0E-6 \qquad (4.27)$$

where: n = number of nodal points or sublayer boundaries in the problem, u_t = pore pressure at each node at time t or $t+Dt$.

Criterion 3: Element Stress

The global change in the effective initial and creep stresses from one iteration to the next (between time t and $t+Dt$):

$$\sum_{1}^{nel}\left[(\sigma'_{t+\Delta t}-\sigma'_t)^2 \Big/ (\sigma'_t)^2\right] \le 1.0E-6 \qquad (4.28)$$

where: nel = number of elements or sublayers in the problem, s'_t = effective stress at each element or sublayer at time t or $t+Dt$. Both the initial and creep effective stresses are checked for convergence.

Criterion 4: Yield Surface

The effective stress in any sublayer after each time step increment does not exceed:

$$(1.0+\mathrm{Tol})\cdot\sigma'_p \qquad (4.29)$$

where: Tol is the yield tolerance (Tol = 0.10 for time-dependent analyses and 0.01 for conventional analyses), σ'_p is the current preconsolidation or critical stress. The value of σ'_p is updated after criteria 1 through 3 are satisfied at each time step.

During a continuous load application, criterion 4 is not checked. However, small time step increments are automatically selected such that the computations produce effective stresses that are close to the yield surface.

4.3.3 Time Step Integration

The time integration scheme for each time step t_{n-1} to t_n uses the approximation:

$$\int_{tn-1}^{tn} \bar{u} \cdot dt = \left[(1-\theta) \cdot \bar{u}_{(tn-1)} + \theta \cdot \bar{u}_{(tn)} \cdot \Delta t\right] \tag{4.30}$$

$$\int_{tn-1}^{tn} w \cdot dt = \left[(1-\theta) \cdot w_{(tn-1)} + \theta \cdot w_{(tn)} \cdot \Delta t\right] \tag{4.31}$$

where $\bar{u}$ is the total head, w is the displacement, and θ is a dimensionless parameter with values ranging from 0 to 1. With time step size changing at each increment, a better approximation is achieved by using two consecutive time steps, t_{n-1}, t_n, t_{n+1} such that θ is recomputed based on the previous time step, t_n and the current time step size, t_{n-1}:

$$\theta = \frac{t_n}{t_n + t_{n-1}} \tag{4.32}$$

For equal values of time step increments, $\theta = 1/2$.

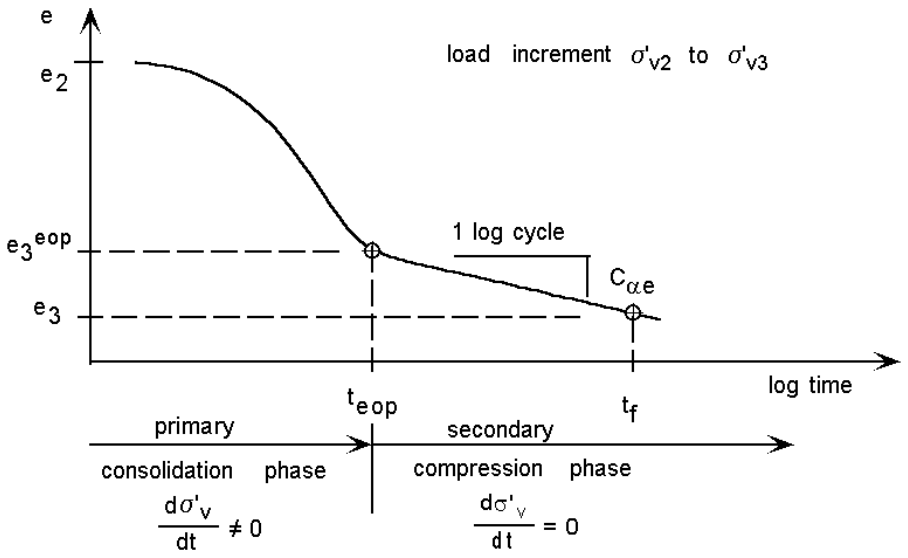

(a) Void ratio versus log time

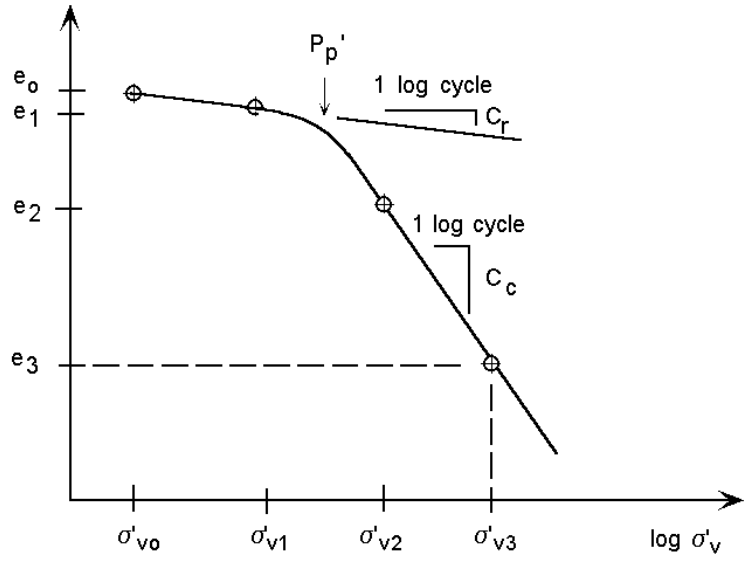

(b) Void ratio versus log effective stress

Figure 4-1: Laboratory strain-time and stress-strain curves for conventional consolidation model

manual/chapter4/fig4_1.cvs

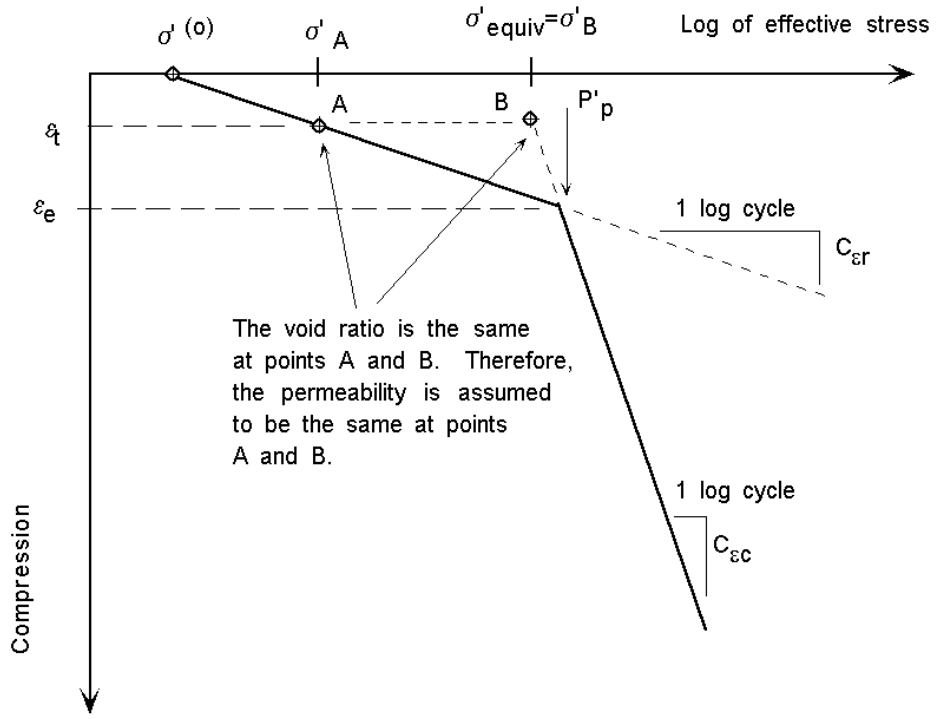

Figure 4-2: Elasto-plastic permeability-strain-effective stress relationship

manual/chapter4/fig4_2.cvs

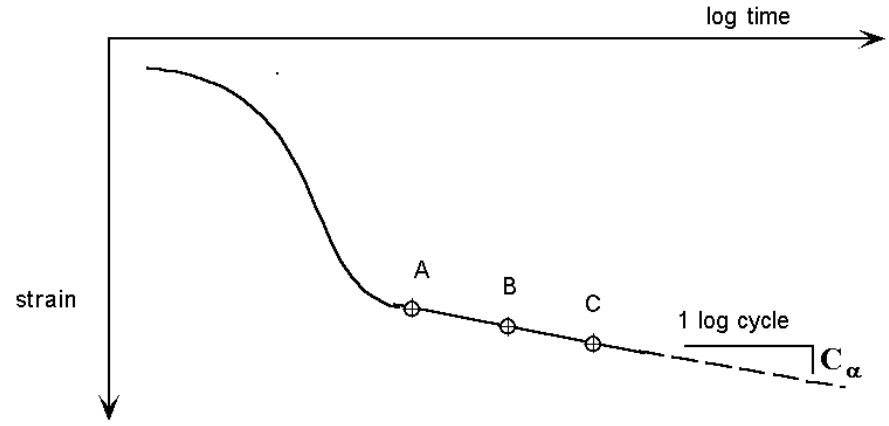

(a) Strain versus time curve for load increment from σ'_o to σ'_f

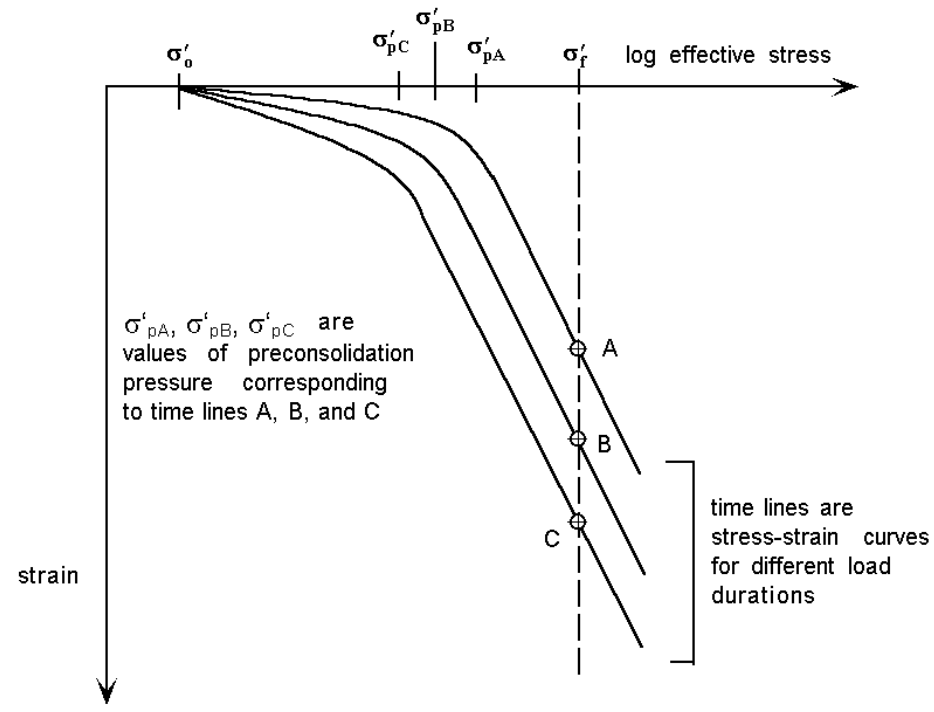

(b) Stress-strain curves

Figure 4-3: Laboratory strain-time and stress-strain curves for time-dependent model

manual/chapter4/fig4_3.cvs

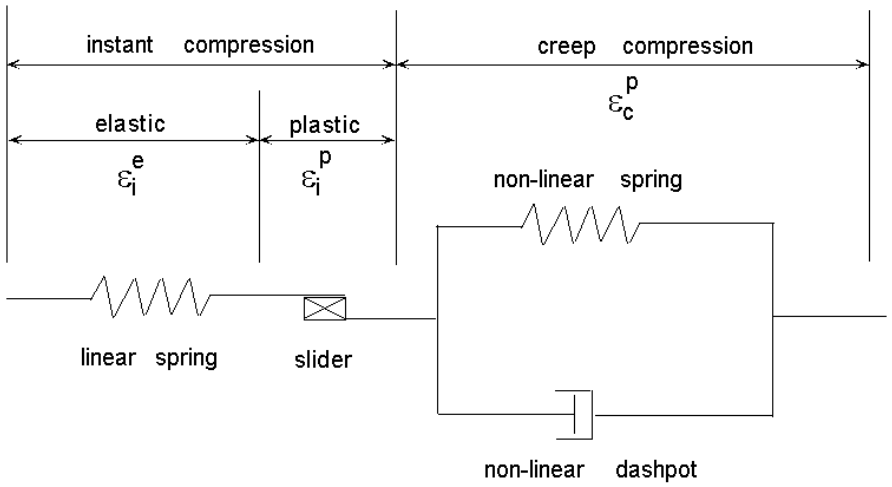

Figure 4-4: Rajot's rheologic mechanical model

manual/chapter4/fig4_4.cvs

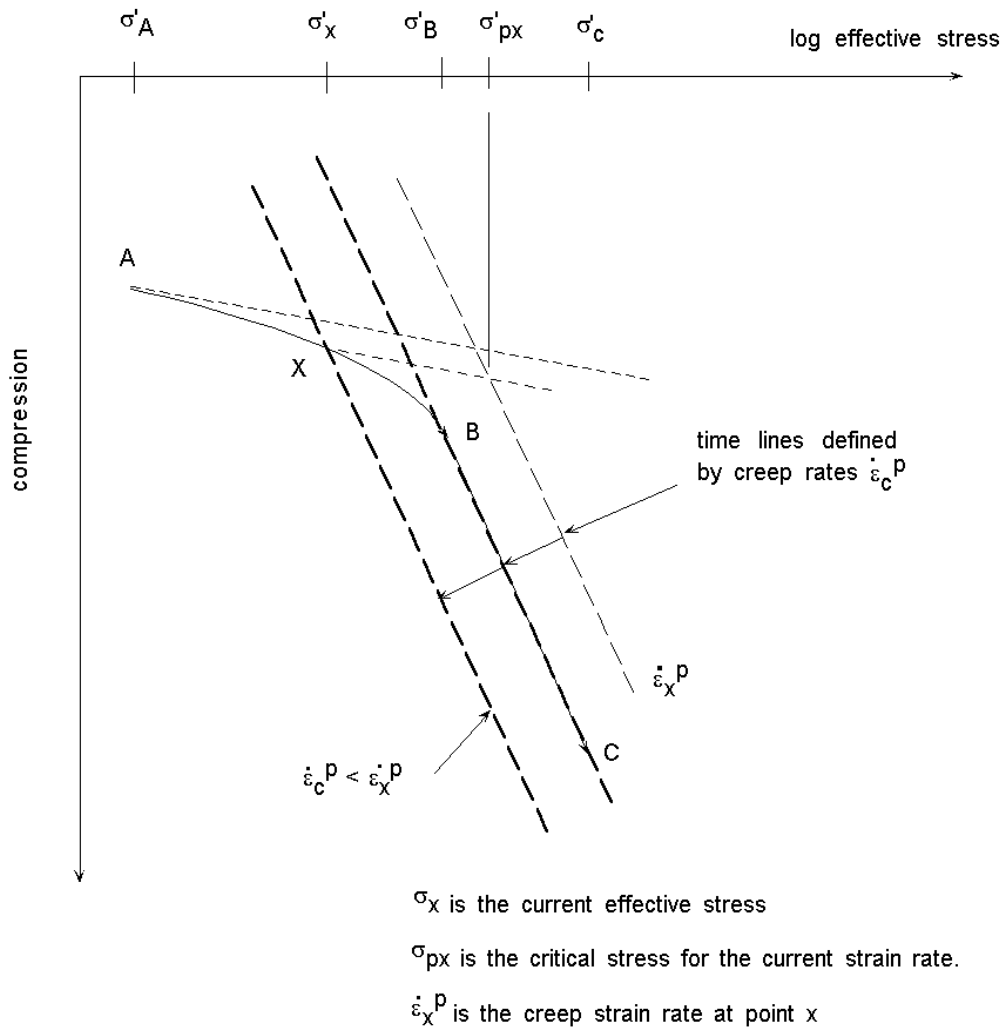

Figure 4-5: Critical stress determination for Rajot's model

manual/chapter4/fig4_5.cvs

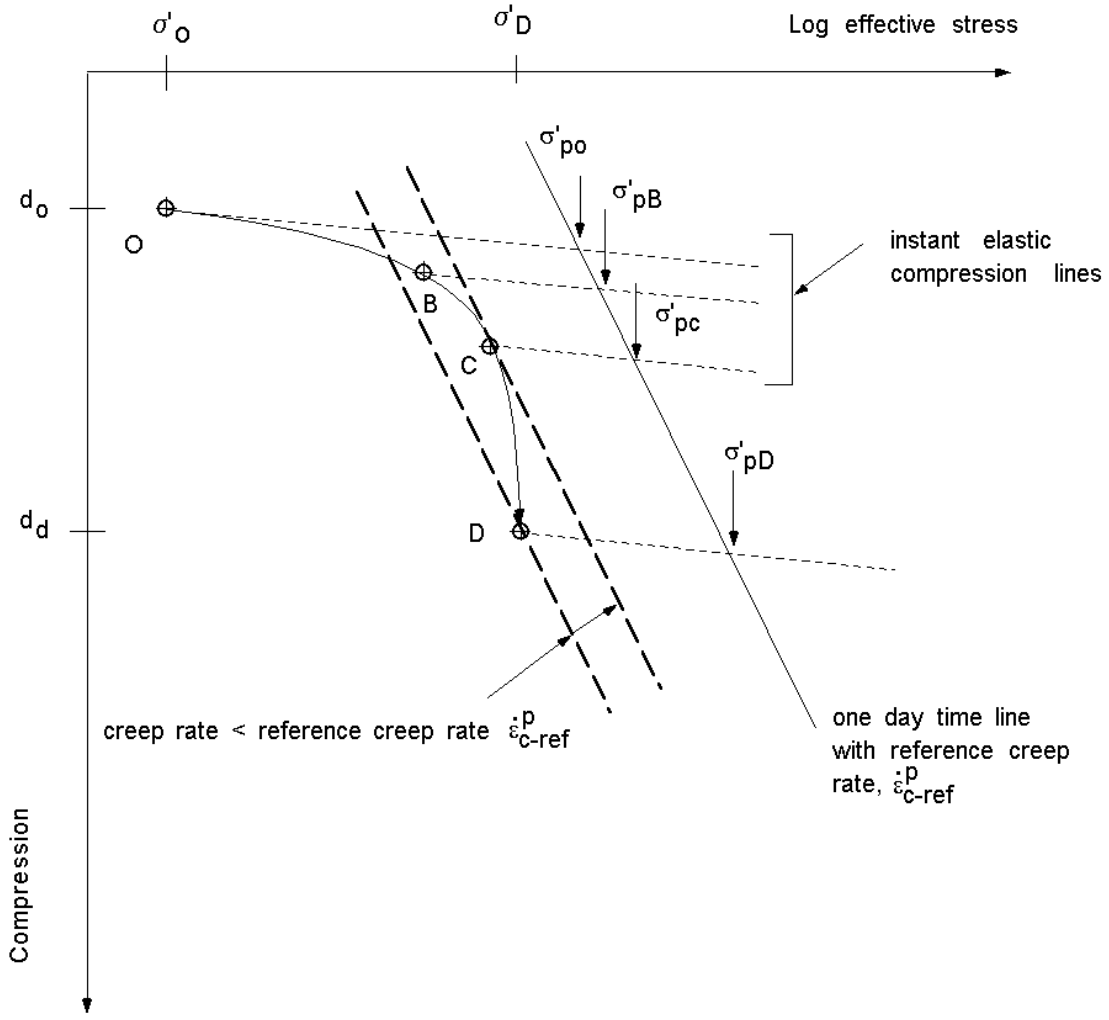

Figure 4-6: Yielding and creep during pore pressure dissipation

manual/chapter4/fig4_6.cvs

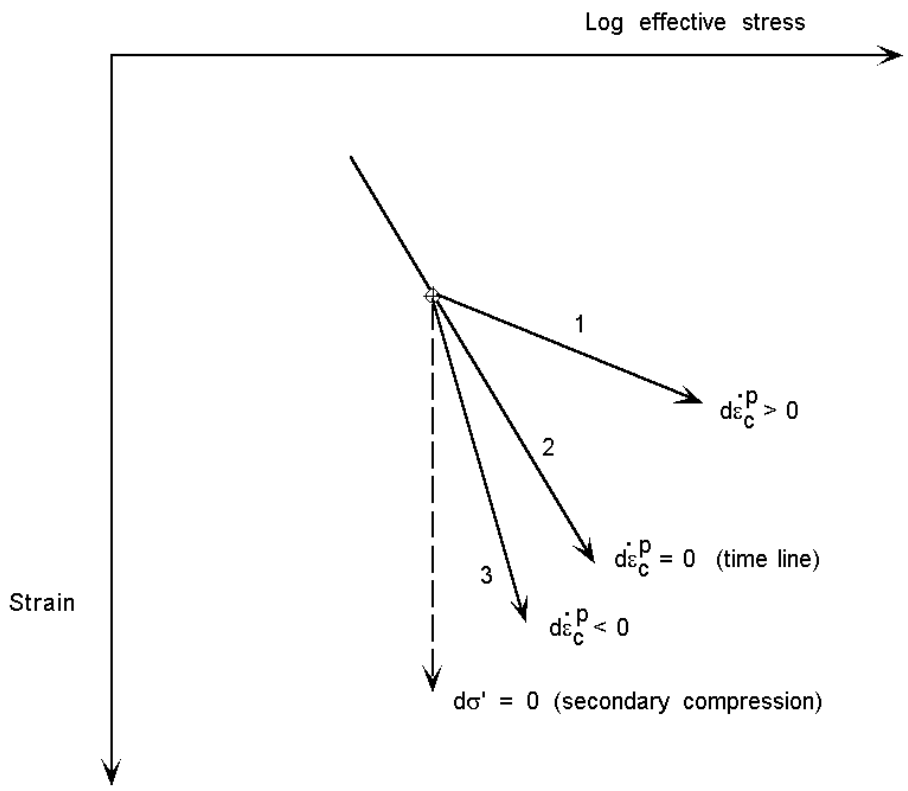

Figure 4-7: Effect of creep rate change on stress-strain paths

manual/chapter4/fig4_7.cvs

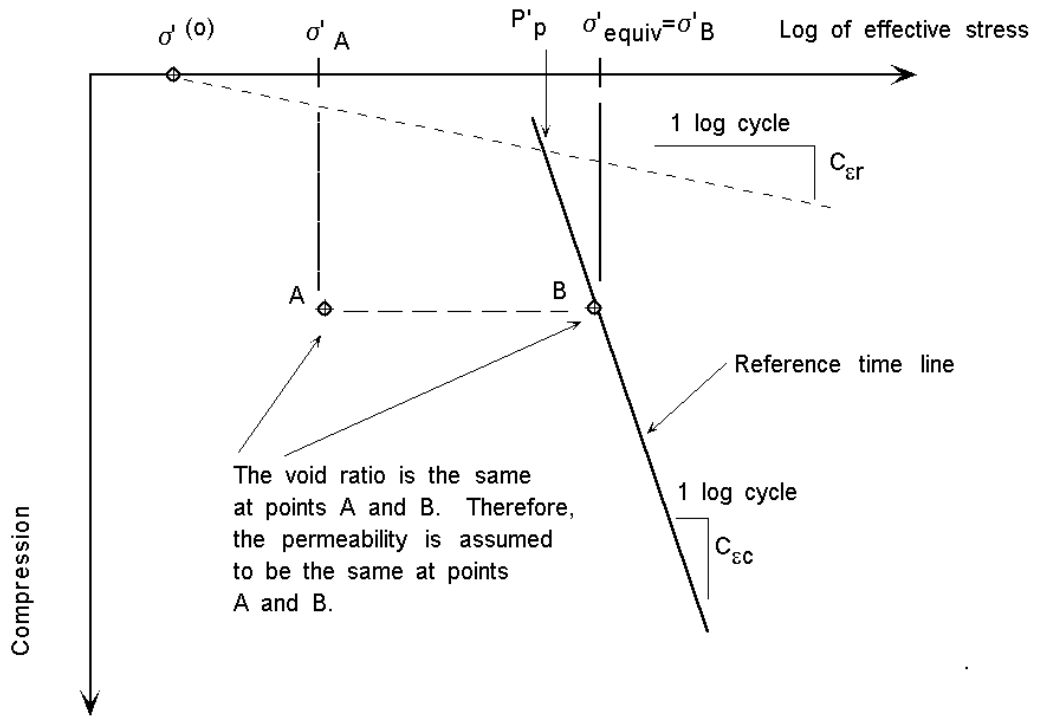

Figure 4-8: Elasto-visco-plastic permeability-strain-effective stress relationship

manual/chapter4/fig4_8.cvs

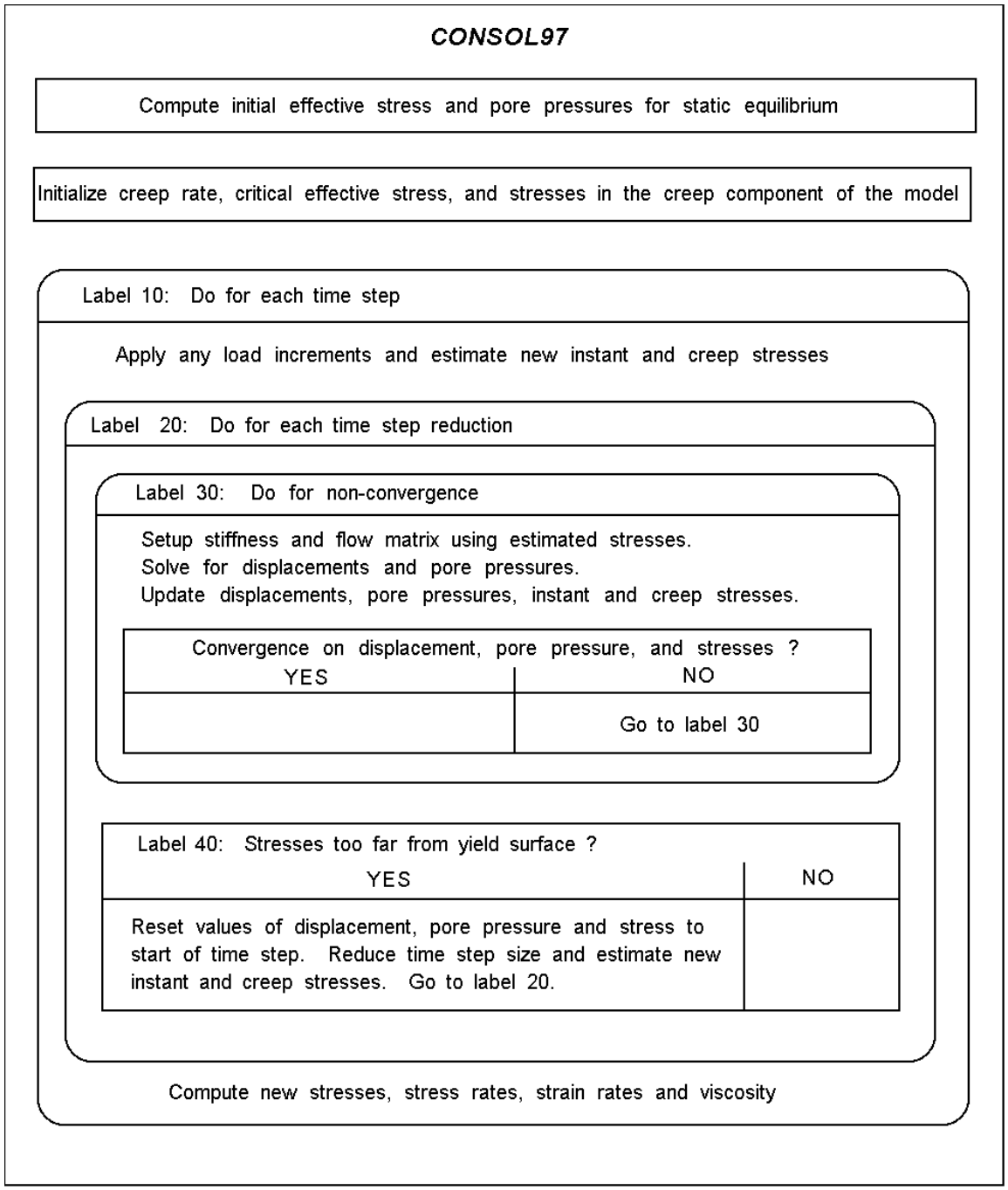

Figure 4-9: Summary of CONSOL97 computational procedures

manual/chapter4/fig4-9.cvs

5. RUN TIME ERROR AND WARNING MESSAGES

Unless otherwise stated, these run time error and warning messages apply to both conventional and time-dependent consolidation analyses.

5.1 WARNING MESSAGES

1. *"More than 10 iterations in current time step."* This message occurs when convergence to the yield surface does not occur in 10 iterations or less. The time increment will be automatically reduced and the computation repeated. No action is required by the user. However, the computational time may become excessive if this message continues to appear. The User may wish to redesign the with thinner sublayers near drainage boundaries.

2. *"Numerical scheme changed to explicit until solution is reached for this time step."* The automatic selection of time step intervals has not produced numerical convergence. The minimum time step size will be used with an explicit time integration procedure.

3. *"This is a warning:*

High frequency oscillations in effective stress are detected.
Still convergence is met within allowable number of iterations
but solution may be off concerning viscous strains.

The User should run another analysis with thinner sublayers near drainage boundaries and a larger loading ramp time, and compare the results of the two analyses.

5.2 ERROR MESSAGES

1. *"This is last output before program stops."* The numerical procedure did not converge for the current time step. This message will be accompanied by other warning and/or error messages.

2. *"Problem detected about pore pressure increase: Vertical effective stress is negative. Could be caused by viscous strains (?)."* Generally due to incorrect data input. Check profile and layer information and the value of the load increments. Positive loading is in a downward direction.

3. *"Too many equations ... memory space."* The number of layers exceeds the declared dimensions of program variables. Use fewer layers.

4. *"Band width too large ... memory space."* The number of layers and loads results in a system of equations that exceed the declared dimensions of the equation solver. Use fewer layers.

5. *"Too many elements ... memory space."* The number of layers exceeds the declared dimensions of the source code. Use fewer elements.

6. *"Too many specified displacement or pore pressure boundary conditions ...memory space."* Use fewer internal drainage layers.

7. *"Too many specified boundary tractions ... memory space."* CONSOL97 computes side forces on each sublayer to produce force equilibrium. These side forces are zero for large areal loads and non-zero for small area surface loads. Use fewer sublayers.

8. *"Too many required output times ... memory space."* Use fewer output times.

9. *"Too many specified loads ... memory space."* Use fewer load options.

10. *"Error on boundary conditions: pore pressure, displacement, or loading conditions were not specified at the boundaries."* Check for errors in the pore pressure, displacement, and loading data input. CONSOL97 internally sets the displacement boundary conditions which consists of zero displacement at the bottom of the soil profile.

11. *"More than 30 iterations for initial conditions ... Program stopped."* Check for errors in the subsurface profile and layer condition data input.

12. *"Initial computed mean effective stress is negative ... (?) Program stopped."* Check for errors in the subsurface profile and layer condition data input.

13. *"Out of plasticity criterion for initial conditions in either part of model ... ?"* Use more sublayers and more time step increments.

14. *"Problem with viscous strains could not be fixed by explicit scheme. Execution is stopped."* Use more sublayers and more time step increments.

15. *"Problem with iteration process could not be fixed by explicit scheme. Execution is stopped."* Use more sublayers and more time time step increments.

16. *"Too far from yield surface even with minimum time step. Execution is stopped."* The computed yield stress is not within the specified tolerance. You should redesign the sublayer mesh by using thinner layers at drainage boundaries.

6. INDEX OF DATA INPUT VARIABLES

Variable	Description
ACONSOL	Dimensional units for coefficient of consolidation.
AGE(J)	Estimated geologic age of soil J.
ARC(N5)	Radius of circular area surcharge for circular load number N5 of load option 5 (circular area fill).
ARS(N4)	Distance from center of strip fill load number N4 of load option 4 (strip fill).
ASTRESS	Dimensional units for stress.
AWATER	"Fresh" or "salt" water.
BMW	Bulk modulus of water. BMW=2.0×10^6 kPa
CC(J,K)	Virgin compression index of soil type J, and lab curve segment K.
CEC2(J,K)	Coefficient of secondary compression for soil type J and lab curve segment K.
CR(J)	Recompression coefficient of soil type J.
CV(J,K)	Coefficient of consolidation of soil type J and lab curve segment K.
DELTA1(J,N1)	Specified stress increase for layer J, load number N1 for load option 1.
DIAMC(N5)	Diameter of circular area load for load number N5 of loadcase 5.
DIAMS(N4)	Width of the strip load for load number N4 of loadcase 4.
ELEV(J)	Elevation of each layer boundary, J.
ELFC(N5)	Elevation of circular fill for load number N5 of loadcase 5. Value is -9999 if HFLC(N5) is specified.
ELFL(N3)	Elevation of areal fill for load number N3 of loadcase 3. Value is -9999 if HFILL(N3) is specified.
ELFS(N4)	Elevation of strip fill for load number N4 of loadcase 4. Value is -9999 if HLFS(N4) is specified.
ELNW(N2)	Elevation of new water level for load number N2 of loadcase 2.
ELSURF0	Surface elevation of overburden soil above compressible layer.
ELW	Elevation of initial water table.
ER(J)	Initial void ratio of soil type J.
ERROR	The allowable convergence error on computed displacements and pore pressures. ERROR= 10^{-2} after load has been applied.
ETA0	The viscosity constant for the creep part of the model. ETA0=10^6 kPa-minutes.
FINAL(J,N6)	Final effective stress for layer J, load number N6, for loadcase 6.
GAMF	Moist unit weight of fill overburden above compressible layer.
GAMFC(N5)	Moist unit weight of new circular fill, load number N5 of loadcase 5.
GAMFL(N3)	Moist unit weight of areal fill for load number N3 of loadcase 3.
GAMFS(N4)	Moist unit weight of strip fill for load number N4 of loadcase 4.
GAMS(J)	Saturated unit weight of soil type J.

Variable	Description
GAMSAT	Saturated unit weight of overburden fill above compressible layer.
GAMSATC(N5)	Saturated unit weight of circular fill for load number N5 of loadcase 5.
GAMSATL(N3)	Saturated unit weight for areal fill for load number N3 of loadcase 3.
GAMSATS(N4)	Saturated unit weight for strip fill for load number N4 of loadcase 4.
GW	Unit weight of water. GW=9.80 kN/m^3
HFILL(N3)	Height of new areal fill for load number N3 of loadcase 3. Value is - 999 if ELFILL(N3) is specified.
HFILLC(N5)	Height of new circular fill for load number N5 of loadcase 5. Value is -999 if ELFC(N5) is specified.
HFILLS(N4)	Height of new strip fill for load number N4 of loadcase 4. Value is -999 if ELFS(N4) is specified.
IBUOYC(N5)	Buoyancy code for load number N5 of loadcase 5. IBUOYC(N5) = 1 correct for buoyancy, = 0 no correction.
IBUOYS(N4)	Buoyancy code for load number N4 of loadcase 4. IBUOYS(N5) = 1 correct for buoyancy, = 0 no correction.
IFILE	Value designates detailed output option: 0 = no detailed output; 1 or greater = detailed output. For conventional elasto-plastic analysis, leave blank.
ITIMAR(K)	Load time attendance roster: 0 =output time VTO(K) is not a load application time; 1 or greater = output time is also a load application time.
LAYDAT(J)	Layer number selected for the output plot file.
LAYOUT	Total number of layers identified for output plot file
LOADCASE(K)	Type of loading: 1 = stress change; 2 = change in groundwater elevation; 3 = large area fill; 4 = strip fill; 5 = circular fill; 6 = specified change in stress and preconsolidation pressure; 7 = underconsolidated.
LUNIT	Code for selecting variable units: 1 = psf,min.; 2 = ksf,min; 3 = tsf,min; 4 = kPa,min; 5 = tsm,min; 6 = psf,day; 7 = ksf,day; 8 = tsf,day; 9 = kPa,day; 10 = tsm,day; 11 = psf,year; 12 = ksf,year; 13 = tsf,year; 14 = kPa,year; 15 = tsm,year.
MATL(K)	Soil type number for layer K.
METHOD	Type of analysis: 0 = time-dependent method; 1 = conventional method.
MODE(K)	Soil model attendance roster: 0 = time-dependent model; 1 or greater = conventional model.
NBDFP	Number of drainage boundaries.
NE(K)	Number of layers (elements) in soil zone K.
NMAT	Number of material types
NMESH(K)	Mesh geometry option for each layer, K: 1 = increasing thickness with depth; 2 = decreasing thickness with depth; 3 = increasing and decreasing thickness with depth; 4 = uniform thickness.
NNP(K)	Node number of drainage boundary K.
NP	Number of points to describe soil zone boundaries.
NTL	Number of times the load is specified.
NTO	Number of requested output times.

Variable	Description
NX1	Number of time steps between successive output times.
OVER(K,N6)	Specified overburden pressure of layer K, load number N6 for loadcase 6.
P1KPA	One kilo-Pascal in pressure units used (determined from LUNIT).
PP(K)	Initial preconsolidation pressure for layer K.
PRECONS(J,N6)	Specified preconsolidation pressure for layer J, load number N6 for loadcase 6.
RAMP(K)	Time duration to fully apply load number K.
SIG(J,K)	Maximum effective stress for segment K of the stress-strain curve for soil type K.
ST(K)	Stress state of subsurface zone K: "UC"= under consolidated, "NC"= normally consolidated, "OC"= over consolidated.
T1(J,K)	Yield surface tolerance for the top (K=1) and bottom (K=2) of layer J. For EVP model, T1 = 0.1; for EP model, T1 = 0.01. Values are used after the load is applied.
T1DAY	One day in time units used (determined from LUNIT).
TAGE(K)	Estimated geologic age of soil type K.
TITL	Description of problem.
TMAX	The maximum value of requested output time.
T0(K)	Reference load duration for soil type K. Usually 24 hours.
VTIME(J)	Time at which load J is applied.
VTO(J)	Time at which output is requested. J = 1 to NTO.

7. REFERENCES

American Society for Testing and Materials (1987). *Annual Book of ASTM Standards, Section 4, Construction, Volume 04.08, Soil and Rock; Building Stones; Geotextiles*, ASTM, 1916 Race Street, Philadelphia, PA, 19103.

Bjerrum, L. (1967). "Engineering geology of Norwegian normally consolidated marine clays as related to settlements of buildings," 7th Rankine Lecture, *Geotechnique*, 17(2), 81-118.

Crawford, C.B., (1964). "Interpretation of the consolidation test," *Journal of the Soil Mechanics and Foundations Division*, Proceedings of the ASCE, 90(5), pp. 87-102.

Crawford, C.B., (1988). "On the importance of rate of strain in the consolidation test," *Geotechnical Testing Journal*, 11(1), pp. 60-62.

Duncan, J.M., Smith, R.W., Brandon, T.L., Wong, K.S. (1988). "Consol Version 2.0: A Computer Program For 1-D Consolidation Analysis of Layered Soil Masses," The Charles E. Via, Jr. department of Civil Engineering, 104 Patton Hall, Virginia Polytechnic Institute and State University, Blacksburg, VA, 24061.

Meijer, K.L. (1984). "Comparison of finite and infinitesimal strain consolidation by numerical experiments," *International Journal for Numerical and Analytical Methods in Geomechanics*, Vol. 8, no. 6.

Rajot, J.P. (1992). "A theory for the time dependent yielding and creep of clay," Ph.D. Thesis, Virginia Polytechnic Institute and State University, Blacksburg, Virginia.

Taylor, D.W., (1942). "Research on Consolidation of Clays," Department of Civil and Sanitary Engineering, Massachusetts Institute of Technology, Cambridge, Massachusetts, Serial 82.

Taylor, D.W., (1948). *Fundamentals of Soil Mechanics*, John Wiley & Sons, New York, 700 pp.

U.S. Navy, (1982). *Navfac DM-7.1, Soil Mechanics, Design Manual 7.1*, Department of the Navy, Naval Facilities Engineering Command, 200 Stovall Street, Alexandria, VA, 22332.

VITA

Vincent J. Perrone

EDUCATION

M.S., Civil Engineering, Massachusetts Institute of Technology, 1978.
Cambridge, Massachusetts

B.S., Civil Engineering, Tufts University, 1973.
Medford, Massachusetts

PROFESSIONAL EXPERIENCE

1985 to 1993: Principal Engineer, Converse Consultants NW, Seattle, Washington.

1982 to 1985: Project Engineer, Dames and Moore, Seattle, Washington.

1980 to 1982: Project Engineer, Converse Consultants, Seattle, Washington.

1978 to 1980: Staff Engineer, Hart Crowser and Associates, Seattle, Washington.

1976 to 1978: Research Assistant, Massachusetts Institute of Technology, Cambridge, Massachusetts.

1973 to 1976: Staff Engineer, Stone and Webster Engineering Co. Inc., Boston, Massachusetts.

REGISTRATIONS

Professional Engineer: Washington and Alaska

PROFESSIONAL AFFILIATIONS

- American Society of Civil Engineers (ASCE)
- Planning Committee of ASCE Seattle Geotechnical Section (1990 to 1993)
- International Society of Soil Mechanics and Foundation Engineering
- Volunteers in Technical Assistance (VITA)
- ASCE Geotechnical Journal Publications (1991 to 1993)